UNIVERSITY OF CALIFORNIA

Los Angeles

Genetic Determinants of Macrocephaly

A dissertation submitted in partial satisfaction of the requirements for the degree of Doctor of

Philosophy in Human Genetics

by

Steven Daniel Klein

2017

ABSTRACT OF THE DISSERTATION


Genetic Determinants of Macrocephaly

by

Steven Daniel Klein

Doctor of Philosophy in Human Genetics

University of California, Los Angeles, 2017

Professor Julian Antonio Martinez, Chair

Measurement of head circumference is a common practice in the care of a developing child as it is a high yield, low cost clinical test to monitor brain development. Macrocephaly, or head circumference greater than two standard deviations above the mean (>98th %ile), can be caused by abnormal brain growth, impaired cerebral spinal fluid drainage, or bone growth. While head circumference is a normally distributed trait with normal variations in the population, extreme variants in head circumference are often associated with underlying disease pathogenesis and, in many cases, accompanying behavioral phenotypes. Understanding the causes of reproducible macrocephaly allows us to better grasp the governing principles of brain growth and furthermore the associated behavioral abnormalities. The clinical workup for a child presenting with macrocephaly is important as it not only dictates testing, but also can be indicative of a more insidious disease process with comorbidities. With the wide spread use of massively parallel sequencing technologies the genetic etiologies of numerous *de novo*, sporadic, and rare genetic syndromes have been recently discovered. We have used this

powerful detection tool to identify mutations in a cohort of cases with Macrocephaly. We

present the phenotypic information for cases with identified mutations in the genes PTEN,

Ptch1, SUFU, mTOR, and DICER1. Furthermore, we have modeled these mutations in human

cell lines and show that their mechanism of action converges on activation of mTOR signaling.

Lastly, we demonstrate that infection of with *Toxoplasmosis Gondi* mirrors this mTOR activation

and explains why congenital infections manifest with macrocephaly. We have dissected the

exact molecular mechanism resulting from each mutation and proposed novel precision

medical approaches to treat these and future cases. The work presented in this dissertation

demonstrates the power and utility of a precision medical approach to patients presenting with

rare disease and abnormal phenotypes.

The dissertation of Steven Daniel Klein is approved.


Eric Vilain

Harley Kornblum

Rita Cantor

Julian Antonio Martinez, Committee Chair



University of California, Los Angeles

2017

DEDICATION

For my loving and supporting family and friends who helped me to believe in myself even when

I did not.

Debbie, Irwin, Mark, Andrea, Kathy, Kiara, Blayne, Ana, Marlowe, Ronit, Bruno, Robert, Kristian,

Stephen(Stinky), Joe, Evan, Brittany, Norah and Bjorn.

Table of Contents

List of Tables and Figures

VITA/Biographical Sketch: Steven Daniel Klein

**Education:**

2012-                UCLA-Caltech Medical Scientist Training Program (MSTP)

                     Anticipated Graduation MD/PhD June 2019

2012-                UCLA Human Genetics PhD Candidate

                     Anticipated Graduation PhD March 2017

2010-                David Geffen School of Medicine at UCLA

                     Anticipated graduation date June 2019

2004-2008            University of Rochester

                     Major: BS Molecular Genetics

                     Minor: American Sign Language


**Research Experience:**

2011-Present         Continuing to work in the laboratory of Julian Martinez-Agosto MD, PhD. Where an

                     ongoing biochemical study aims to describe a novel disease and continuing to elucidate

                     the genetic etiologies of Autism and overgrowth disorders.

2011                 Recipient of the American College of Medical Genetics summer scholar award at UCLA.

                     This was a program designed to stimulate interest in the field of medical genetics. Time

                     was split between doing basic science research and seeing patients in the various

                     genetic clinics at UCLA. Research was carried out in the laboratory of Julian Martinez-

                     Agosto MD, PhD. Two publications are currently under review from this work.

**Publications:**

1.  Danzi S, **Klein S**, Klein I. 2008. Differential regulation of myosin heavy chain genes $\alpha$ and $\beta$ in the rat atria and ventricles: Role of antisense RNA. Thyroid, 18(7):761-768.

2.  **Klein S**, Stroberg A, Ghahremani S, Martinez-Agosto JA. 2012. Phenotypic progression of skeletal anomalies in cloves syndrome. Am J Med Genet Part A. 158A:1690–1695.

3.  **Klein, S,** Sharifi-Hannauer, P, & Martinez-Agosto, J. A. 2013. Macrocephaly as a clinical indicator of genetic subtypes in autism. Autism Res, 6(1), 51-56.

4.  **Klein S**, Lee H, Ghahremani S, Kempert P, Ischander M, Teitell MA, Nelson SF, Martinez-Agosto JA. Expanding the phenotype of mutations in DICER1: mosaic missense mutations in the RNase IIIb domain of DICER1 cause GLOW syndrome. J Med Genet 2014;51(5):294-302.

5.  Martinez-Agosto J and **Klein S**. Referee Report For: Temporal order of RNase IIIb and loss-of-function mutations during development determines phenotype in DICER1 syndrome: a unique variant of the two-hit tumor suppression model [v1; ref status: approved with reservations 1, http://f1000r.es/5l9] F1000Research 2015, 4:214 (doi: 10.5256/f1000research.7245.r9442)

6.  **Klein, S**, Goldman, A, Lee, H, Ghahremani, S, Bhakta, V, UCLA Clinical Genomics Center, Nelson, S. F. and Martinez-Agosto, J. A. Truncating mutations in *APP* cause a distinct neurological phenotype. Ann Neurol., 80: 456–460. doi:10.1002/ana.24727 (2016),

7.  Bramble M. S, Roach L, Lipson A, Vashist N, Eskin A, Ngun T, Goasschalk J. E, **Klein S**, Barseghyan, Arboleda, V. A, and Vilain E. Sex-Specific Effects of Testosterone on the Sexually Dimorphic Transcriptome and Epigenome of Embryonic Neural Stem/Progenitor Cells. *Sci. Rep.* **6**, 36916; doi: 10.1038/srep36916 (2016).

8.  *Mullegama, S.V., ***Klein, S.D.,** Mulatinho, M.V., Senaratne, T.N., Singh, K., Center, U.C.G., Nguyen, D.C., Gallant, N.M., Strom, S.P., Ghahremani, S., et al. De novo loss-of-function variants in STAG2 are associated with developmental delay, microcephaly, and congenital anomalies. Am J Med Genet A. . (2017, **\*Co-First Author)**

**Honors and Awards:**

| | |
|---|---|
| 2016 | Winnder of the David Rimoin Award for Research Excellence in Medical Genetics at the UCLA Human Genetics Department & UCLA Intercampus Medical Genetics Training Program Joint Academic Retreat |
| 2014 | Recipient of the Denis Weatherstone Predoctoral fellowship from Autism Speaks |
| 2013 | Winner of the Leena Peltonen Award in Research Excellence at UCLA at the UCLA Human Genetics Academic Retreat |
| 2013 | 1st place for best poster in the BWF-IT-MD, GATP, SIB joint training grant symposium |
| 2013 | Admitted to the Fellowship at Auschwitz for the Study of Professional Ethics (FASPE) |

**Chapter One**

The heterogeneous genetic etiologies of

macrocephaly: associated phenotypes, novel

neural networks, and impacts on behavior

# Abstract

Measurement of head circumference is a common practice in the care of a developing child as it is a high yield, low cost clinical test to monitor brain development. Macrocephaly, or head circumference greater than two standard deviations above the mean (>98th %ile), can be caused by abnormal brain growth, impaired cerebral spinal fluid drainage, or bone growth. While head circumference is a normally distributed trait with normal variations in the population, extreme variants in head circumference are often associated with underlying disease pathogenesis and, in many cases, accompanying behavioral phenotypes. Understanding the causes of macrocephaly allows us to better grasp the governing principles of brain growth and furthermore the associated behavioral abnormalities. The clinical workup for a child presenting with macrocephaly is important as it not only dictates testing, but also can be indicative of a more insidious disease process with comorbidities. With the wide spread use of massively parallel sequencing technologies the genetic etiologies of numerous sporadic, rare, and *de novo* genetic syndromes have been recently discovered. We have reviewed publications relating to the genetics of macrocephaly. From these publications we have curated a macrocephaly-associated gene list and subjected this list to pathway enrichment analysis, functional analysis, and cross reference to publically available gene sets including those from Online Mendelian Inheritance in Man

(OMIM) and Human Phenotype Ontology (HPO). We focus on associated phenotypes, overrepresented signaling cascades, and functional associations to synthesize a comprehensive review of the genetics of macrocephaly. Most importantly we emphasize the comorbidity of neurological deficits in the reported cases including autism spectrum

disorders, intellectual disability, and developmental delay.  We have found that both the

PI3K/Akt/mTOR pathway and the sonic hedgehog pathway are significantly enriched in

this gene set and furthermore that many of these genes are related to or members of

functional neural networks.  This review helps to characterize the genetic heterogeneity of

macrocephaly, guides the clinical work up of future cases, summarizes known biochemical

data where available, and could shed additional light on future treatment modalities for

syndromes associated with this phenotypic finding.

## Introduction

Measurement of head or occipital frontal circumference (OFC) is a common and recommended practice in the developing newborn and infant. The measurement obtained at each pediatric well child visit and is derived from the placement of a pliable tape measure around the head using the occiput and supraorbital ridges as points of reference. Measurements are plotted on standard growth curves, most commonly those published by the world health organization (WHO) and the centers for disease control (CDC). These charts compare measurements to standard trajectories for age and sex. This routine screening is a first line detection method for numerous conditions relating to alterations in development and function of the skull, brain or its ventricular system. Deviations from normal are first and foremost identified by increased or decreased head size, termed macrocephaly and microcephaly respectively. These terms are defined by growth measurements that are two or more standard deviations from the mean (above the 98th percentile or below the 2nd percentile). Macrocephaly can be the result of numerous underlying medical abnormalities including increased brain size/volume (megalencephaly), cerebral spinal fluid content (CSF), intracranial blood, bone growth, and intracranial pressure (Figure 1). Surveillance and identification of these etiologies is important as it dictates management of the child and the available/appropriate interventions. Megalencephaly results in an enlarged brain, which may be due to increased proliferation and division of brain cells. The cause of the increased proliferation is possibly genetic and in many cases the result of sporadic, *de novo* mutations that affect growth-signaling pathways therefore resulting in their deregulation. Most interestingly this increase in proliferation is associated with behavioral phenotypes including but not limited

to intellectual disability (ID), development delay (DD), and autism spectrum disorders (ASDs). In fact, macrocephaly is the most reproducibly documented physical finding in autism spectrum disorder (ASD) cohorts[1].

Macrocephaly is a key finding in many established overgrowth syndromes where the increased head circumferences is part of a constellation of other somatic overgrowth findings such as tall stature, increased weight, and in many cases deregulated growth processes that present as neoplasms. Understanding the spectrum of reported macrocephaly associated genes is essential for identifying growth signaling pathways that control brain growth and aides in the justification of novel variants which can further cause this phenotypic entity.   We present a review of the current literature on macrocephaly associated genetic conditions as well as their associated phenotypic findings.

Figure 1-1:  Etiologies of altered head size

Flow sheet of the workup and potential etiologies for the patient presenting with abnormal

head size; we focused on macrocephaly, which can have numerous etiologies.

**Measure OFC**

> 98th Percentile
**Macrocephaly**

< 2nd Percentile
Microcephaly

↑Intercranial Pressure (ICP)
(Infection)

↑Blood
(Hemorrhage)

↑Cerebral Spinal Fluid (CSF)
(Hydrocephalus)

↑**Brain Volume/Mass
(Megalencephaly)**

↑Bone
(Skeletal Dysplasia)

Mass Lesion
(Cast, Tumor, Abcess)

**Anatomic**

Metabolic
(Leukodystrophy/Lysosomal)

**Sporadic**

Familial

**Genetic**

Environmental
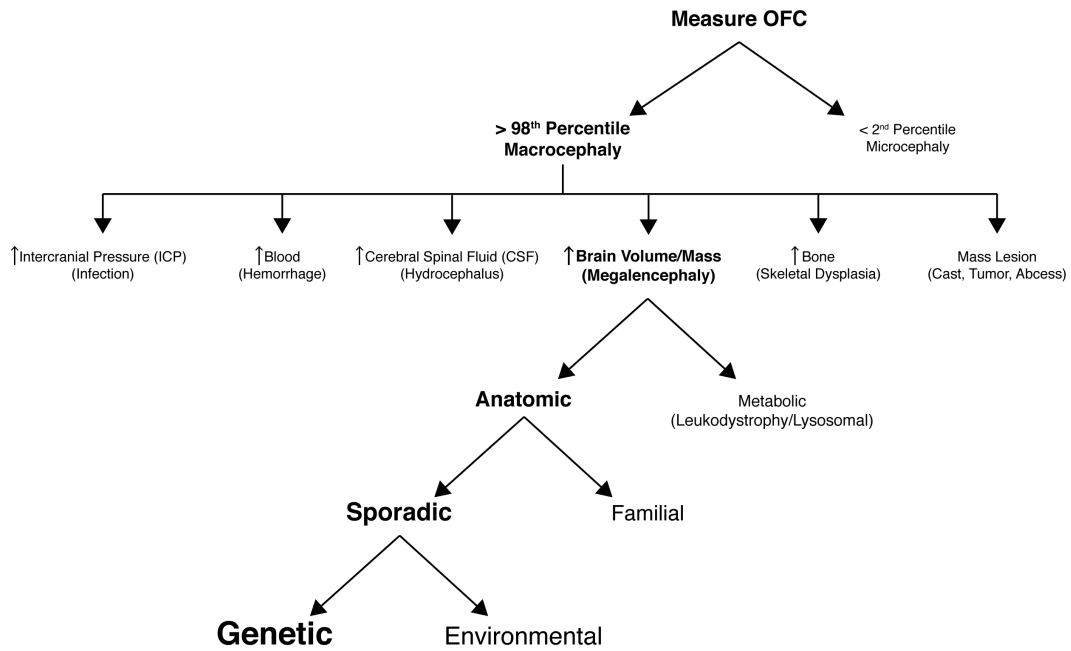
*Types of Macrocephaly: Extreme, Relative or Disproportionate; Progressive or Static*

The definition of macrocephaly as having an OFC greater than two standard deviations

from the mean encompasses many subtypes of macrocephaly. Extreme macrocephaly is

described as macrocephaly greater than three standard deviations above the mean and is

most commonly associated with mutations in PTEN [2-4]. Relative and disproportionate

macrocephaly refers to the relationship between head circumference and height. The

definition of this term utilizes the "Klein Ratio (KR)" a derived value of height

percentile/head circumference percentile. This measurement allow us to make the

distinction between cases with large heads and increased height, relative macrocephaly

(KR > .7), and cases with large heads and disproportionately shortened stature,

disproportionate macrocephaly (KR < .7) [2]. We have found that the clinical findings within

these two sub categories are distinct, possibly pointing to a differential involvement of

organ systems and distinct genetic etiologies. Macrocephaly is also described and

differentiated by state, where progressive macrocephaly worsens during development and

static macrocephaly remains constant. Although the trajectory of head growth is a

fascinating subject for understanding temporal brain development, we will not highlight

this throughout the review, as we believe the data on these cases is incomplete due to the

lack of reported true developmental measurements over standard lengths of time, such as

at every well-child visit. Lastly the sub category of familial macrocephaly is a term used to

describe specific cases which have (1) an absence of craniofacial, neurocutaneous or

somatic anomalies (syndromic), (2) normal brain radiographs, and (3) a relative (parent or

sibling) with reported macrocephaly[5] (Figure 2).

Figure 1-2: Classifications of macrocephaly sub types

Within macrocephaly there are numerous subgroups. We show and define the common grouping used throughout this review.



| Extreme | Relative | Disproportionate | Normal | Familial |
|---------|----------|------------------|--------|----------|
| HC > 3 SD | HC > 2 SD | HC > 2 SD | | |
| | HT > 2 SD | HT < 2 SD | | |

**Progressive**

**Static**
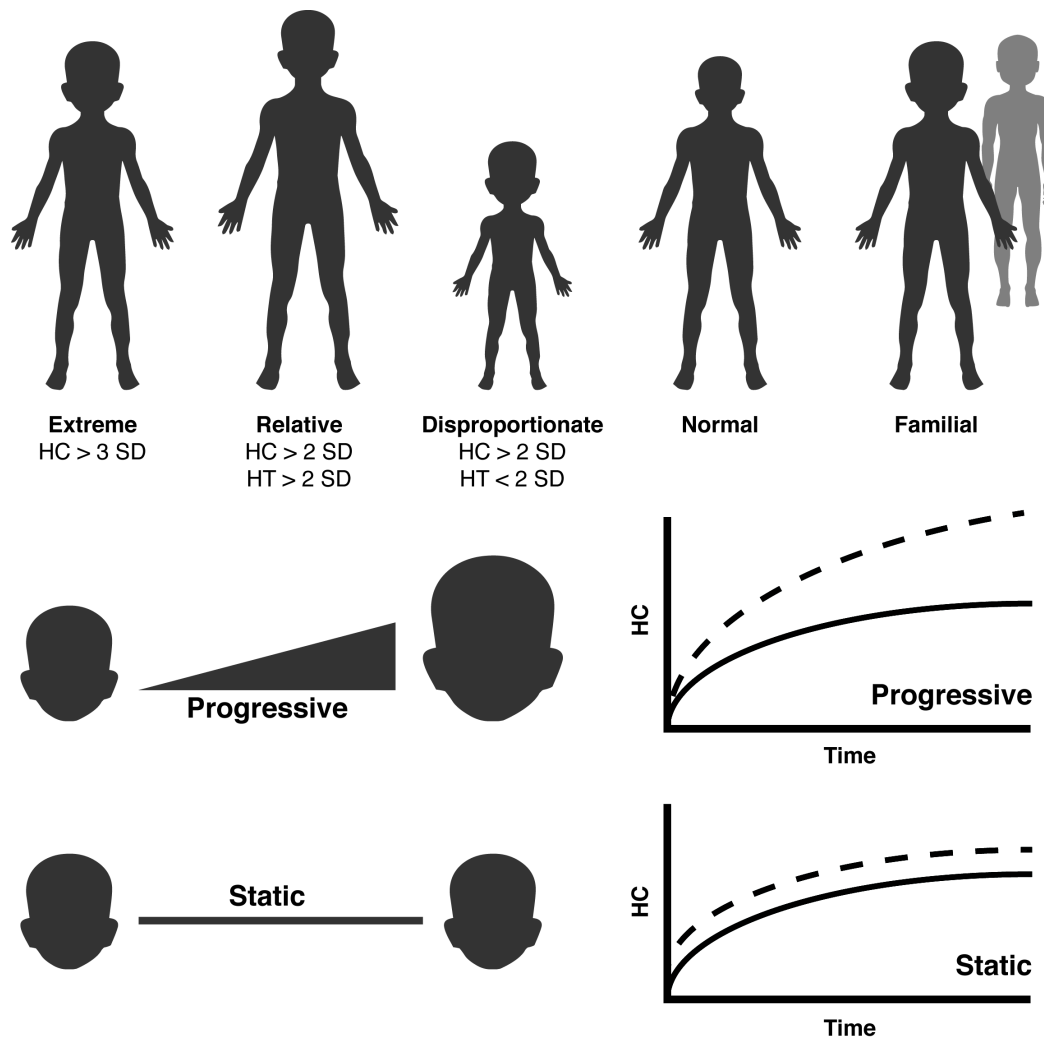
*A note on Hydrocephalus*

Increased head circumference secondary to increased cerebral spinal fluid is referred to as hydrocephaly. While the etiology of hydrocephaly can be infection, birth defect, hemorrhage, and/or injury, the large majority of cases are caused by obstructed ventricular outflow. Cases with macrocephaly in the perinatal period, which may be present at birth or have a sudden onset, undergo a diagnostic work-up to determine the type (communicating versus non-communicating), and in some cases the etiology. There are also genetic syndromic cases where the hydrocephaly is part of a larger reproducible phenotype. We have identified a list of 350 genes associated with syndromes where hydrocephaly is a key component. Most interestingly these genes show statistically significant enrichment for components of the cilium (n=64, p=5.6 x 10$^{-34}$) and microtubule cytoskeleton (n=59, p=5.7x10$^{-13}$). Pertinent examples of hydrocephaly-associated genetic syndromes include: hydrocephalus due to aqueductal stenosis (OMIM: 307000) and Peters-plus syndrome (OMIM: 261540). The overlap between hydrocephaly- and megalencephaly-associated genes is striking and includes genes such as *PTEN, AKT3* and *PIK3CA*. For that reason we do not attempt to use hydrocephaly as an exclusion criterion for the remaining conditions as there is phenotypic, genetic, or functional overlap between these two clinical entities.

## Macrocephaly Associated Genes

We conducted a compressive literature search for all reported macrocephaly genes by querying PubMed <https://www.ncbi.nlm.nih.gov/pubmed> for the key words "macrocephaly gene" on March 13th 2017. This search yielded 707 publications, which were curated manually. We excluded publications in animal models (n=77), publications

with no genetic information or cases with macrocephaly, and publications deemed "outside of the scope" of the search (n=130). We were then left with 539 articles that were composed of 23 relating to the clinical management of cases, 73 reviews, and 443 primary articles reporting novel genetic and clinical associations.  The novel genetic findings subgroup was composed of 289 single nucleotide variations (SNVs) and 155 copy number variations (CNVs, Figure 3).

Figure 1-3: Comprehensive macrocephaly literature review.

To better curate the genes associated with macrocephaly phenotypes, we undertook a review of all literature obtained through PubMed for the search term "macrocephaly gene." We then filtered out all the articles without clinical macrocephaly and those that were reported in animal models. Of the 539 remaining articles we focused on the 443 with novel genetic findings/associations. Within this group we found 289 single nucleotide variants (SNVs) and 154 copy number variants (CNV). We collected all genetic and phenotypic information from these reports into a master gene list.
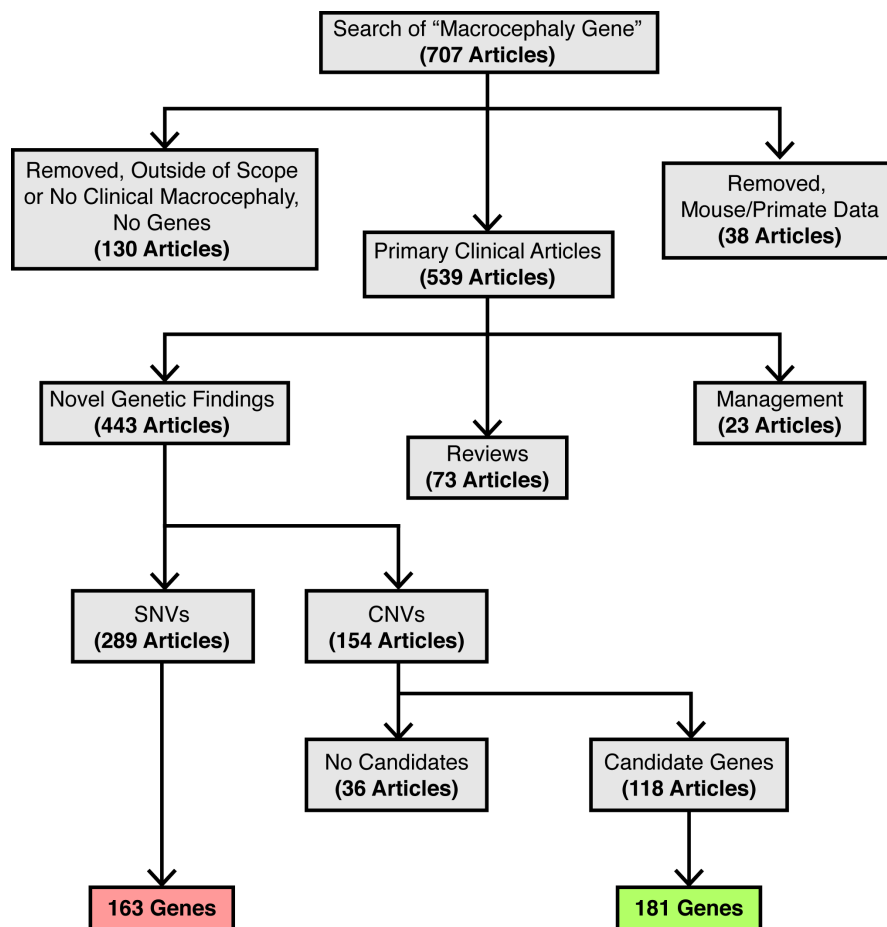
The genes from the SNV articles (n=163) were combined into a master gene list and to this list, those genes from the CNV articles that were listed as potential candidates with any degree of experimental functional or predictive evidence were added (n=183). These lists were compared to one another and showed overlap of 31 shared genes, 125 unique SNV genes, 148 unique CNV candidate genes, and an aggregate total of 299 genes from the literature (Figure 4). We will herein refer to this list as the literature-associated macrocephaly gene list or "Lit-Macro" (complete gene list, reference list and annotations presented in the supplement).

Figure 1-4: Generating a master gene list from the available literature.

Comparison of genes with reported single nucleotide variations (SNVs) and candidate

genes in the copy number variations (CNVs) revealed 125 unique SNV genes, 148 unique

CNV genes, and 31 shared genes which were combined into a master gene list of 304

macrocephaly associated genes from the literature.
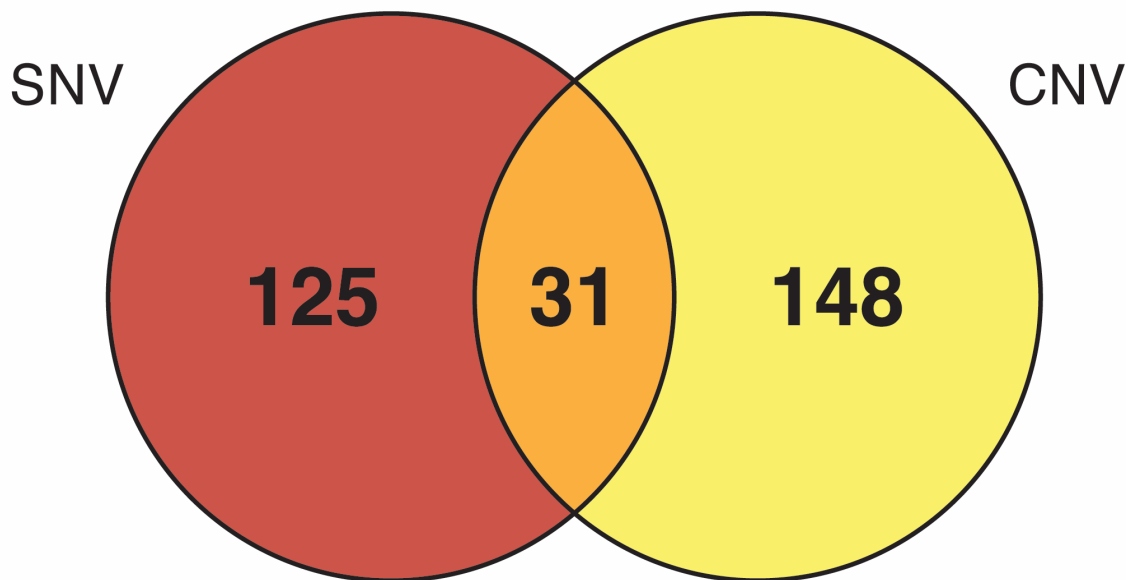
*Comparison of literature gene list to established macrocephaly gene lists*

Using the Online Inheritance in Man (OMIM) database we ascertained a list of all genes associated with syndromic macrocephaly by querying the terms "macrocephaly" and "megalencephaly." From this source we identified 499 distinct clinical entities. After filtering through the data set and removing repeated genes we found a final gene list of 251 genes. We will herein refer to this gene list as the online inheritance in man (OMIM)-associated gene list "OMIM-Macro" (complete gene list, reference list, and annotations presented in the supplement). We also queried Human Phenotype Ontology (HPO) for an additional gene list using the term "macrocephaly" (HPO:0000256) which yielded a list of 192 genes. We will herein refer to this gene list as the human phenotype ontology (HPO) macrocephaly-associated gene list "HPO-Macro" (complete gene list, reference list and annotations presented in the supplement). Comparing the three genes lists revealed 34 genes shared by all three lists, and 104 genes shared by two of the three gene lists. This analysis also shows that there are 135 OMIM-Macro specific genes, 84 HPO-Macro specific genes, and 213 specific Lit-macro genes. We finally combined the three lists in a master gene list of 570 genes, which we will herein refer to as the combined macrocephaly-associated gene list "Comb-Macro" (Figure 5, complete gene list, reference list and annotations presented in the supplement).

Figure 1-5: Comparison of publically available gene lists to the gene list generated from the literature

We compared the master gene list generated from the literature to those available from online mendelian inheritance in man (OMIM) and human phenotype ontology (HP). While there is overlap reported in these gene lists, we found 213 genes additional genes not in our curated list, which demonstrates the power of manually curating literature-associated gene lists.
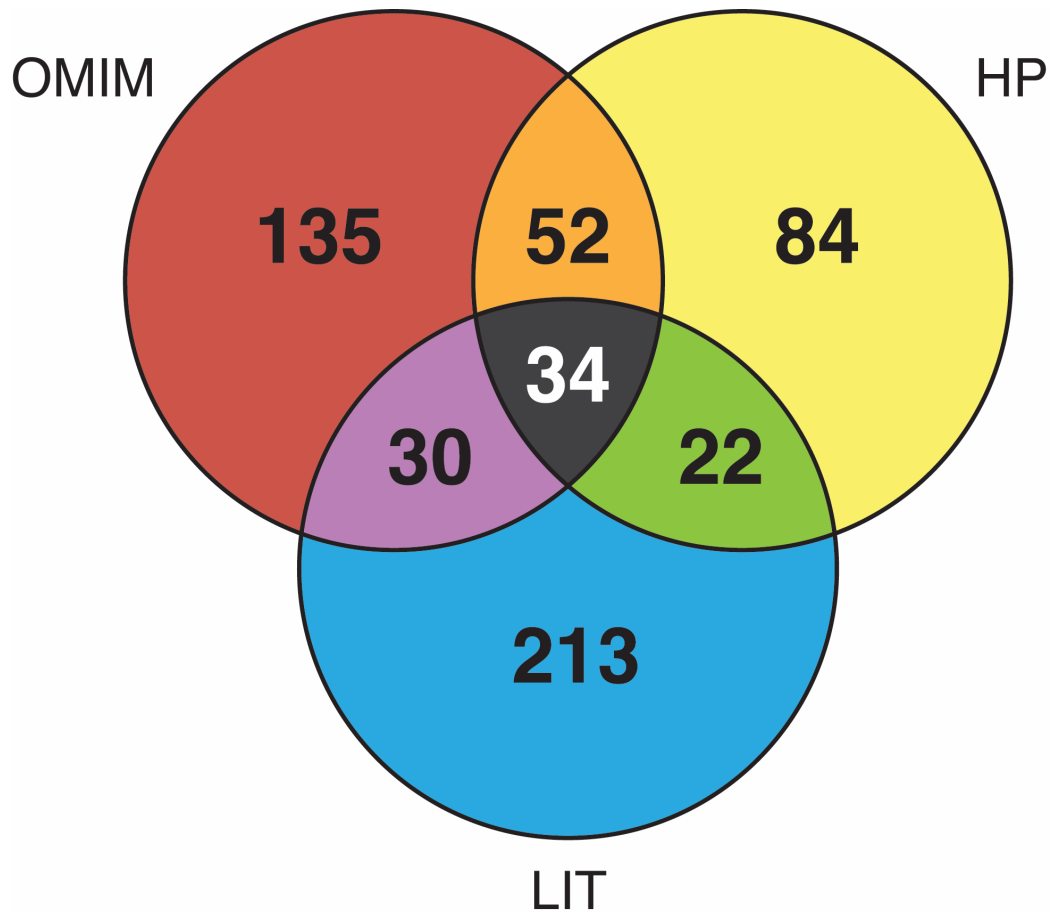
*Functional enrichment analysis*

We subjected the Lit-Macro gene list to functional and pathway cluster enrichment analysis using the ToppFun tool in the ToppGene suite <https://toppgene.cchmc.org/>. Which identifies enriched clusters in gene lists. We used the probability density function to estimate p-values and the Bonferroni correction method for multiple tests. We also used a level of significance of 0.05 and gene limits 1≤n≤2000. The clusters which were enriched most significantly in this gene set were central nervous system development, neurogenesis, generation of neurons, head development, neuron differentiation, and brain development (n=78, 97, 89, 62, 80, 58; corrected p-values= $2.33 \times 10^{-30}$, $1.14 \times 10^{-29}$, $7.12 \times 10^{-26}$, $6.13 \times 10^{-23}$, $3.60 \times 10^{-22}$, $4.88 \times 10^{-21}$). We compared this enrichment to the Comb-Macro gene list and found biologically relevant similarities with the most enriched clusters being neurogenesis, central nervous system development, cell projection organization, generation of neurons, head development, brain development (n= 152, 117, 137, 141, 98, 92; corrected p-values= $3.31 \times 10^{-38}$, $3.25 \times 10^{-37}$, $2.68E \times 10^{-35}$, $2.94 \times 10^{-34}$, $5.62 \times 10^{-32}$, $1.29 \times 10^{-29}$). We also found enrichment for the localization/cell types where these genes are expressed. For the Lit-Macro gene list, we observed enrichment for the neuron projection, neuron part, somatodendritic compartment, excitatory synapse, and axon (n=63, 66, 44, 23, 32; corrected p-value= $6.15 \times 10^{-16}$, $3.21 \times 10^{-12}$, $8.33 \times 10^{-10}$, $4.91 \times 10^{-09}$, $7.88 \times 10^{-08}$). The Comb-Macro list showed similar enrichment: cell projection part, neuron projection, neuron part, ciliary part and cilium (n=94, 87, 100, 42, 51; corrected p-value= $8.97 \times 10^{-19}$, $5.92 \times 10^{-14}$, $5.84 \times 10^{-13}$, $1.82 \times 10^{-12}$, $1.40 \times 10^{-11}$). Interestingly, the cilium and ciliary part clusters, we believe, are enriched because these genes are reported in publically available "macrocephaly" gene lists (OMIM and HPO); however, this is due to cases of underlying

hydrocephaly and as already discussed, these genes show over-representation of cilium associated genes. This finding exemplifies the need for well-curated gene lists and the potential pit falls of using publically available gene lists for analysis.

*Pathway-enrichment*

We found significant enrichment for the following pathways in the Lit-Macro gene list: signaling by NGF, signaling by FGFR, PI3K-Akt signaling pathway, signaling by ERBB2, and Hedgehog signaling Pathway (n=26, 18, 25, 16, 7; corrected p-value= $3.37x10^{-07}$,$7.65x10^{-06}$,$9.57x10^{-05}$,$3.25x10^{-04}$,$3.34x10^{-04}$). We found significant enrichment in the Comb-Macro gene list for Insulin receptor-related events triggered by IGF1R, Hedgehog signaling pathway, ErbB signaling pathway, signaling by EGFR, and estrogen signaling pathway (n= 21, 10, 18, 25, 17; corrected p-value= $3.39x10^{-09}$,$2.68x10^{-06}$,$3.04E^{-06}$,$6.74x10^{-06}$,$1.59E^{-04}$). Manually searching these enriched clusters made it evident that PI3K-AKT and hedgehog signaling cascades are central to these enrichments, we provide a review of the pertinent mutations and associated phenotypes for these pathways and their targets.

## The PI3K-AKT Pathway

The PI3K/AKT pathway is a central signaling axis that relays external stimuli to numerous intercellular effector pathways. Mutations to genes within this pathway result in human overgrowth phenotypes. Through our analysis we have identified mutations in (1) core components of the pathway, (2) secondary FGF receptors, (3) collagen types 1 and 2 chains, and (3) components of the RAS signaling cascade that may interact with this pathway. Furthermore, these variants highlight the genetic heterogeneity of macrocephaly

17

and show the striking association between deregulation of this pathway and macrocephaly phenotypes.

*PI3K/AKT/mTOR Core components*

At every level of the core canonical mTOR-signaling pathway, mutations result in macrocephaly-associated overgrowth phenotypes. These mutations present as one of two varieties: inactivating mutations in negative regulators of the pathway or activating mutations in positive regulators of the pathway. The inactivating mutations are confined to PTEN, TSC1, and TSC2, all negative regulators. These cases largely present as germline mutations in widely distributed affected phenotypes. Mutations in PTEN cause a spectrum of genetic syndromes collectively referred to as the PTEN Hamartoma Tumor Syndromes. This collection of phenotypically diverse syndromes include Bannayan-Riley-Ruvalcaba syndrome (BRRS, MIM: 153480), Cowden syndrome 1 (CD1, MIM: 158350), and macrocephaly/autism syndrome (MIM: 605309). These syndromes have distinct phenotypic manifestations such as the characteristic penile freckling observed in BRRS and the multiple tissue neoplasms observed in CD1; however, they also share common phenotypes including macrocephaly[3,6,7], obesity/somatic overgrowth, and dysmorphic facial features. The mutations reported in PTEN are all suspected to be loss of function[8]. Even with this increased understanding, there is a lack of genotype-phenotype correlation and it is not yet fully understood what underlies the exact genetic pathophysiology in each syndrome. Further down the signaling cascade inactivating mutations in TSC1 and TSC2 cause Tuberous sclerosis-1 (TSC1, MIM: 191100) and Tuberous sclerosis-2 (TSC2, MIM: 613254) these diseases are characterized by multiple, benign hamartomas in numerous organ systems. The macrocephaly in these patients is a result of hemimegalencephaly and

18

focal megalencephaly [9,10]. The lack of genotype-phenotype correlation within these syndromes is still poorly understood; however there are some developments which point to temporal mTOR activation as being a pivotal factor in TSC signaling [11]. The remaining mutations in the core pathway represent activating mutations in drivers that increase signaling. Activating mutations are clustered on nucleotides that affect specific amino acids resulting in either constitutive activation or a loss of ability to be inhibited. These mutations present largely as mosaic most likely due to the fact that they are not tolerated as germline mutations in keeping with Happle's Hypothesis[11,12]. As such, these mutations present with phenotypes of varying severity depending on the extent of affected tissue types. Mutations to PIK3CA are associated with megalencephaly-capillary malformation-polymicrogyria syndrome (MACP, MIM: 602501)[13], CLOVES syndrome (MIM: 612918)[14], and Cowden syndrome 5 (CWS5, MIM: 615108)[15]. MCAP is characterized by polymicrogyria, megalencephaly, and overgrowth as well as asymmetry of the brain, asymmetry of the body, vascular malformations, and syndactyly. CLOVES syndrome is associated with irregular dysplastic adipose tissue, truncal vascular malformations, scoliosis, and enlarged bony structures. CWS5 is a genetic variant of PTEN-associated CWS1 and therefore shows strong phenotypic overlap with associated PTEN mutations[16]. Mutations in PIK3R2 are associated with megalencephaly-polymicrogyria-polydactyly-hydrocephalus syndrome 1 (MPPH1, MIM: 603387). MPPH1 is associated with megalencephaly, macrocepahly, polymicrogyria, hydrocephalus and sometimes polydactyly. Mutations in AKT1 are associated with the proteus syndrome (MIM: 176920) and Cowden syndrome 6 (CWS6, MIM: 615109). Proteus syndrome is characterized by asymmetric overgrowth, vascular malformations, megaspondylodysplasia, connective

tissue and epidermal nevi, and irregular adipose tissue. CWS6 is a genetic variant of PTEN and therefore shows strong phenotypic overlap with associated PTEN mutations[16]. Mutations in AKT3 are associated with megalencephaly-polymicrogyria-polydactyly-hydrocephalus syndrome 2 (MPPH2, MIM: 615937) a genetic variant of MPPH1 that is phenotypically identical. Mutations in mTOR are associated with Smith-Kingsmore syndrome (SKS, MIM:616638) which is characterized by intellectual disability, seizures, macrocephaly, and dysmorphia.

### *Mutations in members of the PP2A Family*

PP2A is a direct negative regulator of AKT. Mutations in members of the protein phosphatase 2A (PP2A) regulatory subunit B family including *PPP2R5D*, *PPP2R5C, and PPP2R5B* are associated with an overgrowth syndrome(s) and are predicted to disrupt this inhibitory action, thus activating AKT function.[17] These mutations, first reported by Loveday et al, currently have no formal syndromic name; however, they are characterized by somatic overgrowth, macrocephaly and intellectual disability.

### *Mutations of the FGF Receptor*

The FGF receptor lies upstream of the PI3K signaling cascade and, when activated, can increase not only PI3K signaling, but also coordinated activation of RAS/MAPK, STAT and PLCY[18,19]. Interestingly, gain of function mutations in FGFR2 and FGFR3 are associated with macrocephaly syndromes. Gain of function mutations in FGFR2, including p.Try290Cys and p.Ser351Cys, cause Pfeiffer syndrome (PS; MIM:101600) which results in a phenotype including  brachydactyly, craniosynostosis, dysmorphia, variable syndactyly, and can be associated with macrocephaly[20,21]. The murine model solidified the role of these mutations where mutants demonstrate megalencephaly among other congruent phenotypes including

midline disorders and ventricular wall alterations [22]. Likewise, specific mutations in FGFR3, p.Pro250Arg, cause Muenke Syndrome (MNKES, MIM: 602849) which result in macrocephaly as well as synostosis, dysmorphia, thimble-shaped middle phalanges, brachydactyly, deafness, and developmental delay[23,24]. In combination, these variants show that pathogenic activation of the FGF receptor results in striking phenotypes with both common and unique findings to those of core PI3K mutations; the unique findings are possibly the result of other pathway activation while we argue the macrocephaly is a result of AKT activation.

*Mutations in Components of the Extracellular Matrix*

The extracellular matrix (ECM) is a complex collection of secreted proteins that surround and support neighboring cells. The ECM is also involved in complex signaling cascades that aide the cells in determining and responding to external stimuli. Specifically, components of the ECM interact with membrane embedded TGFβ receptors and causes dimerization which then transduces the signaling into cytoplasmic signaling cascades. TGFβRII and TGFβRI dimerize and activate a number of substrates including, but not limited to SOS1, PI3K, Rac, and RhoA. We are most interested in the interaction of the ECM with the PI3K pathway as mutations to components of the ECM have been reported in cases with macrocepahly-associated phenotypes. Mutations in collagen fiber type I alpha chains (COL1A1 and COL1A2) are associated with osteogenesis imperfecta (OI) which is characterized by severely weakened bones that are prone to fractures, hearing loss, and short stature. In its progressively deforming type (OI Type III), macrocephaly with enlarged ventricles is seen; barrel chest deformity and blue sclera are also common phenotypic findings within this subgroup [25]. Similarly, mutations in the collagen type II alpha chain

(COL2A1) have been reported in association with macrocephaly. A mother/child case report with documented dominant COL2A1 nonsense mutation showed that these mutations are associated with short stature, macrocephaly, skeletal dysplasia, hearing loss, and dysmorphia[26]. Additionally, a case was reported to have mutations in both COL2A1 and Gli3, an effector of Sonic Hedgehog Signaling (discussed later). This patient presented with macrocephaly in addition to syndactylies and severe skeletal dysplasia [27]. Mutations to the collagen type III chain were reported in a mother/child series with Ehlers-Danlos syndrome (EDS). Although macrocephaly does not fall into the common phenotypic spectrum of EDS these patients presented with macrocephaly, secondary to hydrocephaly in infancy[28]. Lastly, mutations to the laminin beta subunit LAMB1, another component of the ECM, have been reported to be associated with macrocephaly. In addition, these cases present with severe progressive neurodegeneration, epilepsy, optic atrophy, anterior subcapsular lens opacities, and deafness; the macrocephaly was characterized by enlargement of the ventricles[29]. As a whole, ECM-associated macrocephalic cases are a distinct entity with unique phenotypes including varying degrees of short stature, skeletal dysplasia, and hearing loss. The macrocephaly is in many cases secondary to hydrocephaly and can be characterized by increased ventricular size. Also, the macrocephaly is disproportionate which as previously discussed means the head circumference is increased in comparison to the smaller than average body (Figure 2) therefore making the difference more pronounced. Ultimate diagnosis results from a combination of genetic and clinical evaluations and has strong implications for prognosis.

    *RAS Signaling*

The RAS-ERK signaling cascade relays diverse signals from the environment into adaptive cellular activity.   Similar to the PI3K pathway signaling begins at receptor tyrosine kinases and continues into the cytoplasm/nucleus. Specifically Grb2 and SOS1 assemble at the receptor to facilitate the transfer of a phosphate to RAS-bound GDP forming active Ras-GTP. The cascade continues with Ras-GTP signaling Raf, MEK, ERK and finally RSK in the canonical core-signaling unit.  This pathway has numerous effectors and cross talks with additional signaling cascades. We highlight cross talk to the PI3K signaling pathway. Starting closest to the receptor, Ras-GTP can interact directly with PI3K and activate it. Additionally, Erk secondary signaling can activate PI3K and directly activate mTORC1. Erk and RSK are furthermore involved in complex negative feedback mechanisms that inactivate TSC1 and TSC2.  This cross talk is not unidirectional as activated AKT signaling can inhibit Raf[30-36]. The high level of interconnected signaling demonstrates a delicate balancing in these two pathways. Interestingly, mutations in members of the Ras-ERK signaling pathway result in syndromes that are associated with macrocephaly.  Ras has three isoforms (HRAS, KRAS and NRAS), which are each associated with a constellation of overlapping and unique phenotypes. Gain of function mutations (most commonly G12S) in HRAS are associated with Costello syndrome (CSTLO, MIM: 218040). This syndrome is associated with macrocephaly, papillomata, dysmorphic facial features, hypertrophic cardiomyopathy, neoplasms, and developmental delay. The macrocephaly in these cases is the result of cerebellar enlargement and results in progressive frontal bossing [37].  Similar to the macrocephaly-capillary malformation syndrome (described above) cerebellar tonsillar herniation is a common finding that is proposed to arise from abnormal and unregulated genesis of neuronal cells as well as structural abnormalities[38,39]. Mutations in KRAS and

23

NRAS are associated with Noonan syndromes 3 (NS3, MIM: 609942) and 6 (NS6, MIM: 613224). In addition to macrocephaly, NS3 and NS6 are associated with cardiac septal defects, developmental delay, short stature, myelomonocytic leukemia, webbed neck, and sagittal suture synostosis [40-44]. Lastly SOS1 mutations, upstream of the RAS isoforms, are associated with Noonan Syndrome 4 (NS4, MIM: 610733). This form of Noonan syndrome is characterized by macrocephaly, increased pulmonic stenosis, keratosis pilaris, curly hair, and a lack of atrial septal defects [45,46]. Finally mutations in MAP2K2, a map kinase downstream of Ras signaling, cause an overlapping phenotype named Cardiofaciocutaneous Syndrome 4 (CFC4, MIM: 615280) which is characterized by macrocepahly, cardiac septal defects, cardiomyopathy, craniofacial dysmorphia, xerosis, hyperkeratosis, eczema, pigmented moles, and hemangiomas [47]. Additionally, MAP2K2 is a candidate gene in the 19p13.3 microduplication syndrome, which is associated with macrocephaly, developmental delay, hypotonia, speech delay and dysmorphia [48,49]. As a whole these activating mutations in KRAS, HRAS, NRAS, MAP2K2, and SOS1 represent a group of macrocephaly-associated conditions that are molecularly and clinically distinct. We stress the presence of macrocephaly in each of the conditions and attribute this to the cross talk between the RAS and PI3K signaling pathways.

*Mutations in PI3K Targets outside of mTOR canonical signaling*

Outside of canonical mTOR signaling there are numerous targets and inputs of PI3K/AKT signaling in which mutations are associated with macrocephaly. These include MCL1, GNB3, CCND2, and EFNA3. MLC-1 is downstream target of AKT signaling, via the intermediate GSK, and is a potent inhibitor of apoptosis. Mutations in MLC-1 are associated with megalencephalic leukoencephalopathy with subcortical cysts (MIM: 604004). This

disease demonstrates autosomal receive inheritance. It is clinically characterized by neurologic deterioration, epilepsy, spasticity, and macrocephaly [50,51]. Cyclin D2, CCND2, is another downstream target of AKT signaling and involved in cell cycle regulation. Mutations in CCND2 have been associated with megalencephaly-polymicrogyria-polydactyly-hydrocephalus syndrome 3 (described above, MPPH, MIM: 615938). These mutations occur surrounding a residue that is phosphorylated by GSKB .The mutant proteins are shown to be resistant to degradation [52]. It has been hypothesized that Cyclin D2 stabilization is the ultimate cause of MPPH, which can be caused by specific mutations to CCND2 itself or PI3K/AKT activation secondary to gain of function mutations. The *GNB3* locus codes for the GB3 protein. This protein associates with additional subunits and activates signaling cascades including PI3K and AKT. Most interestingly, loss of *GBN3* is associated with decreased AKT phosphorylation[53].  Duplications involving *GBN3* have been reported to be associated with macrocephaly as well as intellectual disability, obesity, and seizures[54]. It should be noted that this association may also be due to contribution of other genes within the duplication; however, mouse models do support *GBN3*s role in somatic overgrowth and show expression in the brain.  *EFNA3* codes for Ephrin A3, which binds to receptor tyrosine kinases and, via IRS1, can signal PI3K. Additionally, *EFNA3* deletions in malignant peripheral nerve sheath tumors (MPNST) increases the expression of PI3K, while overexpression of *EFNA3* decreases PI3K expression via mechanisms not yet understood [55].  Recently a mutation in *EFNA3* was reported in the Autism-Epilepsy phenotype with macrocephaly, which we propose has strong phenotypic overlap to mutations in PTEN due to PI3K/AKT over activity. In aggregate, these mutations confirm the role of PI3K signaling and implicate targets of the pathway in ultimate pathogenesis.  It

is important to evaluate the potential interconnectedness of variants identified in

Macrocephaly cases for cross talk to the PI3K/AKT pathway, which is central to its

development.  (Mutations Summarized in Table 1 and Figure 6)

Table 1-1: PI3k/AKT/mTOR signaling-macrocephaly-associated syndromes

These genes were identified via our pathway enrichment analysis; for each gene, we

present the syndrome associated with it and the reference which first reported its

association.

Table 1-1: PI3k/AKT/mTOR signaling-macrocephaly-associated syndromes

These genes were identified via our pathway enrichment analysis; for each gene, we present the syndrome associated with it and the reference which first reported its association.

## PI3K/AKT/mTOR Core Components

| Gene | | Associated Syndrome(s) | Reference |
|------|---|------------------------|-----------|
| PIK3CA | phosphatidylinositol-4,5-bisphosphate 3-kinase catalytic subunit alpha | CLOVES Syndrome, Cowden Syndrome 5, Megalencephaly-capillary malformation-polymicrogyria syndrome | [14, 56, 57, 15, 13] |
| PIK3R2 | phosphoinositide-3-kinase regulatory subunit 2 | Megalencephaly-polymicrogyria-polydactyly-hydrocephalus syndrome 1 | [58] |
| PTEN | phosphatase and tensin homolog | PTEN hamartoma tumor syndrome | [3] |
| AKT1 | AKT serine/threonine kinase 1 | Cowden syndrome 6, Proteus syndrome, | [15,59] |
| AKT3 | AKT serine/threonine kinase 3 | Megalencephaly-polymicrogyria-polydactyly-hydrocephalus syndrome 2 | [56,57] |
| TSC1 | tuberous sclerosis 1 | Tuberous sclerosis-1 | [60] |
| TSC2 | tuberous sclerosis 2 | Tuberous sclerosis-2 | [61] |
| MTOR | mechanistic target of rapamycin | Smith-Kingsmore syndrome | [56,62] |

## PP2A Family

| Gene | | Associated Syndrome(s) | Reference |
|------|---|------------------------|-----------|
| PPP2R5D | protein phosphatase 2 regulatory subunit B'delta | Novel Overgrowth Syndrome | [17] |
| PPP2R5B | protein phosphatase 2 regulatory subunit B'beta | Novel Overgrowth Syndrome | [17] |
| PPP2R5C | protein phosphatase 2 regulatory subunit B'gamma | Novel Overgrowth Syndrome | [17] |

## FGF Signaling

| Gene | | Associated Syndrome(s) | Reference |
|------|---|------------------------|-----------|
| FGFR3 | fibroblast growth factor receptor 3 | Pfeiffer syndrome | [63,64] |

| FGFR2 | fibroblast growth factor receptor 2 | Muenke syndrome | 24 |
|---|---|---|---|

## Extracellular Matrix Components

| COL1A1 | collagen type I alpha 1 chain | Osteogenesis Imperfecta | 65 |
|---|---|---|---|
| COL1A2 | collagen type I alpha 2 chain | Osteogenesis Imperfecta | 65 |
| COL2A1 | collagen type II alpha 1 chain | Greig syndrome with a severe form of SED | 27 |
| COL3A1 | collagen type III alpha 1 chain | Ehlers-Danlos | 28 |
| LAMB1 | laminin subunit beta 1 | Lissencephaly 5 | 29 |

## RAS Signaling

| HRAS | HRas proto-oncogene, GTPase | Costello syndrome | 66 |
|---|---|---|---|
| KRAS | KRAS proto-oncogene, GTPase | Noonan syndrome 3 | 44 |
| NRAS | neuroblastoma RAS viral oncogene homolog | Noonan syndrome 6, Schimmelpenning-Feuerstein-Mims syndrome, | 40 |
| SOS1 | SOS Ras/Rac guanine nucleotide exchange factor 1 | Noonan syndrome 4 | 67 |
| MAP2K2 | mitogen-activated protein kinase kinase 2 | Cardiofaciocutaneous syndrome 4. 19p13.3 deletion Candidate Gene | 49,68 |

## Uncharacterized

| MCL1 | BCL2 family apoptosis regulator | Megalencephalic leukoencephalopathy with subcortical cysts | 69 |
|---|---|---|---|
| GNB3 | G protein subunit beta 3 | Childhood obesity syndrome | 54 |
| CCND2 | cyclin D2 | Megalencephaly-polymicrogyria-polydactyly-hydrocephalus syndrome 3 | 52 |
| EFNA3 | ephrin A3 | Autism-Epilepsy Phenotype with Macrocephaly | 70 |

Figure 1-6: The PI3K/AKT/mTOR signaling pathway and associated signaling in macrocephaly

We show the canonical PI3K/AKT/mTOR signaling pathway highlighted in yellow. Additionally, we draw attention to the cross talk of the FGFR and RAS/MAPK signaling pathways. Additionally, we include the AKT target GSK3B, which provides a link between PI3K signaling and the regulation of CCND2 and MCL1, which are both associated with macrocephaly phenotypes.
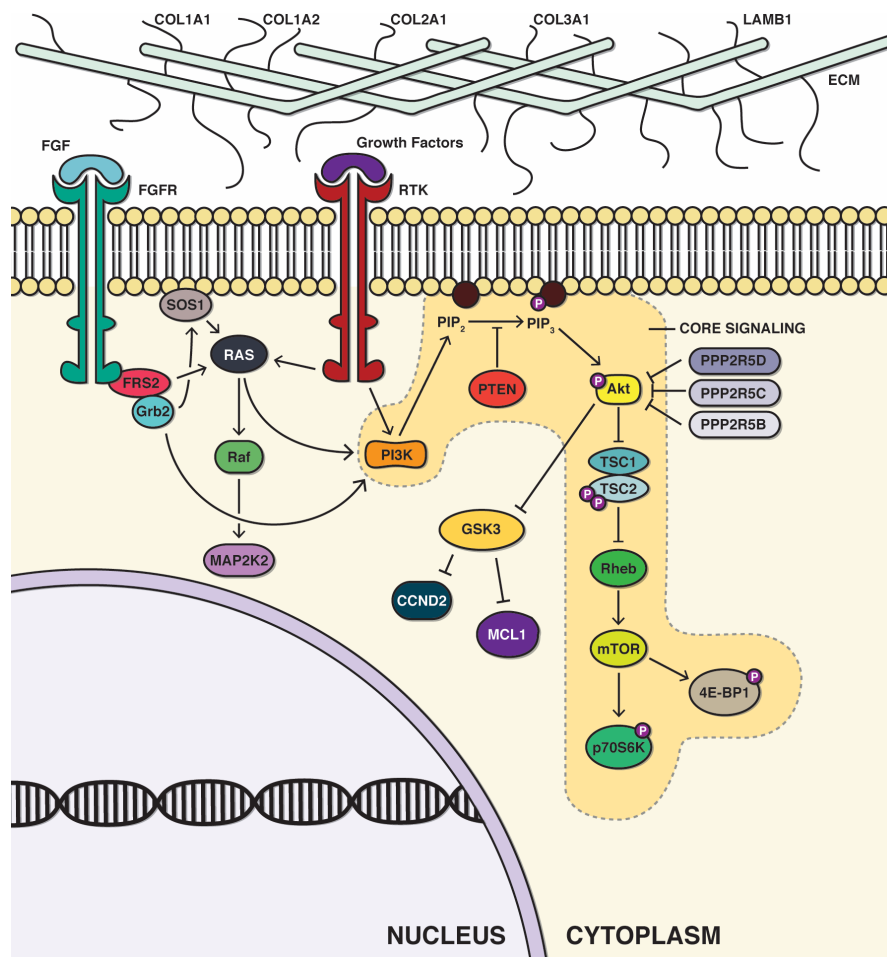
## Sonic Hedgehog Signaling

Another pathway that showed significant enrichment in our macrocephaly associated gene list was the Hedgehog signaling pathway. Similar to the core PI3K/AKT pathway, we observe that mutations at nearly every level, from receptor to effector, manifests with overlapping yet unique phenotypes.  The Hedgehog signaling cascade begins with the binding of numerous ligands, including Sonic Hedgehog (SHH) and Indian hedgehog (IHH), to the PTCH1 or PTCH2 membrane-bound receptors.   Mutations to SHH that cause early termination are associated with Holoprosencephaly 3 (MIM: 142945). This condition is associated with a failure to develop two cerebral hemispheres and normal ventricular structures as well as midface hypoplasia and proboscis.  This association demonstrates the importance of SHH in the developing brain and exemplifies the consequence of its loss[71]. More recently, a familial 7q36.3 duplication encompassing RBM33 and SHH was reported in association with macrocephaly, agenesis of the corpus collosum, intellectual disability, widely spaced eyes, and broad forehead[72]. These studies, in combination, point to SHH being essential for brain development and increased dosage of SHH resulting in macrocephaly. In addition to SHH, duplications involving IHH have been associated with a macrocephaly phenotype also including extensive polysyndactyly, agenesis of the corpus callosum, dysplastic ears, severe hypertelorism, and psychomotor delay[73].  This phenotype is most similar to acrocallosal syndrome (ACLS, MIM: 200990) and Joubert syndrome-12 (JBTS12, MIM: 200990), two autosomal recessive macrocephaly-associated conditions caused by mutations in *KIF7.*  ACLS is further characterized by mental retardation, agenesis of the corpus callosum, dysmorphic facial features, and polydactyly. JBTS12 has strong phenotypic overlap with ACLS; however, it is distinct in the

presence of the molar tooth sign (MTS). KIF7 interacts with the SHH pathway and has been shown to regulate its signal transduction as well as its final effectors (Gli1-3)[74,75].

Following ligand binding PTCH1/2 are inactivated and can no long exert an inhibitory effect on Smoothened (SMO).  Mutations to these negative regulators are also associated with macrocephaly phenotypes.  Mutations in *PTCH1* and *PTCH2* are associated with the basal cell nevus syndrome (BCNS, MIM: 109400). Additionally, PTCH1 is associated with holoprosencephaly 7 (HPE7, MIM: 610828). PTCH1 mutations causing HPE7 are inherited in an autosomal dominant pattern and present with macrocephaly, mental retardation, and dysmorphia[76]. A reciprocal duality exists for PTCH1 as loss of function results in macrocephaly phenotypes while reported duplications result in microcephaly[77].  BCNS is a clinically distinct syndrome characterized by jaw cysts, basal cell tumors, skeletal abnormalities, and in many cases macrocephaly [78,79].  BCNS is caused by mutations in either *PTCH1, PTCH2* or *SUFU*. *SUFU* is normally bound to the ultimate effector (Gli1-3) and keeps it sequestered in the cytoplasm where it cannot activate expression of its target genes, but when inactivated the PTCH receptor subsequently activates the smoothened (SMO) membrane bound protein. Gain of function, mosaic mutations in *SMO* have been associated with Curry-Jones syndrome (MIM: 601707). This syndrome is characterized by patchy skin lesions, polysyndactyly, craniosynostosis, iris colobomas, microphthalmia, and intestinal malrotation[80].   Major findings from this initial report included megalencephaly, hemimegalencephaly, ventriculomegaly, and polymicrogyria which show overlap and are also associated with activating mutations in the PI3K/AKT/mTOR pathway.  These mutations are suspected to be gain of function and result in ligand-independent, constitutive activation of Hedgehog signaling.

The ultimate result of Hedgehog signaling is translocation of the effectors GLI1-3 into the nucleus where they are transcription factors, which coordinate the expression of multiple target genes. Mutations in GLI2 are associated with holoprosencephaly 9 (HPE9, MIM: 610829) which is characterized by midline dysmorphology, pituitary hypoplasia, postaxial polydactyly, agenesis of the corpus collosum, and macrocephaly[81,82]. These mutations are inherited in an autosomal dominant fashion and are suspected to be loss of function. Additionally, mutations in GLI3 are associated with Greig Cephalopolysyndactyly syndrome (GCPS, MIM: 175700), which is characterized by polydactyly, syndactyly, hypertelorism, and macrocephaly. The association of GLI2 and GLI3 with phenotypes that so closely resemble those in the upstream pathway components support that activated hedgehog is pathogenic in those cases (Mutations summarized in Table 2, Figure 7)

Table 1-2: Hedgehog (Hh) signaling-macrocephaly-associated syndromes

We present the genes from our pathway enrichment analysis, which were grouped and
identified as members of the Hh signaling pathway. For each gene, we present the genetic
syndrome and the reference that first reported the association.

## Hedgehog Ligands

| Gene Symbol | Gene Name | Associated Syndrome (S) | Refereences |
|---|---|---|---|
| SHH | sonic hedgehog | Holoprosencephaly 3 | [72] |
| IHH | indian hedgehog | Acrocallosal Syndrome | [73] |

## Membrane Bound Receptors

| | | | |
|---|---|---|---|
| PTCH1 | patched 1 | Basal cell nevus syndrome | [83] |
| PTCH2 | patched 2 | Basal cell nevus syndrome | [84] |
| SMO | | Curry-Jones Syndrome | [80] |

## Cytoplasmic/Nuclear Signaling

| | | | |
|---|---|---|---|
| SUFU | SUFU negative regulator of hedgehog signaling | Basal cell nevus syndrome | [85] |
| GLI2 | GLI family zinc finger 2 | Culler-Jones syndrome, Holoprosencephaly 9 | [81] |
| GLI3 | GLI family zinc finger 3 | Greig cephalopolysyndactyly syndrome | [27] |
| KiF7 | Kinesin family member 7 | Acrocallosal syndrome, Joubert syndrome 12 | [86] |

Figure 1-7: The Hedgehog signaling pathway

We show the interactions of the Hh signaling pathway and highlight the genes identified in

our analysis.
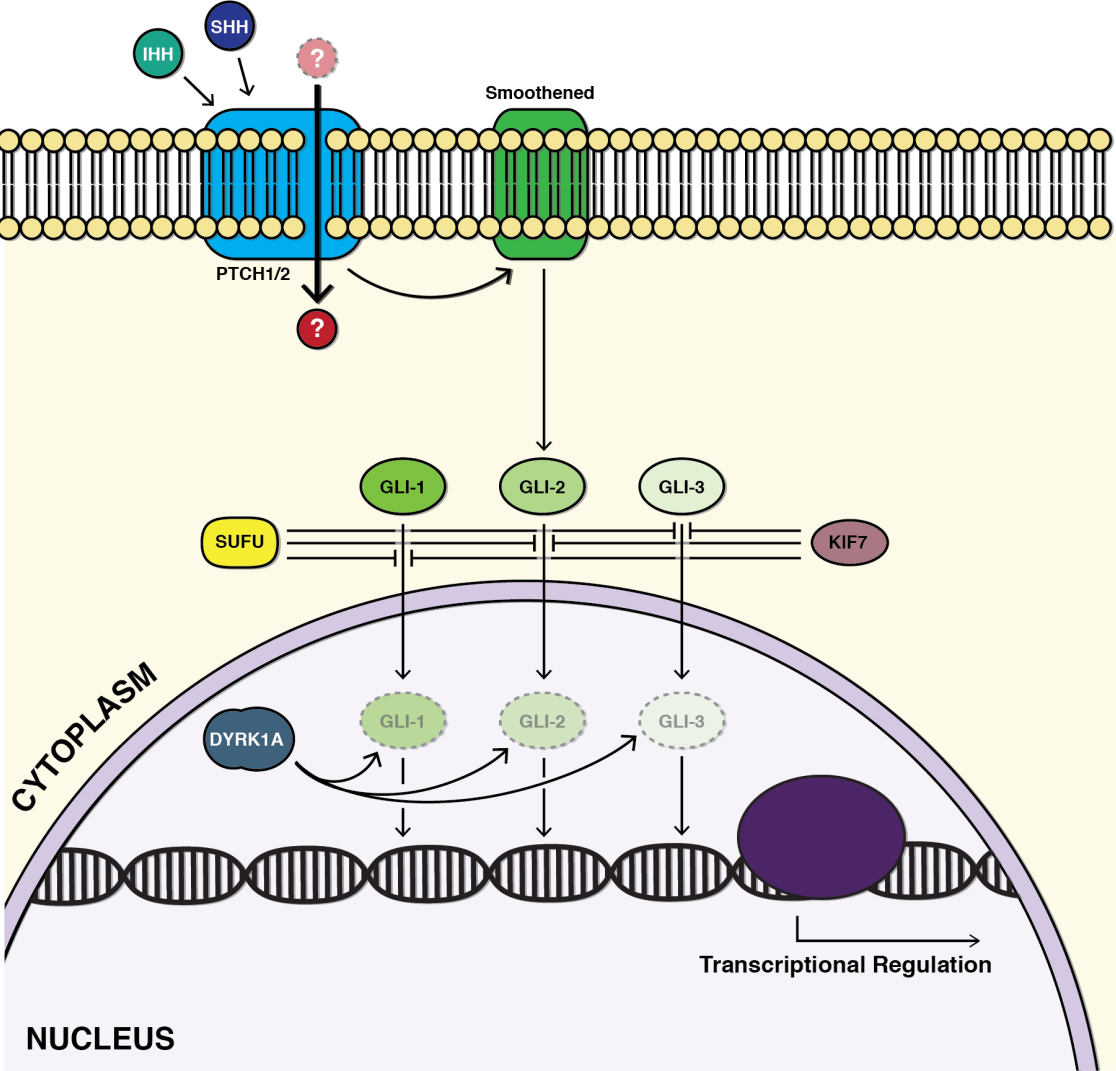
## Macrocephaly Associated Phenotypes

We thought it was most appropriate to compare macrocephaly-associated genes based upon additional phenotypes associated with the cases and relate this to the underlying genetics for each entity.

*Neurological/Behavioral Phenotypes*

Neurological and behavioral phenotypes are the most frequently observed comorbidities with macrocephaly. We found such phenotypes in 91% (134/147) of entities. It is highly plausible that where we see brain development abnormalities that are drastic enough to alter brain size, skull formation, and/or structural organization they directly result in altered brain function. The most common finding within these syndromes is developmental delay (55%) which is characterized by delays in age appropriate developmental mile stones. More specifically, many of these syndromes show delays in speech (37%) and/or cognitive acquisition. Also common are mental retardation (45%) and seizures (40%). The occurrence of seizures within these cases that is suspected to be a direct result of altered brain organization. We also find brain atrophy in a subset of cases (18%), which may be recognized later in development and shows interesting insight into the temporal nature of brain development. The finding of hypotonia (33%) is also common and demonstrates the general dysfunction of the central nervous system affecting control of motor functions and muscle tone. Lastly, we searched for the association of autism with these syndromes and found that 13% are associated with autism or autistic traits. This is an important observation that we will expand upon with a more comprehensive explanation in a later

section.   A summary of the neurological/behavioral phenotypes is presented below (Table 3) with the full table in the supplement.

Table 1-3: Most common neurologic phenotypes associated with macrocephaly

We provide the most over-represented neurologic and behavioral phenotypes associated with macrocephaly. More than half of the syndromes display developmental delays; also common are mental retardation (MR), seizures, and hypotonia.

| Phenotype | Percentage of cases |
|---|---|
| Developmental Delay | 55.22% |
| Speech | 25.37% |
| Language | 8.96% |
| MR | 45.52% |
| Autistic | 8.96% |
| Autism | 4.48% |
| Seizures | 40.30% |
| Brain Atrophy | 17.91% |
| Hypotonia | 32.84% |

*Skeletal findings*

 Skeletal abnormalities were the second most common phenotype with 61% (90/147) of associated syndromes having some pathology present. The associated anomalies in skeletal development with macrocephaly were present in two main forms: (1) bone overgrowth, which is more striking in syndromes such as the Proteus syndrome where affected bones grow asymmetrically faster than the unaffected bones and can be seen clinically or measured with bone age studies (2) underdeveloped bones which manifest as weakened bones that are prone to fracture and short stature as is seen in osteogenesis imperfecta. The latter comprises a group of disorders collectively called skeletal dysplasias almost and exclusively present with short stature and disproportionate macrocephaly while the former presents with megalencephaly or hemi-megalencephaly depending on the extent of tissue involvement. Another finding within this group is abnormal bone age. Bone age is determined by comparing x-rays from the subject to normalized radiographs from controls of the same age in size, shape and characterization of bones.  Interestingly, conditions associated with overgrowth show advanced bone age, such as Sotos syndrome, and conditions of undergrowth with disproportional macrocephaly and delayed bone age, such as Cantu Syndrome. "Limb abnormalities" are the most common abnormalities within the macrocephaly-associated group with 60% of the conditions associated with findings such as clinodactyly (19%), brachydactyly (14%), syndactyly (11%), and hypermobility (4%). Additionally pathologies of the spine are observed with scoliosis (32%), kyphosis (12%), and lordosis (4%).  Finally there are recognizable defects to the skull itself that are present in 12% of these syndromes and include synostosis (7%). A summary of the skeletal findings is presented below (Table 4; the full table is available in the supplement)

Table 1-4: Most common skeletal findings associated with macrocephaly

We present the four most common skeletal systems associated with the macrocepahly phenotype. Abnormalities to the limbs, spine, skull, and those affecting overall bone health were most reproducible. We broke down each system into specific phenotypes and show their corresponding percentages in the overall macrocephaly phenotype

| System | Phenotype | Percentage of Cases |
|---|---|---|
| Limbs | Limb Abnormalities | 59.60% |
| | Clinodactyly | 19.19% |
| | Syndactyly | 11.11% |
| | Polydactyly | 9.09% |
| | Brachydactyly | 14.14% |
| | hypermobility | 4.04% |
| Spine | Scoliosis | 32.32% |
| | Kyphosis | 12.12% |
| | Lordosis | 4.04% |
| Skull | Skull | 12.12% |
| | Synostosis | 7.07% |
| Bone Health | Osteosclerosis | 3.03% |
| | Osteoporosis | 5.05% |
| | Fractures | 5.05% |
| | Bone Age | 15.15% |
| | dysplasia | 8.08% |

*Undergrowth*

Somatic undergrowth defined as having short stature, growth parameters <3$^{rd}$ percentile, intrauterine growth restriction, or failure to thrive is present in 44 (29%) of macrocephaly-associated conditions. All of these syndromes present with disproportionate macrocephaly and represent an interesting group of conditions where skull/brain growth seems to be sheltered from the overall defects of somatic growth. All associated conditions are presented in the table below. Since this group of disorders is distinct from classically described macrocephaly, we subjected the gene list of these conditions to functional enrichment analysis. We found that there are two novel associations with this gene set and these conditions: 8/44 of these genes are involved in canonical Wnt signaling (DVL3, SOX9, FGFR3, AMER1, THRA, MED12, ROR2, DVL1) and 6/44 of these genes are involved in B-catenin binding (DVL3, SOX9, AMER1, HDAC6, MED12, DVL1). Additionally, we found that alterations in 9/44 (XYLT1, SOX9, FGFR3, AMER1, NF1, THRA, SERPINH1, H19, ROR2) of these genes cause abnormal endochondral bone ossification in the murine model which confirms the presence of skeletal dysplasias and dwarfism in this subset (Table 5).

| MIM Number | Title | Cytogenetic Location | Gene |
|---|---|---|---|
| #300373 | Osteopathia Striata With Cranial Sclerosis; Oscs | Xq11.2 | AMER1 |
| #261540 | Peters-plus Syndrome | 13q12.3 | B3GLCT |
| #115150 | Cardiofaciocutaneous Syndrome 1; Cfc1 | 7q34 | BRAF1 |
| #300354 | Mental Retardation, X-linked, Syndromic, Cabezas Type; Mrxsc | Xq24 | CUL4B |
| #616331 | Robinow Syndrome, Autosomal Dominant 2; Drs2 | 1p36.33 | DVL1 |
| #616894 | Robinow Syndrome, Autosomal Dominant 3; Drs3 | 3q27.1 | DVL3 |
| #127000 | Kenny-caffey Syndrome, Type 2; Kcs2 | 11q12.1 | FAM111A |
| #146000 | Hypochondroplasia; Hch | 4p16.3 | FGFR3 |
| #606812 | Fumarase Deficiency; Fmrd | 1q43 | FH |
| #300699 | Mental Retardation, X-linked, Syndromic, Wu Type; Mrxsw | Xq25 | GRAI3 |
| #253220 | Mucopolysaccharidosis, Type Vii; Mps7 | 7q11.21 | GUSB |
| #180860 | Silver-russell Syndrome; Srs | 7p11.2 | H19/IGF2 |
| #300863 | Chondrodysplasia With Platyspondyly, Distinctive Brachydactyly, Hydrocephaly, And Microphthalmia | Xp11.23 | HDAC6 |
| #236680 | Hydrolethalus Syndrome 1; Hls1 | 11q24.2 | HYLS1 |
| #614099 | Cranioectodermal Dysplasia 3; Ced3 | 14q24.3 | IFT43 |
| #616489 | Growth Restriction, Severe, With Distinctive Facies; Grdf | 11p15.5 | IGF2 |
| #258480 | Opsismodysplasia; Opsmd | 11q13.4 | INPPL1 |
| #613385 | Autoimmune Disease, Multisystem, With Facial Dysmorphism; Admfd | 20q11.22 | ITCH |
| #220210 | Ritscher-schinzel Syndrome 1; Rtsc1 | 8q24.13 | KIAA0196 |
| #603546 | Spondyloepimetaphyseal Dysplasia With Joint Laxity, Type 2; Semdjl2 | 16p11.2 | KIF22 |
| #200990 | Acrocallosal Syndrome; Acls | 15q26.1 | KIF7 |
| #303350 | Masa Syndrome | Xq28 | L1CAM |
| #248500 | Mannosidosis, Alpha B, Lysosomal; Mansa | 19p13.13 | MAN2B1 |
| #305450 | Opitz-kaveggia Syndrome; Oks | Xq13.1 | MED12 |
| #252150 | Molybdenum Cofactor Deficiency, Complementation Group A; Mocoda | 6p21.2 | MOCS1 |
| #601321 | Neurofibromatosis-noonan Syndrome; Nfns | 17q11.2 | NF1 |
| #193520 | Watson Syndrome; Wtsn | 17q11.2 | NF1 |
| #602849 | Muenke Syndrome; Mnkes | 4p16.3 | NF1 |
| #252010 | Mitochondrial Complex I Deficiency | Numerous | Numerous |
| #614813 | Short Stature, Onychodysplasia, Facial Dysmorphism, And Hypotrichosis; Soft | 3p21.2 | POC1A |
| #615139 | Facial Dysmorphism, Immunodeficiency, Livedo, And Short Stature; Fils | 12q24.33 | POLE1 |
| #613075 | Macs Syndrome | 20p11.23 | RIN2 |
| #615355 | Noonan Syndrome 8; Ns8 | 1q22 | RIT1 |
| #268310 | Robinow Syndrome, Autosomal Recessive; Rrs | 9q22.31 | ROR2 |
| #607812 | Craniolenticulosutural Dysplasia; Clsd | 14q21.1 | SEC23A |
| #616294 | Cole-carpenter Syndrome 2; Clcrp2 | 4q26 | SEC24D |
| #613848 | Osteogenesis Imperfecta, Type X; Oi10 | 11q13.5 | SERPINH1 |
| #607721 | Noonan Syndrome-like Disorder With Loose Anagen Hair; Nslh | 10q25.2 | SHOC2 |
| #615085 | Osteopetrosis, Autosomal Recessive 8; Optb8 | 7p15.2 | SNX10 |
| #617140 | Zttk Syndrome; Zttks | 21q22.11 | SON |
| #610733 | Noonan Syndrome 4; Ns4 | 2p22.1 | SOS1 |

| #114290 | Campomelic Dysplasia | 17q24.3 | SOX9 |
|---------|----------------------|---------|------|
| #614450 | Hypothyroidism, Congenital, Nongoitrous, 6; Chng6 | 17q21.1 | THRA |
| #615503 | Short-rib Thoracic Dysplasia 8 With Or Without Polydactyly; Srtd8 | 7q36.3 | WDR60 |
| #615777 | Desbuquois Dysplasia 2; Dbqd2 | 16p12.3 | XYLT1 |
| #617302 | Optic Atrophy 11; Opa11 | 10p12.1 | YMEIL1 |
| #259050 | Primrose Syndrome; Prims | 3q13.31 | ZBTB20 |

Table 1-5: Macrocephaly-associated syndromes which present with somatic undergrowth.

We present the MIM#, name, cytogenetic location, and genes associated with not only

macrocephaly, but also somatic undergrowth.

*Somatic Overgrowth*

The somatic overgrowth associated with macrocephaly subgroup represents some of the most classically described "overgrowth syndromes." We used the criteria of reported growth measurements >95th percentile, reproducibly reported "tall stature" , "macrosomia" or "large for gestational age" to be included within this group (Table 6). Within this group we have identified some of the most classically described overgrowth syndromes including SOTOs syndrome, the proteus syndrome, weaver syndrome and Perlman syndrome.  Ubiquitous human overgrowth conditions are a fascinating subset of the macrocephaly-associated syndromes. In these cases it is thought that widespread distribution of mutations inherited in a germ line mechanism caused increased growth trajectories for a wide breath of tissues, bones and organs. There are exceptions to this observed distribution as some of these overgrowth syndromes are caused by mosaic patterning of mutations and the resulting overgrowth of only those tissues which carrying the mutations. Such is the case with the Proteus syndrome and Megalencephaly-capillary Malformation-polymicrogyria Syndrome (MCAP). Taken together, these syndromes offer insight into the conserved role of human growth across tissue types and additionally have elucidated the roles of specific members of growth signaling pathways in this pathogenesis.

Table 1-6: Macrocephaly-associated syndromes which present with somatic overgrowth. We present the MIM#, name, cytogenetic location, and genes associated with not only macrocephaly, but also somatic overgrowth.

| MIM Number | Title | Cytogenetic Location | Gene |
|---|---|---|---|
| #613675 | Chromosome 17q11.2 Deletion Syndrome, 1.4-mb | 17q11.2 | 17q11.2 |
| #239850 | Cantu Syndrome | 12p12.1 | ABCC9 |
| #176920 | Proteus Syndrome | 14q32.33 | AKT1 |
| #615032 | Autism, Susceptibility to, 18; Auts18 | 14q11.2 | CHD8 |
| #267000 | Perlman Syndrome; Prlmns | 2q37.1 | DIS3L2 |
| #277590 | Weaver Syndrome; Wvs | 7q36.1 | EZH2 |
| #617107 | Thauvin-robinet-faivre Syndrome; Trofas | 11q13.1 | FIBP |
| #613670 | Mental Retardation With Language Impairment and With or Without Autistic Features | 3p13 | FOXP1 |
| #312870 | Simpson-golabi-behmel Syndrome, Type 1; Sgbs1 | Xq26.2 | GPC3 |
| #617011 | Macrocephaly, Dysmorphic Facies, and Psychomotor Retardation; Mdfpmr | 15q22.31 | HERC1 |
| #218040 | Costello Syndrome; Cstlo | 11p15.5 | HRAS |
| #616728 | Cleft Palate, Psychomotor Retardation, and Distinctive Facial Features; Cprf | 1p36.12 | KDM1A |
| #616638 | Smith-kingsmore Syndrome; Sks | 1p36.22 | MTOR |
| #614753 | Sotos Syndrome 2; Sotos2 | 19p13.13 | NFIX |
| #117550 | Sotos Syndrome 1; Sotos1 | 5q35.3 | NSD1 |
| #615398 | Multiple Congenital Anomalies-hypotonia-seizures Syndrome 3; Mcahs3 | 20q13.12 | PIGT |
| #602501 | Megalencephaly-capillary Malformation-polymicrogyria Syndrome; Mcap | 3q26.32 | PIK3CA |
| #616355 | Mental Retardation, Autosomal Dominant 35; Mrd35 | 6p21.1 | PPP2R5D |
| #158350 | Cowden Syndrome 1; Cws1 | 10q23.31 | PTEN |
| #153480 | Bannayan-riley-ruvalcaba Syndrome; Brrs | 10q23.31 | PTEN |
| #605309 | Macrocephaly/autism Syndrome | 10q23.31 | PTEN |
| #616260 | Tenorio Syndrome; Tnors | 18q12.1 | RNF125 |
| #614192 | Macrocephaly, Macrosomia, and Facial Dysmorphism Syndrome; Mmfd | 17q11.2 | RNF135 |
| #616831 | Luscan-lumish Syndrome; Lls | 3p21.31 | SETD2 |
| #606232 | Phelan-mcdermid Syndrome; Phmds | 22q13.33 | SHANK3 |
| #229200 | Brittle Cornea Syndrome 1; Bcs1 | 16q24.2 | ZNF469 |

*Neoplasms*

The overlap between macrocephaly and neoplastic conditions is reflective of the over-representation of mutations in growth signaling pathways that in turn regulate cellular proliferation. Tumors within this subgroup vary in involvement of the kidney (Wilms tumor), brain tissue (meduloblastoma), and thyroid. These neoplasms are, in many cases, malignant and justify surveillance and appropriate management. Early identification of the underlying genetic syndrome in the child presenting with macrocephaly allows testing to be focused and pointed towards ruling in/out the most devastating pathogenesis and clinical sequelae (Table 7).

Table 1-7: Macrocephaly-associated syndromes which present with neoplasms.
We present the name, genes, and, specific tumor types associated with macrocephaly
syndromes.

| Syndrome | Gene | Neoplasm |
|---|---|---|
| Chromosome 17q11.2 Deletion Syndrome, 1.4-mb | 17q11.2 | Optic glioma, Malignant peripheral nerve sheath tumors |
| Proteus Syndrome | AKT1 | Ovarian cystadenoma Parotid monomorphic adenoma |
| Perlman Syndrome; Prlmns | DIS3L2 | Wilms tumor |
| Hypothalamic Hamartomas | GLI3 | Hypothalamic hamartoma , Brain stem glioma |
| Simpson-golabi-behmel Syndrome, Type 1; Sgbs1 | GPC3 | Embryonal tumors, Wilms tumor |
| Silver-russell Syndrome; Srs | H19/IGF2 | Craniopharyngioma, Testicular seminoma, Wilms tumor, Hepatocellular carcinoma |
| Costello Syndrome; Cstlo | HRAS | Epithelioma , Bladder carcinoma, Rhabdomyosarcoma, Vestibular schwannoma |
| Muenke Syndrome; Mnkes | NF1 | Optic glioma, Neurofibromas, |
| Neurofibromatosis-noonan Syndrome; Nfns | NF1 | Optic glioma, Neurofibromas |
| Neurofibromatosis, Type I; Nf1 | NF1 | Optic glioma, Meningioma, Hypothalamic tumor , Rhabdomyosarcoma, Duodenal carcinoid |
| Noonan Syndrome 6; Ns6 | NRAS | juvenile myelomonocytic leukemia (JML) |
| Sotos Syndrome 1; Sotos1 | NSD1 | Wilms tumor |
| Megalencephaly-capillary Malformation-polymicrogyria Syndrome; Mcap | PIK3CA | meningioma, Wilms tumor, leukemia |
| Megalencephaly-polymicrogyria-polydactyly-hydrocephalus Syndrome 1; Mpph1 | PIk3R2 | medulloblastoma |
| Basal Cell Nevus Syndrome; Bcns | PTCH1, PTCH2, SUFU | Medulloblastoma, - Basal cell carcinoma |
| Bannayan-riley-ruvalcaba Syndrome; Brrs | PTEN | Meningioma, Thyroid follicular cell tumor |
| Cowden Syndrome 1; Cws1 | PTEN | Breast cancer, Ovarian carcinoma, Cervical carcinoma, Uterine adenocarcinom, Thyroid cancer (follicular cell), Meningioma, Mucosal neuromas |
| Noonan Syndrome 4; Ns4 | SOS1 | -Multiple giant cell granulomas (bones, joints, soft tissues) |

46

*Epidermal changes*

Numerous epidermal phenotypes were observed within the macrocephaly-associated

conditions.  Cafe au lait spots are reported in 22% (11/50) syndromes.  Also, nevi of

various descriptions, including nevous flamous, are reported in 16% (8/50) syndromes. A

complete list of all macrocephaly-associated syndromes with epidermal changes is

presented in the table below (Table 8).

| Syndrome | Gene | Epidermal Changes |
|---|---|---|
| Chromosome 17q11.2 Deletion Syndrome, 1.4-mb | 17q11.2 | Neurofibromas, subcutaneous, Neurofibromas, cutaneous, Plexiform neurofibroma, Cafe au lait spots, Axillary freckling, Inguinal freckling |
| Chromosome 1p32-p31 Deletion Syndrome | 1p32 | Cutis marmorata |
| Cantu Syndrome | ABCC9 | Lymphedema |
| Proteus Syndrome | AKT1 | Cerebriform connective tissue nevus, Lymphangioma, Lipoma, Lipohypoplasia, Epidermal nevi, Hypertrophy of skin of soles, Depigmentation/hyperpigmentation, Hemangiomata, especially thorax and upper abdomen ,Skin Histology, Highly collagenized connective tissue, Acanthosis, Hyperkeratosis, Dermal hypoplasia, |
| Megalencephaly-polymicrogyria-polydactyly-hydrocephalus Syndrome 2; Mpph2 | AKT3 | Skin hyperextensibility, Connective tissue dysplasia, Cutis marmorata |
| Shashi-pena Syndrome; Shapns | ASXL2 | Nevus flammeus, glabellar, Capillary malformations |
| Peters-plus Syndrome | B3GLCT | Single transverse palmar creases, Deep foot creases |
| Meester-loeys Syndrome; Mrls | BGN | Skin striae |
| Cardiofaciocutaneous Syndrome 1; Cfc1 | BRAF1 | Severe atopic dermatitis, Ichthyosis , Hyperkeratosis (especially extensor surfaces), Cavernous hemangioma, Keratosis pilaris, Multiple palmar creases, Multiple lentigines, |
| Mental Retardation, X-linked, Syndromic, Cabezas Type; Mrxsc | CUL4B | Striae |
| Multiple Acyl-coa Dehydrogenase Deficiency; Madd | ETFDH, EFTA, EFTB | Jaundice |
| Weaver Syndrome; Wvs | EXH2 | Loose skin,Increased pigmented nevi |
| Hypochondroplasia; Hch | FGFR3 | Acanthosis nigricans |
| Fumarase Deficiency; Fmrd | FH | Cutaneous leiomyomata (heterozygote carriers) |
| Sturge-weber Syndrome; Sws | GNAQ | Hemangiomata in at least first branch (ophthalmic) of trigeminal nerve distribution, unilateral, occasionally bilateral |
| Simpson-golabi-behmel Syndrome, Type 1; Sgbs1 | GPC3 | Coccygeal skin tags |
| Silver-russell Syndrome; Srs | H19/IGF2 | Cafe au lait spots |
| Costello Syndrome; Cstlo | HRAS | Cutis laxa (especially hands and feet), Loose, redundant skin , Dark skin pigmentation, Papillomas (perioral, nasal, and anal regions) , Acanthosis nigricans, Palmar nevi, Deep palmar creases |
| Cranioectodermal Dysplasia 3; Ced3 | IFT43 | Skin laxity, Dry skin |
| Growth Restriction, Severe, With Distinctive Facies; Grdf | IGF2 | Pigmented nevi |
| Spondyloepimetaphyseal Dysplasia With Joint Laxity, Type 2; Semdjl2 | KIF22 | Velvety skin |
| Al-gazali-bakalinova Syndrome; Agbk | KIF7 | Soft and lax skin |
| Opitz-kaveggia Syndrome; Oks | MED12 | Facial wrinkling , Sacral dimple, Perianal skin tags, Single transverse palmar crease, Persistent fetal fingertip pads |
| Coloboma, Osteopetrosis, Microphthalmia, Macrocephaly, Albinism, And Deafness; Commad | MITF | Lack of pigment in skin |
| Waardenburg Syndrome, Type 2a; Ws2a | MITF | Congenital partial albinism (leukoderma) on face, trunk, or limbs |
| Smith-kingsmore Syndrome; Sks | MTOR | Cafe au lait spots |
| Neurofibromatosis, Type I; Nf1 | NF1 | Neurofibromas, Plexiform neurofibroma, Cafe au lait spots, Axillary freckling, Inguinal freckling, |

| | | |
|---|---|---|
| Watson Syndrome; Wtsn | NF1 | Multiple cafe au lait spots, Neurofibromas, Axillary freckling, |
| Muenke Syndrome; Mnkes | NF1 | Cafe au lait spots, Axillary freckling, Inguinal freckling, Neurofibromas, |
| Neurofibromatosis-noonan Syndrome; Nfns | NF1 | Cafe au lait spots, Axillary freckling, Inguinal freckling, Neurofibromas, |
| Sotos Syndrome 2; Sotos2 | NFIX | Livedo reticularis, generalized |
| Noonan Syndrome 6; Ns6 | NRAS | Hyperkeratosis, 2cafe au lait spots |
| Simpson-golabi-behmel Syndrome, Type 2; Sgbs2 | OFD1 | Facial capillary hemangioma, Transverse palmar creases |
| Megalencephaly-capillary Malformation-polymicrogyria Syndrome; Mcap | PIK3CA | Thick, loose, doughy skin, Patchy, reticular stains, Cutis marmorata |
| Facial Dysmorphism, Immunodeficiency, Livedo, And Short Stature; Fils | POLE1 | Livedo, Telangiectasia on the cheeks |
| Basal Cell Nevus Syndrome; Bcns | PTCH1, PTCH2, SUFU | Basal cell nevi, Pits of palms and soles |
| Cowden Syndrome 1; Cws1 | PTEN | Multiple facial papules, Acral keratoses, Palmoplantar keratoses, Multiple skin tags, Facial trichilemmomas, Subcutaneous lipomas, |
| Bannayan-riley-ruvalcaba Syndrome; Brrs | PTEN | Tan macules on glans penis and penile shaft, Acanthosis nigricans, Angiokeratoma, Cafe au lait spots, Lipoma, Hemangiomas, |
| Macs Syndrome | RIN2 | Soft, redundant skin, Ichthyosis, Hyperextensible skin, Multiple pigmented moles, Easy bruising |
| Robinow Syndrome, Autosomal Recessive; Rrs | ROR2 | Nevus flammeus |
| Craniolenticulosutural Dysplasia; Clsd | SEC23A | Hyperpigmentation, Capillary hemangioma (forehead) |
| Phelan-mcdermid Syndrome; Phmds | SHANK3 | Tendency to overheat, Lack of perspiration |
| Noonan Syndrome-like Disorder With Loose Anagen Hair; Nslh | SHOC2 | Darkly pigmented skin, Eczema (in some patients), Keratosis pilaris (in some patients), Ichthyosis (in some patients), Increased fine wrinkles (in some patients), Deep palmar creases (in some patients), |
| Noonan Syndrome 4; Ns4 | SOS1 | Ectodermal symptoms, Keratosis pilaris |
| Campomelic Dysplasia | SOX9 | Cutaneous dimpling over bowed tibia |
| Campomelic Dysplasia | SOX9 | Cutaneous dimpling over bowed tibia |
| Legius Syndrome | SPRED1 | Cafe au lait spots, Axillary freckling |
| Hypothyroidism, Congenital, Nongoitrous, 6; Chng6 | THRA | Dry skin, Doughy skin (in some patients) |
| Desbuquois Dysplasia 2; Dbqd2 | XYLT1 | Doughy or puffy skin, Simian crease (in some patients) |
| Brittle Cornea Syndrome 1; Bcs1 | ZNF469 | Scarring, Molluscoid pseudotumor, Excessive wrinkled skin (palms and soles) |

Table 1-8: Macrocephaly-associated syndromes which present with epidermal abnormalities.

We present the name, genes, and specific epidermal phenotypes associated with macrocephaly syndromes

*Vascular Abnormalities*

We found that vascular abnormalities are present in a subset of macrocephaly-associated syndromes with the most common observed defects being patent ductus arteriosus, and capillary malformations such as hemangiomatas. Additional phenotypes include: raynaud phenomenon, renal artery stenosis, hypertension, and tortuosity of arteries. In general vascular malformations are complex and progressive worsening with time. There are two forms of cutaneous vascular abnormalities (1) fast flow and (2) slow flow. Fast flow malformations are cutaneous markings which are normally red, comorbid with lymphedema, and painful. Conversely, slow flow malformations present as diffuse "port-wine stain" colorings, functional impairment of affected area localized intravascular coagulopathy[87]. Both forms are observed in the macrocephaly-associated syndromes. Non-cutaneous vascular malformations including those affecting large, central vessels are additionally observed. The syndromes and their associated vascular abnormalities are presented below (Table 9)

Table 1-9: Macrocephaly-associated syndromes which present with vascular malformations. We present the name, genes, and specific vascular phenotypes associated with macrocephaly syndromes.

| Syndrome | Gene | Vascular |
|---|---|---|
| Cantu Syndrome | ABCC9 | Patent ductus arteriosus |
| Hypermethioninemia Due To Adenosine Kinase Deficiency | ADK | Coarctation of the aorta (1 patient) |
| Proteus Syndrome | AKT1 | Capillary malformations, Venous malformations, Lymphatic malformations, Deep vein thrombosis, |
| Megalencephaly-polymicrogyria-polydactyly-hydrocephalus Syndrome 2; Mpph2 | AKT3 | Vascular malformations |
| Osteopathia Striata With Cranial Sclerosis; Oscs | AMER1 | Patent ductus arteriosus |
| Meester-loeys Syndrome; Mrls | BGN | Aneurysm of aortic root, Aneurysm of ascending aorta, Aortic dissection, Pulmonary artery aneurysm, Cerebral aneurysm, |
| Robinow Syndrome, Autosomal Dominant 3; Drs3 | DVL3 | Patent ductus arteriosus |
| Thauvin-robinet-faivre Syndrome; Trofas | FIBP | Varicose veins, severe |
| Sturge-weber Syndrome; Sws | GNAQ | Facial hemangiomata, Choroidal hemangiomata |
| Simpson-golabi-behmel Syndrome, Type 1; Sgbs1 | GPC3 | Transposition of great vessels, Patent ductus arteriosus |
| Cranioectodermal Dysplasia 3; Ced3 | IFT43 | Peripheral pulmonary stenosis |
| Neurofibromatosis, Type I; Nf1 | NF1 | Renal artery stenosis, Hypertension |
| Sotos Syndrome 1; Sotos1 | NSD1 | Patent ductus arteriosus |
| Simpson-golabi-behmel Syndrome, Type 2; Sgbs2 | OFD1 | Facial capillary hemangioma |
| Multiple Congenital Anomalies-hypotonia-seizures Syndrome 3; Mcahs3 | PIGT | Patent ductus arteriosus |
| Megalencephaly-capillary Malformation-polymicrogyria Syndrome; Mcap | PIK3CA | Cutaneous malformations |
| Cowden Syndrome 1; Cws1 | PTEN | Vascular anomalies (50% of patients), Intracranial developmental venous anomalies |
| Tenorio Syndrome; Tnors | RNF125 | Raynaud phenomenon |
| Hypothyroidism, Congenital, Nongoitrous, 6; Chng6 | THRA | Low resting blood pressure, Tortuosity of arteries of dorsal hands and feet (in some) |

*Heart Defects*

Finally, we looked at the occurrence of heart defects within these conditions and found that they are somewhat common and can present as atrial septal defects, cardiomegaly, and ventricular septal defects. As these conditions require management in the first few years of life, we believe using macrocephaly as an early warning sign to these conditions may accelerate the identification and treatment of at risk cases (Table 10).

Table 1-10:  Macrocephaly-associated syndromes which present with cardiac defects.

We present the name, genes, and specific cardiac manifestation associated with

macrocephaly syndromes.

| Title | Gene | Heart |
|---|---|---|
| D-2-hydroxyglutaric Aciduria 1; D2hga1 | D2HGDH | Cardiomyopathy, Aortic insufficiency |
| Chromosome 17q11.2 Deletion Syndrome, 1.4-mb | 17q11.2 | Heart, Congenital heart defects |
| Cantu Syndrome | ABCC9 | Cardiomegaly, Pericardial effusions, Congenital hypertrophy of left ventricle, Bicuspid aortic valve |
| Hypermethioninemia Due To Adenosine Kinase Deficiency | ADK | Cardiac defects (in some), Atrial septal defect (2 patients), Pulmonary stenosis (1 patient) |
| Osteopathia Striata With Cranial Sclerosis; Oscs | AMER1 | Ventricular septal defect, Atrial septal defect |
| Shashi-pena Syndrome; Shapns | ASXL2 | Atrial septal defect |
| Peters-plus Syndrome | B3GLCT | Atrial septal defect, Ventricular septal defect, Pulmonary stenosis |
| Meester-loeys Syndrome; Mrls | BGN | Mitral valve insufficiency, Aortic valve insufficiency |
| Cardiofaciocutaneous Syndrome 1; Cfc1 | BRAF1 | Atrial septal defects, Pulmonic stenosis, Hypertrophic cardiomyopathy |
| Sifrim-hitz-weiss Syndrome; Sihiwes | CHD4 | Congenital heart defects, Coarctation of the aorta, Tetralogy of Fallot, Septal defects |
| D-2-hydroxyglutaric Aciduria 1; D2hga1 | D2HGDH | Cardiomyopathy, Aortic insufficiency |
| Desmosterolosis | DHCR24 | Total anomalous pulmonary venous drainage |
| Perlman Syndrome; Prlmns | DIS3L2 | Interrupted aortic arch |
| Robinow Syndrome, Autosomal Dominant 3; Drs3 | DVL3 | Ventricular septal defect,  Patent foramen ovale, Pulmonary atresia, Hypoplastic right heart, Tricuspid regurgitation |
| Seizures, Scoliosis, And Macrocephaly Syndrome; Ssms | EXT2 | Ventricular septal defect |
| Thauvin-robinet-faivre Syndrome; Trofas | FIBP | Ventricular septal defect, Mitral valve prolapse (patient A) |
| Fragile X Mental Retardation Syndrome | FMR1 | Mitral valve prolapse |
| Hypothalamic Hamartomas | GLI3 | Congenital heart defect |
| Simpson-golabi-behmel Syndrome, Type 1; Sgbs1 | GPC3 | Cardiac conduction defects, Ventricular septal defect, Pulmonic stenosis, Cardiomyopathy |
| Mucopolysaccharidosis, Type Vii; Mps7 | GUSB | Valvular heart disease |
| Silver-russell Syndrome; Srs | H19/IGF2 | Cardiac defects |
| Costello Syndrome; Cstlo | HRAS | Hypertrophic cardiomyopathy,  Pulmonic stenosis,  Mitral valve prolapse,  Ventricular septal defect,  Atrial septal defect,  Dysrhythmias,  Arrhythmias, |
| Hydrolethalus Syndrome 1; Hls1 | HYLS1 | Atrioventricular cana,  Ventricular septal defect |
| Growth Restriction, Severe, With Distinctive Facies; Grdf | IGF2 | Persistent ductus arteriosus, Ventricular septal defect, small |
| Ritscher-schinzel Syndrome 1; Rtsc1 | KIAA0196 | Ventricular septal defect,  Atrial septal defect,  Tetralogy of |

| | | Fallot,  Double outlet right ventricle,  Hypoplastic left heart, Aortic stenosis,  Pulmonic stenosis, |
|---|---|---|
| Acrocallosal Syndrome; Acls | KIF7 | Septal defects, Pulmonary valve defects |
| Smith-kingsmore Syndrome; Sks | MTOR | Aortic sinus to right atrial fistula |
| Muenke Syndrome; Mnkes | NF1 | Pulmonic stenosis |
| Neurofibromatosis-noonan Syndrome; Nfns | NF1 | Pulmonic stenosis |
| Watson Syndrome; Wtsn | NF1 | Pulmonary valvular stenosis |
| Noonan Syndrome 6; Ns6 | NRAS | hypertrophic cardiomyopathy and pulmonic stenosis. |
| Sotos Syndrome 1; Sotos1 | NSD1 | Atrial septal defect, Ventricular septal defect |
| Mitochondrial Complex I Deficiency | Numerous | Hypertrophic cardiomyopathy |
| Multiple Congenital Anomalies-hypotonia-seizures Syndrome 3; Mcahs3 | PIGT | Restrictive cardiomyopathy |
| Hyperphosphatasia With Mental Retardation Syndrome 1; Hpmrs1 | PIGV | Ventral septal defect |
| Megalencephaly-capillary Malformation-polymicrogyria Syndrome; Mcap | PIK3CA | Heart,  Ventricular septal defect |
| Megalencephaly-polymicrogyria-polydactyly-hydrocephalus Syndrome 1; Mpph1 | PIk3R2 | Atrial septal defect,  Ventricular septal defect,  Vascular ring, Mitral regurgitation |
| Basal Cell Nevus Syndrome; Bcns | PTCH1, PTCH2, SUFU | Cardiac fibroma |
| Macs Syndrome | RIN2 | Mild aortic dilatation (rare) |
| Noonan Syndrome 8; Ns8 | RIT1 | Hypertrophic cardiomyopathy,  Atrial septal defect, Ventricular septal defect,  Pulmonic stenosis,  Valvular insufficiency, |
| Robinow Syndrome, Autosomal Recessive; Rrs | ROR2 | Right ventricular outlet obstruction |
| Noonan Syndrome-like Disorder With Loose Anagen Hair; Nslh | SHOC2 | Atrial septal defect,  Ventricular septal defect, Mitral/tricuspid valve dysplasia,  Pulmonic stenosis, Hypertrophic cardiomyopathy, |
| Zttk Syndrome; Zttks | SON | Congenital heart defects |
| Campomelic Dysplasia | SOX9 | Congenital heart defects |

## Overlapping Phenotypes and Groupings

We next looked at the association between phenotypes as a way to further delineate functional interactions within subgroups. We found the following the most compelling:

*Somatic Overgrowth, Neoplasms, and Vascular Abnormalities.*

A common overlap was seen between the overgrowth and neoplasms group (Figure 8). This overlap is unsurprising as these disorders often result from mutations to tumor suppressors in growth signaling pathways such as PTEN or activating mutations in oncogenes such as PIK3CA and AKT1. We also see numerous somatic overgrowth conditions that present with vascular and/or epidermal findings. This triad of presentations has long been the standard for suspicion of underlying pathologic overgrowth syndromes (Figure 9 & 12).

Figure 1-8: Overlap of overgrowth and neoplastic macrocephaly-associated phenotypes

We compared the gene lists for somatic overgrowth and neoplasms associated with

macrocephaly and show that there is overlap between these two lists.
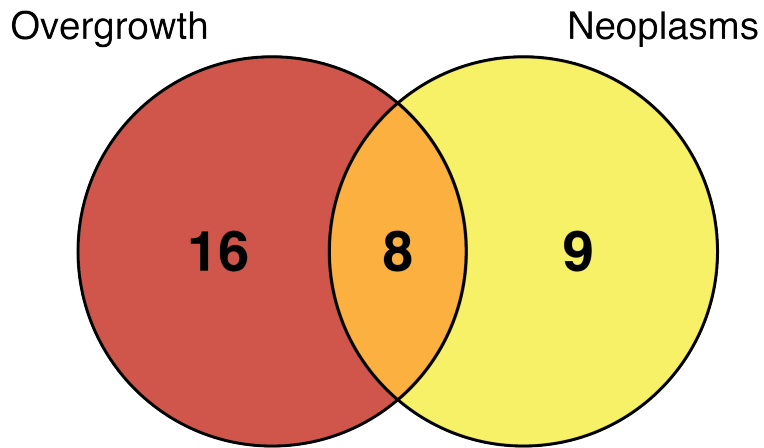
Figure 1-9: Overlap of overgrowth, epidermal, and neoplastic macrocephaly-associated phenotypes

We compared the gene lists for somatic overgrowth, neoplasms, and epidermal abnormalities associated with macrocephaly to show that there is overlap between these three lists. This triad makes up the core of the classical overgrowth syndromes.
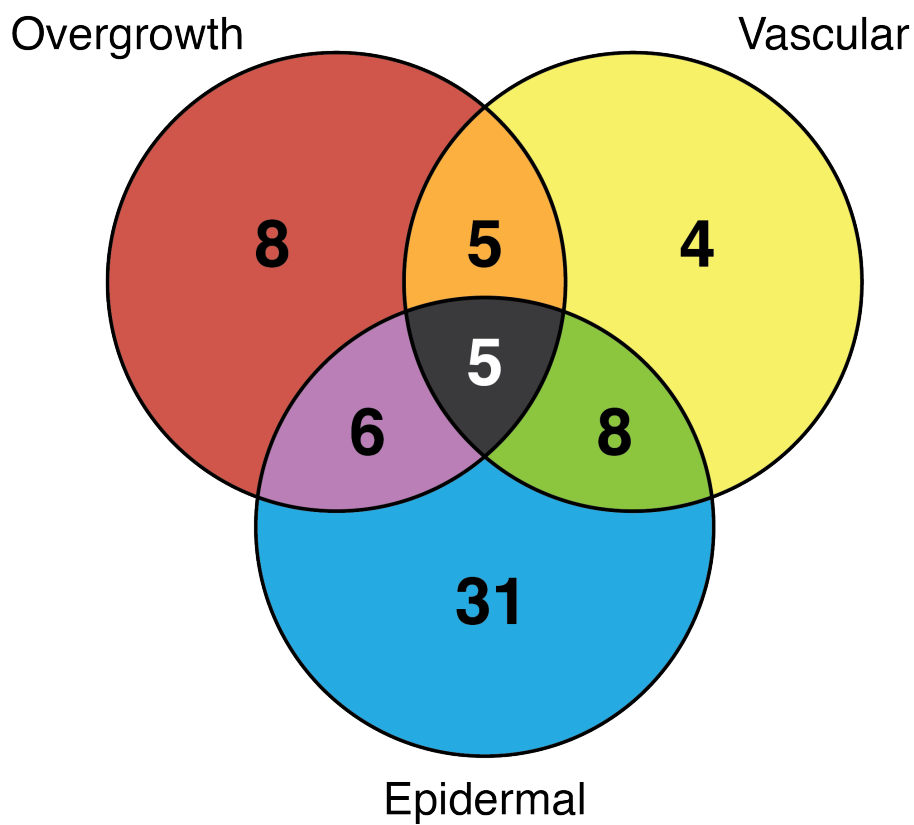
## Somatic Undergrowth, Skeletal abnormalities, and Heart Defects

We see significant overlap between the physical findings of somatic undergrowth and skeletal changes with 40 conditions. This overlap represents the skeletal dysplasia disorders, which have numerous defects of skull development (Figure 10). Additionally within this group we see that many of these skeletal-undergrowth conditions are associated with heart defects (Figure 11-12).

Figure 1-10: Overlap of undergrowth and skeletal macrocephaly-associated phenotypes

We compared the gene lists for somatic undergrowth and skeletal abnormalities associated with macrocephaly and show that there is overlap between these two lists. This supports that idea that disproportionate macrocephaly in the undergrowth cases are associated with skeletal dysplasia.
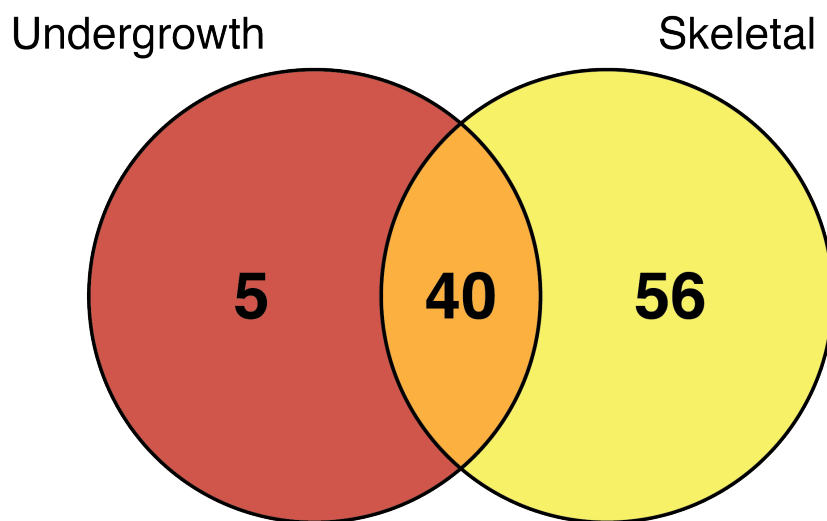
Figure 1-11: Overlap of undergrowth, skeletal, and cardiac macrocephaly-associated

phenotypes

We compared the gene lists for somatic undergrowth, skeletal abnormalities, and cardiac

defects associated with macrocephaly and show that there is overlap between these three

lists. This triad constitutes a novel triad of somatic undergrowth, skeletal, and cardiac

syndromes.
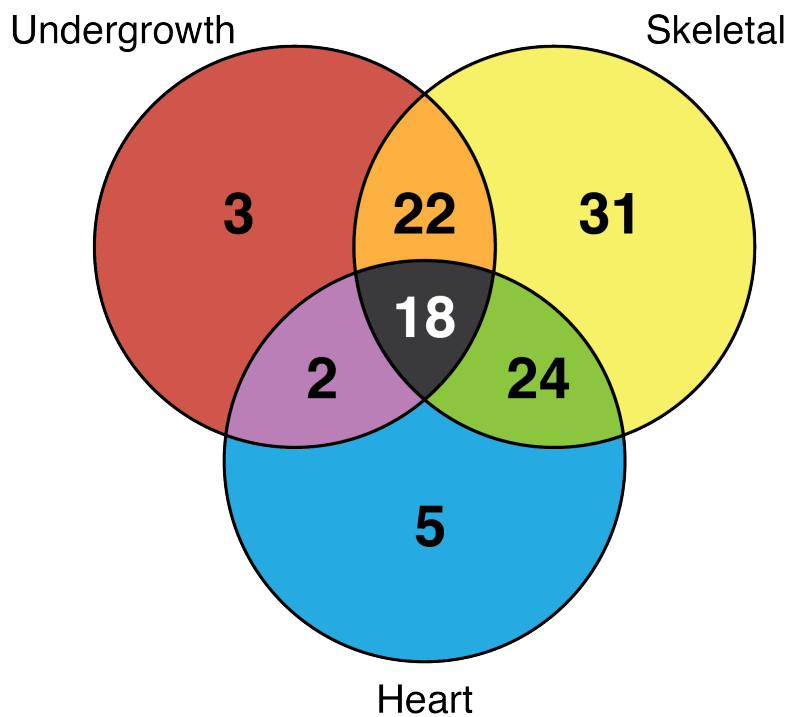
Figure 1-12: Main phenotypic subgroupings.

We summarize our two main phenotypic subgroup triads those with macrocephaly, somatic overgrowth, neoplastic predisposition, and vascular abnormalities and those with macrocephaly, somatic undergrowth, skeletal abnormalities, and cardiac defects.
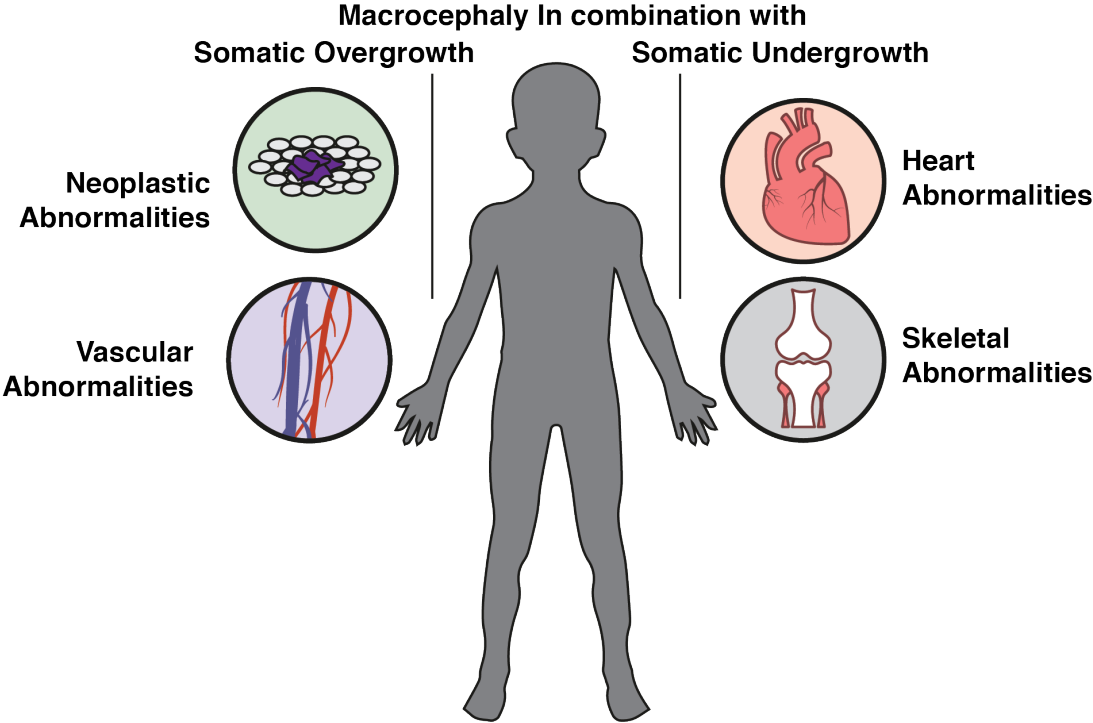
## Autism/Macrocephaly

The association between macrocephaly and autism has been classically and reproducibly reported.[1,2,88-90].  Most recently, it has been show that abnormal brain growth is not only associated with autism but can be predictive of future development[91]. This study compared neuroimaging from 106 infants in high-risk autism families to 42 low risk infants. They identified 15 infants who were diagnosed with autism at 24 months of age and these cases show hyperexpansion of cortical surface, which precedes the increase in brain volume observed between 12 and 24 months. The researchers used these measurements to train a deep learning algorithm which was predictive for autism with a predictive value of 81%[91]. We hypothesized that many of the genes we identified in the literature and public database search may overlap with known/emerging autism associated genes because they may display similar altered growth trajectories. To answer this, we compared our "comb-macro" gene list to the gene list curated by SFARI, which includes many new autism-associated genes. We found that 84 of the macrocephaly genes overlap with genes curated in the SFARI Database. We call this gene list the autism-macrocephaly or "aut-macro" gene list (Figure 13).

Figure 1-13: Overlap macrocephaly- and autism associated gene lists

We compared our "comb-macro" gene list, which is a collection of all publically available genes, as well as those curated from the literature to the "SFARI-ASD" gene list; this is a curated gene list from the SFARI database. We show that 84 genes are present on both gene lists and deem this group the autism-macrocephaly (Aut-Macro) gene list.



Combined Macro  SFARI-ASD

486   84   564
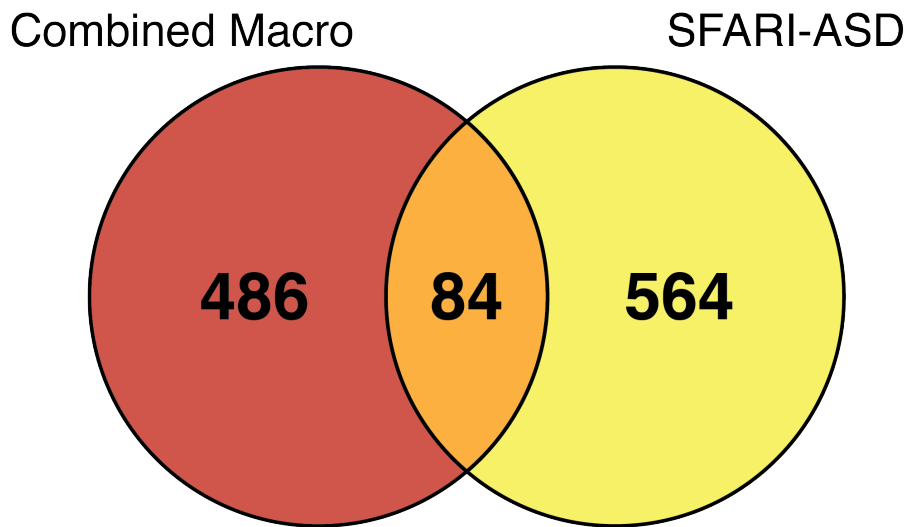
We then visualized the potential for there to be a novel gene network within this aut-macro gene list utilizing the cytoscape reactome app. We were able to generate the follow autism-macrocephaly associated gene network (Figure 14). Additionally, we confirmed interactions with GeneNETs software on the same 84 genes and built the following two communities of genes (Figure 15 and 16).

Figure 1-14: Novel neural autism-macrocephaly associated neural network

We analyzed the aut-macro gene list using the cytoscape reactome app and show that they
assemble into a potentially novel network. We see the presence of three well known
signaling pathways including Wnt, RAS, and PI3K/AKT/mTOR as well as less well
understood interactions between these growth signaling pathways and the identification of
novel pathway intermediates including:IL6, GRIN2B, PFAH1B1, YWAE and DAB1.
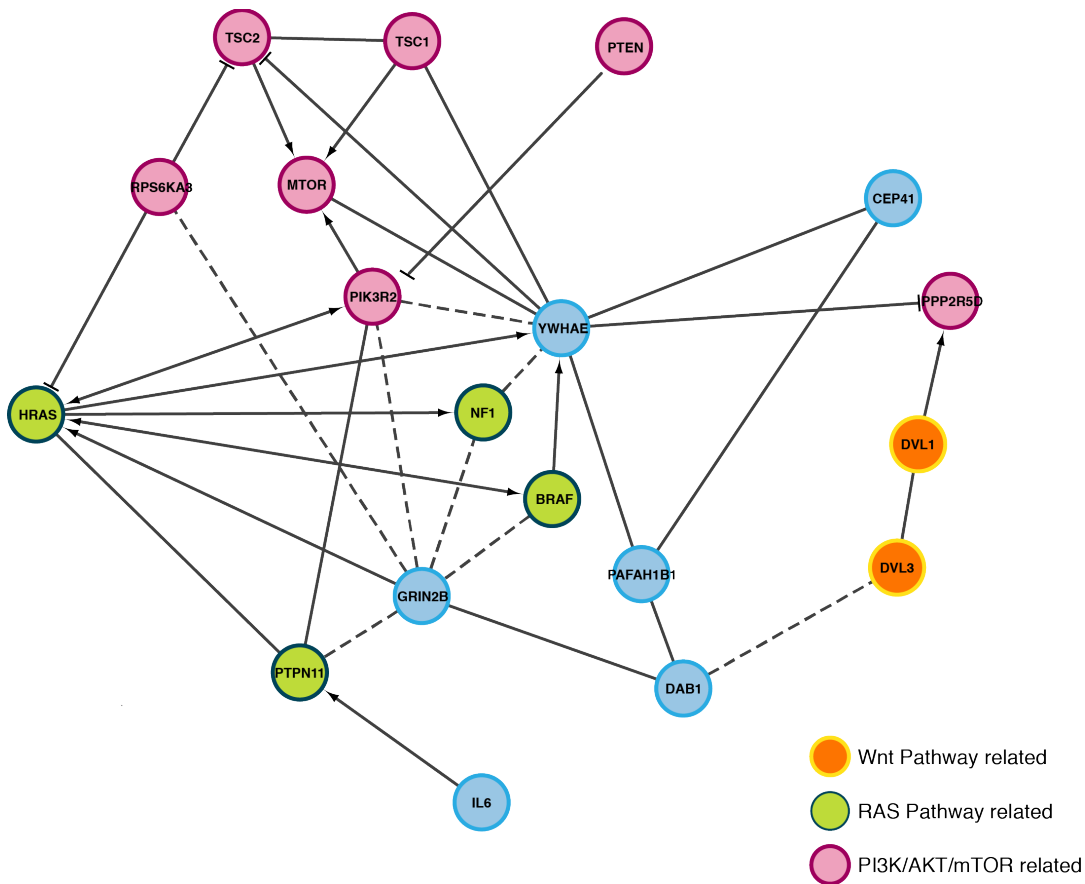
Figure 1-15: Autism-macrocephaly related community #1

Using GeneNets software we were able to generate this community from the aut-macro gene list. These highly interconnected genes represent a potential novel neural network that is implicated in the development of the autism-macrocephaly phenotype.
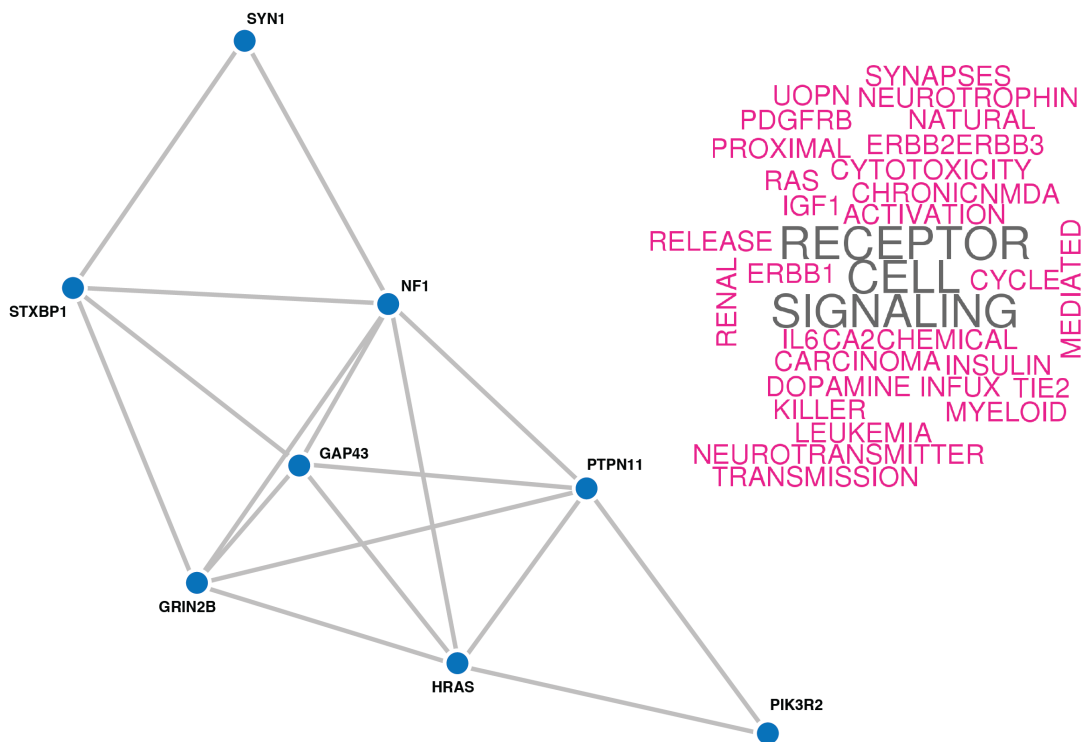
Figure 1-16: Autism-macrocephaly related community #2

Using GeneNets software we were able to generate this community from the aut-macro gene list. These highly interconnected genes represent a potential novel neural network that is implicated in the development of the autism-macrocephaly phenotype.
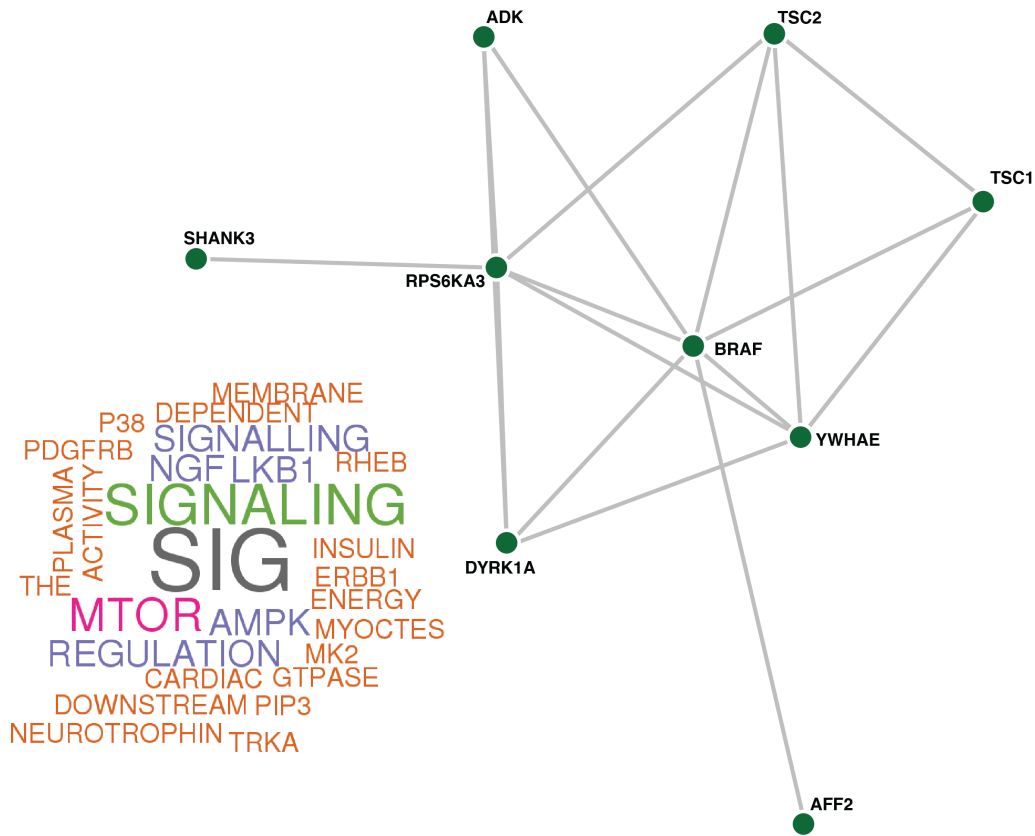
Overall, these communities and potential novel neural networks make a convincing argument for the overlap of macrocephaly and autism. They potentially explain why mutations in these genes result in similar brain phenotypes. Lastly, the appearance of distinct genetic syndromes with unique somatic phenotypes may be partially due to the downstream and interpathway effects of these variants outside of known canonical signaling cascades.

## Conclusions

Macrocephaly is a distinct clinical finding resulting from numerous etiologies. In the setting of the abnormally developing child it can be an early indicator of insidious structural deficits as well as underlying genetic mutations. We have summarized the available literature of genetic cases of macrocephaly and shown that functionally these genes are involved with central nervous system development, neurogenesis, generation of neurons, head development, neuron differentiation, and brain development. More specifically, many of these genes cluster within two well-known pathways: the PI3K/AKT/mTOR pathway and the Hedgehog-signaling pathway.  Furthermore, we have performed a comprehensive review of the associated phenotypes and shown that many macrocephaly-associated syndromes are associated with changes to the skeletal, epidermal, and vascular systems. Additionally, examining the neurologic phenotypes, we show that a striking number of syndromes are associated with developmental delays, autism, and hypotonia. By demonstrating the overlap of macrocephaly- and autism-associated genes, we have identified potential novel networks and gene clusters which may

lead to a better understanding of this phenotype.  This work also highlights the intersection

of abnormal brain growth and associated alterations in normal neurologic development.

# References

1.  Sacco, R., Gabriele, S. & Persico, A.M. Head circumference and brain size in autism spectrum disorder: A systematic review and meta-analysis. *Psychiatry Res* **234**, 239-51 (2015).

2.  Klein, S., Sharifi-Hannauer, P. & Martinez-Agosto, J.A. Macrocephaly as a clinical indicator of genetic subtypes in autism. *Autism Res* **6**, 51-6 (2013).

3.  Butler, M.G. *et al.* Subset of individuals with autism spectrum disorders and extreme macrocephaly associated with germline PTEN tumour suppressor gene mutations. *J Med Genet* **42**, 318-21 (2005).

4.  Lynch, N.E., Lynch, S.A., McMenamin, J. & Webb, D. Bannayan-Riley-Ruvalcaba syndrome: a cause of extreme macrocephaly and neurodevelopmental delay. *Arch Dis Child* **94**, 553-4 (2009).

5.  DeMyer, W. Megalencephaly: types, clinical syndromes, and management. *Pediatr Neurol* **2**, 321-8 (1986).

6.  Hanssen, A.M., Werquin, H., Suys, E. & Fryns, J.P. Cowden syndrome: report of a large family with macrocephaly and increased severity of signs in subsequent generations. *Clin Genet* **44**, 281-6 (1993).

7.  Bannayan, G.A. Lipomatosis, angiomatosis, and macrencephalia. A previously undescribed congenital syndrome. *Arch Pathol* **92**, 1-5 (1971).

8.  Spinelli, L., Black, F.M., Berg, J.N., Eickholt, B.J. & Leslie, N.R. Functionally distinct groups of inherited PTEN mutations in autism and tumour syndromes. *J Med Genet* **52**, 128-34 (2015).

9. Griffiths, P.D., Gardner, S.A., Smith, M., Rittey, C. & Powell, T. Hemimegalencephaly and focal megalencephaly in tuberous sclerosis complex. *AJNR Am J Neuroradiol* **19**, 1935-8 (1998).

10. Cuddapah, V.A. *et al.* Hemispherectomy for Hemimegalencephaly Due to Tuberous Sclerosis and a Review of the Literature. *Pediatr Neurol* **53**, 452-5 (2015).

11. Magri, L. *et al.* Timing of mTOR activation affects tuberous sclerosis complex neuropathology in mouse models. *Dis Model Mech* **6**, 1185-97 (2013).

12. Happle, R. Lethal genes surviving by mosaicism: a possible explanation for sporadic birth defects involving the skin. *J Am Acad Dermatol* **16**, 899-906 (1987).

13. Riviere, J.B. *et al.* De novo germline and postzygotic mutations in AKT3, PIK3R2 and PIK3CA cause a spectrum of related megalencephaly syndromes. *Nat Genet* **44**, 934-40 (2012).

14. Kurek, K.C. *et al.* Somatic mosaic activating mutations in PIK3CA cause CLOVES syndrome. *Am J Hum Genet* **90**, 1108-15 (2012).

15. Orloff, M.S. *et al.* Germline PIK3CA and AKT1 mutations in Cowden and Cowden-like syndromes. *Am J Hum Genet* **92**, 76-80 (2013).

16. Molvi, M., Sharma, Y.K. & Dash, K. Cowden Syndrome: Case Report, Update and Proposed Diagnostic and Surveillance Routines. *Indian J Dermatol* **60**, 255-9 (2015).

17. Loveday, C. *et al.* Mutations in the PP2A regulatory subunit B family genes PPP2R5B, PPP2R5C and PPP2R5D cause human overgrowth. *Hum Mol Genet* **24**, 4775-9 (2015).

18. Hardy, K.M., Yatskievych, T.A., Konieczka, J., Bobbs, A.S. & Antin, P.B. FGF signalling through RAS/MAPK and PI3K pathways regulates cell movement and gene

expression in the chicken primitive streak without affecting E-cadherin expression. *BMC Dev Biol* **11**, 20 (2011).

19.    Kwabi-Addo, B., Ozen, M. & Ittmann, M. The role of fibroblast growth factors and their receptors in prostate cancer. *Endocr Relat Cancer* **11**, 709-24 (2004).

20.    Oliveira, N.A., Alonso, L.G., Fanganiello, R.D. & Passos-Bueno, M.R. Further evidence of association between mutations in FGFR2 and syndromic craniosynostosis with sacrococcygeal eversion. *Birth Defects Res A Clin Mol Teratol* **76**, 629-33 (2006).

21.    Gonzales, M. *et al.* Vertebral anomalies and cartilaginous tracheal sleeve in three patients with Pfeiffer syndrome carrying the S351C FGFR2 mutation. *Clin Genet* **68**, 179-81 (2005).

22.    Khonsari, R.H. *et al.* Central nervous system malformations and deformations in FGFR2-related craniosynostosis. *Am J Med Genet A* **158A**, 2797-806 (2012).

23.    Abdel-Salam, G.M. *et al.* Muenke syndrome with pigmentary disorder and probable hemimegalencephaly: An expansion of the phenotype. *Am J Med Genet A* **155A**, 207-14 (2011).

24.    Kruszka, P., Addissie, Y.A., Agochukwu, N.B., Doherty, E.S. & Muenke, M. Muenke Syndrome. in *GeneReviews(R)* (eds. Pagon, R.A. *et al.*) (Seattle (WA), 1993).

25.    Steiner, R.D., Adsit, J. & Basel, D. COL1A1/2-Related Osteogenesis Imperfecta. in *GeneReviews(R)* (eds. Pagon, R.A. *et al.*) (Seattle (WA), 1993).

26.    Bedeschi, M.F. *et al.* Prenatal manifestation and management of a mother and child affected by spondyloperipheral dysplasia with a C-propeptide mutation in COL2A1: case report. *Orphanet J Rare Dis* **6**, 7 (2011).

27.    Sobetzko, D., Eich, G., Kalff-Suske, M., Grzeschik, K.H. & Superti-Furga, A. Boy with syndactylies, macrocephaly, and severe skeletal dysplasia: not a new syndrome, but two dominant mutations (GLI3 E543X and COL2A1 G973R) in the same individual. *Am J Med Genet* **90**, 239-42 (2000).

28.    Kroes, H.Y., Pals, G. & van Essen, A.J. Ehlers-Danlos syndrome type IV: unusual congenital anomalies in a mother and son with a COL3A1 mutation and a normal collagen III protein profile. *Clin Genet* **63**, 224-7 (2003).

29.    Tonduti, D. *et al.* Cystic leukoencephalopathy with cortical dysplasia related to LAMB1 mutations. *Neurology* **84**, 2195-7 (2015).

30.    Mendoza, M.C., Er, E.E. & Blenis, J. The Ras-ERK and PI3K-mTOR pathways: cross-talk and compensation. *Trends Biochem Sci* **36**, 320-8 (2011).

31.    Murillo, M.M. *et al.* RAS interaction with PI3K p110alpha is required for tumor-induced angiogenesis. *J Clin Invest* **124**, 3601-11 (2014).

32.    Adapala, N.S., Barbe, M.F., Tsygankov, A.Y., Lorenzo, J.A. & Sanjay, A. Loss of Cbl-PI3K interaction enhances osteoclast survival due to p21-Ras mediated PI3K activation independent of Cbl-b. *J Cell Biochem* **115**, 1277-89 (2014).

33.    Guenther, M.K., Graab, U. & Fulda, S. Synthetic lethal interaction between PI3K/Akt/mTOR and Ras/MEK/ERK pathway inhibition in rhabdomyosarcoma. *Cancer Lett* **337**, 200-9 (2013).

34.    Castellano, E. & Downward, J. RAS Interaction with PI3K: More Than Just Another Effector Pathway. *Genes Cancer* **2**, 261-74 (2011).

35.    Tsutsumi, K., Fujioka, Y., Tsuda, M., Kawaguchi, H. & Ohba, Y. Visualization of Ras-PI3K interaction in the endosome using BiFC. *Cell Signal* **21**, 1672-9 (2009).

36. Wang, J. *et al.* Protein interaction data set highlighted with human Ras-MAPK/PI3K signaling pathways. *J Proteome Res* **7**, 3879-89 (2008).

37. Gripp, K.W., Hopkins, E., Doyle, D. & Dobyns, W.B. High incidence of progressive postnatal cerebellar enlargement in Costello syndrome: brain overgrowth associated with HRAS mutations as the likely cause of structural brain and spinal cord abnormalities. *Am J Med Genet A* **152A**, 1161-8 (2010).

38. Conway, R.L., Danielpour, M. & Graham, J.M., Jr. Surgical management of cerebellar tonsillar herniation in three patients with macrocephaly-cutis marmorata telangiectatica congenita. Report of three cases. *J Neurosurg* **106**, 296-301 (2007).

39. Segal, D., Heary, R.F., Sabharwal, S., Barry, M.T. & Ming, X. Severe holocord syrinx in a child with megalencephaly-capillary malformation syndrome. *J Neurosurg Pediatr* **18**, 79-82 (2016).

40. De Filippi, P. *et al.* Germ-line mutation of the NRAS gene may be responsible for the development of juvenile myelomonocytic leukaemia. *Br J Haematol* **147**, 706-9 (2009).

41. Kraoua, L. *et al.* Constitutional NRAS mutations are rare among patients with Noonan syndrome or juvenile myelomonocytic leukemia. *Am J Med Genet A* **158A**, 2407-11 (2012).

42. Denayer, E. *et al.* NRAS Mutations in Noonan Syndrome. *Mol Syndromol* **3**, 34-38 (2012).

43. Cirstea, I.C. *et al.* A restricted spectrum of NRAS mutations causes Noonan syndrome. *Nat Genet* **42**, 27-9 (2010).

44.     Schubbert, S. *et al.* Germline KRAS mutations cause Noonan syndrome. *Nat Genet* **38**, 331-6 (2006).

45.     Roberts, A.E. *et al.* Germline gain-of-function mutations in SOS1 cause Noonan syndrome. *Nat Genet* **39**, 70-4 (2007).

46.     Tartaglia, M. *et al.* Gain-of-function SOS1 mutations cause a distinctive form of Noonan syndrome. *Nat Genet* **39**, 75-9 (2007).

47.     Rauen, K.A. Cardiofaciocutaneous Syndrome. in *GeneReviews(R)* (eds. Pagon, R.A. *et al.*) (Seattle (WA), 1993).

48.     Nevado, J. *et al.* PIAS4 is associated with macro/microcephaly in the novel interstitial 19p13.3 microdeletion/microduplication syndrome. *Eur J Hum Genet* **23**, 1615-26 (2015).

49.     Risheg, H. *et al.* Clinical comparison of overlapping deletions of 19p13.3. *Am J Med Genet A* **161A**, 1110-6 (2013).

50.     Leegwater, P.A. *et al.* Mutations of MLC1 (KIAA0027), encoding a putative membrane protein, cause megalencephalic leukoencephalopathy with subcortical cysts. *Am J Hum Genet* **68**, 831-8 (2001).

51.     Patrono, C. *et al.* Genetic heterogeneity of megalencephalic leukoencephalopathy and subcortical cysts. *Neurology* **61**, 534-7 (2003).

52.     Mirzaa, G.M. *et al.* De novo CCND2 mutations leading to stabilization of cyclin D2 cause megalencephaly-polymicrogyria-polydactyly-hydrocephalus syndrome. *Nat Genet* **46**, 510-5 (2014).

53.     Tummala, H. *et al.* The D153del mutation in GNB3 gene causes tissue specific

        signalling patterns and an abnormal renal morphology in Rge chickens. *PLoS One* **6**,

        e21156 (2011).

54.     Goldlust, I.S. *et al.* Mouse model implicates GNB3 duplication in a childhood obesity

        syndrome. *Proc Natl Acad Sci U S A* **110**, 14990-4 (2013).

55.     Wang, Z., Liu, Z., Liu, B., Liu, G. & Wu, S. Dissecting the roles of Ephrin-A3 in

        malignant peripheral nerve sheath tumor by TALENs. *Oncol Rep* **34**, 391-8 (2015).

56.     Lee, J.H. *et al.* De novo somatic mutations in components of the PI3K-AKT3-mTOR

        pathway cause hemimegalencephaly. *Nat Genet* **44**, 941-5 (2012).

57.     Mirzaa, G.M. *et al.* Megalencephaly-capillary malformation (MCAP) and

        megalencephaly-polydactyly-polymicrogyria-hydrocephalus (MPPH) syndromes:

        two closely related disorders of brain overgrowth and abnormal brain and body

        morphogenesis. *Am J Med Genet A* **158A**, 269-91 (2012).

58.     Nakamura, K. *et al.* AKT3 and PIK3R2 mutations in two patients with

        megalencephaly-related syndromes: MCAP and MPPH. *Clin Genet* **85**, 396-8 (2014).

59.     Lindhurst, M.J. *et al.* A mosaic activating mutation in AKT1 associated with the

        Proteus syndrome. *N Engl J Med* **365**, 611-9 (2011).

60.     Ali, J.B., Sepp, T., Ward, S., Green, A.J. & Yates, J.R. Mutations in the TSC1 gene

        account for a minority of patients with tuberous sclerosis. *J Med Genet* **35**, 969-72

        (1998).

61.     Kandt, R.S. *et al.* Linkage of an important gene locus for tuberous sclerosis to a

        chromosome 16 marker for polycystic kidney disease. *Nat Genet* **2**, 37-41 (1992).

62.    Baynam, G. *et al.* A germline MTOR mutation in Aboriginal Australian siblings with intellectual disability, dysmorphism, macrocephaly, and small thoraces. *Am J Med Genet A* **167**, 1659-67 (2015).

63.    Anderson, J., Burns, H.D., Enriquez-Harris, P., Wilkie, A.O. & Heath, J.K. Apert syndrome mutations in fibroblast growth factor receptor 2 exhibit increased affinity for FGF ligand. *Hum Mol Genet* **7**, 1475-83 (1998).

64.    Chun, K., Siegel-Bartelt, J., Chitayat, D., Phillips, J. & Ray, P.N. FGFR2 mutation associated with clinical manifestations consistent with Antley-Bixler syndrome. *Am J Med Genet* **77**, 219-24 (1998).

65.    Marini, J. & Smith, S.M. Osteogenesis Imperfecta. in *Endotext* (eds. De Groot, L.J. *et al.*) (South Dartmouth (MA), 2000).

66.    Aoki, Y. *et al.* Germline mutations in HRAS proto-oncogene cause Costello syndrome. *Nat Genet* **37**, 1038-40 (2005).

67.    Lepri, F. *et al.* SOS1 mutations in Noonan syndrome: molecular spectrum, structural insights on pathogenic effects, and genotype-phenotype correlations. *Hum Mutat* **32**, 760-72 (2011).

68.    Yoon, G., Rosenberg, J., Blaser, S. & Rauen, K.A. Neurological complications of cardio-facio-cutaneous syndrome. *Dev Med Child Neurol* **49**, 894-9 (2007).

69.    Singhal, B.S., Gorospe, J.R. & Naidu, S. Megalencephalic leukoencephalopathy with subcortical cysts. *J Child Neurol* **18**, 646-52 (2003).

70.    Marchese, M., Valvo, G., Moro, F., Sicca, F. & Santorelli, F.M. Targeted Gene Resequencing (Astrochip) to Explore the Tripartite Synapse in Autism-Epilepsy Phenotype with Macrocephaly. *Neuromolecular Med* **18**, 69-80 (2016).

71.    Roessler, E. *et al.* Mutations in the human Sonic Hedgehog gene cause holoprosencephaly. *Nat Genet* **14**, 357-60 (1996).

72.    Wong, K. *et al.* A familial 7q36.3 duplication associated with agenesis of the corpus callosum. *Am J Med Genet A* **167A**, 2201-8 (2015).

73.    Yuksel-Apak, M. *et al.* A large duplication involving the IHH locus mimics acrocallosal syndrome. *Eur J Hum Genet* **20**, 639-44 (2012).

74.    Li, Z.J. *et al.* Kif7 regulates Gli2 through Sufu-dependent and -independent functions during skin development and tumorigenesis. *Development* **139**, 4152-61 (2012).

75.    Liem, K.F., Jr., He, M., Ocbina, P.J. & Anderson, K.V. Mouse Kif7/Costal2 is a cilia-associated protein that regulates Sonic hedgehog signaling. *Proc Natl Acad Sci U S A* **106**, 13377-82 (2009).

76.    Ribeiro, L.A., Murray, J.C. & Richieri-Costa, A. PTCH mutations in four Brazilian patients with holoprosencephaly and in one with holoprosencephaly-like features and normal MRI. *Am J Med Genet A* **140**, 2584-6 (2006).

77.    Derwinska, K. *et al.* PTCH1 duplication in a family with microcephaly and mild developmental delay. *Eur J Hum Genet* **17**, 267-71 (2009).

78.    Kimonis, V.E. *et al.* Clinical and radiological features in young individuals with nevoid basal cell carcinoma syndrome. *Genet Med* **15**, 79-83 (2013).

79.    Kimonis, V.E. *et al.* Clinical manifestations in 105 persons with nevoid basal cell carcinoma syndrome. *Am J Med Genet* **69**, 299-308 (1997).

80.    Twigg, S.R. *et al.* A Recurrent Mosaic Mutation in SMO, Encoding the Hedgehog Signal Transducer Smoothened, Is the Major Cause of Curry-Jones Syndrome. *Am J Hum Genet* **98**, 1256-65 (2016).

81. Ribeiro, L.A., Guerini Rde, C. & Richieri-Costa, A. Holoprosencephaly with microphthalmia, hypoplastic ears, vertebral segmentation defects, and congenital heart defects. *Am J Med Genet A* **136A**, 350-1 (2005).

82. Roessler, E. *et al.* Loss-of-function mutations in the human GLI2 gene are associated with pituitary anomalies and holoprosencephaly-like features. *Proc Natl Acad Sci U S A* **100**, 13424-9 (2003).

83. Guion-Almeida, M.L., Zechi-Ceide, R.M. & Richieri-Costa, A. Cerebro-oculo-nasal syndrome: 13 new Brazilian cases. *Am J Med Genet A* **143A**, 3252-66 (2007).

84. Fujii, K. *et al.* Frameshift mutation in the PTCH2 gene can cause nevoid basal cell carcinoma syndrome. *Fam Cancer* **12**, 611-4 (2013).

85. Evans, D.G. & Farndon, P.A. Nevoid Basal Cell Carcinoma Syndrome. in *GeneReviews(R)* (eds. Pagon, R.A. *et al.*) (Seattle (WA), 1993).

86. Ali, B.R., Silhavy, J.L., Akawi, N.A., Gleeson, J.G. & Al-Gazali, L. A mutation in KIF7 is responsible for the autosomal recessive syndrome of macrocephaly, multiple epiphyseal dysplasia and distinctive facial appearance. *Orphanet J Rare Dis* **7**, 27 (2012).

87. Enjolras, O., Chapot, R. & Merland, J.J. Vascular anomalies and the growth of limbs: a review. *J Pediatr Orthop B* **13**, 349-57 (2004).

88. Huang, W.C., Chen, Y. & Page, D.T. Hyperconnectivity of prefrontal cortex to amygdala projections in a mouse model of macrocephaly/autism syndrome. *Nat Commun* **7**, 13421 (2016).

89. Parente, D.J. *et al.* Neuroligin 2 nonsense variant associated with anxiety, autism, intellectual disability, hyperphagia, and obesity. *Am J Med Genet A* **173**, 213-216 (2017).

90. Reis, V.N. *et al.* Integrative Variation Analysis Reveals that a Complex Genotype May Specify Phenotype in Siblings with Syndromic Autism Spectrum Disorder. *PLoS One* **12**, e0170386 (2017).

91. Hazlett, H.C. *et al.* Early brain development in infants at high risk for autism spectrum disorder. *Nature* **542**, 348-351 (2017).

**Chapter Two**


# Not all Mutations in PTEN are created equally.

# Associations with Autism Macrocephaly,

# activation of mTORC2, and dominant negatives.

## Abstract

The *PTEN* gene on chromosome ten contains nine exons that code for the PTEN protein, a 403 amino acid, 47 kDA, negative regulator of PI3K/AKT/mTOR signaling. PTEN is a true tumor suppressor gene and loss of function mutations are associated with numerous sporadic cancers including, but not limited to prostate, breast, endometrial, and those in the central nervous system. In addition to its role in solid tumors PTEN plays a role in normal human development. The important regulatory function in somatic growth, brain development, and epidermal maturity is deduced from a spectrum of human phenotypes, which are caused by germ line, and in many cases *de novo,* mutations and associated syndromes. These syndromes; Cowden Syndrome, Bannayan-Riley-Ruvalcaba syndrome, and macrocephaly/autism syndrome are collectively referred to as the PTEN hamartoma tumor syndromes (PHTSs). PHTS is characterized by accelerated growth and is distinguished by the presence of specific neoplasms, epidermal phenotypes, increased head circumference (macrocephaly), developmental delays, or autism. Although there is strikingly phenotypic overlap between the syndromes there are central differences which to date have no unifying genotype-phenotype correlation. Complicating this effort there are emerging roles for PTEN dimerization, localization, and cooperation tha may contribute in varying degrees to distinct phenotypic expression. We aimed to study the role of PTEN in the macrocephaly/autism via the generation of neural progenitor cells (NPCs) from induced pluripotent stem cells (iPSCs) derived from affected patients with confirmed PTEN mutations and unaffected parental controls. We compare the signaling changes in the PI3K pathway between each patient line derived, additionally we have compared these signaling changes to those observed from CRISPR-Cas9 deletion of PTEN. From these studies we

have made numerous observations that help to elucidate the exact signaling changes that result from PTEN point mutations and deletions. From these studies we show that nuclear sparing distribution is a unique phenotype observed in extreme autism/macrocephaly cases; additionally, PTEN deletion/knockdown is associated with strong mTORC2 activation a phenomenon that has not yet been fully recognized in these syndromes. Lastly, we show that different PTEN mutations activate mTORC1 and mTORC2 differently. We believe that this is the central difference between these three classically described syndromes and furthermore that mTORC2 signaling is central to the presentation of macrocepahly/autism in the absence of neoplasms. We have tried to restore baseline PI3K/AKT/mTOR signaling levels via pharmacological interventions and show that they may respond better to a combined mTORC1/mTORC2 inhibitor TORIN-1 than the strong mTORC1 inhibitor Rapamycin. This finding is of central importance to the management and potential treatment of these cases, which based upon our data may require a personalized/precision approach.

# Introduction

### *General PTEN Function and Structure*

The phosphatase and tensin homolog, *PTEN,* gene is located on chromosome ten (HG38; 87863438-87971930) adjacent to Killin, *KLLN*, and contains nine exons that when translated, transcribe for the PTEN protein. PTEN contains 403 amino acids, the molecular weight is 47 kDA, and it has five domains. The domains including the PB (1-15), Phosphatase (15-185), C2 (185-351), Tail-PEST-PDZ (351-403) domains[1]. Functionally, PTEN is best characterized as a negative regulator of PI3K/AKT/mTOR signaling, where it's focal substrate is activated phosphatidylinositol (3,4,5)-trisphosphate (PIP3). PTEN is a phosphatase and hydrolyzes PIP3 into inactive PIP2 (phosphatidylinositol (4,5)-bisphosphate). The PIP3 secondary messenger integrates extracellular signaling into intracellular cascades, which allow the cells to adapt and respond appropriately.  This symphony is coordinated by numerous inputs, feedback loops, and redundant signaling motifs[2].  The role of cytoplasmic PTEN is largely to maintain base levels of PI3K signaling and prevent aberrant activation. PTEN also plays a role in the nucleus where it maintains genomic stability, inhibits cell cycle, and affects gene expression[3-5].

### *PTEN in Somatic Cancer*

PTEN is a classic tumor suppressor gene, as somatic loss and function mutations result in activation of downstream pathways and subsequent solid tumor formation[6].  This function has been well established in numerous cancer studies that have identified PTEN mutations in glioblastoma[7], thyroid[8], prostate[9], and breast cancers[10]. In fact, if large cancer studies are queried it is observed that PTEN mutations are very common in specific tumor types such

as uterine corpus endometrial carcinoma (67%)[11], prostate adenocarcinomas (49%)[12],

glioblastomas (41%)[13; 14], and stomach adenocarcinomas (27%)[15] (Figure 1). Also there are

specific residues of PTEN, which demonstrate overrepresentation and enrichment in

sporadic tumors (Figure 2)[1].

Figure 2-1: Domains of PTEN and specific mutations in COSMIC

Figure recreated from Chalhoub, 2009[1] analysis of the catalogue of somatic tumors in cancer (COSMIC) reveals that there are specific residues that are recurrently mutated in tumors.
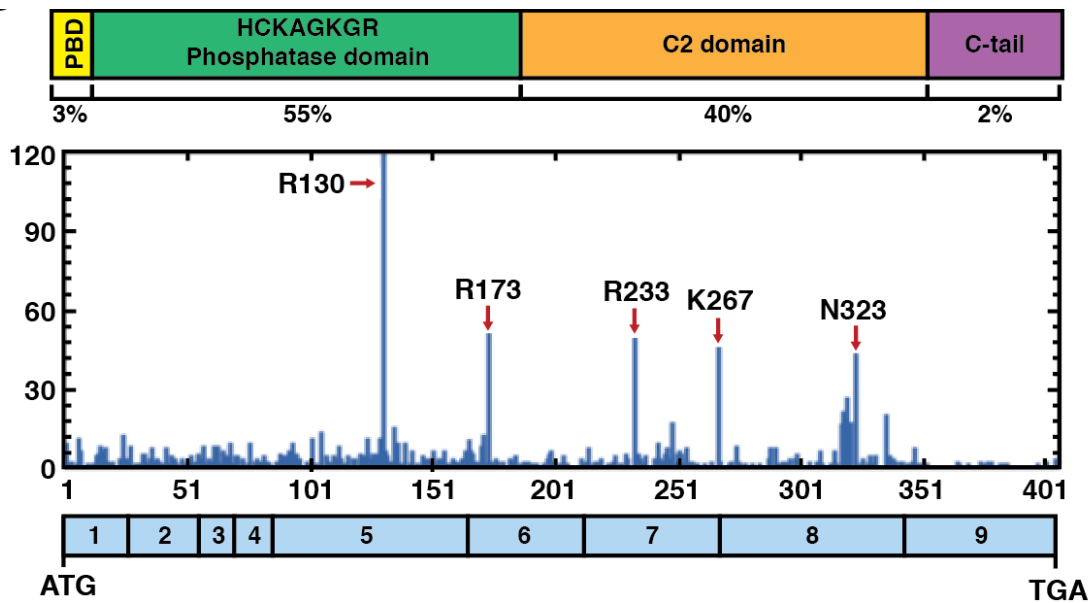
Figure 2-2: Prevalence of PTEN mutations in specific tumor types

We queried large tumor studies that collected sequencing data from cohorts of cases with tumors. We combined the data from these studies to show the prevalence of PTEN mutations in these tumor types. We have found that PTEN mutations occur in 67% of uterine corpus endometrial carcinomas [11], 49% of prostate adenocarcinomas[12], 41% of glioblastomas[13; 14], and 27% of stomach adenocarcinomas[15]

**Percentage of Cases with PTEN Mutations**
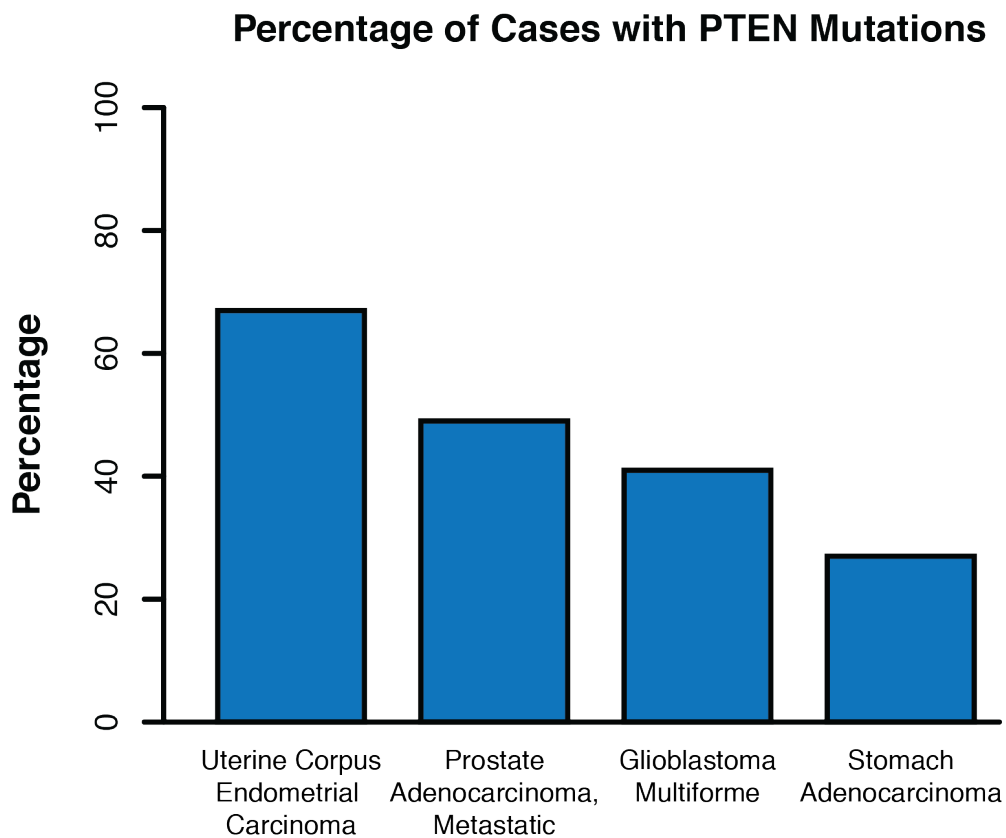
Perhaps surprisingly, tumor formation stratifies to tissues where expression of PTEN is the

highest and potentially play a critical role in growth suppression.  Using a monoclonal

antibody, Gimm et. al. explored PTEN expression in the developing human and found that it

is most highly expressed in the central nervous system, skin, and thyroid[16]. Most

interestingly, these tissues are also those affected in cases with germ line inherited or *de*

*novo* mutations in PTEN which present with well characterized syndromic phenotypes.


<u>PTEN in Syndromes</u>

It has been well established that somatic mutations in PTEN result in deregulated growth

and resulting tumors. Also, more widespread germ line mutations in PTEN are associated

with genetic overgrowth syndromes. Collectively, these syndromes are referred to as the

PTEN Hamartoma Syndromes and are clinically unified by the presentation of somatic

and/or brain overgrowth each; however, varying degrees of cancer predisposition,

behavioral phenotypes, and associated epidermal manifestations that makes them distinct.


*Cowden Syndrome*

Cowden syndrome (CS1, MIM: 158350) was first described and recognized as a clinical

syndromic entity in 1963[17]. However, the link to PTEN mutations was not established until

14 years later in 1997[18]. This syndrome is largely characterized by cancer predisposition

which manifests as increased lifetime risks of specific tumor types including breast (25-

50%), endometrial (2-28%), renal (34%), colon (9-16%), thyroid (3-17%) and melanoma

(6%)[18].  Outside of neoplastic findings there are major phenotypic features that define this

syndrome including increased head circumference (macrocephaly), macular pigmentation on the glans of the penis, and mucocutaneous lesions (including trichilemmomas, palmoplantar pits, hyperkeratotic papules, neuromas, and papillomas). Less common minor diagnostic criteria include lipomas, vascular abnormalities, esophageal glycogenic acanthosis, autism spectrum disorder, and intellectual disability[18].

*BRRS Syndrome*

Bannayan-Riley-Ruvalcaba syndrome (BRRS, MIM: 152480) was first described in 1971 as a syndrome of overlapping angiomatosis, lipomatosis, and macrocephaly[19].  The genetic etiology was first mapped in 1997 to the region of 10q23[20] and then refined to the location of the PTEN gene via the study of a case with a deletion incorporating the gene[21].  The association of PTEN mutations in this syndrome was subsequently solidified via more sensitive sequencing methods[22; 23].  The phenotypic presentation has been expanded from the classic triad of angiomatosis, lipomatosis, and macrocephaly to include intestinal hamartomatous polyps and developmental delay[24]. There is significant clinical overlap with CS1 which have led some to suggest that they are "allelic[21]" or perhaps even a single entity[25]. Supporting this latter claim there is truly no unifying genotype-phenotype correlation between the two disorders. For example mutations associated with CS1 do not cluster in known functional domains and are not enriched for truncating or missense mutations. One PTEN associated phenotype that is clinically distinct however is PTEN associated macrocephaly/autism[25].

*Macrocephaly/Autism*

Macrocephaly/autism syndrome (MIM: 605309) has been more recently described with the first suspected cases identified in 1991[26] and 2000[27]. However, at that time their behavioral phenotypes were not diagnosed as autism but instead described as major delays in social and language development without accompanying delays in motor function, which was deemed "autistic." In 2005 the genetic etiology was confirmed with the largest cohort of patients to date, which identified mutations in PTEN and also made the observation that in many cases there was extreme macrocephaly (>3SD, overall range 2.5-8SD above the mean)[28].  We have also described a cohort of patients (33) with the macrocepahly/autism phenotype.  Within this cohort we were able to identify mutations in PTEN. Similar to the findings of Butler et. al we find that the cases with PTEN mutations all display extreme macrocephaly, and furthermore overwhelmingly demonstrate somatic overgrowth with height and weight also being above the 95th percentile[29].

Table 2-1:  Genetic and Phenotypic findings in patients with autism macrocephaly

This previously reported cohort[29] shows the recurrent prevalence of PTEN mutations in autism macrocephaly. Additionally, the PTEN patients in this cohort demonstrate extreme macrocephaly. We have derived iPSCs from patients 2 and 3 in this cohort.

| | Individuals with confirmed PTEN Mutations | | | | | ADM (Autism with Disproportionate Macrocephaly) | | | | | | | | | |
|---|---|---|---|---|---|---|---|---|---|---|---|---|---|---|---|
| Number | 1 | 2 | 3 | 4 | 5 | 6 | 7 | 8 | 9 | 10 | 11 | 12 | 13 | 14 | 15 |
| Gender | M | M | M | M | M | M | M | M | M | F | M | M | F | M | M |
| Age | 15 years | 3 years | 4 years | 2 years 6 months | 4 years 4 months | 18 years 11 months | 17 years | 5 years 4 months | 3 years | 3 years 2 months | 6 years 11 months | 17 years 6 months | 7 years | 2 years 8 months | 2 years 9 months |
| Height cm (%ile) | 169 (50) | 102 (>95) | 125.6 (>95) | 99 (>95) | 106.8 (75) | 158 (<5) | 168.3 (15) | 106.5 (20) | 92.5 (25) | 91.8 (25) | 117.5 (25) | 174.5 (48) | 123 (53) | 92 (50) | 95 (60) |
| Weight kg (%ile) | 62.6 (74) | 17.4 (95) | 24.8 (>95) | 13.2 (50) | 18.7 (80) | 91.8 (93) | 73.6 (76) | 17.3 (25) | 14.3 (50) | 14.2 (50) | 35.8 (>95) | 61.9 (30) | 26.5 (80) | 14.5 (73) | 16.6 (95) |
| HC cm (%ile) | 58.5 (>99.7) | 56 (>99.7) | 56 (>99.7) | 55.5 (>99.7) | 53 (92) | 62.5 (>99.7) | 57.3 (85) | 53 (87) | 53 (>97) | 51 (92) | 53.5 (85) | 58 (91) | 54 (>97) | 51 (85) | 53 (>97) |
| HC SD | >3 | >3 | >3 | >3 | 1–3 | >3 | 1–3 | 1–3 | 1–3 | 1–3 | 1–3 | 1–3 | 1–3 | 1–3 | 1–3 |
| HT/HC %ile | .5 | .98 | .98 | .96 | .82 | .05 | .18 | .23 | .25 | .27 | .29 | .53 | .55 | .59 | .62 |
| Hypotonia | – | + | – | – | – | + | + | + | + | + | – | – | + | – | + |
| Flat Nasal Bridge | – | – | – | – | – | + | + | + | – | – | + | – | + | – | – |
| Clinodactyly | – | – | – | – | – | – | – | – | – | + | – | + | – | – | – |
| CMA | ? | ? | ? | ? | – | ? | dup6 q23.2 | – | – | – | – | – | – | – | ? |
| PTEN | P38H | R130X | Y68N | R130L | V255A | – | – | – | – | – | – | – | – | – | ? |

| | ARM (Autism with Relative Macrocephaly) | | | | | | | | | | | | AMSO (Autism Macrocephaly with Somatic Overgrowth) | | | | | |
|---|---|---|---|---|---|---|---|---|---|---|---|---|---|---|---|---|---|---|
| Number | 16 | 17 | 18 | 19 | 20 | 21 | 22 | 23 | 24 | 25 | 26 | 27 | 28 | 29 | 30 | 31 | 32 | 33 |
| Gender | F | F | M | F | M | F | M | M | M | M | M | M | M | F | M | M | M | M |
| Age | 7 years 10 months | 2 years 7 months | 3 years 1 months | 4 years 7 months | 3 years 10 months | 2 years 7 months | 7 years | 3 years 8 months | 4 years 8 months | 6 years | 1 years 6 months | 3 years 2 months | 3 years | 3 years 6 months | 14 years 4 months | 3 years 1 months | 4 years 1 months | 6 years 11 months |
| Height cm (%ile) | 129 (74) | 94 (75) | 98 (73) | 107.5 (74) | 104 (76) | 94.6 (85) | 126.7 (80) | 104.5 (89) | 112 (89) | 120 (80) | 87.5 (95) | 102 (93) | 113 (>95) | 109.8 (>95) | 181.3 (>95) | 104.8 (>95) | 116.7 (>95) | 140.3 (>95) |
| Weight kg (%ile) | 32.3 (91) | 17.6 (>95) | 16.8 (91) | 17.5 (50) | 17.2 (80) | 17.5 (>95) | 24.9 (74) | 18.4 (92) | 21 (90) | 23.3 (80) | 13.1 (80) | 17.1 (90) | 35 (>95) | 20.3 (>95) | 70.3 (92) | 19 (>95) | 22.2 (>95) | 56.7 (>95) |
| HC cm (%ile) | 55.5 (>97) | 53 (>97) | 52 (93) | 52.5 (95) | 53 (96) | 55.5 (>99.7) | 54 (90) | 54 (>97) | 54 (>97) | 53.5 (90) | 52.5 (>99.7) | 52.5 (96) | 55 (>99.7) | 52 (>97) | 57.5 (96) | 53 (>97) | 54.5 (>97) | 56 (>97) |
| HC SD | + | + | + | + | + | >3SD | + | + | + | + | >3SD | + | >3SD | + | + | + | + | + |
| HT/HC %ile | .76 | .77 | .79 | .79 | .79 | .85 | .89 | .91 | .91 | .89 | .95 | .97 | .98 | .98 | .98 | .98 | .98 | .98 |
| Hypotonia | – | – | + | – | – | + | – | – | – | – | – | – | – | – | – | + | – | – |
| Flat Nasal Bridge | + | – | – | + | – | – | – | – | – | – | – | – | + | – | – | – | + | – |
| Clinodactyly | – | – | – | – | + | – | – | + | – | + | + | + | + | – | – | – | – | – |
| CMA | ? | – | ? | – | – | ? | – | – | – | ? | del10 q24.32 | – | ? | – | – | – | – | – |
| PTEN | – | ? | ? | ? | – | ? | – | – | ? | ? | ? | ? | ? | – | ? | – | – | – |

CMA, chromosomal microarray; HC, head circumference; HT, height; %ile: percentile; ?, unknown; +, feature present; –, normal or not present; SD, standard deviation.

Similar to CS1 and BRRS, there does not seem to be a genotype-phenotype correlation

within autism macrocepahly cases that may explain the divergence of this syndromic

entity. There is a single report which claims that "autism-associated" PTEN mutations are

less severe than those associated with "severe PHTS" in that the "autism-associated"

mutations are less likely to be complete loss of function frame shift and nonsense.

Furthermore, retain some ability to suppress AKT signaling[30]. While the results of this

study are suggestive, they do not take into account the recurrent observation of complete

loss of function frameframe shift and nonsense mutations in macrocephaly autism cases,

including the R130X mutation from our report[30] and in others[31].  It is possible that the

newly emerging data on PTEN homo-dimer formation and localization provides additional

insight into the role of PTEN mutations and the spectrum of phenotypic manifestations.


### *PTEN Forms Catalytically Active Homo-Dimers*

It has been recently described that PTEN forms homo-dimers both in solution[32] and in the

living cell[33].  Most interestingly, these dimers are catalytically active and formation is

controlled partly through the phosphorylation of the C-terminal tail. It has been shown that

dimers, which contain a mutated partner, are catalytically inactive. Thus, mutations that

cause loss of phosphatase activity but maintain an intact C-terminal tail can exert a

dominant negative effect[33] (Figure 3). In addition to the dominant negative effects,

mutations may disrupt residues that are essential for trafficking signals where PTEN is

shuttled between the membrane, cytoplasm and nucleus.

Figure 2-3: PTEN can act in a dominant negative or true heterozygous mechanism

Based upon the emerging data that PTEN forms catalytically active homo dimers *in vitro* and *in vivo,* we present three states of PTEN function. In the wild-type setting all copies of PTEN protein are functional and able to form active homodimers. When a dominant negative copy of PTEN protein is made it randomly can form homo dimers with either wild-type functional copies or other negative copies. This dominant negative mechanism results in the decreased availably of functional homo dimers. In settings of true loss of function frame shift and nonsense mutations, homo dimer formation with mutant PTEN is not possible. Therefore there, are no catalytically dead homo dimers; Rather, there is a reduced frequency of functional complexes (LOF=Loss of Function).



93
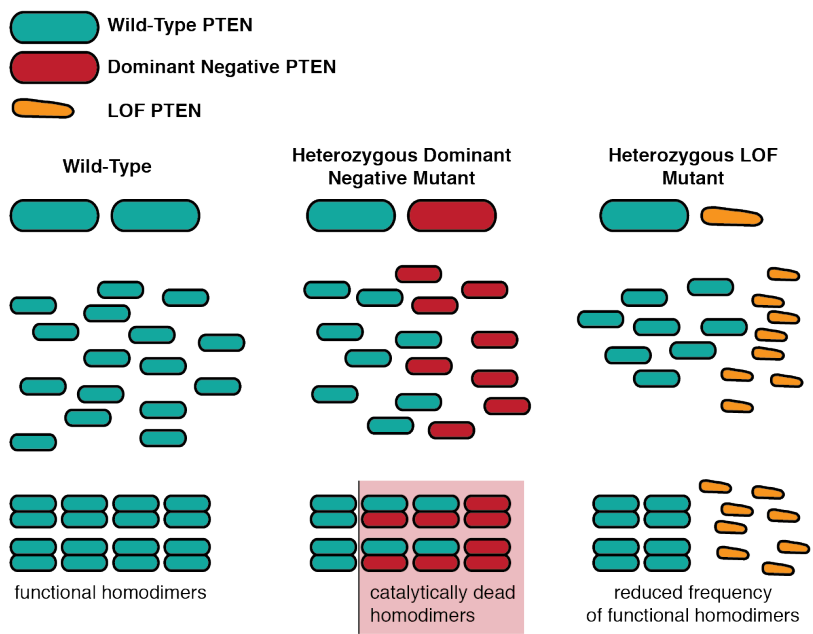
PTEN can be found in three main cellular locations. Cytoplasmic PTEN is the most conventionally discussed and its role in suppression of AKT signaling is well understood. In addition, it can transiently associate with the plasma membrane, which is stabilized by interactions between acidic motifs in phospholipids with basic amino acid motifs throughout the PTEN protein. In the membrane, PTEN can interact with PIP2 via a binding site on the N-terminus[34; 35]. Alternatively PTEN can be localized in the nucleus, which is mediated via a nuclear localization signal, which includes ubiquitination on the N-terminus in the C2 Domain and SUMOylation in the C2 Domain (Figure 4). A number of cellular stressors including radiation causes PTEN to exit the nucleus. However, posttranslational modifications may additionally regulate the location of PTEN in a biologically relevant manner[36] (Figure 5). To better understand the role of PTEN mutations in the autism/macrocepahly phenotype we aimed to model them via three approaches (1) Crispr/Cas9 deletion, (2) viral knockdown, and (3) generation of NPCs from iPSCs of affected patients.

Figure 2-4: Nuclear localization signals and protein modifications of PTEN

Figure recreated from Chalhoub, 2009[1] phosphorylation, ubiquitination on the N-terminus in the C2 Domain and SUMOylation in the C2 Domain coordinate the nuclear localization signal on PTEN.
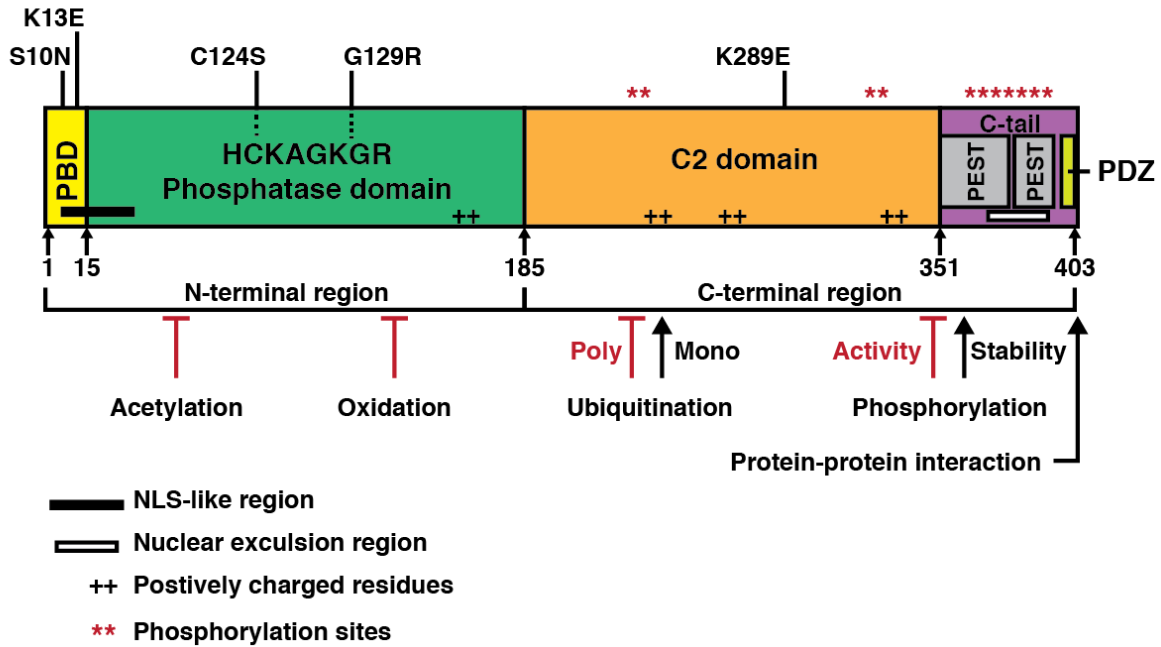
Figure 2- 5: Cytoplasmic and nuclear roles of PTEN

In the cytoplasm, PTEN acts a negative regulator or the PI3K/AKT pathway via its
phosphatase activity on PIP3. When translocated to the nucleus PTEN plays additional
roles in chromatin remodeling, cell cycle, double stranded break repair, and centromere
stability
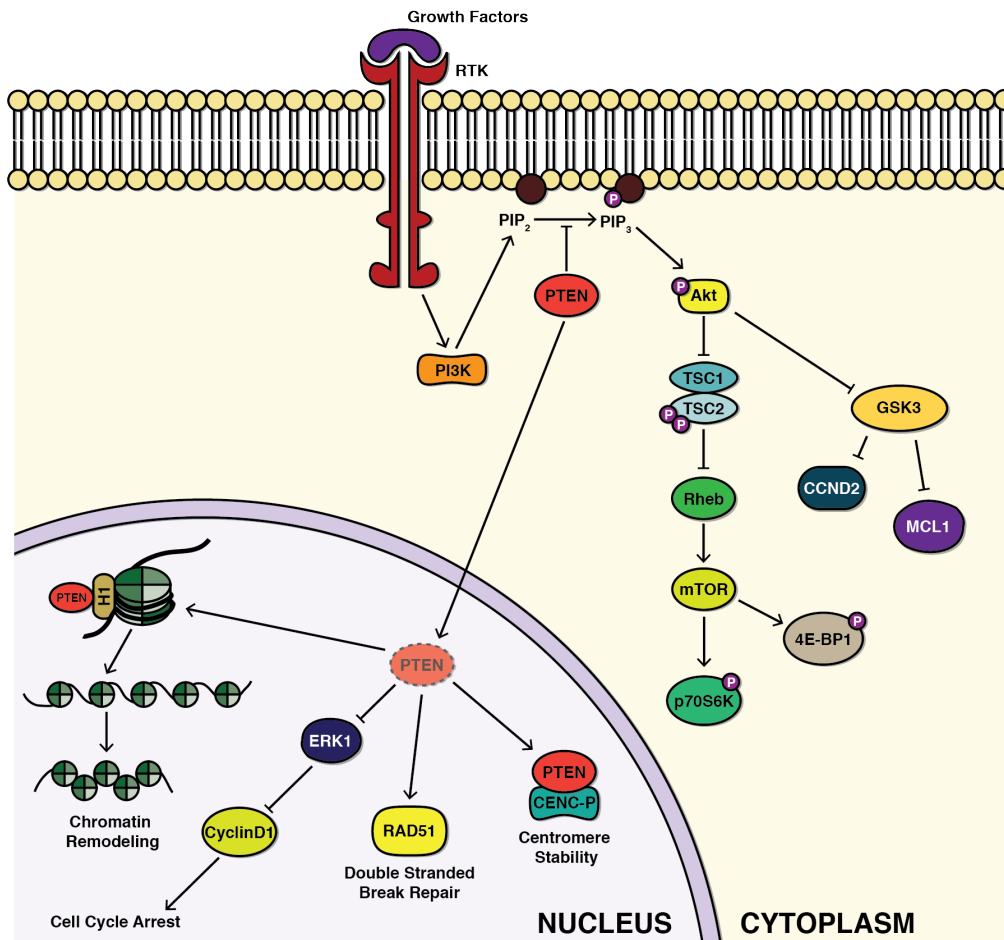
We aimed to explore the exact molecular mechanism of PTEN mutations via Crispr/Cas9 deeletion in human neural stem cells and generation of neural stem cells from affected patients.

## Materials and Methods:

### *Crispr/Cas9 Cloning*

*PTEN and GSK3B* were deleted from HEK293T cells utilizing the Crispr/Cas9 plasmid (pSpCas9(BB)-2A-Puro (PX459) V2.0, #62988[37]) from addgene.   Guide RNAs (gRNAs) were designed using Benchling software. gRNAs were selected based on which showed the highest "on-target" score[38] and "off-target" score[39]. The 20Bp gRNAs were flanked with CACC-on the 5'end of their forward oligo and AAAC- on the 5'end of their reverse oligo. These overhangs facilitate ligation into the parental plasmid once it is digested with BbsI. Briefly the oligos were annealed and phosphorylated using T4 PNK enzyme (NEB, M0201S), annealed oligos were then diluted an added to a digestion-ligation reaction containing parental plasmid, tango buffer (Life Tech, By5), DTT, ATP, BbsI (Thermo, FD1014) and T7 Ligase (NEB, M03185). After six cycles of $37^0C$ for five minutes and $23^0C$ for 5 min the reaction was treated with plasmid safe exonulease (Epicentre, E3101K). Finally plasmids were transformed in Stbl3 E.Coli and grown under ampicillin selection. Plasmid mini-preps were performed on three colonies and sanger sequencing confirmed the cloning event using the human U6 primer sequence: 5'-CGATACAAGGCTGTTA-3'.

gRNA Sequences:

| ID | Sequence |
|---|---|
| PTEN Upstream 2 F | 5'-**CACC**-GGTGGGTTATGGTCTTCAAA-3' |
| PTEN Upstream 2 R | 5'-**AAAC**-TTTGAAGACCATAACCCACC-3' |
| PTEN Downstream 1 F | 5'-**CACC**-GAGAGGCCCTAGATTTCTATG-3' |
| PTEN Downstream 1 R | 5'-**AAAC**-CATAGAAATCTAGGGCCTCTC-3' |
| PTEN Downstream 2 F | 5'-**CACC**-GATTCACTGTAAAGCTGGAAA-3' |
| PTEN Downstream 2 R | 5'-**AAAC**-TTTCCAGCTTTACAGTGAATC-3' |
| GSK3B Upstream 1F | 5'-**CACC**-GAAAAGGAGTGAAAAGCCAAG-3' |
| GSK3B Upstream 1R | 5'-**AAAC**-CTTGGCTTTTCACTCCTTTTC-3' |
| GSK3B Downstream 1 F | 5'-**CACC**-GGTTTCTTATTTTAAGGGCG-3' |
| GSK3B Downstream 1 R | 5'-**AAAC**-CGCCCTTAAAATAAGAAACC-3' |

### *HEK293T Cell Culture and Transfections:*

Cells were maintained with basal media including DMEM, PSN and 10% fetal bovine serum (FBS). Twenty-four hours before transfection cells were liberated from T25 flask with TrypLE™ Express Enzyme (1X). Cell concentration and viability was determined with the Invitrogen Countess I. After plating $2x10^5$ viable cells onto a 12-well culture dish, volume was brought to 1ml of basal media. On the day of transfection media was aspirated, and 500ul of basal media was added to each well. GeneIn Transfection reagent was combined with 2ug of plasmid, brought to a final volume of 200ul, vortexed and then incubated at room temperature for 15 minutes then added to each well. Cells were incubated for 24 hours, followed by a 12-hour nutrient starvation in DMEM lacking glutamine, glucose and FBS.

*Crispr/Cas9 mRNA approach in ipNPCs*

Due to a lack of transfection efficiency of plasmids we switched methodologies to achieve genome editing in ipNPCs. Cas9 and gRNA mRNAs are transfected in combination as follows:  Cells were maintained in basal media composed of NeuralX  NSC Medium, GlutaGro, MEM nonessential amino acids, GS22 Neural Supplement, FGF/EGF, and LIF. 24 hours before transfection, cells were liberated from T75 flask with 5ml of TrypLE™ Express Enzyme (1X) and replated onto a LDEV-free, Geltrex coated T75 flask. On the day of transfection, cells were liberated from T75 flask with 5ml of  TrypLE™ Express Enzyme (1X).Cell concentration and viability were determined with the Invitrogen Countess I. After cells were counted, 500ul of basal media were added to each well of a 24-well culture dish and $7.0 \times 10^4$ viable cells were added. After adding the cells, 2ul of EditPro Stem transfection reagent, 65ng of Cas9 mRNA, and 50ul of OptiMem were added. 24 hours after the cells were transfected with Cas9 mRNA, 2ul of EditPro Stem transfection reagent, 50ng of each guide RNA, and 50ul of OptiMem were added to each well. Cells were incubated for 24 hours prior to analysis.

gRNA mRNA Sequences:

| ID | Sequence |
|---|---|
| PTEN Upstream 2 F | 5'- GGTGGGTTATGGTCTTCAAA-3' |
| PTEN Downstream 1 F | 5'- GAGAGGCCCTAGATTTCTATG-3' |
| PTEN Downstream 2 F | 5'- GATTCACTGTAAAGCTGGAAA-3' |

To model PTEN loss we chose to analyze populations of cells which had been edited,

instead of clonally expanding individual cell lines (Figure 6).

Figure 2-6: Experimental design for generation of PTEN deletion populations in

HEKS293Ts

Guide RNAs (gRNAs) were designed using benching software, which maximizes efficiency

and mina mizes off target effects. These gRNAs are then cloned into parental Crispr

plasmids that additionally carry puromycin selection. Follow transfection and selection we

analyzed populations of cells, which are advantageous because of the few passages

required which allow the cells less time to compensate, and biological differences to be
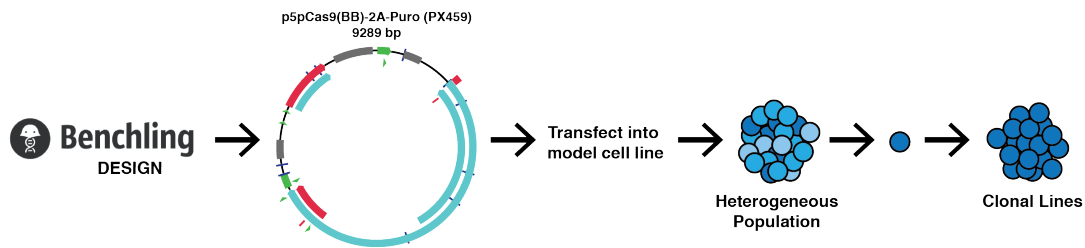
observed.



| Clonal Lines | "Population Studies" |
| --- | --- |
| Timely | Fast |
| Multiple Passages | Few Passages |
| Allows time for compensation | Compensation is less likely as cells are analyzed with 2 passages |

*Patient Enrollment*

Patients were referred to determine the genetic etiology of their pathology. Key factors, which led to PTEN testing were autism with head circumference greater than the 95th percentile, history of pediatric neoplasms, or freckling of the glans of the penis. Genetic testing was ordered to sequence all exons of PTEN in either a gene-specific or whole exome format. For this study, patients and parents were asked to sign an IRB approved consent form covering the generation of iPSCs and analysis for research purposes. Unaffected non-carrier parents will be enrolled to serve as controls for each case.

*Sample Collection*

Venipuncture was performed by trained personnel at UCLA. Two CPT tubes containing 8 ml of blood were drawn for each participant. Specimens were centrifuged, screened for blood-borne diseases (HBV, HCV, HIV) and placed on ice.

*iPSC Generation*

We used a non-integrating system to avoid random insertion of proviral DNA into the genome to generate the patient iPSC lines. Specifically, a combination of episomal plasmids containing the reprogramming factors Oct-4, Sox-2, Klf-4, L-Myc, Lin-28, SV40 Large T Antigen ("SV40LT"), and short hairpin RNAs targeting p53 ("shRNA-p53") were utilized in a defined reprogramming media (Figure 7).

*Generation and characterization of NSCs from iPSCs*

Following generation of iPSCs, we generated forebrain, cortex-like neural progenitor cell

cultures. We used an adaptation of a protocol for the differentiation of cortical

progenitors[31].  The Pax6/Nestin positive neural stem cells were expanded in EGF and bFGF

to generate neurospheres prior to use. We verifed that each culture contained multipotent

neural stem cells, clonal neurospheres will be differentiated in the absence of mitogens and

cells stained for neural and glial markers, including markers of glutamatergic and

GABAergic neurons (Figure 8).

Figure 2-7: Generation of ipNPCs from autism macrocephaly patients

CPT tubes were drawn for each participant. From the blood samples, mono-nucleated cells were isolated and reprogramed using episomal plasmids containing the reprogramming factors Oct-4, Sox-2, Klf-4, L-Myc, Lin-28, SV40 Large T Antigen ("SV40LT") and short hairpin RNAs targeting p53 ("shRNA-p53"). From the iPSCs, we generated forebrain, cortex-like neural progenitor cell cultures (ipNPCs)



.
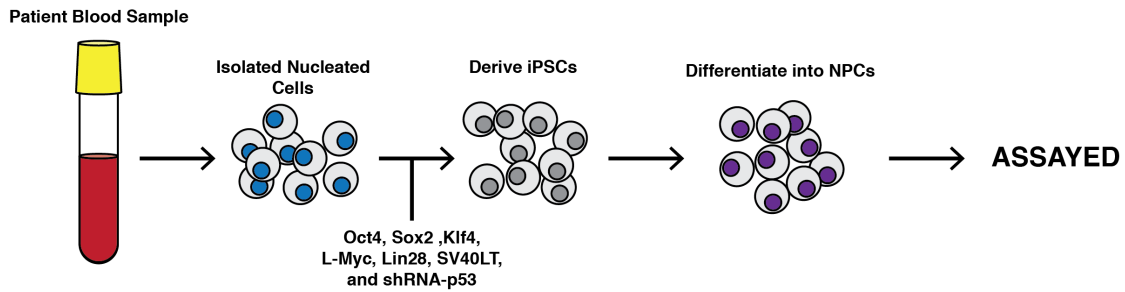
Figure 2-8: Validation of ipNPC cell identity

We use the markers Pax6 and Nestin to confirm that the cells were progenitors.

Additionally, we confirmed that the cultures contained multipotent neural stem cells by

assaying the ability of clonal neurospheres to differentiate in the absence of mitogens.
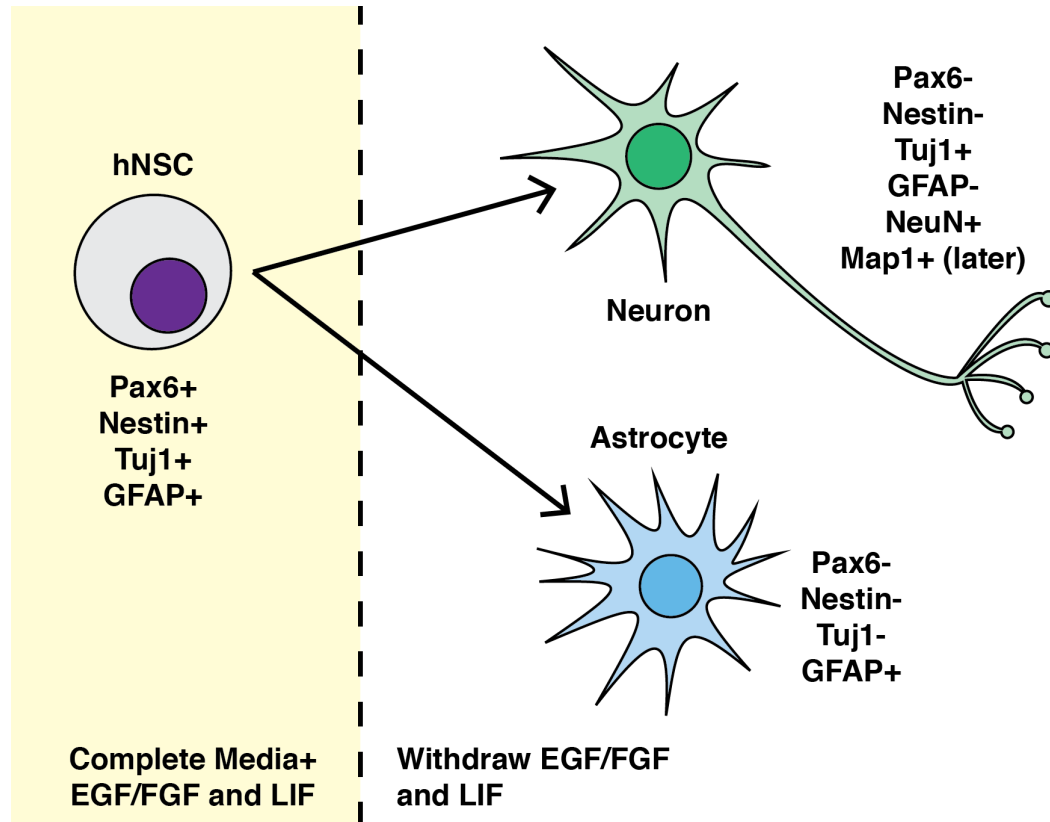
*Confirmation of Patient Mutations*

All exons of PTEN were amplified via PCR and then Sanger sequenced. Traces were
manually screened for the presence of mutations, which were then mapped to the human
genome to predict cDNA and Protein changes.

| PTEN Sequencing Primers | |
|---|---|
| **PTEN1FWD1:** | ACA TTT TGC TGC CGG TCA ATT ATT CGT CTT CTC CCC ATT CCG |
| **PTEN1REV1:** | TCC TTT GTC GAT ACT GGT AAA GAA AGC AAT CGG TGG CTT GA |
| **PTEN2FWD1:** | ACA TTT TGC TGC CGG TCA ACC TGA ATA CTG TCC ATG TGG AAG TTA CC |
| **PTEN2REV1:** | TCC TTT GTC GAT ACT GGT ACA AAT GAA CTG TAT CCC CCT GAA GTC |
| **PTEN3FWD1:** | ACA TTT TGC TGC CGG TCA AAC CCA TAG AAG GGG TAT TTG TTG G |
| **PTEN3REV1:** | TCC TTT GTC GAT ACT GGT AGC TCT TGG ACT TCT TGA CTT AAT CGG |
| **PTEN4FWD2:** | ACA TTT TGC TGC CGG TCA GTG GCA TCA CAA GTT TTT AAG CA |
| **PTEN4REV2:** | TCC TTT GTC GAT ACT GGT ATC TCA CTC GAT AAT CTG GAT GAC TCA TT |
| **PTEN5FWD1:** | ACA TTT TGC TGC CGG TCA TCC GTA TAG CGT AAA TTC CCA GA |
| **PTEN5REV1:** | TCC TTT GTC GAT ACT GGT ACA GAT CCA GGA AGA GGA AAG GAA AA |
| **PTEN6FWD1:** | ACA TTT TGC TGC CGG TCA GAG CGC TGT TGT GAC CTT TGA ATA A |
| **PTEN6REV1:** | TCC TTT GTC GAT ACT GGT AGA ATT GGG CTG TAT TTG GTG GTT |
| **PTEN7FWD1:** | ACA TTT TGC TGC CGG TCA GGA CCT TAT TTT GAA GGT TCA AAC TGG AG |
| **PTEN7REV1:** | TCC TTT GTC GAT ACT GGT AGT TAC AAT GCC ATA AGG CCT TTT CC |
| **PTEN8FWD2:** | ACA TTT TGC TGC CGG TCA TGC AAC AGA TAA CTC AGA TTG CC |
| **PTEN8REV2:** | TCC TTT GTC GAT ACT GGT ACT TTT TTG ACG CTG TGT ACA TTG GG |
| **PTENEX9 FWD:** | ACA TTT TGC TGC CGG TCA AGA GGG TCA TTT AAA AGG CCT C |
| **PTENEX9REV:** | TCC TTT GTC GAT ACT GGT AAG TGT CAA AAC CCT GTG GAT GT |
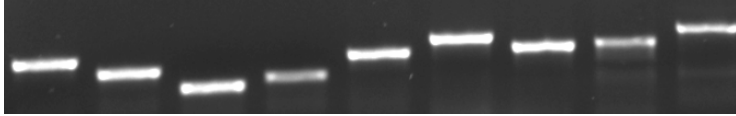
PCR showing amplification of all exons in PTEN for sequencing


*Western Blot Analysis*

Cells were lysed on 24 well or 12 well plates in 200µl or 400ul of passive lysis buffer,

prepared with phosphatase and protease inhibitors, and incubated by shaking at $4^0$C for

one hour. After lysis tubes were spun at 7500 Rcf for 5 minutes to collect debris.

Supernatant was transferred to a new tube then protein concentration determined with the

Coomassie Plus Bradford (Life Technologies) reagent following manufacture instructions.

Protein samples were diluted to a final concentration of 10µg/20 µl into Western loading

buffer with beta-mercaptoethanol and then boiled for 5 minutes.  Western blots were run

on 12% acrylamide gels followed by transfer onto nitrocellulose membranes utilizing the

Transblot Turbo® apparatus from Biorad. The membrane was blocked in 5% bovine

serum albumin in Tris buffered saline plus Tween (TBST) for 30 minutes, then incubated in

primary antibodies (Listed Below) for 24 hours. Blots were then rinsed with Tris buffered

saline (TBS) and washed three times with TBST. Blots were then incubated in rabbit or

mouse secondary antibodies conjugated to horseradish peroxidase at a dilution of 1/3750.

Following secondary incubation membranes were rinsed with TBS then washed twice with

TBST. Blots were exposed using Western Clarity reagents from BioRad and imaged on the

Bio Rad ChemiDoc and viewed in ImageLab Software.


| Antibodies |
|---|

| Antibody | Manufacturer | Cat # | Dilution |
|---|---|---|---|
| pmTOR 2448 | Cell Signaling | 5536 | 1:1000 |
| AKT 473 | Cell Signaling | 4060 | 1:2000 |
| B-actin | Cell Signaling | 4970 | 1:4000 |
| p4EBP1 S65 | Cell Signaling | 9451 | 1:1000 |
| PTEN | Cell-Signaling | 9188 | 1:1000 |
| pTSC2 | Cell-Signaling | 3611 | 1:2000 |
| pGSK3a/b | Cell-Signaling | 9331 | 1:1000 |
| pPTEN | Cell-Signaling | 9551 | 1:1000 |
| pAKT308 | Cell-Signaling | 13038 | 1:1000 |
| pAKT450 | Cell-Signaling | 9267 | 1:1000 |
| P4EBP1 | Cell-Signaling | 2855 | 1:1000 |
| pmTOR2481 | Cell-Signaling | 2974 | 1:500 |
| pS6Kinase | Cell-Signaling | 9234 | 1:1000 |
| pSGK(Ser422) | Santa Cruz | Sc-16745 | 1:200 |
| pRAPTOR (Ser792) | Cell-Signaling | 2083 | 1:1000 |

*Statistical Analysis*

Western blots were run in biological sextets, which gave us the power to perform Mann-Whitney U tests for non-parametric data. The p-values for these tests were Bonferroni corrected for multiple tests in the event of numerous comparisons.

*Immunofluorescence*

One hundred thousand human neural stem cells were plated on GelTrex (Invitrogen) coated coverslips. After 24 hours of growth cells were fixed using paraformaldehyde for 20 minutes then blocked with 10% normal goat serum in TBST overnight. The following day,

coverslips were washed three times in TBST. Coverslips were incubated in primary

antibody (listed below) in 3% BSA in TBST for one hour. Coverslips were then washed

three times in TBST and incubated in secondary antibody (Jackson Laboratories, AffiniPure

Donkey Anti-Rabbit, 711-165-152, Dilution 1/1000 and Invitrogen, Alexa Fluor® 647

Phalloidin, A22287, dilution 1/100) in 3% BSA in TBST for one hour. Coverslips were then

washed three times in TBST and then three times in water. Coverslips were mounted on

glass slides using ProLong® Gold Antifade Mountant with DAPI (Invitrogen, P36931).

Slides were imaged using a Zeiss LSM-800.

| Staining | | | |
|----------|--------------|-------------|----------|
| **Antibody** | **Manufacturer** | **Cat #** | **Dilution** |
| PTEN | Cell Signaling | 9188 | 1:500 |
| Phalloidin 647 | Thermo | A22287 | 1:250 |
| Rb-Cy3 | Jackson | 711-165-152 | 1:1000 |
| Ms-DL469 | Jackson | | 1:4000 |

## Results

*Deletion of PTEN from HEK293Ts*

We first modeled loss of PTEN in HEK293T cells. Following transfection of PTEN gRNA

plasmids and 48-hour puromycin selection, we confirmed PTEN deletion via PCR analysis

utilizing a primer set, which flanks the cut sites. We observed the presence of an edited

band in addition to the wild type band. This band is of the expected size, which confirms

that the Crispr/Cas9 system is cutting efficiently and correctly (Figure 9a). We then wanted

to assay how the pathway activation of PTEN+/- cells vs wildtype cells which have only

received the empty Crispr/Cas9 plasmid lacking any cloned guide RNA.  Protein extracts

from these cells were then subjected to western blot analysis, which demonstrated that the

PTEN+/- cells have increased phosphorylation of mTORC2-associated targets including

pAKT473, pAKT450 and pSGK1-422 (Figure 9b-c). There was no increase in the mTORC1

targets assessed including p4EBP1 37/46 and pmTOR2448 (Figure 9b-c).  We then assayed

the activation of GSK3α/β in these cells and show that there is strong activation of both

proteins via loss of their inhibitory phosphorylation events at Ser21 and Ser9 respectively

(Figure 9d). We observed an increase in the autophagy component LC3A (Figure 9d) To

better understand the interplay between GSK3B and mTORC2 we engineered GSK3B$^{(+/-)}$

interestingly these show decreases in mTORC1 substrates and markers including

pmTOR2448 and p4EBP1, however show an increase in the mTORC2 target pAKT473.

Figure 2-9: Deletion of PTEN and GSK3B from HEK293T Cells

(a) PCR showing deletion of critical exon 5 in PTEN (b) western blot analysis of PTEN$^{(+/-)}$ cells which demonstrate increased mTORC2 targets including pAKT473, pAKT450, and pSGK1(422) (c) Quantification of western blots, standard deviations are shown with black vertical bars, * denotes significant difference <.05 (d) Western blot analysis showing that PTEN$^{(+/-)}$ cells have less pGSK3a(Ser21) and pGSK3b (Ser9) (e) proposed model for decreases in GSK3a/b activity (f) PCR showing deletion of critical exon 1 and 5' UTR in GSK3B (g) western blot showing consequence of GSK3B loss including increased pAKT473, decreased pmTOR2448, and p4EBP1(37/46).

To explore the effect of PTEN loss on brain progenitor cells we modified our approach to genetically engineer PTEN loss in induced pluripotent derived neural progenitors. These cells do not transfect with circular DNA plasmids with high enough efficiency to be conducive for Crispr/Cas9. Therefore we used an mRNA Crispr/Cas9 system where the Cas9 mRNA is transfected along side gRNA mRNAs. To establish this approach we first validated that ipNPCs can be transfected with GFP mRNA (Figure 10a). We then confirmed that these cells express Cas9 when transfected with Cas9 mRNA (Figure 10b). Finally we transfected Cas9 with both gRNA mRNAs we observed the presence of an edited band in addition to the wild type band. This band is of the expected size, which confirms that the Crispr/Cas9 system is cutting efficiently and correctly (Figure 10c). We then wanted to assay how the pathway activation of PTEN+/- ipNPCs versus wildtype cells which have only received Cas9 or gRNA mRNA. Protein extracts from these cells were then subjected to western blot analysis, which demonstrated that the PTEN+/- cells have increased phosphorylation of mTORC2-associated targets including pAKT473, pAKT450, and pmTOR 2481 (Figure 10d). There was no increase in the mTORC1 targets assessed including p4EBP1 Ser65, pAKT308 and pmTOR2448 and in fact we see slight decreases in these targets (Figure 10d). We additionally observed an increased in pRAPTOR, which is an inhibitory signaling on the mTORC1 complex. Lastly we observe an increase in the autophagy component LC3A (Figure 10d)

*Figure 2-10: Deletion of PTEN from ipNPCs*

(a) transfection efficiency of mRNA is superior to plasmid delivery as evidenced by GFP

mRNA (b) confirmation of Cas9 expression following Cas9 mRNA transfection (c) PCR

showing deletion of critical exon 5 in PTEN in ipNPCc (d) western blot analysis of PTEN[(+/-)]

ipNPCs showing activation of mTORC2 targets pAKT473, pAKT450, pmTOR2481, and

decreased mTORC1 targets including pmTOR2448, p4EBP1(Ser65) and also increased

inhibition of mTORC1-realted pRAPTOP (e) summary of mTORC1 and mTORC2 Targets.
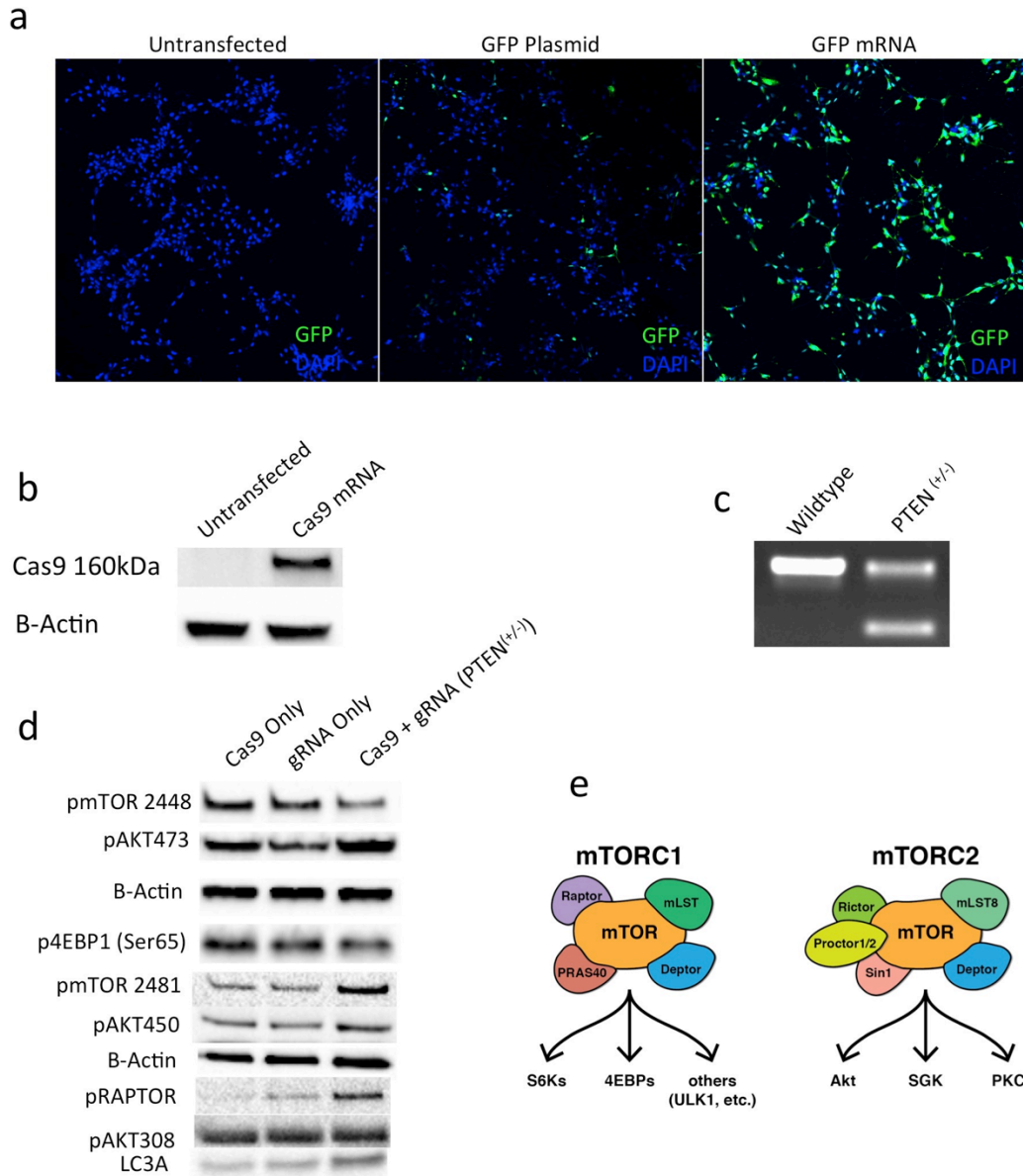
*Patient Derived NPCs*

To model specific mutations in PTEN we generated ipNPCS from patients with Autism-macrocephaly and different PTEN mutations. We first validated the genotype of the iPSC derived NPCs via full length sequencing of the exons of PTEN. We confirm that Case #1 carriers a single base pair substitution which results in the protein change p.Y68N. Case #2 is a carrier of a frame shift mutation which results in the protein change (p.R130X, Figure 11a). The identity of these cells was confirmed via staining for Pax6 and Nestin, two well-described markers for neural progenitor cells (Figure 11b). We next determined the effect of these mutations on cell signaling via Western blot analysis. We show that these mutations have different effects on downstream signaling. Cells derived from case 1 show elevated phosphorylation of pAKT308, and moderately decreased p4EBP1S65 and unchanged levels of pmTOR2448 and 2481 when compared to control. Patient 007's cells show increased pAKT473 and pAKT308, they also demonstrate decreased levels of pmTOR2448 and 2481, p4EBP1Ser65 and Thr37/46 when compared to control(Figure 12a-b). We additionally have observed that components of autophagy are increased in the 007 line however not in the 001 line (Figure 12a-b). We finally determined the effect of these mutations on PTEN localization and expression via immunofluorescence. We have observed that the 001 cells show PTEN staining that excludes the nucleus, while the 007 and wild type iPSC control cells show nuclear and cytoplasmic staining (Figure 12c).

Figure 2-11: Confirmation of PTEN mutations and neural progenitor identity

(a) Sanger sequencing plots from ipNPCs derived from case 1 and case 2 which show the
presence of mutations in PTEN (b) ipNPCs from case 1 and case 2 which stain positive for
Pax6/Nestin confirming that they are neural progenitors.
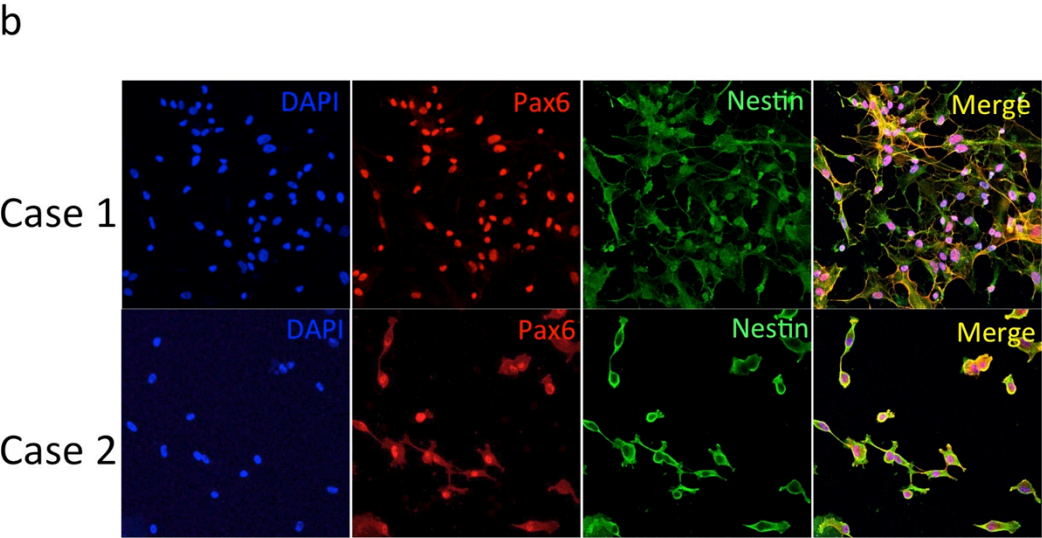
Figure 2-12: Consequence of PTEN mutation on patient derived ipNPCs

(a) Western blot analysis of ipNPCS derived from autism-macrocephaly patients compared to a control ipNPC line showing differential activation of the PI3K/AKT/mTOR signaling pathway. (b, c) (c) Quantification of western blots, standard deviations are shown with black vertical bars, * denotes significant difference <.05 (d) ipNPCs stained with PTEN antibody at 63x showing the effect of PTEN mtuations on PTEN localization, yellow dotted lines outline the nucleus.
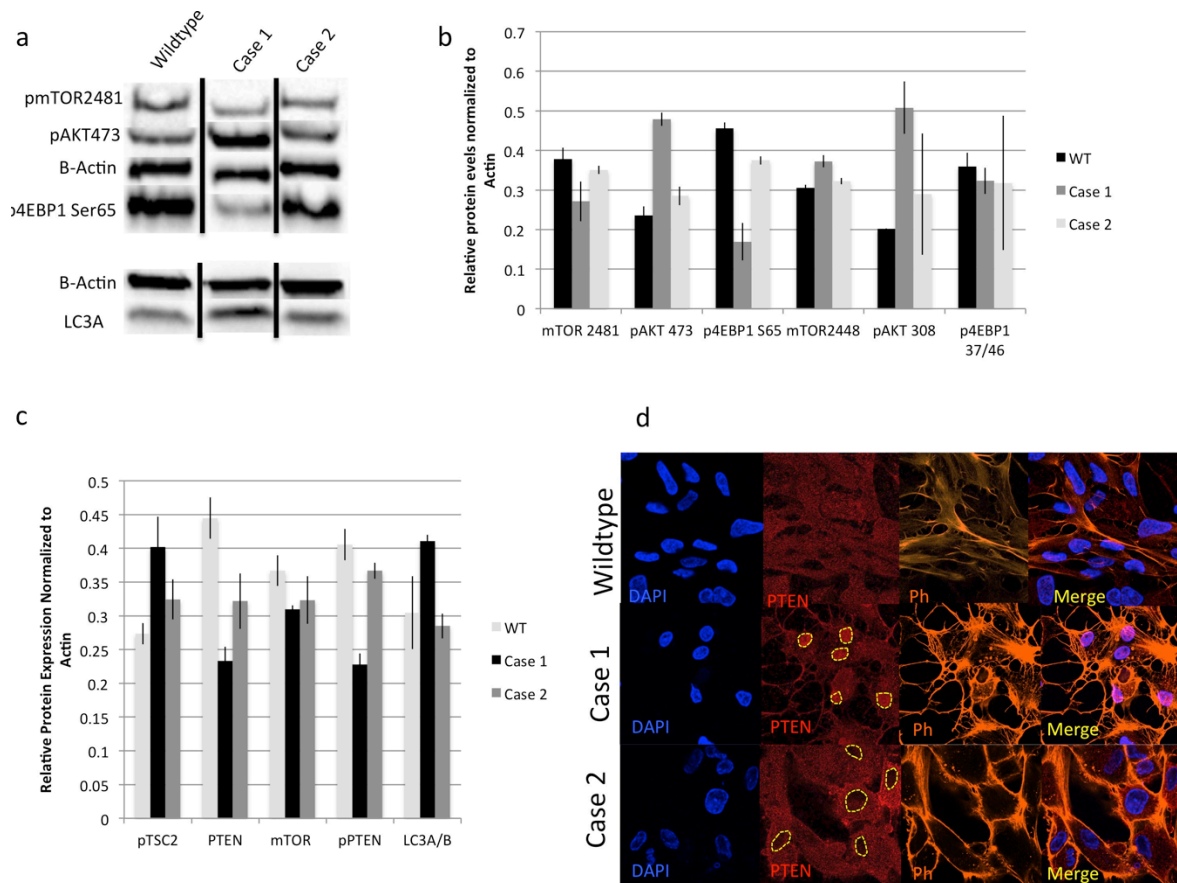
# Discussion

*PTEN Deletion results in mTORC2 Activation*

mTOR exists as part of at least two distinct complexes, mTORC1 and mTORC2. mTORC1 is composed of Raptor, Deptor, and PRAS40 and thought to be the complex which is most responsive to environmental nutrient cues and in relaying these signals into its two main targets 4EBP1 and 70S6Kinase. Overall the mTORC1 targets have been shown to affect protein translation, and cell proliferation/growth[40]. Conversely mTORC2 is composed of Rictor, mSin1, and Deptor and is responsive to ribosomal inputs as well as feedback via mTORC1 from which it modulates the signaling to its targets AKT, SGK1, PKC and additionally on mTOR. The unique functional role of mTORC2 activation is reported to be more associated with cell migration[40]. It should be noted however that the exact mechanisms of mTORC1 and mTORC2 activation are hard to assay independently as there are multiple cross talk points in both signaling cascades. A compelling difference has been recently described in the CNS, which shows that mTORC1 is necessary for axon-regeneration, however mTORC2 and GSK3B signaling are inhibitory for this same process[41]. Our data shows that PTEN deletion in the HEK293T, ipNPCS and the Y68N patient derived iPSC NPC line have activation of mTORC2-associated targets including pAKT473, pAKT450, pSGK1-422, and pmTOR2481. Most interestingly, these cells lines have unchanged or decreased phosphorylation of p4EBP1 demonstrating either isolated mTORC2 activation or mTORC2 activation with mTORC1 inhibition. The link between PTEN and mTORC2 has been reported in Grade IV gliomas[42], murine prostate cancers models[43], bladder cancer[44], breast cancer[45] and leukemia[46]. However, to our knowledge, this is the first reporting of such activation in non-cancerous CNS tissues. In addition we

have observed activation of autophagy in these cells via increases in the autophagy components LC3A/B.  This observation is somewhat paradoxical as classic canonical mTOR signaling is thought to inhibit autophagy. We propose for the first time that activation of mTORC2 is associated with increases in autophagy, which may be playing a role in the balance of increased growth, and autophagy. Additional studies are needed to see if this effect is due to feedback or are a direct result of the mTOR activation.  To support the link between mTORC2 and autophagy further, it has been shown that autophagy can activate mTORC2[47]

*Autism Associated Mutations activate Downstream signaling differently*

We compared the signaling of two PTEN mutations associated with Autism and Macrocephaly, Y68N and R130X in patient derived iPSC NPCs. We observed distinct pathway activation associated with each mutation. The R130X (Case 2) mutation activates only pAKT308 and shows moderate decreases in p4EBP1Ser65. The Y68N (case 1) mutation however demonstrates marked increases in pAKT473, pAKT308 decreases in pmTOR2481, pAKT2448, p4EBP165 and p4EBP137/46. These two states represent two potentially different mechanisms by which these mutations act. Additionally imaging of these cells show that the R130X mutation causes PTEN to be exported from the nucleus and results in a  "nuclear sparing" staining pattern not observed in Y68N.  As the Y68N mutation results in a complete protein with an intact C-terminal tail we propose that it can in fact form catalytically "dead" heterodimers with wildtype PTEN and acts in a dominant negative mechanism, most interestingly this causes PTEN to translocate to the nucleus as we have shown increased nuclear staining in these cells.  The result of this dominant

negative signaling is strongly activated AKT as evidenced by increased phosphorylation at residues 308 and 473. Interestingly the downstream targets of this signaling show decreases including mTOR (2481 and 2448) as wells as 4EBP1 (65, 37/46). We believe that in the setting of dominant negative mutations the activation of AKT is so profound that is causes negative feedback to the downstream components, including phosphorylation of mTOR itself (Figure 15). This work, for the first time, presents evidence that the ultimate culprit in the autism macrocephaly phenotype due to dominant negative mutations may be do to an AKT branch point and not ultimate activation of mTOR. This is confirmed with the R130X mutation, which cannot form heterodimers as it lack the c-terminal tail which is a requirement[33], as there was no increase in any downstream target assayed. Interestingly these cells show loss of nuclear PTEN, which itself may be the pathogenic mechanism for these mutations. Nuclear PTEN plays a role in signaling apoptosis, arresting cell cycle, and coordinating double stranded break repair[5] (Figure 17). Ultimately these results lead us to propose that that in the setting of non-cancerous CNS tissue, the effect of dominant-negative versus loss of function is mechanistically different but perhaps converge on the same targets. As we have shown loss of PTEN activates GSK3A/B via loss of the inhibitory phosphorylation events at Ser9 and 21 respectively. Down stream of GSK3B lies CyclinD2, which is an essential regulator of cell cycle progression. Additionally loss of the PTEN from the nucleus removes inhibition of ERK and ultimate inhibition of CyclinD1 and the cell cycle. It is possible that the common node in these mutations is deregulation of the cyclin family and resulting increased proliferation, which manifests as macrocephaly and may additionally be responsible for the behavioral phenotype of autism in these cases.

Figure 2-13:  Effect of dominant negative and true loss of function mutations

Out proposed model that explains the difference in dominant negative mutations and true loss of function mutations. The dominant negative mutations are associated with PTEN translocation into the nucleus and increased pAKT308 and 473 while true loss of function mutations are associated with a nuclear sparing staining pattern.
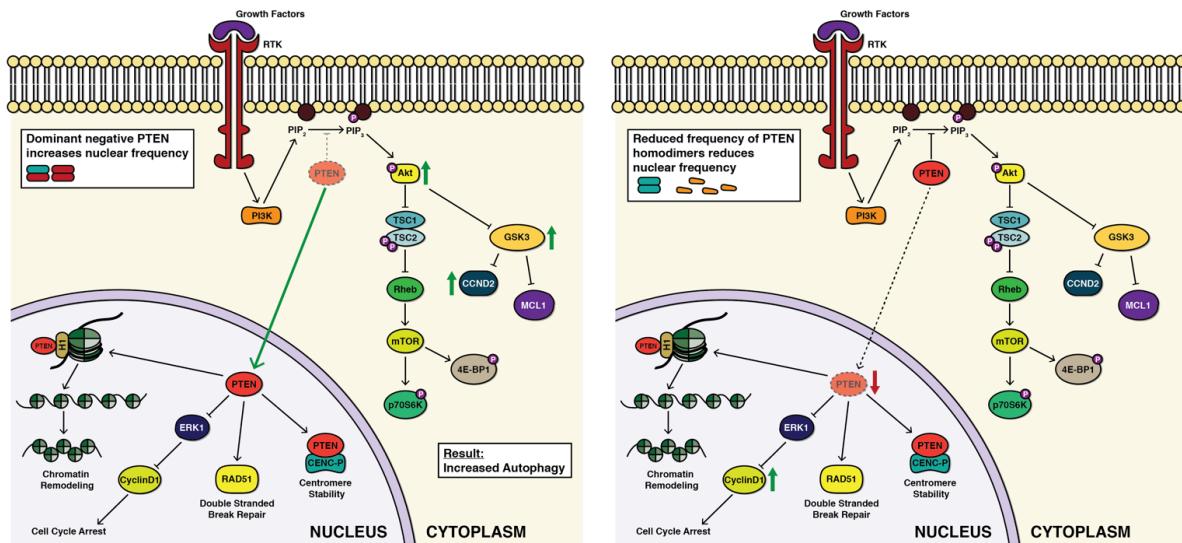
*Potential role for mTORC1/mTORC2 Inhibitors in treatment*

Treatment for the PI3K-relatied overgrowth/neoplastic disorders has been largely focused on step-specific inhibition of components of the conical mTOR signaling cascade[48]. Specific inhibitors of PI3K, AKT and mTOR are available, as well as drugs that demonstrate a combined effect on multiple targets within the pathway. As we have described, specific mutations in PTEN affect cell signaling in distinct patterns with potentially common targets. The data demonstrates that the activation effects of the PTEN mutations on mTORC1/mTORC2 are distinct which we believe has broad implications for the potentially unique treatment strategies, and make a compelling case for individual case based medical approaches. Specifically individuals carrying a mutation in PTEN, which acts as dominate negative, may benefit from use of an inhibitor that strongly targets mTORC2 focusing on AKT phosphorylation. To evaluate the relative actions of mTORC1 vs mTORC1/mTORC2 inhibition we compared the most widely used mTOR inhibitor Rapamycin to a newer mTORC1/mTORC2 inhibitor TORIN-1 (Figure 14).

Figure 2-14:  mTORC1 and mTORC2 inhibitors may be beneficial in the treatment of PTEN associated syndromes

(a) HEK293T cells treated with decreasing doses of Rapamycin, TORIN-1 and a combination approach. (b) ipNPCs treated with Rapamycin and TORIN-1. We propose that the decreases in pAKT473 seen with TORIN-1, but not Rapamycin are mTORC2 specific knockdowns which is an important consideration for patient with a PTEN mutation.
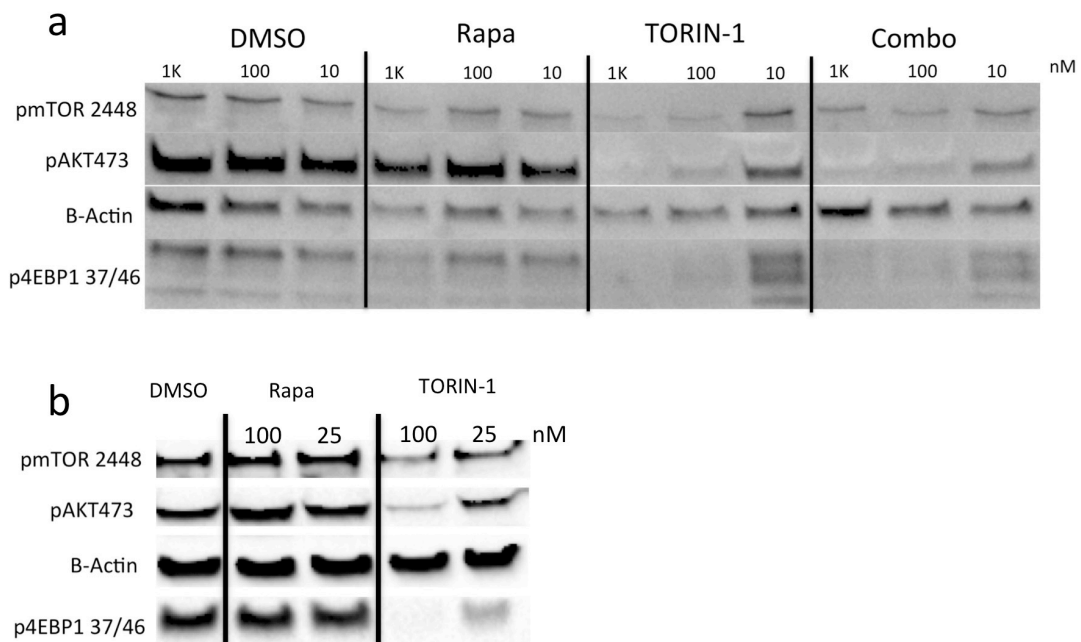
We show that even at low doses TORIN1 inhibits or ablates AKT phosphorylation at Ser473, which may be a signaling event central to the pathogenic phenotype in these cases. Conversely patients with mutations that do not act as dominate negatives may benefit from a direct cell-cycle inhibitor, or a different agent, which facilitates shuttling PTEN into the nucleus where it can play its essential role in cell cycle inhibition.

## Conclusions:

We have used a combination of approaches to determine the role that loss of/mutations in PTEN affect cell signaling. From these studies we determine that true heterozygous PTEN loss in neural progenitor cells results in isolated activation of pAKT308 and translocation of PTEN out of the nucleus. Mutations in PTEN that result in dominant negative mechanisms of action are associated with not only increased pAKT308 but also strong pAKT473 activation and decreases in mTORC1 targets such as p4EBP1. We believe that these signaling event culminate in functional effects outside of canonical mTOR signaling mainly deregulation of the cell cycle. These distinctions help to explain the spectrum of molecular mechanisms that can result in macrocephaly associated autism, and predict varying response to treatment modalities based upon molecular etiology.

# References

1. Chalhoub, N., and Baker, S.J. (2009). PTEN and the PI3-kinase pathway in cancer. Annu Rev Pathol 4, 127-150.

2. Hopkins, B.D., Hodakoski, C., Barrows, D., Mense, S.M., and Parsons, R.E. (2014). PTEN function: the long and the short of it. Trends Biochem Sci 39, 183-190.

3. Zhang, Z., Hou, S.Q., He, J., Gu, T., Yin, Y., and Shen, W.H. (2016). PTEN regulates PLK1 and controls chromosomal stability during cell division. Cell Cycle 15, 2476-2485.

4. Ho, J., Bassi, C., and Stambolic, V. (2015). Characterization of nuclear PTEN and its post translational modifications. Methods 77-78, 104-111.

5. Planchon, S.M., Waite, K.A., and Eng, C. (2008). The nuclear affairs of PTEN. J Cell Sci 121, 249-253.

6. Di Cristofano, A., and Pandolfi, P.P. (2000). The multiple roles of PTEN in tumor suppression. Cell 100, 387-390.

7. Li, D.M., and Sun, H. (1998). PTEN/MMAC1/TEP1 suppresses the tumorigenicity and induces G1 cell cycle arrest in human glioblastoma cells. Proc Natl Acad Sci U S A 95, 15406-15411.

8. Weng, L.P., Gimm, O., Kum, J.B., Smith, W.M., Zhou, X.P., Wynford-Thomas, D., Leone, G., and Eng, C. (2001). Transient ectopic expression of PTEN in thyroid cancer cell lines induces cell cycle arrest and cell type-dependent cell death. Hum Mol Genet 10, 251-258.

9. Wise, H.M., Hermida, M.A., and Leslie, N.R. (2017). Prostate cancer, PI3K, PTEN and prognosis. Clin Sci (Lond) 131, 197-210.

10. Reed, D.E., and Shokat, K.M. (2017). INPP4B and PTEN Loss Leads to PI-3,4-P2 Accumulation and Inhibition of PI3K in TNBC. Mol Cancer Res.

11. Cancer Genome Atlas Research, N., Kandoth, C., Schultz, N., Cherniack, A.D., Akbani, R., Liu, Y., Shen, H., Robertson, A.G., Pashtan, I., Shen, R., et al. (2013). Integrated genomic characterization of endometrial carcinoma. Nature 497, 67-73.

12. Grasso, C.S., Wu, Y.M., Robinson, D.R., Cao, X., Dhanasekaran, S.M., Khan, A.P., Quist, M.J., Jing, X., Lonigro, R.J., Brenner, J.C., et al. (2012). The mutational landscape of lethal castration-resistant prostate cancer. Nature 487, 239-243.

13. Network, T.C. (2013). Corrigendum: Comprehensive genomic characterization defines human glioblastoma genes and core pathways. Nature 494, 506.

14. Cancer Genome Atlas Research, N. (2008). Comprehensive genomic characterization defines human glioblastoma genes and core pathways. Nature 455, 1061-1068.

15. Wang, K., Kan, J., Yuen, S.T., Shi, S.T., Chu, K.M., Law, S., Chan, T.L., Kan, Z., Chan, A.S., Tsui, W.Y., et al. (2011). Exome sequencing identifies frequent mutation of ARID1A in molecular subtypes of gastric cancer. Nat Genet 43, 1219-1223.

16. Gimm, O., Attie-Bitach, T., Lees, J.A., Vekemans, M., and Eng, C. (2000). Expression of the PTEN tumour suppressor protein during human development. Hum Mol Genet 9, 1633-1639.

17. Lloyd, K.M., 2nd, and Dennis, M. (1963). Cowden's disease. A possible new symptom complex with multiple system involvement. Ann Intern Med 58, 136-142.

18. Liaw, D., Marsh, D.J., Li, J., Dahia, P.L., Wang, S.I., Zheng, Z., Bose, S., Call, K.M., Tsou, H.C., Peacocke, M., et al. (1997). Germline mutations of the PTEN gene in Cowden disease, an inherited breast and thyroid cancer syndrome. Nat Genet 16, 64-67.

19. Bannayan, G.A. (1971). Lipomatosis, angiomatosis, and macrencephalia. A previously undescribed congenital syndrome. Arch Pathol 92, 1-5.

20. Zigman, A.F., Lavine, J.E., Jones, M.C., Boland, C.R., and Carethers, J.M. (1997). Localization of the Bannayan-Riley-Ruvalcaba syndrome gene to chromosome 10q23. Gastroenterology 113, 1433-1437.

21. Arch, E.M., Goodman, B.K., Van Wesep, R.A., Liaw, D., Clarke, K., Parsons, R., McKusick, V.A., and Geraghty, M.T. (1997). Deletion of PTEN in a patient with Bannayan-Riley-Ruvalcaba syndrome suggests allelism with Cowden disease. Am J Med Genet 71, 489-493.

22. Marsh, D.J., Dahia, P.L., Zheng, Z., Liaw, D., Parsons, R., Gorlin, R.J., and Eng, C. (1997). Germline mutations in PTEN are present in Bannayan-Zonana syndrome. Nat Genet 16, 333-334.

23. Longy, M., Coulon, V., Duboue, B., David, A., Larregue, M., Eng, C., Amati, P., Kraimps, J.L., Bottani, A., Lacombe, D., et al. (1998). Mutations of PTEN in patients with Bannayan-Riley-Ruvalcaba phenotype. J Med Genet 35, 886-889.

24. Hendriks, Y.M., Verhallen, J.T., van der Smagt, J.J., Kant, S.G., Hilhorst, Y., Hoefsloot, L., Hansson, K.B., van der Straaten, P.J., Boutkan, H., Breuning, M.H., et al. (2003). Bannayan-Riley-Ruvalcaba syndrome: further delineation of the phenotype and management of PTEN mutation-positive cases. Fam Cancer 2, 79-85.

25. Marsh, D.J., Kum, J.B., Lunetta, K.L., Bennett, M.J., Gorlin, R.J., Ahmed, S.F., Bodurtha, J., Crowe, C., Curtis, M.A., Dasouki, M., et al. (1999). PTEN mutation spectrum and genotype-phenotype correlations in Bannayan-Riley-Ruvalcaba syndrome suggest a single entity with Cowden syndrome. Hum Mol Genet 8, 1461-1472.

26. Cole, T.R., and Hughes, H.E. (1991). Autosomal dominant macrocephaly: benign familial macrocephaly or a new syndrome? Am J Med Genet 41, 115-124.

27. Naqvi, S., Cole, T., and Graham, J.M., Jr. (2000). Cole-Hughes macrocephaly syndrome and associated autistic manifestations. Am J Med Genet 94, 149-152.

28. Butler, M.G., Dasouki, M.J., Zhou, X.P., Talebizadeh, Z., Brown, M., Takahashi, T.N., Miles, J.H., Wang, C.H., Stratton, R., Pilarski, R., et al. (2005). Subset of individuals with autism spectrum disorders and extreme macrocephaly associated with germline PTEN tumour suppressor gene mutations. J Med Genet 42, 318-321.

29. Klein, S., Sharifi-Hannauer, P., and Martinez-Agosto, J.A. (2013). Macrocephaly as a clinical indicator of genetic subtypes in autism. Autism Res 6, 51-56.

30. Spinelli, L., Black, F.M., Berg, J.N., Eickholt, B.J., and Leslie, N.R. (2015). Functionally distinct groups of inherited PTEN mutations in autism and tumour syndromes. J Med Genet 52, 128-134.

31. Varga, E.A., Pastore, M., Prior, T., Herman, G.E., and McBride, K.L. (2009). The prevalence of PTEN mutations in a clinical pediatric cohort with autism spectrum disorders, developmental delay, and macrocephaly. Genet Med 11, 111-117.

32. Heinrich, F., Chakravarthy, S., Nanda, H., Papa, A., Pandolfi, P.P., Ross, A.H., Harishchandra, R.K., Gericke, A., and Losche, M. (2015). The PTEN Tumor Suppressor Forms Homodimers in Solution. Structure 23, 1952-1957.

33. Papa, A., Wan, L., Bonora, M., Salmena, L., Song, M.S., Hobbs, R.M., Lunardi, A., Webster, K., Ng, C., Newton, R.H., et al. (2014). Cancer-associated PTEN mutants act in a dominant-negative manner to suppress PTEN protein function. Cell 157, 595-610.

34. Leslie, N.R., Batty, I.H., Maccario, H., Davidson, L., and Downes, C.P. (2008). Understanding PTEN regulation: PIP2, polarity and protein stability. Oncogene 27, 5464-5476.

35. Leslie, N.R., Kriplani, N., Hermida, M.A., Alvarez-Garcia, V., and Wise, H.M. (2016). The PTEN protein: cellular localization and post-translational regulation. Biochem Soc Trans 44, 273-278.

36. Bassi, C., Ho, J., Srikumar, T., Dowling, R.J., Gorrini, C., Miller, S.J., Mak, T.W., Neel, B.G., Raught, B., and Stambolic, V. (2013). Nuclear PTEN controls DNA repair and sensitivity to genotoxic stress. Science 341, 395-399.

37. Ran, F.A., Hsu, P.D., Wright, J., Agarwala, V., Scott, D.A., and Zhang, F. (2013). Genome engineering using the CRISPR-Cas9 system. Nat Protoc 8, 2281-2308.

38. Doench, J.G., Fusi, N., Sullender, M., Hegde, M., Vaimberg, E.W., Donovan, K.F., Smith, I., Tothova, Z., Wilen, C., Orchard, R., et al. (2016). Optimized sgRNA design to maximize activity and minimize off-target effects of CRISPR-Cas9. Nat Biotechnol 34, 184-191.

39. Hsu, P.D., Scott, D.A., Weinstein, J.A., Ran, F.A., Konermann, S., Agarwala, V., Li, Y., Fine, E.J., Wu, X., Shalem, O., et al. (2013). DNA targeting specificity of RNA-guided Cas9 nucleases. Nat Biotechnol 31, 827-832.

40. Jhanwar-Uniyal, M., Amin, A.G., Cooper, J.B., Das, K., Schmidt, M.H., and Murali, R. (2017). Discrete signaling mechanisms of mTORC1 and mTORC2: Connected yet apart in cellular and molecular aspects. Adv Biol Regul.

41. Miao, L., Yang, L., Huang, H., Liang, F., Ling, C., and Hu, Y. (2016). mTORC1 is necessary but mTORC2 and GSK3beta are inhibitory for AKT3-induced axon regeneration in the central nervous system. Elife 5, e14908.

42. Bhattacharya, K., Maiti, S., and Mandal, C. (2016). PTEN negatively regulates mTORC2 formation and signaling in grade IV glioma via Rictor hyperphosphorylation at Thr1135 and direct the mode of action of an mTORC1/2 inhibitor. Oncogenesis 5, e227.

43. Guertin, D.A., Stevens, D.M., Saitoh, M., Kinkel, S., Crosby, K., Sheen, J.H., Mullholland, D.J., Magnuson, M.A., Wu, H., and Sabatini, D.M. (2009). mTOR complex 2 is required for the development of prostate cancer induced by Pten loss in mice. Cancer Cell 15, 148-159.

44. Hau, A.M., Leivo, M.Z., Gilder, A.S., Hu, J.J., Gonias, S.L., and Hansel, D.E. (2017). mTORC2 activation is regulated by the urokinase receptor (uPAR) in bladder cancer. Cell Signal 29, 96-106.

45. Lee, S.L., Chou, C.C., Chuang, H.C., Hsu, E.C., Chiu, P.C., Kulp, S.K., Byrd, J.C., and Chen, C.S. (2013). Functional Role of mTORC2 versus Integrin-Linked Kinase in Mediating Ser473-Akt Phosphorylation in PTEN-Negative Prostate and Breast Cancer Cell Lines. PLoS One 8, e67149.

46. Magee, J.A., Ikenoue, T., Nakada, D., Lee, J.Y., Guan, K.L., and Morrison, S.J. (2012). Temporal changes in PTEN and mTORC2 regulation of hematopoietic stem cell self-renewal and leukemia suppression. Cell Stem Cell 11, 415-428.

47. Bernard, M., Dieude, M., Yang, B., Hamelin, K., Underwood, K., and Hebert, M.J. (2014). Autophagy fosters myofibroblast differentiation through MTORC2 activation and downstream upregulation of CTGF. Autophagy 10, 2193-2207.

48. Keppler-Noreuil, K.M., Parker, V.E., Darling, T.N., and Martinez-Agosto, J.A. (2016). Somatic overgrowth disorders of the PI3K/AKT/mTOR pathway & therapeutic strategies. Am J Med Genet C Semin Med Genet 172, 402-421.

**Chapter Three**


# A spectrum of macrocephaly phenotypes are caused by allele specific gain of function mutations in mTOR

# Abstract

Human overgrowth is characterized by enhanced growth parameters that exceed those for age. A broad phenotypic spectrum is observed amongst cases with syndromic overgrowth. Specifically macrocephaly, or overgrowth of the head, is a distinct phenotypic finding and commonly associated with behavioral abnormalities and/or developmental delay. Massively parallel sequencing has facilitated the discovery of numerous genetic etiologies of human overgrowth with and without macrocephaly, revealing common alterations in distinct signaling pathways. One prominent example is the PI3K/AKT pathway, a key regulator of cellular growth. A number of mutations have been identified in upstream components of this pathway such as *PIK3CA, PTEN* and *AKT*. Although it is commonly suggested that these mutations act to ultimately activate mTOR, it is not known if mTOR activation is sufficient to cause human overgrowth or if in fact other signaling pathways are involved as AKT is a major growth signaling node. We have identified pathogenic gain of function variants in the FAT domain of MTOR that phenocopy established overgrowth syndromes, confirming that mTOR activation is sufficient to cause human overgrowth. Most interestingly these mutations are associated with a spectrum of phenotypes that range from severe hemi-megalencephaly to megalencephaly-capillary malformation-polymicrogyria syndrome (MCAP) to more moderate symmetric brain overgrowth. Functional analysis of these variants revealed that they all activate mTOR by different degrees. We demonstrate *in situ* strong mTOR activation in fibroblasts and in a distinct population of cells within hemimegalencephalic brain regions that histologically resemble focal cortical dysplasia (FCD). We conclude that the absolute amount of mTOR activation results in mutation specific phenotypes that range from hemi-megalencephaly to

132

polymicrogyria to extreme macrocephaly. These findings provide insight into the distinct role of mTOR in regulating growth and development, and furthermore how varying degrees of activation in the same pathway can cause a diverse spectrum of phenotypes.

## Author Summary

Human overgrowth is characterized by excessive body growth that usually presents with increased height, weight or head size. In addition, rare genetic overgrowth syndromes are associated with other findings, including increased risk for certain cancers and skin manifestations. Specifically macrocephaly, or overgrowth of the head, is a distinct phenotypic finding and commonly associated with behavioral abnormalities and/or developmental delay in these syndromes. Many of these human overgrowth syndromes have been associated with mutations in components of the PI3K/AKT pathway. Despite the common activation of this pathway, in many of these syndromes their phenotypic findings are distinct for each entity. The mechanistic basis for this diversity of phenotypes remains elusive given that they should all result in ultimate activation of its effector mTOR. We demonstrate that mutations in mTOR that increase its activity result in a spectrum of overgrowth phenotypes, reflective of the plethora of clinical findings associated with mutations in upstream components of the PI3K/AKT pathway. The level of absolute activation of mTOR dictates this diversity of phenotypes. For the first time we have demonstrated that these distinct mutations cause varying levels of mTOR activation and conclude that phenotypes caused by mutations upstream in the pathway may follow a similar pattern explaining their unique constellation of phenotypic findings.

## Introduction

Human growth is a tightly controlled and highly complex trait, with numerous environmental and genetic factors that determine final body size. Overgrowth is characterized by deregulation of these processes, resulting in excessive height, weight, and/or head circumference (HC) when compared to age- and sex-matched controls [1]. Rare overgrowth syndromes can occur as sporadic genetic entities associated with *de novo*, in many cases mosaic [2-5], gain-of-function mutations in upstream components of the PI3K/AKT pathway [1,3,5-8]. This pathway is essential for the control of cellular growth and is regulated by the availability of nutrients in the environment. Mutations at distinct levels of this pathway result in characteristic overgrowth syndromes, including but not limited to megalencephaly-polymicrogyria-polydactyly-hydrocephalus syndrome (MPPH, [MIM: 603387]), megalencephaly-capillary malformation-polymicrogyria syndrome (MCAP, [MIM: 602501]) [8] and macrocephaly autism (MIM: 605309) [9].

Mutations in components upstream of *PI3K/AKT* signaling can occur as either germline, where every cell of the body carries the variant, or mosaic, where the distribution of the mutation is restricted to certain tissues. Sequence changes which result in heterozygous loss of function of negative regulators of the pathway, including *PTEN (MIM:601728)*, *TSC1(MIM: 605284)* and *TSC2 (MIM: 19109),* are primarily germline in distribution. Conversely, activating mutations in drivers of the pathway, including *PIK3CA* (MIM: 171834)*, AKT1 (MIM: 164730), AKT3* (MIM: 611223), and *PIK3R2* (MIM: 603157) are primarily mosaic. The difference in mutation distribution patterns manifests with distinct phenotypic consequences, as the latter present with hemi-megalencephaly and/or hemi-hyperplasia, and the former present with symmetric macrocephaly and somatic

overgrowth. The association of macrocephaly across these syndromes demonstrates the importance of this pathway in regulating brain growth.  However, there is a paucity of data supporting why these subgroups manifest distinct phenotypes given the large number of potential downstream targets of AKT, a major signaling node. One well-documented target of AKT is mTOR, a multi protein complex that regulates key cellular processes including autophagy, cell cycle, protein biosynthesis, survival, and cytoskeletal organization [10,11].  It has been hypothesized that mTOR activation is the crucial event in the pathogenesis of overgrowth; however until now it is not know is this event is in fact sufficient.

In this study we demonstrate that rare mutations in mTOR are sufficient to cause a spectrum of overgrowth phenotypes. Next generation sequencing identified distinct *de novo* missense gain of function mutations in the FAT domain of mTOR. These variants are overrepresented in specific cancers and functional analysis revealed varying degrees of mTOR activation that correlate with mosaic versus germline distribution of the mutation. Our findings demonstrate that varying levels of mTOR activation are sufficient to cause a spectrum of specific overgrowth phenotypes that mirror those observed when components PI3K/AKT pathway upstream of mTOR are mutated.

## Methods:

### *Cases*

All subjects were consented under a UCLA approved IRB protocol. Samples included in DNA analysis included peripheral mononuclear blood cells, cultured skin fibroblasts from a skin biopsy, and surgically resected brain tissue.  All individuals underwent chromosomal microarray analysis and PTEN mutation testing, all of which was normal.

135

## DNA Isolation

DNA was isolated from mononuclear peripheral blood cells using QIAGEN QIAamp Blood Mini Kit. DNA was isolated from tumor samples embedded in paraffin using QIAGEN QIAamp DSP DNA FFPE Tissue Kit.

## Exome Sequencing

Clinical exome sequencing was performed on all three cases and identified variants confirmed to be *de novo* via analysis of their parents (complete description of methods in supplement).

## Pyro Sequencing

Pyrosequencing was performed on DNA isolated from blood, cultured skin fibroblasts and resected brain tissue isolated from paraffin blocks (case one) to determine allele abundance. Pyrosequencing reactions were performed on all samples in triplicate according to the standard vacuum prep protocol for the PSQ 96 MA instrument from QIAGEN. This method has been validated for the quantification of allele distribution within a heterogeneous population of alleles [12,13]. Complete list of primers presented in supplemental material.

## Generation of mTOR site directed mutagenesis plasmids

Site directed mutagenesis was performed with the Agilent QuikChange II XL Site-Directed Mutagenesis Kit on the pcDNA3-Flag-mTOR-wt plasmids obtained from Addgene. Using

100 ng plasmid per reaction (primer list in supplement), plasmids were transformed into

MAX Efficiency® DH5$\alpha$™ Competent Cells. Plasmids were isolated using ZymoPURE™

Plasmid Maxiprep Kit (D4202). Full-length cDNA was sequenced to confirm the presence of

a single mutation (complete list of primers presented in supplement).


### HEK293T Transfection

Cells were maintained with basal media including DMEM, PSN and 10% fetal bovine serum

(FBS). Twenty-four hours before transfection cells were liberated from T25 flask with

TrypLE™ Express Enzyme (1X). Cell concentration and viability was determined with the

Invitrogen Countess I. After plating $2x10^5$ viable cells onto a 12-well culture dish, volume

was brought to 1ml of basal media. On the day of transfection media was aspirated, and

500ul of basal media was added to each well. GeneIn Transfection reagent was combined

with 2ug of plasmid, brought to a final volume of 200ul, vortexed and then incubated at

room temperature for 15 minutes then added to each well. Cells were incubated for 24

hours, followed by a 12-hour nutrient starvation in DMEM lacking glutamine, glucose and

FBS.

### Cell Lysis and Western Blot Analysis

Media was aspirated from each well, and a single wash of 1x PBS was performed. The 500ul

of Passive Lysis Buffer was supplemented with 500ul of Halt Phosphatase inhibitor

(Thermo) and 500ul of protease inhibitor cocktail (Sigma). Lysis buffer was protected from

light and stored at $4^0$C. Once the lysis buffer was added, plates were incubated for 1 hour at

$4^0$C with gentle shaking. Following a one-hour incubation the lysate was transferred to

1.5ml tubes and spun 7500 RCF for 5 minutes to form cell debris pellets. The supernatant

was transferred to a new tube and the concentration determined with Coomassie Plus (Bradford) Assay Kit (Invitrogen). Proteins were diluted to a final concentration of 5ug/20ul with western loading buffer supplemented with beta mercaptoethanol. Samples were boiled for 5 minutes and then either run immediately or frozen at -20$^0$C. Western blot analysis was performed using 12% BioRad TGX™ FastCast™ acrylamide gels. Transfers were performed on the Trans-Blot® Turbo™ Transfer System according to the manufacturer's specification. Following transfer, blots were blocked in 5% bovine serum albumin in TBST (Tris buffered saline with 0.2% Tween) for 30 minutes and incubated in primary antibody overnight at 4$^0$C (Beta-Actin (13E5 Cell Signaling #4970) 1/4000; mTOR (7C10 Cell Signaling #2983) 1/1000; p4EBP1 Ser65 (Cell Signaling # 9451) 1/1000; p-p70-S6kinaseThr389 (Cell Signaling #9234) 1/500; DYKDDDDK Tag Flag (Cell Signaling #2369) 1/500). After primary blots were rinsed with TBS (Tris buffered saline), three 10-minute washes with TBST were performed. Blots were incubated in secondary antibody (Bio Rad Immun-Star Goat Anti-Rabbit (GAR)-HRP Conjugate) at a concentration of 1/3750 diluted in 5% milk in TBST. Secondary blots were rinsed with TBS then washed with TBST two times for 10 minutes, followed by a final TBS wash. Blots were incubated in Clarity Western ECL Substrate for 5 minutes then imaged on the Biorad ChemiDoc XRS+. Bands were quantified across replicates and normalized to beta-actin controls using the Biorad image lab software.

*Immunohistochemical analysis*

Formalin fixed paraffin embedded blocks were sectioned into 6 um thick slices onto charged glass slides for immunofluorescence labeling. Slides were first deparaffinized at $37^0$C overnight, then immersed in three xylene baths and then rehydrated in graded ethanol baths (100%- 70%) into deionized water.  Following deparaffinization and rehydration of tissue, heat induced antigen retrieval was then performed by immersing the tissue sections in 10 mmol citrate buffer pH 6.0 and heating samples to $104^0$C for 20 min using a pressure cooker.  Sections were then cooled to room temperature and blocked with 5% normal donkey serum and TBST. Tissue was then immunolabeled with primary antibodies against NeuN  (1:100 Millipore MAB 377) and p4EBP1 (1/200 Cell Signaling #2855) overnight at $4^0$C.  Following primary antibody labeling, sections were washed with TBST and fluorescently labeled with Alexaflour 488 anti-mouse (Life Technologies) for NeuN and Alexaflour 568 anti-rabbit (Life Technologies) for p4EBP1 for 1 hour at room temperature.  Slides were finally counterstained with DAPI and coverslipped using liquid mountant (Life Technologies). Skin fibroblasts were maintained in basal media DMEM, PSN and 10% FBS then liberated from T25 flask with TrypLE™ Express Enzyme (1X). Cell concentration and viability was determined with the Invitrogen Countess I. $5x10^4$ viable cells were plated on uncoated glass coverslips in a 24 well plate. Twenty-four hours later media was aspirated and cells were fixed with 3.5% PFA for 20 minutes. Following fixation cells were permeabilized with TBS with 0.4% Triton X for 20 minutes then blocked with 10% NGS in TBS with 0.4% Triton X at $4^0$C overnight. Cells were stained with primary antibodies histone (1/500, Clone H11-4 Millipore MAB3422), p4EBP1 (1/200 Cell Signaling #2855), and phalloidin-648 (1/500 Invitrogen) for 1 hour at room temperature and then secondary for 1 hour at room temperature (Alexa Fluor 568 donkey anti-rabbit

(Life Technologies A10042, Alexa Fluor 488 donkey anti- mouse (Life Technologies

A21202)). Fibroblasts were imaged with the Carl Zeiss 310 laser-scanning microscope.


### *Assessment of cancer variants*

Data was pooled for comparison to previously described cancer mutations from the

following publically available databases: The Cancer Genome Atlas (TCGA), Cancer Cell Line

Encyclopedia (CCLE), International Cancer Genome Consortium (ICGC), and Catalogue of

Somatic Mutations in Cancer (COSMIC) databases[14-18].  TCGA and CCLE data was accessed

through the cBio Portal [14,15] while COSMIC and ICGC data was accessed directly though

their respective data portals.


## Results

### *De novo germline and mosaic mutations within the FAT Domain of mTOR*

Amongst a cohort of individuals with macrocephaly who underwent whole exome

sequencing (WES) we identified a subset that carried mutations in components of the PI3K

pathway. Specifically three individuals carried *de novo* mutations in mTOR. Case one is a

6.5-year-old female with macrocephaly (HC: 54cm, >97th percentile, +2SD), left

hemimegalencephaly (Fig 1A-B, Fig 2A-B, S1), hypomelanosis of ITO (Figure 1C-D), and

seizures. Histochemical staining of resected brain tissue revealed a single focus in the

superficial cortex with a cluster of balloon-like cells of the type seen in focal cortical

dysplasia (FCD) International League Against Epilepsy (ILAE) Type IIB  (Fig 2D-E). NeuN

staining of the same tissue showed prominent disorganized neurons in subcortical white

matter (Fig 2F-G). WES identified a mutation C1483Y in mTOR (chr1: g.11217230 C>T,

NM_004958.3: c.4448G>A, p.Cys1483Tyr). Case two is an 8-month-old male who presented with extreme macrocephaly (HC 51.5cm >97th percentile +4SDs, Fig 1E), polymicrogyria (Fig 2C), hemi-hypertrophy (Fig 1G), and hyperpigmented skin lesions (Fig 1H). WES identified a mutation T1977I (chr1: g.11188164C>T, NM_004958: c.5390C>T, p.Thr1977Ile). Case three is an 8-year-old female with somatic overgrowth and extreme macrocephaly (HC: 59 cm, >97th percentile, +3SDs, Fig 1I-J). WES identified a mutation E1799K (chr1:g. 11190804C>T, NM_004958.3:c.5395G>A, p.Glu1799Lys, additional phenotypic information is presented in S2).

Figure 3-1. Phenotypic features associated with mutations in the FAT domain of mTOR

Case 1 images (A-D) showing (A) down-slanting palpebral fissures, (B) macrocephaly, (C) hypomelanosis of Ito on left leg, and (D) hypomelanosis of Ito on abdomen. Case 2 images (E-H) showing (E) extreme macrocephaly (HC 51.5cm, >97th percentile +4SDs), down-slanting palpebral fissures, short upturned nose, flattened nasal bridge, hypertelorism, (F) low-set ears, micrognathia, (G) hemi-hyperplasia (leg length discrepancy 0.5cm right>left) , and (H) hyperpigmented lesions. Case 3 (I-J) images showing (I) down-slanting palpebral fissures, hypertelorism, short upturned nose, (J) extreme macrocephaly (OFC: 59 cm, >98thpercentile, +3SDs), flattened nasal bridge, and frontal bossing.

Figure 3-2. Anatomical and histological brain findings associated with mTOR activation

(A) MRI (case 1) showing left hemimegalencephaly; red arrow points to overgrown left occipito-temporal lobe. (B) PET scan (case 1) showing asymmetric glucose uptake in region of overgrowth. (C) Axial T2 MRI (case 2) showing polymicrogyria in the bilateral perisylvian and bilateral frontal lobes. (D) H & E staining of normal brain region (case 1) shows absence of balloon cells and normal cellular architecture. (E) H & E staining of abnormal brain region (case 1); red arrow points to single focus of a cluster of balloon-like cells of the type seen in focal cortical dysplasia ILAE Type IIB. (F) NeuN staining (case 1) of normal brain region showing patterned and normally sized neurons. (G) NeuN staining (case 1) of abnormal brain region showing prominent, disorganized neurons in subcortical white matter



.
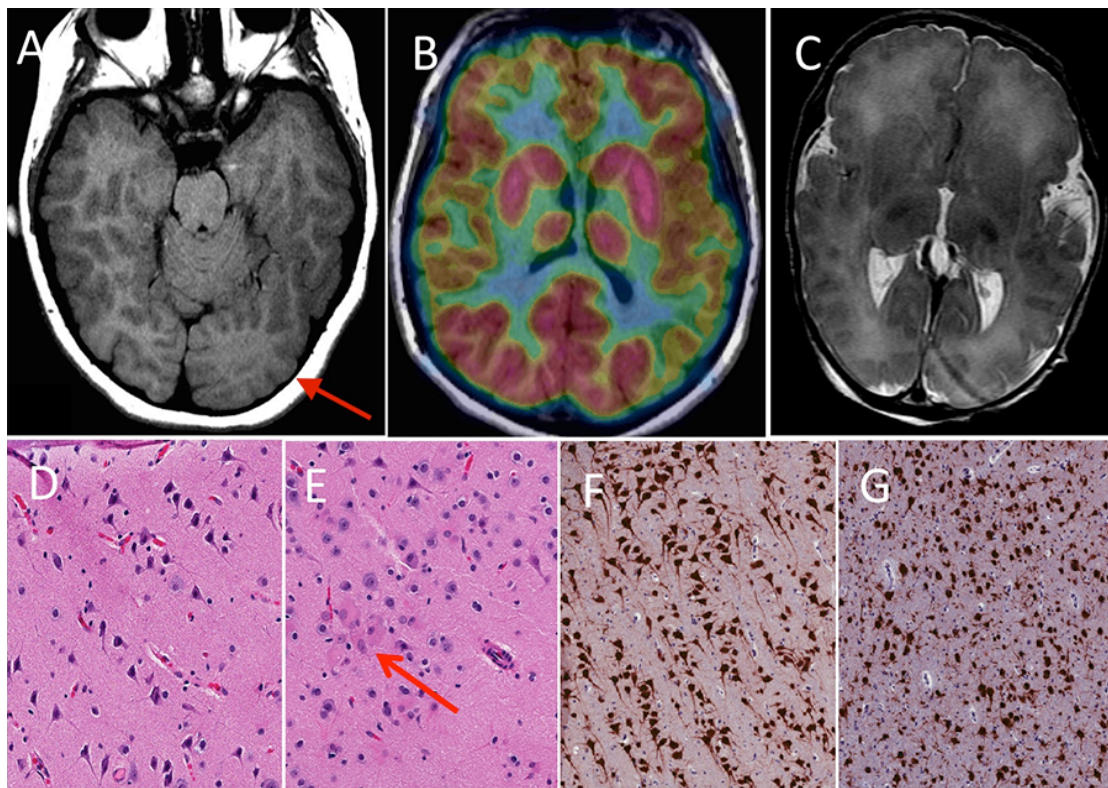
While the E1799K variant was equally distributed in mononuclear blood cells (S3), the

C1483Y variant in Case 1 was present in 36% of the reads from skin fibroblasts but in only

2 of 192 (1%) total reads from mononuclear blood cells (S4). Mutation abundance was

confirmed with pyrosequencing and was undetectable in blood and the parental samples

(S5). The mutation abundance in skin was confirmed to be 39.2%, as well as unevenly

distributed within three distinct areas of resected brain with measured abundances

ranging from 17.9%-55.9% (Fig 3). Similarly, the T1977I variant in Case 2 was unequally

distributed in exome sequencing reads and in Sanger peak distribution confirmation

studies. The unequal distribution of reference/alternate alleles led us to conclude that the

C1483Y and T1977I variants represent *de novo,* post-zygotic, mosaic mutations, while

E1799K is *de novo* germline.

Figure 3-3. Mosaic distribution of C1483Y mutation

Mutation abundance determined by pyro sequencing for g. 1:11217230, c.4448 G>A, with

reference allele (G) in red and alternate allele (A) in blue. Varying allele frequencies

demonstrate somatic mosaicism. Black bars represent standard deviations. Images of

resected brain tissue displayed above each bar.
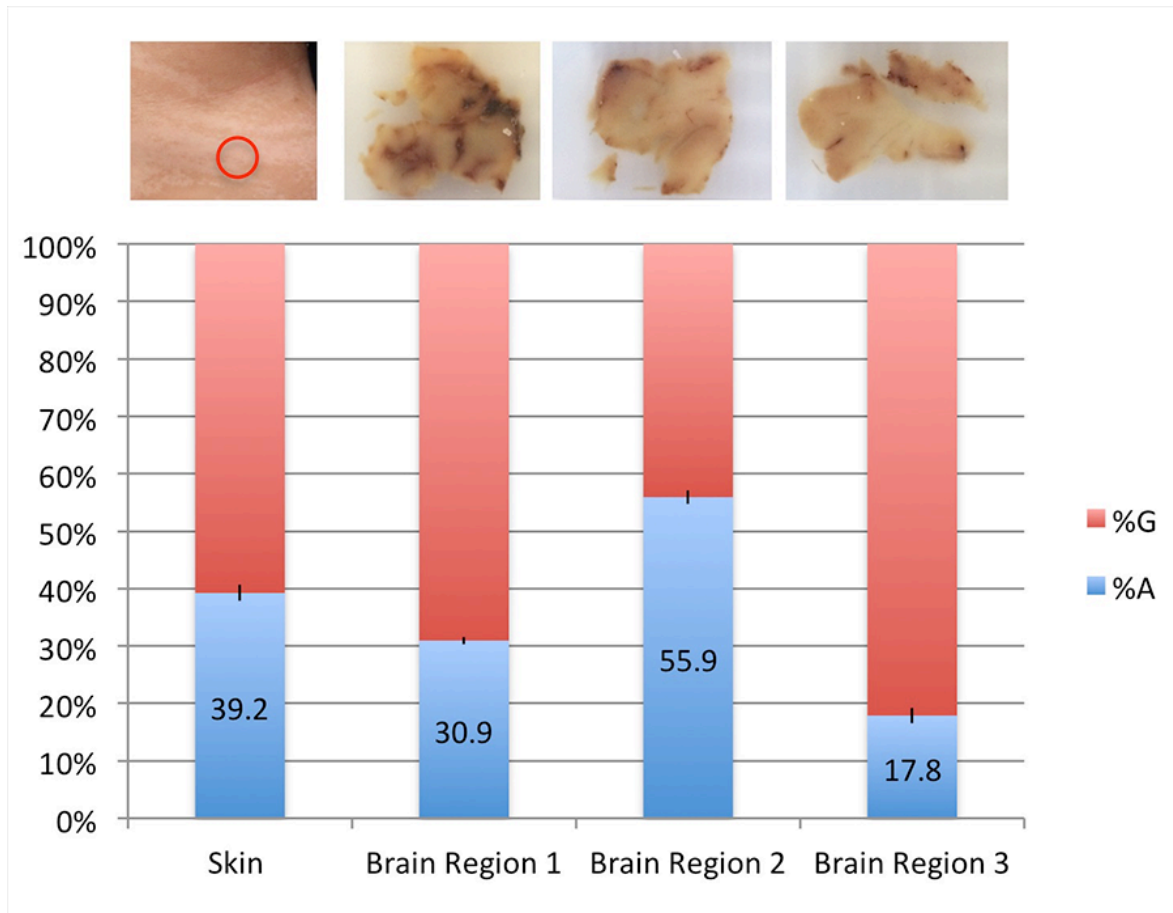
*Identified mutated residues overlap with "hot spots" in the FAT domain of mTOR in somatic tumors*

We next ascertained the potential pathogenicity of these mutations by querying publicly available bioinformatics databases (cBio, COSMIC, ICGC, CCLE) for cancer-associated mutations in mTOR, which might support a gain-of-function mechanism [2,3].  Interestingly, recurrent "hot spot" mutations in the C1483, E1799 and T1977 amino acid residues have been identified in a number of neoplasms with an overrepresentation of specific tissue types.  These specific residues demonstrate relative enrichment compared to others in the FAT domain (Fig 4A).  The glutamic acid at 1799 is exclusively mutated to a lysine, and is the most common mutation in the FAT domain, while the C1483 and T1977 residues are more varied in their amino acid substitutions. The C1483 and T1977 variants show a distinct tissue distribution, with renal tumors being the most common (58% and 46% respectively), while the E1799K mutation is over-represented in uterine/cervical tissues (57%) (Fig 4B).  These findings support a model in which specific allelic mutations in the FAT domain of mTOR contribute to tumor growth within distinct tissue types (full list of tumor mutations presented in supplemental materials S6).

Figure 3-4. Distribution of neoplastic and syndromic mutations within the FAT domain of mTOR

(A) Location and frequency of reported mutations within the FAT domain of mTOR. Each point represents a single tumor, cancer cell line, case of FCD or syndromic case. (B) Distribution of tumor tissue types by residue for the three mutations identified in syndromic cases. cBio: cBioPortal for Cancer Genomic, COSMIC: Catalogue of somatic mutations in cancer, ICGC: International Cancer Genome Consortium, FCD: Focal cortical dysplasia [19]. Additional syndromic cases C1483Y [20], C1483F [21], and E1799K [22,23]. Dashed black line represents frequency greater than eight district tumors or cases of FCD.
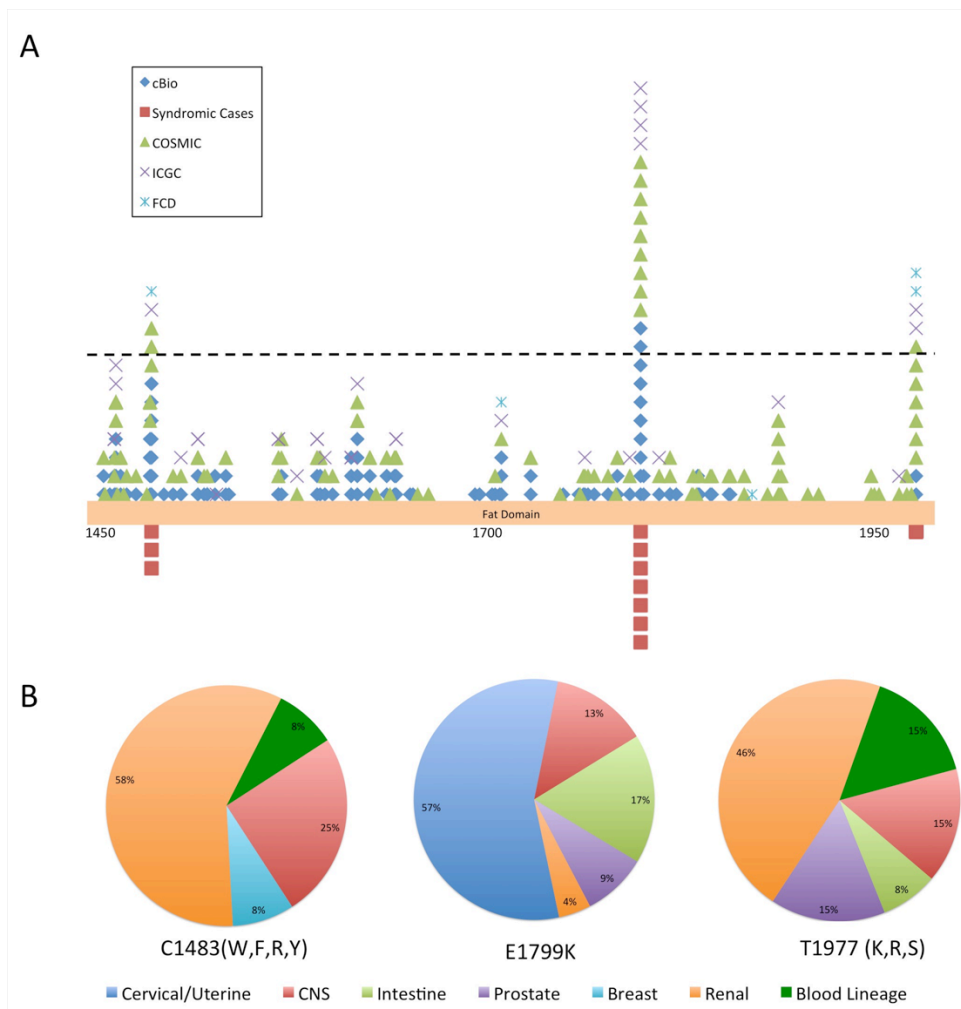
**Mutation specific increases in mTOR activity are associated with distinct phenotypes**

We validated the pathogenicity of identified variants by introducing flag-tagged mTOR plasmids carrying the mutations into human embryonic kidney cells (HEK293T) and assayed activation of downstream mTOR targets. All three of the plasmids activate the downstream components of mTOR p4EBP1 (Ser 65 and Thr37/46) and pS6kinase (Thr389, Figure 5A). Most interestingly the three variants differ in the amount of absolute mTOR activation, measured by these three independent targets, with C14Y having the most activation, E17K having the least activation and T19I being intermediate (Figure 5B-D). We confirmed mTOR activation *in situ* via staining for p4EBP1, which is increased in C1483Y patient-derived fibroblasts and resected brain samples. Patient-derived fibroblasts confirm increased mTOR activity and have increased p4EBP1 staining when compared to wild type (Figure 6). The resected brain sections showed increased p4EBP1 staining and its translocation into the nucleus in NeuN-positive cells (S7). These cells are distinct from the balloon cells most commonly observed in focal cortical dysplasia, and their identity remains unknown. These findings demonstrate that gain-of-function mutations in mTOR activate signaling to different degrees leading to specific phenotypic findings that range in severity proportionate to the level of activation.

Figure 3-5: Functional analysis of mTOR variants

(A) Western blot analysis demonstrates activation of mTOR (p4EBP1(S65, Thr37/46) and pS6Kinase (Thr389)) for each syndrome associated mutation. (B-D) Quantification of relative protein levels for each substrate measured confirms gain of function. "*": p-value <.05 (One way ANOVA weighted) Emp: transfection reagent without plasmid, WT: wild type mTOR, C1483Y: g. 1:11217230, c.4448 G>A, p.Cys1483Tyr, T1977I: chr1: g.11188164C>T, NM_004958: c.5390C>T, p.Thr1977Ile, E1799K: g. 1:11190804, c.5395G>A, p.Glu1799Lys.
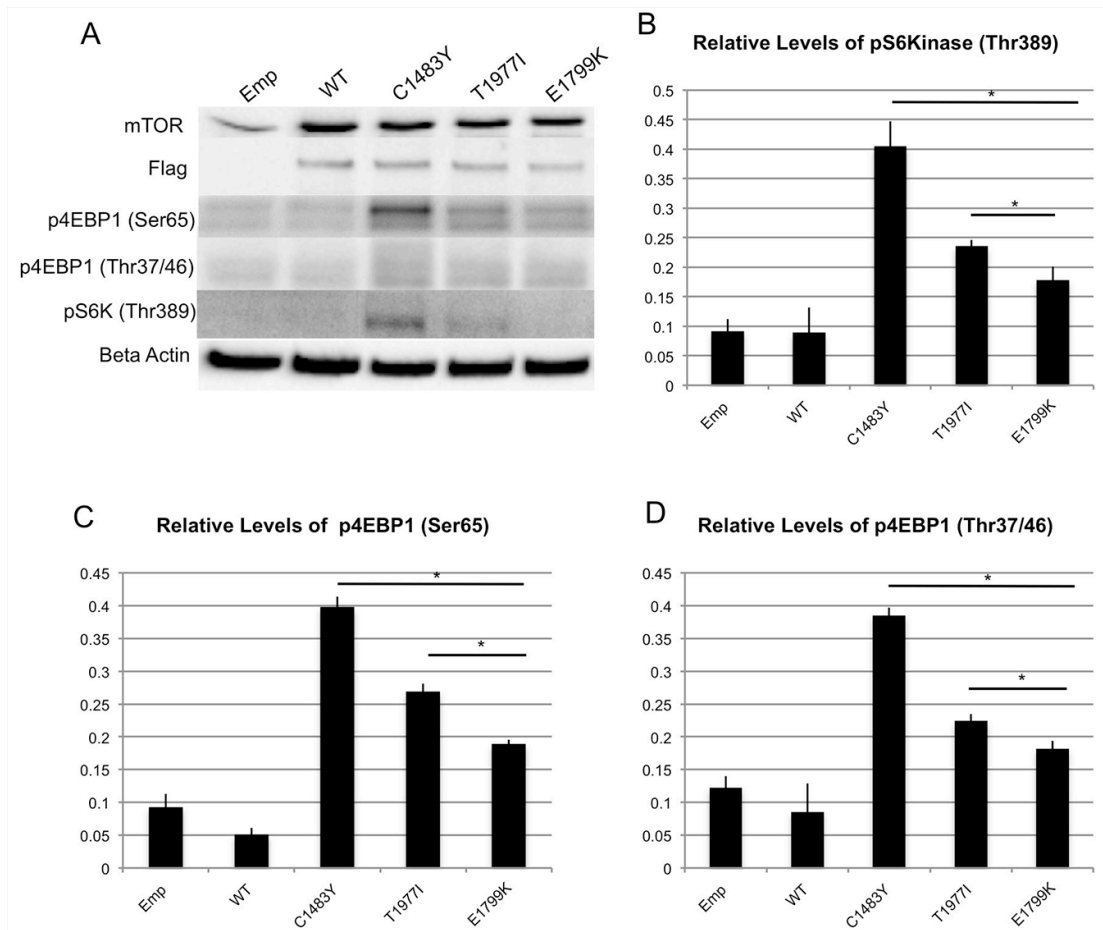
Figure 3-6: mTOR activation in C1483Y fibroblasts

Immunofluorescence staining of fibroblasts demonstrates an increase in p4EBP1 staining

(60x) when compared to wild type fibroblasts.
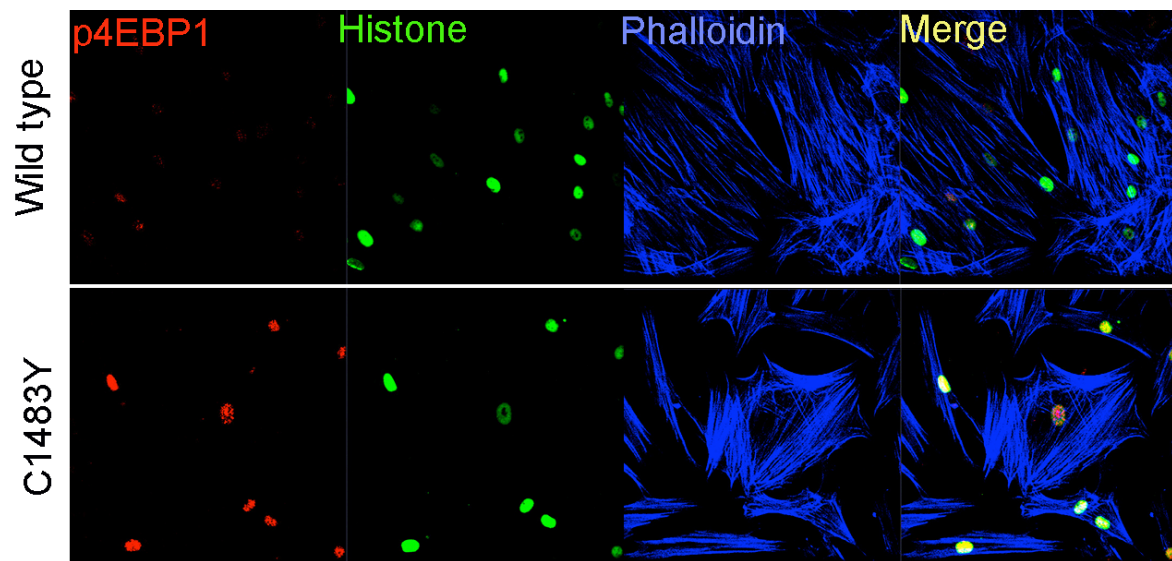
## Discussion

We have herein reported activating mutations in mTOR which cause overgrowth, establishing its central role and sufficiency in the pathogenesis of human overgrowth phenotypes. Additionally these findings clarify the spectrum of macrocephaly overgrowth phenotypes associated with mutations upstream of mTOR. While mosaic mutations in *PIK3CA* (MIM: 171834)*, AKT3* (MIM: 611223) and *PIK3R2* (MIM: 603157) cause hemimegalencephaly, megalencephaly-polymicrogyria-polydactyly-hydrocephalus syndrome (MPPH) and megalencephaly-capillary malformation-polymicrogyria syndrome (MCAP)[8], germline mutations in *PTEN* (MIM: 601728) cause macrocephaly associated with autism (MIM: 605309), Cowden syndrome (CS, [MIM: 158350]) and Bannayan-Riley-Ruvalcaba syndrome (BRRS, [MIM: 153480]), collectively known as the PTEN Hamartoma syndromes. Generalized symmetric brain overgrowth associated with E1799K germline mutations is most reminiscent of PTEN associated brain phenotypes, where brain asymmetry and malformations are rare but extreme macrocephaly is one of its main phenotypic manifestations [9,24].  Conversely focal, asymmetric, and abnormal brain patterning phenotypes due to C1483Y and T1977I mosaic mutations resemble *PIK3CA, AKT3* and *PIK3R2* associated hemimegalencephaly/megalencephaly/polymicrogyria phenotypes [7,8] (Fig 7). Interestingly, mutations in the C1483 and T1977 residues have been reported in sporadic cases of FCD [19,25]. The E1799K mutation however, although associated with germline and wide spread phenotypes, is not yet associated with focal cortical dysplasia possibly because the activation of mTOR is too low to meet the threshold for this pathologic entity.

Figure 3-7: mTOR activation and associated overgrowth phenotypes

Summary of phenotypic findings associated with mutations in the residues C1483, T1977 and E1799 and corresponding levels of mTOR activation.  M/G: Mosaic/Germline distribution, M: Mosaic Distribution, G: Germline Distribution, G?: single case reported to be germline but not confirmed, HMI: Hypomelanosis of ITO,  GDD: Global developmental delay, SD: speech delay, ASD: Autism Spectrum Disorder, A: Lee et al.[20], B: Smith et al.[21], C: Mroske et al.[23], D: Baynam et al. [22].

| C1483Y/F | | | T1977I | | | E1799K | | |
|---|---|---|---|---|---|---|---|---|
| Cases | Phenotype | M/G | Cases | Phenotype | M/G | Cases | Phenotype | M/G |
| **Case 1** | Hemi-Megalencephaly, HMI, Seizures | M | **Case 2** | Hemi-Hypertrophy, Hyperpigmented Skin Lesion, GDD, Macrocephaly | M | **Case 3** | Macrocephaly, Somatic Overgrowth, GDD | G |
| 1[A] | Hemi-Megalencephaly, HMI | M | | | | 2[C] | Macrocephaly, Somatic Overgrowth*, ASD, Iris Coloboma, | G |
| 1[B] | Megalencephaly, Seizures | G? | | | | 3[D] | Macrocephaly, SD, GDD, Seizures, Small Chest | G |

| Mosaic Distribution | Mosaic Distribution | Germline |
|---|---|---|
| Global Developmental Delay | Global Developmental Delay | Global Developmental Delay |
| Hemi-Megalencephaly | Macrocephaly | Autism Spectrum Disorder |
| Hypomelanosis of ITO | Hemi-Hyperplasia | Macrocephaly |
| Seizures | Hyperpigmented Skin Lesions | Somatic Overgrowth |
| | | Seizures |

mTOR Activity

Our findings demonstrate that specific macrocephaly-associated phenotypes arise from distinct degrees of mTOR activation. In particular, gain of function mutations with predilection for strong mTOR activation may behave similar to gain-of- function mutations in *PIK3CA, AKT3* and *PIK3R2*, while gain-of-function mutations that only mildly activate mTOR resemble inactivating mutations in *PTEN*. Supporting this comparison, inactivating mutations in *PTEN* are repeatedly observed to be germline similar to the E1799K *MTOR* variant, while activating mutations in *PIK3CA, AKT3, AKT1* and *PIK3R2* have a predilection towards mosaic distribution, as observed for the C1483Y and the T1977I *MTOR* variants*. The observation that most activating mutations of PI3K/AKT signaling are observed as mosaic leads us to hypothesize that strong activation of mTOR is not compatible with fetal development, while germline mutations that only mildly increase mTOR (E1799K) can be tolerated. As growth signaling pathways are highly complex and branch extensively, we cannot rule out that additional pathway intermediates may play distinct roles upstream of the activation of mTOR and account for further genotype-phenotype variations [26].

In conclusion, our findings establish gain-of-function mutations in *mTOR* as causative for a range of distinct human macrocephaly-associated phenotypes that result from allele specific effects on pathway activation and mosaic distribution. These findings provide insight into the etiology of human overgrowth and establish mTOR activation as sufficient for deregulation of this process, with implications for therapeutic approaches and prognosis.

## Acknowledgements

## References:

1. Tatton-Brown, K. & Weksberg, R. Molecular mechanisms of childhood overgrowth. *American journal of medical genetics. Part C, Seminars in medical genetics* **163**, 71-5 (2013).

2. Lindhurst, M.J. *et al.* Mosaic overgrowth with fibroadipose hyperplasia is caused by somatic activating mutations in PIK3CA. *Nat Genet* **44**, 928-33 (2012).

3. Lindhurst, M.J. *et al.* A mosaic activating mutation in AKT1 associated with the Proteus syndrome. *N Engl J Med* **365**, 611-9 (2011).

4. Klein, S. *et al.* Expanding the phenotype of mutations in DICER1: mosaic missense mutations in the RNase IIIb domain of DICER1 cause GLOW syndrome. *J Med Genet* **51**, 294-302 (2014).

5. Kurek, K.C. *et al.* Somatic mosaic activating mutations in PIK3CA cause CLOVES syndrome. *Am J Hum Genet* **90**, 1108-15 (2012).

6. Astuti, D. *et al.* Germline mutations in DIS3L2 cause the Perlman syndrome of overgrowth and Wilms tumor susceptibility. *Nat Genet* **44**, 277-84 (2012).

7. Mirzaa, G.M., Riviere, J.B. & Dobyns, W.B. Megalencephaly syndromes and activating mutations in the PI3K-AKT pathway: MPPH and MCAP. *American journal of medical genetics. Part C, Seminars in medical genetics* **163**, 122-30 (2013).

8. Riviere, J.B. *et al.* De novo germline and postzygotic mutations in AKT3, PIK3R2 and PIK3CA cause a spectrum of related megalencephaly syndromes. *Nat Genet* **44**, 934-40 (2012).

9.      Butler, M.G. *et al.* Subset of individuals with autism spectrum disorders and extreme macrocephaly associated with germline PTEN tumour suppressor gene mutations. *J Med Genet* **42**, 318-21 (2005).

10.     Laplante, M. & Sabatini, D.M. mTOR signaling in growth control and disease. *Cell* **149**, 274-93 (2012).

11.     Laplante, M. & Sabatini, D.M. mTOR Signaling. *Cold Spring Harb Perspect Biol* **4**(2012).

12.     Cheesman, S. *et al.* Validation of Pyrosequencing for accurate and high throughput estimation of allele frequencies in malaria parasites. *Mol Biochem Parasitol* **152**, 213-9 (2007).

13.     Wasson, J., Skolnick, G., Love-Gregory, L. & Permutt, M.A. Assessing allele frequencies of single nucleotide polymorphisms in DNA pools by pyrosequencing technology. *Biotechniques* **32**, 1144-6, 1148, 1150 passim (2002).

14.     Cerami, E. *et al.* The cBio cancer genomics portal: an open platform for exploring multidimensional cancer genomics data. *Cancer Discov* **2**, 401-4 (2012).

15.     Gao, J. *et al.* Integrative analysis of complex cancer genomics and clinical profiles using the cBioPortal. *Sci Signal* **6**, pl1 (2013).

16.     Barretina, J. *et al.* The Cancer Cell Line Encyclopedia enables predictive modelling of anticancer drug sensitivity. *Nature* **483**, 603-7 (2012).

17.     Forbes, S.A. *et al.* COSMIC: mining complete cancer genomes in the Catalogue of Somatic Mutations in Cancer. *Nucleic Acids Res* **39**, D945-50 (2011).

18.     International Cancer Genome, C. *et al.* International network of cancer genome projects. *Nature* **464**, 993-8 (2010).

19.     Lim, J.S. *et al.* Brain somatic mutations in MTOR cause focal cortical dysplasia type II leading to intractable epilepsy. *Nat Med* **21**, 395-400 (2015).

20.     Lee, J.H. *et al.* De novo somatic mutations in components of the PI3K-AKT3-mTOR pathway cause hemimegalencephaly. *Nat Genet* **44**, 941-5 (2012).

21.     Smith, L.D. *et al.* Exome Sequencing Reveals De Novo Germline Mutation of the Mammalian Target of Rapamycin (MTOR) in a Patient with Megalencephaly and Intractable Seizures. *Journal of Genomes and Exomes* **2**, 63-72 (2013).

22.     Baynam, G. *et al.* A germline MTOR mutation in Aboriginal Australian siblings with intellectual disability, dysmorphism, macrocephaly, and small thoraces. *Am J Med Genet A* **167**, 1659-67 (2015).

23.     Mroske, C. *et al.* Germline activating MTOR mutation arising through gonadal mosaicism in two brothers with megalencephaly and neurodevelopmental abnormalities. *BMC Med Genet* **16**, 102 (2015).

24.     Klein, S., Sharifi-Hannauer, P. & Martinez-Agosto, J.A. Macrocephaly as a clinical indicator of genetic subtypes in autism. *Autism Res* **6**, 51-6 (2013).

25.     Nakashima, M. *et al.* Somatic Mutations in the MTOR gene cause focal cortical dysplasia type IIb. *Ann Neurol* **78**, 375-86 (2015).

26.     Neuman, N.A. & Henske, E.P. Non-canonical functions of the tuberous sclerosis complex-Rheb signalling axis. *EMBO Mol Med* **3**, 189-200 (2011).

27.     Lee, H. *et al.* Clinical exome sequencing for genetic identification of rare Mendelian disorders. *JAMA* **312**, 1880-7 (2014).

28.     McKenna, A. *et al.* The Genome Analysis Toolkit: a MapReduce framework for analyzing next-generation DNA sequencing data. *Genome Res* **20**, 1297-303 (2010).

29.    DePristo, M.A. *et al.* A framework for variation discovery and genotyping using next-generation DNA sequencing data. *Nat Genet* **43**, 491-+ (2011).

30.    Yourshaw, M., Taylor, S.P., Rao, A.R., Martin, M.G. & Nelson, S.F. Rich annotation of DNA sequencing variants by leveraging the Ensembl Variant Effect Predictor with plugins. *Brief Bioinform* (2014).

31.    Rehm, H.L. *et al.* ACMG clinical laboratory standards for next-generation sequencing. *Genetics in Medicine* **15**, 733-47 (2013).

32.    Richards, C.S. *et al.* ACMG recommendations for standards for interpretation and reporting of sequence variations: Revisions 2007. *Genetics in Medicine* **10**, 294-300 (2008).

33.    Strom, S.P. *et al.* Assessing the necessity of confirmatory testing for exome-sequencing results in a clinical molecular diagnostic laboratory. *Genetics in Medicine* **16**, 510-515 (2014).

**Supplemental Material**
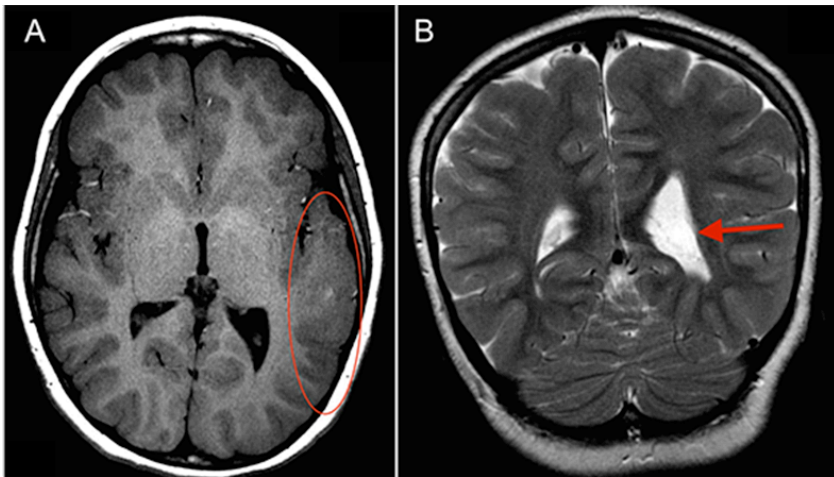


**S1. Supplemental Figure 1: Additional anatomical images of associated with mTOR C1483Y mutation**

(A) Axial MRI showing overgrowth of the left occipito-temporal lobe, indicated by red circle. (B) Coronal MRI showing asymmetry to the ventricles, red arrow pointing to the larger left ventricle.

### S2. Supplemental Document 1: Full clinical case reports

**Case One:**

Case two is a female born NSVD at 37 weeks gestation to a 29-year-old G3P2 mother; paternal age was 29 years at birth. Pregnancy was complicated by maternal occupational exposure to lead, which was confirmed at birth. Fetal movements were decreased, but ultrasounds were normal. Birth weight was 7 pounds, 2 ounces (25th %ile) and length was 21.5cm (95th %ile). Family history was significant for maternal dextrocardia, a maternal grandmother with uterine cancer, a paternal aunt and grandfather with kidney failure, and a paternal first cousin with autism, seizures, and learning disabilities. At birth severe hypotonia and small areas of hypopigmentation on the patient's abdomen, legs, and hands were noted.

At 6.5 years of age she presented with focal epilepsy and hypomelanosis of Ito (Figure 1e and 1f), left hemimegalencephaly, and global developmental delay. She was also found to have decreased visual acuity and tracking with salt and pepper pigmentary changes in her retina. Physical examination showed a height of 121.92 cm (90th %ile) and head circumference of 54cm (>97th %ile). Hand length was 13.5 cm and foot length was 17.4 cm, however, both hands and feet were symmetric in size. Dysmorphic facial features were noted including down slanting palpebral fissures, long eyelashes and a short upturned nose (Figure 1c and d). She displayed symmetric motor movements on both sides of her extremities but had difficulty swallowing food. She also had a history of asthma. Her developmental milestones were delayed: pull to standing at 3.5 years old and walking at 4.5 years old, she was not toilet trained and did not use any words.

Seizure history began at 2.5 months of age and progressively worsened. Her seizures presented as one of two types: type 1, which is less frequent, was clinically characterized by relative behavioral arrest, slow forceful eye blinking, right > left arm stiffening, rightward gaze deviation, suggestion of fencer posturing (right arm extended, left flexed), followed by slow left head/eye deviation 16 seconds after onset. Electroencephalogram showed a build-up of sharply-contoured, rhythmic alpha-theta maximal T3/T5 waves, spreading posteriorly to parietal/occipital region after 5 seconds, thereafter remaining confined to the left posterior quadrant with evolution in frequency/amplitude lasting 5 minutes, the last four of which were comprised of broad ~1Hz T5 spike-wave discharges. The second type manifested clinically as subtle

behavioral arrests. These events were associated with generalized background attenuation with superimposed symmetric or occasionally left > right fast activity lasting 30-45 seconds, often terminating in and/or momentarily disrupted by a high-amplitude 3-5 second burst of monomorphic notched delta wave with shifting hemispheric predominance. Trials of phenobarbital, lamotrigine with levetiracetam, topiramate, oxcarbazepine, and diazepam were unsuccessful in controlling the seizures. Additional pharmacological regimen included clobazam, clonazepam, felbamate, and primidone with limited success.

MRI of the brain revealed asymmetry of the temporal-occipito lobes, and ventricles, consistent with left hemimegalencephaly (Figure 2a, Supplemental Figure 1A and B). Additionally a PET scan was performed which showed asymmetric glucose uptake in the temporo-occipito lobes (Figure 2b). A limited left temporo-occipito-parietal lobe resection with electrocorticography was performed in an attempt to control her seizures. Histopathological examination of the left lateral temporal neocortex from the resection showed multifocal, slight to moderate cortical disorganization. A single focus in the superficial cortex showed a cluster of balloon-like cells of the type seen in focal cortical dysplasia ILAE Type IIB (Figure 2c and d). Prominent neurons were observed in subcortical white matter (Figure 2e and f). Minimal Chaslin's gliosis was also noted. There was no evidence of neoplasm, vascular malformation or active inflammation. The surgery greatly improved her seizures, as they have decreased in prevalence from >10 per day to less than 1 per week. Genetic analysis was limited to trio Clinical Exome Sequencing (CES) ordered on genomic DNA isolated from blood as well as genomic DNA isolated from a skin punch biopsy at the border between the hypopigmented and normal skin areas.

**Case Two:**

Case two is an 8 month old male born to a 37 year old G1P2 mother and 35 year old father. Pregnancy was free of any teratogenic exposures. Family history was significant for a paternal uncle born with a clubfoot, but otherwise unremarkable. Pregnancy was complicated by a decrease in amniotic fluid first noticed at about 3 months. At this time ultrasound revealed an increase in head size. Pregnancy delivery occurred at 35 weeks due to breach presentation. At birth the neonate had extreme macrocephaly, macrosomia, and a right clubfoot. Additional findings at birth included an umbilical hernia, right kidney cyst,

161

and hydrocele. A brain MRI was performed and showed polymicrogyria. The neonate was discharged on day 10 of life.  Surveillance of the kidney demonstrated persistent cyst, and by three months of age linear hyperpigmented lesions were first noticed on the legs, abdomen and back. Overgrowth of the head continued postnatally and interfered with normal motor development, causing difficulty in sitting unassisted, rolling from back to stomach, and holding his head up. Exome sequencing revealed a mosaic variant in the mTOR gene. At 8 months old he presented with overgrowth with length of 78.4cm (>>97th %ile, +3SD), weight 12.8Kg (>>97th%ile + 3.48 SD), and OFC 51.5cm (>>97th %ile, +5.28SD).  Additionally, he presented with right sided hemi-hyperplasia with a leg length discrepancy of 0.5cm, calf circumference discrepancy of 0.5cm, and hand length discrepancy of 0.5cm. Linear hyperpigmentation was present, and dysmorphic facial features included low set ears, down slanting palpebral fissures, and hypertelorism.

**Case Three:**

Case three is a female born via normal spontaneous vaginal delivery (NSVD) at 36 weeks gestation to a primigravida 32-year-old mother; paternal age at birth was 36. Pregnancy was complicated by oligohydramnios. At birth torticollis was noted.  Birth length was 19cm (25%ile) and weight was 7 pounds (25%ile). There were no neonatal complications. Family history was negative for any suspected genetic conditions on either side of the family. Physical therapy was started for torticollis and hypotonia at 3 months of age, when motor delay was also noted. Developmental milestones were delayed with sitting at 16 months of age, crawling at 19 months of age, and first words at 13 months of age. At 21 months of age she was evaluated for macrocephaly and global developmental delay. At that age, palpebral fissures were noted to be 3cm on the left and 2.5 cm on the right (>90th %ile). Hypertelorism was noticed with an intercanthal distance of 3cm (75-97th %ile), interpupillary distance of 5cm and outer canthal distance of 8.5cm (97th %ile). Additionally, a flattened nasal bridge and mild pectus excavatum were observed. Plagiocepahly was also noted and MRI of the brain was normal. Developmental delays continued with walking at 25 months of age, and by eight years of age her speech was composed of moderately complex sentences of three to six words, mostly echolalia. Fine motor skills were delayed and writing was impaired.  At eight years old she presented with global developmental delay, and learning disabilities.  Physical exam showed weight 33.2 kg  (90th %ile), height of 140.6 cm (>95th %ile), and head circumference of 159 cm (>98th%ile). Additionally

phenotypic features at this time included over crowding of the teeth, flattened nasal bridge (Figure 1a and b), pes planus, and a wide based gait. Genetic workup included SNP chromosomal microarray, PTEN mutation analysis, and fragile X testing, all of which were normal.
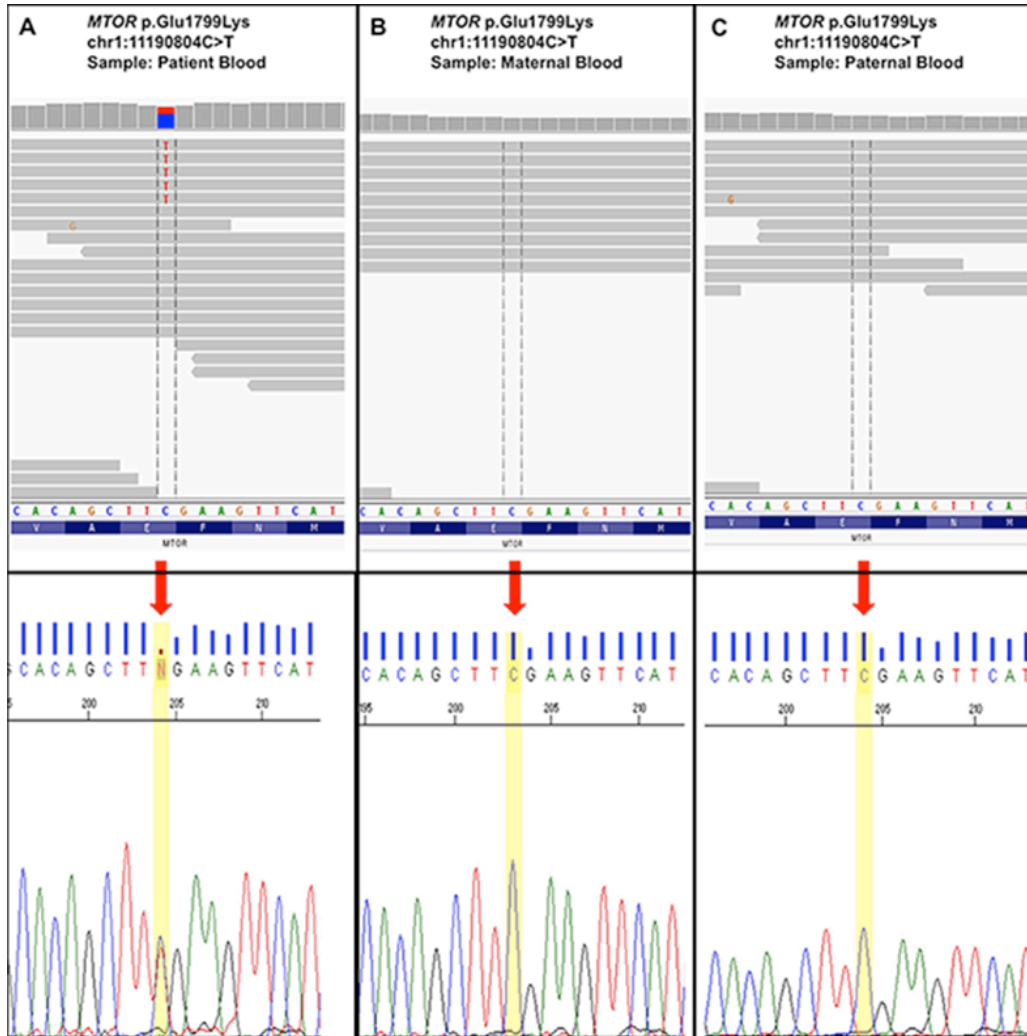
**S3. Supplemental Figure 2: Sequencing reads and confirmation of mutation in Case 1**

Integrative Genomics Viewer alignments and the Sanger chromatograms showing the presence of the mutation in the patient (A) and its absence in the parental samples (B and C). Germline distribution of the mutation was deduced from Sanger chromatograms due to low depth of coverage (14X, 11X and 10X in the patient, father and mother, respectively) by exome sequencing.

**S4. Supplemental Figure 3: Sequencing reads of mutation in Case 1**

The Integrative Genomics Viewer of the alignment file demonstrates the presence of this mutation in (A) 2 of 192 total reads in the patient blood; (B) 83 of 231 reads in skin; (C) 0 of 198 reads in maternal blood; and (D) 0 of 201 reads in the paternal blood sample.
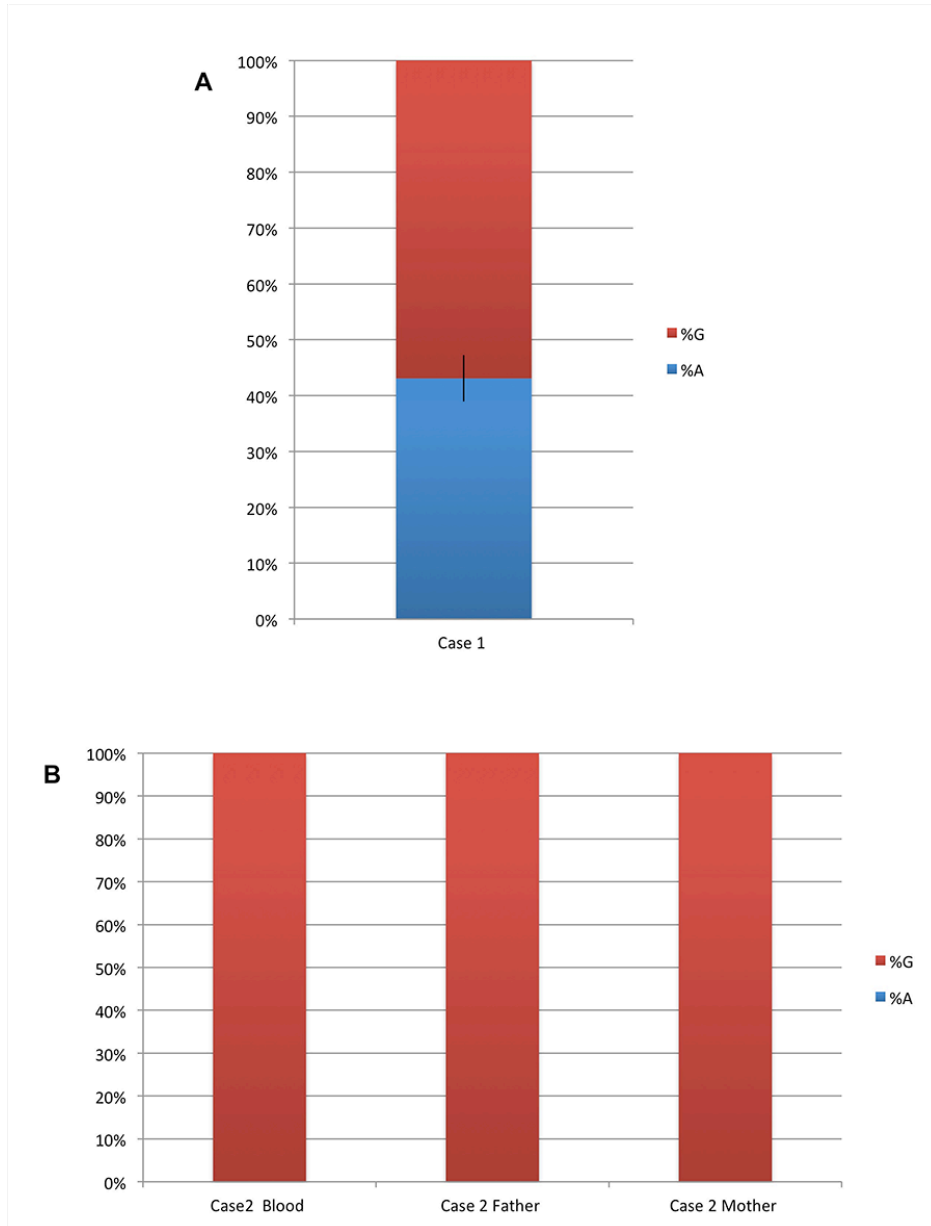
**S5. Supplemental Figure 4: Pyrosequencing confirmation of germline E1799K mutation**
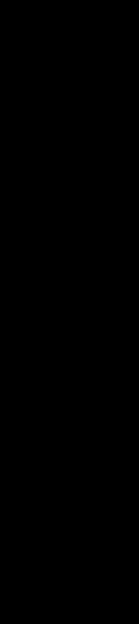
Mutation abundance determined by pyrosequencing for Case 1 (g. 1:11190804, c.5395G>A, p.Glu1799Lys) and case 2 (g. 1:11217230, c.4448 G>A), with reference allele (G) in red and alternate allele (A) in blue. (A) Allele frequencies demonstrate germline

distribution. (B) Mutations not detectable in blood samples from Case 2, or the parents. Black bars represent standard deviations. Images of resected brain tissue displayed above each bar.

| Mutation | Source | Type | Source | Replicate Present (Y/N) | Tissue Designation | Total Number |
|---|---|---|---|---|---|---|
| **E1799K** | **cBio** | **Endometrium** | **CCLE** | **Y** | **Cervical/Unterine** | |
| **E1799K** | **cBio** | **Kidney** | **CCLE** | **Y** | **Renal** | |
| **E1799K** | **cBio** | **CNS** | **CCLE** | **Y** | **CNS** | |
| E1799K | cBio | Cervical | TCGA | N | **Cervical/Unterine** | |
| E1799K | cBio | Colorectal Adenocarcinoma | TCGA | N | **Intestine** | |
| E1799K | cBio | Colorectal Adenocarcinoma | TCGA | N | **Intestine** | |
| E1799K | cBio | Colorectal Adenocarcinoma | MSKCC | N | **Intestine** | |
| E1799K | cBio | MM | Broad | N | **Blood Lineage** | |
| E1799K | cBio | Prostate | Broad/Cornell | N | **Prostate** | |
| E1799K | cBio | Uterine | TCGA | N | **Cervical/Unterine** | |
| E1799K | cBio | Uterine | TCGA | N | **Cervical/Unterine** | |
| E1799K | cBio | Uterine | TCGA | N | **Cervical/Unterine** | |
| E1799K | ICGC | Uterine corpus endometrial carcinoma | UCEC-US | N | **Cervical/Unterine** | |
| E1799K | ICGC | Uterine corpus endometrial carcinoma | UCEC-US | N | **Cervical/Unterine** | |
| E1799K | ICGC | Cervical squamous cell carcinoma | CSC-US | N | **Cervical/Unterine** | |
| E1799K | ICGC | Glioblastoma multiforme | GBM-US | N | **CNS** | |
| E1799K | COSMIC | Glioma | COSMIC | N | **CNS** | |
| E1799K | COSMIC | Cervix | COSMIC | N | **Cervical/Unterine** | |

| | | | | | | |
|---|---|---|---|---|---|---|
| E1799K | COSMIC | Endometrium | COSMIC | N | **Cervical/Unterine** | |
| E1799K | COSMIC | Endometrium | COSMIC | N | **Cervical/Unterine** | |
| E1799K | COSMIC | Endometrium | COSMIC | N | **Cervical/Unterine** | |
| E1799K | COSMIC | Endometrium | COSMIC | N | **Cervical/Unterine** | |
| E1799K | COSMIC | Large Intestine | COSMIC | N | **Intestine** | |
| E1799K | COSMIC | Prostate | COSMIC | N | **Prostate** | |
| **E1799K** | **CCLE** | **Glioma** | **CCLE** | **Y** | **CNS** | |
| **E1799K** | **CCLE** | **Clear Cell Renal Carcinoma** | **CCLE** | **Y** | **Renal** | |
| **E1799K** | **CCLE** | **endometrium adenocarcinoma** | **CCLE** | **Y** | **Cervical/Unterine** | **23** |
| C1483W | cBio | Breast | Broad | N | **Breast** | |
| **C1483Y** | **cBio** | **acute_lymphoblastic_T_cell_leukaemia** | **CCLE** | **Y** | **Blood Lineage** | |
| C1483R | cBio | Glioblastoma multiforme | TCGA | N | **CNS** | |
| C1483Y | cBio | Clear Cell Renal Carcinoma | TCGA | N | **Renal** | |
| C1483F | cBio | Clear Cell Renal Carcinoma | TCGA | N | **Renal** | |
| C1483F | cBio | Clear Cell Renal Carcinoma | TCGA | N | **Renal** | |
| C1483Y | cBio | Clear Cell Renal Carcinoma | TCGA | N | **Renal** | |
| C1483R | ICGC | Glioblastoma multiforme | GBM-US | N | **CNS** | |
| C1483Y | COSMIC | Kidney | COSMIC | N | **Renal** | |
| C1483F | COSMIC | KIDNEY | COSMIC | N | **Renal** | |
| C1483F | COSMIC | KIDNEY | COSMIC | N | **Renal** | |
| C1483R | FCD | CNS | Lim et al. | N | **CNS** | |
| **C1483Y** | **CCLE** | **acute_lymphoblastic_T_cell_leukae** | **CCLE** | **Y** | **Blood Lineage** | **12** |

| | | mia | | | | |
|---|---|---|---|---|---|---|
| T1977K | cBio | Clear Cell Renal Carcinoma | TCGA | N | **Renal** | |
| T1977R | cBio | Prostate | TCGA | N | **Prostate** | |
| T1977K | ICGC | Renal Cell Carcinoma | RECA-EU | N | **Renal** | |
| T1977K | ICGC | Renal Cancer | KIRC-US | N | **Renal** | |
| T1977R | Cosmic | Kidney | Cosmic | N | **Renal** | |
| T1977R | Cosmic | Large Intestine | Cosmic | N | **Intestine** | |
| T1977R | Cosmic | Prostate | Cosmic | N | **Prostate** | |
| T1977K | Cosmic | Lymphoid | Cosmic | N | **Blood Lineage** | |
| T1977K | Cosmic | Kidney | Cosmic | N | **Renal** | |
| T1977K | Cosmic | Kidney | Cosmic | N | **Renal** | |
| T1977S | Cosmic | Lymphoid | Cosmic | N | **Blood Lineage** | |
| T1977K | FCD | CNS | Lim et al. | N | **CNS** | |
| T1977K | FCD | CNS | Lim et al. | N | **CNS** | 13 |

## S6. Supplemental Spreadsheet 1: Merged data from mTOR mutations in cancer spreadsheet
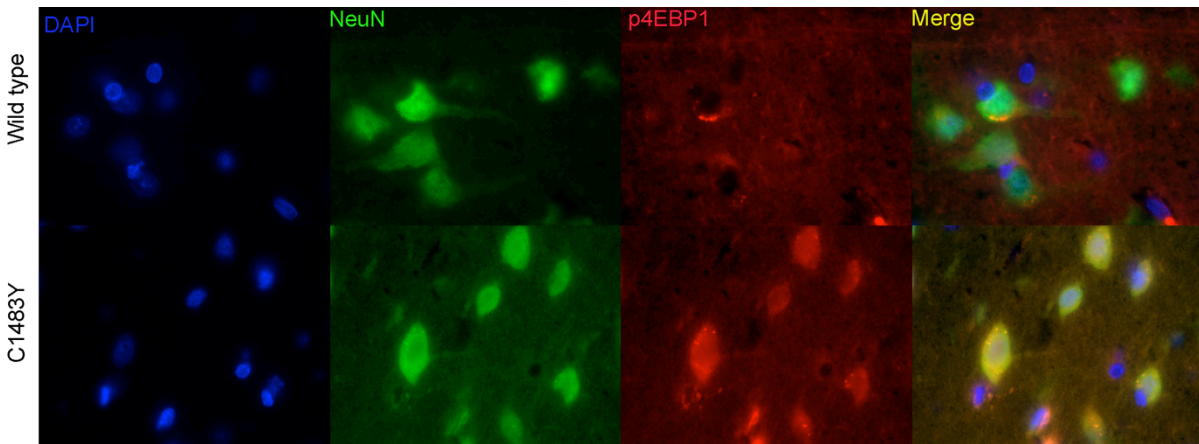
**S7. Supplemental Figure 7: mTOR activated cells in brain samples**

Immunofluorescence staining of brain tissue showing strong activation of p4EBP1 in NeuN

positive cells.  C1483Y:  g. 1:11217230 G>A, c.4448 G>A, p.Cys1483Tyr,

**S8. Supplemental Document 2: Detailed materials and methods**

Exome Sequencing

Cases 1 and 2 were sequenced at the UCLA Clinical Genomics Center and case 3 was sequenced at an outside clinical laboratory. Clinical exome sequencing at UCLA was performed following the validated protocol as described by Lee et al.[27] Briefly, exome capture was performed using Agilent SureSelect Human All Exon V2 50Mb and sequencing was performed on an Illumina HiSeq 2500 as 100-bp paired-end runs. Mean coverage across the RefSeq protein-coding exons and flanking intronic sequence (±2 bp) was >100-fold with > 93% of these base positions being sequenced at >9×. Sequence reads were aligned to the human reference genome (hg19/NCBI Build 37) using Novoalign V2.07.15b (Novocraft, http://www.novocraft.com/main/index.php). PCR duplicates were marked using Picard-tools-1.42 (http://picard.sourceforge.net/). Indel (insertions and deletions) realignment, quality score recalibration, variant calling, recalibration and variant eval were performed using the Genome Analysis Toolkit (GATK) v1.1-33 [28,29]. All variants were annotated using Variant Annotator eXtras (VAX)[30] and deposited into MySQL 5.2 database for filtering. Amino acid altering *de novo*, hemizygous, homozygous, compound heterozygous and inherited heterozygous variants with minor allele frequency (MAF) less than 1% (based on data from the 1000 genomes project (1Kg), NHLBI exome sequencing project (ESP), NIEHS environmental genome project (EGP) and HapMap, without the distinction of ethnic background) that were relevant to the patient's phenotype were considered for further analysis. The pathogenicity of a variant was determined according to current ACMG sequence interpretation guidelines. [31,32] Only variants with a QUAL score (a

172

scaled probability of a variant being present at a certain position based on the GATK data) lower than 500 (an empirically determined cutoff), and all small indels were confirmed by Sanger sequencing.[33]

Pyro Primer Sequences:

c.4448 Pyro F 5' AGGACGACCCAGAGCTGATG 3'

c.4448 Pyro R 5' CTCACCATTCCCCCAAGG 3' (5' Biotin)

c.4448 Pyro Seq 5' TGGGCCGCATGCGCT 3'

c.5395 Pyro F 5' ATGCGTGGGCAGTGATGA 3' (5' Biotin)

c. 5395 Pyro R 5' ATCGCGGGCTTGGTTCTG 3'

c. 5395 Pyro Seq 5' ATGTTTGTAGTGTAGCACAG 3'

mTOR site directed mutagenesis primers

E1799K:

F Primer : CATGCGTGGGCAGTGATGAACTTCAAAGCTGTGCTACACTAC

R Primer: GTAGTGTAGCACAGCTTTGAAGTTCATCACTGCCCACGCATG

C1483Y:

F Primer: CTGGGCCGCATGCGCT**A**CCTCGAGGCCTTGGGGGAATG

R Primer: CATTCCCCCAAGGCCTCGAGG**T**AGCGCATGCGGCCCAG


T1977I:

F Primer: GGCCCTCATCTACCCACTGA**T**AGTGGCTTCTAAGTCTACC

R Primer: GGTAGACTTAGAAGCCACTATCAGTGGGTAGATGAGGGCC


Sequencing Primers:

| | |
|---|---|
| mTOR_CMV_F | CGC AAA TGG GCG GTA GGC GTG |
| mTOR_F_1 | GGA GTC TAC TCG CTT CTA TGA CC |
| mTOR_F_2 | GAC AAC ATT TTT GTG GCC GT |
| mTOR_F_3 | TAC AGC CCC AGC AGT CAA AT |
| mTOR_F_4 | TGC TGG ACA TCA TCC GAG |
| mTOR_F_5 | AGC TTT GAA TTT GAA GGC CA |
| mTOR_F_6 | CCT TTG TCA TGC CTT TCC TG |
| mTOR_F_7 | GAG CCC TAC AGG AAG TAC CCT |
| mTOR_F_8 | GTT CCT GCC CCA GGT CAT |
| mTOR_F_9 | CTG AAG CTC CAC TGC CAT CT |
| mTOR_F_10 | GAA GAA ACT GCA CGT CAG CA |
| mTOR_F_11 | CGA GCA TAT GCC AAA GCA CT |
| mTOR_F_12 | AGT GGG ACA GCA TGG AAG AA |
| mTOR_F_13 | AGT ATG CAA GCC TGT GCG G |
| mTOR_F_14 | GCG TGG GCA GTG ATG AAC T |
| mTOR_F_15 | TAG TGG AGG GGG TGA AGC |

| | |
|---|---|
| mTOR_F_16 | ATG CTA TGA TGG AAC GGG G |
| mTOR_F_17 | AAG ATC TGC GCC AGG ATG |
| mTOR_F_18 | TTT AGC GGT CAT GTC AAT GG |
| mTOR_F_19 | AAA TTT TGG ACG GTG TGG AA |
| mTOR_R_1 | AGA TGC CAC CTT TCC TCT CA |

**Chapter Four**


Mutations in the Sonic Hedgehog Pathway cause

Macrocephaly-associated conditions due to cross talk

to the PI3K/AKT/mTOR pathway

Abstract

The hedgehog (Hh) pathway is a highly evolutionarily conserved signaling cascade that plays an essential role in the patterning of the developing embryo of many species.  In many organ systems, including the developing limb bud and neural tube, the spatial and temporal patterning of Hh ligands is well studied. Due to its role in promoting cellular proliferation, mutations in the Hh pathway are often observed in sporadic solid tumors of numerous tissues.  Additionally, more widespread genetic mutations in components of this pathway are associated with reproducible human phenotypes and syndromic conditions. The phenotypic manifestations of individuals presenting with Hh pathway mutations depends on which component of the pathway is mutated, and while there are unique findings associated with each syndrome there is strong phenotypic overlap. Common to these syndromes are the findings of polydactyly/syndactyly and brain overgrowth with macrocephaly.  The latter is a finding most commonly observed with syndromic overgrowth associated with mutations in the PI3K/AKT/mTOR pathway. We have identified novel Hh pathway mutations and structural copy number variations in individuals with somatic overgrowth, macrocephaly, dysmorphic facial features and developmental delay.  We hypothesize that the brain overgrowth and phenotypic overlap with syndromic overgrowth syndromes in these cases may be due to cross talk between the Hh and PI3K/AKT/mTOR pathways. To test this we modeled disease associated variants by generating PTCH1 and SUFU heterozygote cell lines? using the Crispr/Cas9 system. These cells demonstrate activation of PI3K signaling and increased phosphorylation of its downstream target p4EBP1 as well as a distinct cellular phenotype that includes cellular hyperplasia.  To investigate the mechanism underlying this cross talk

we treated primary human neural stem cells with sonic hedgehog ligand and performed transcriptional analysis of multiple components of the mTOR pathway. These studies identified decreased expression of a set of mTOR negative regulators that appeared to show decreased expression. Transcription factor binding analysis revealed that these down regulated genes all share transcription factor binding sites for LyF and many share an Nkx2.2 binding site. These transcription factors are known to be Hh responsive supporting our hypothesis. We conclude that there is significant cross talk between the SHH and PI3K/AKT/mTOR pathway which underlies the brain overgrowth observed in these cases. We also present behavioral information regarding our patient cohort, focusing on the occurrence of developmental delay in this cohort and propose that mutations in PTCH1 and SUFU mimic PTEN-associated Hamartoma Syndromes.

Introduction

　　Sonic HedgeHog *Signaling*

Hedgehog (Hh) signaling was first described in Drosophila melanogaster as a central

regulator of "Wingless" (Wnt) orthologue signaling and patterning of the wing during

development[1; 2].  In vertebrates, a parallel role for limb development was confirmed as well

as more complex involvement in neural cell type differentiation[3] and organ development[4].

Hh Signaling begins with the binding of Hh ligands to their receptor.  In humans there are

three main Hh ligands sonic, indian, and desert, hedgehog (SHH, IHH, and DHH) and two

receptors Patched 1 (PTCH1) and Patched 2 (PTCH2). The effect of ligand binding is

inhibition of PTCH, which then inhibits smoothened (SMO). Inhibition of SMO leads to

inhibition of Suppressor of Fused (SUFU) and Kinesin family member 7 (KIF7).  With SUFU

inhibited the main effectors of Hh signaling Glioma-associated oncogenes 1-3 (Gli1-3) can

translocate to the nucleus where they act as transcription factors and modulate the

expression of numerous target genes[5-7]. This translocation event is additionally regulated

by via the Dual-Specificity Tyrosine Phosphorylation-Regulated Kinase (DYRK1A, Figure

1)[5; 8]. The transcriptional targets of Gli1-3 coordinate crosstalk with numerous other

signaling cascades including Wnt, TGFβ and Notch[9; 10]. These coordinated pathways play

important roles in not only embryogenesis but additionally stemness[11], protein synthesis[12]

and cell migration[13]. With the wide spread effects and roles of Hh signaling it has been

shown that genetic disruptions to Hh components result in multiple developmental

abnormalities and neoplasms.

Figure 4-1: Hedgehog Signaling Pathway

Initial ligand binding activates hedgehog signaling; Sonic hedgehog binds to the receptor PTCH1, which inhibits the membrane-bound Smoothened. When activated, Smoothened activates SUFU, which facilitates the translocation of Gli1-3 into the nucleus. Once in the nucleus, the Gli1-3 transcription factors coordinate the expression of numerous genes.
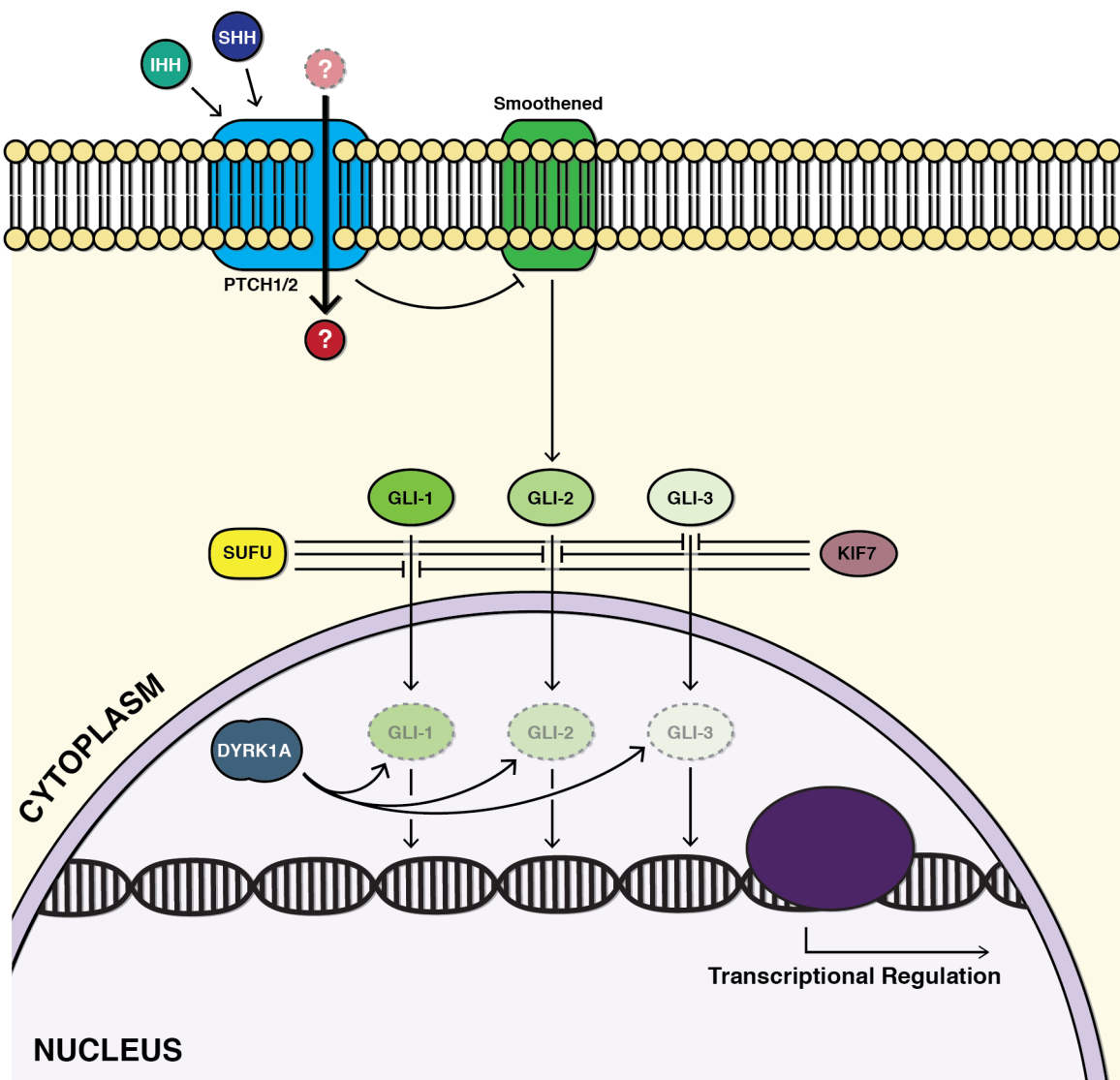
*SHH Mutations In Cancer*

Mutations in the Hh signaling pathway that cause constitutive activation have been most described in basal cell carcinomas[14] and medulloblastoma[15]. Additionally, altered Hh signaling has also been reported in numerous other cancer types including breast[16], pancreas[17] and prostate[18]. Due to its wide spread effects on cell proliferation, migration and differentiation Hh inhibitors have emerged as potential anti-cancer therapies (Figure 2). The goal of these therapies is to dampen Hh signaling and inhibit some of its proliferative and anti-apoptotic functions[19-21]. In addition to being associated with numerous sporadic solid tumors, wide spread disruption of the Hh pathway leads to a plethora of human phenotypes and syndromic presentations.

Figure 4-2: Chemical and Pharmacological inhibition of the hedgehog pathway.

Due to its involvement in numerous sporadic tumor types, inhibitors of the Hh pathway

activity have been developed and discovered. The two main targets of inhibition are

Smoothened and Gli1.
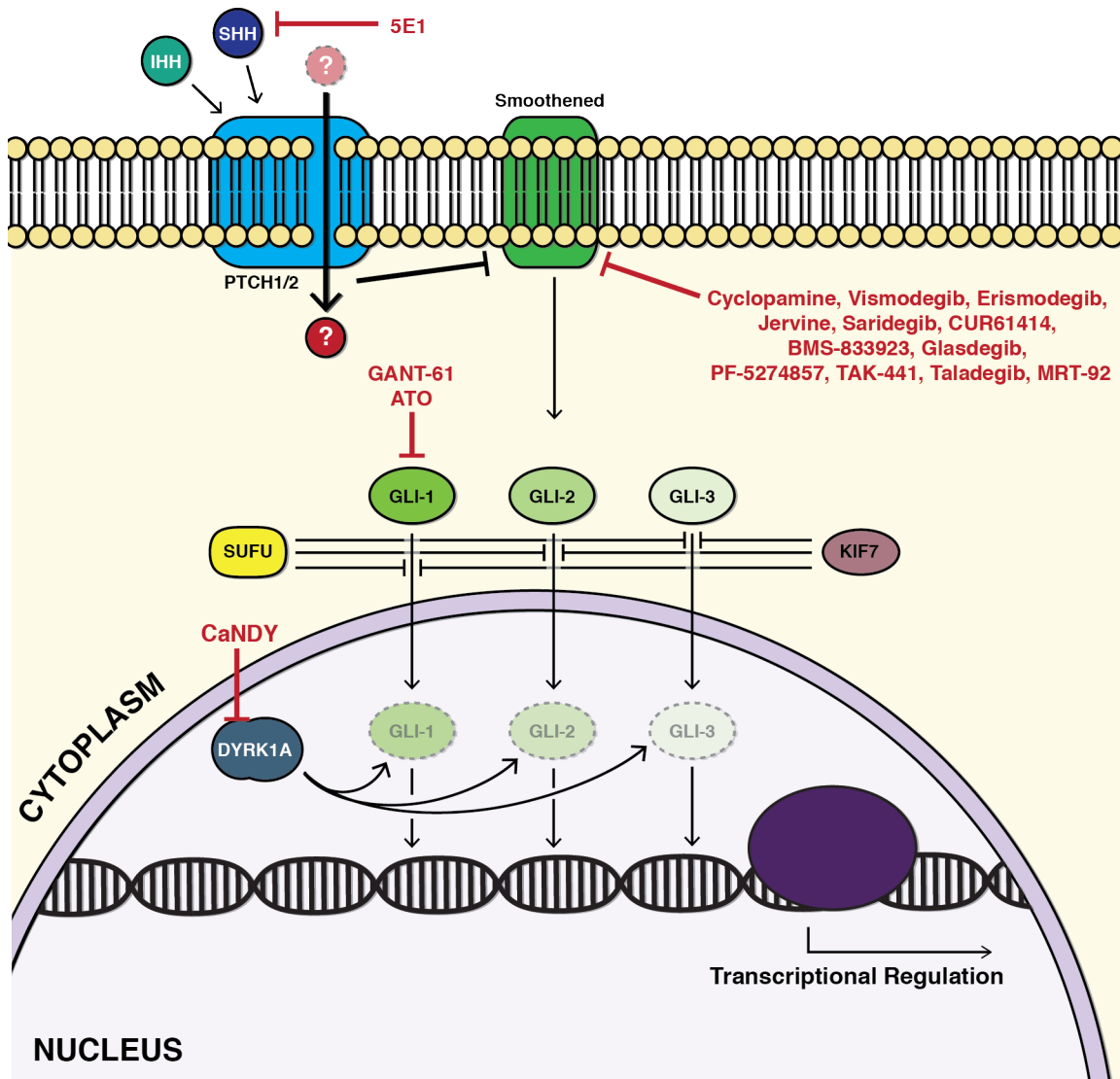
*SHH Mutations in Genetic Syndromes*

A comprehensive review of the genetic syndromes associated with Hh appears in Chapter 1. For this chapter we focused on the phenotypic overlap between these conditions as a way to highlight the common consequences of deregulated Hh signaling.  We compared the brain, limb, neoplasm and facial dysmorphic traits of each of the Hh associated syndromes. From this we have observed trends in each tissue type that help to unify certain roles for Hh signaling in the developing human embryo. As initially described, Hh signaling plays an essential role in the patterning and segmentation of the limbs. Nearly every condition demonstrates limb phenotypes with polydactyly being the most common. Additionally, pharyngeal arch migration is implicated, as facial dysmorphologies are common.   The neoplasms observed in these syndromic conditions mirror those observed in Hh pathway associated sporadic tumors including basal cell carcinomas and medulloblastoma, confirming the important role of Hh signaling the in skin and the brain. The brain phenotypes are varied and present in a range from widespread holoprosencephaly and megalencephaly to more focal and specific agenesis of the corpus callosum, hemimegalencephaly and anterior pituitary hypoplasia.  The triad of brain-limb-dysmorphic phenotypes helps to define the Hh-associated syndromes, albeit with varying degrees and specific findings unique to each genetic etiology. Less well understood or reported are the behavioral phenotypes and general somatic growth trends for many of these conditions (Table 1, Figure 3).

Table 4-1: Syndromes associated with mutations in the Hh signaling pathway and associated phenotypes

We presented a list of the congenital genetic syndromes associated with mutations to the Hh pathway. We stress the occurrence of brain, limb neoplastic and dysmorphic phenotypes within this group.

## Hedgehog Ligands

| Gene Symbol | Gene Name | Associated Syndrome (S) | Type of Mutation/ Effect on pathway | Ref | Brain Phenotype | Limb Phenotype | Neoplasms | Dysmorphic |
|---|---|---|---|---|---|---|---|---|
| SHH | Sonic hedgehog | Holoprosencephaly 3 | Inactivating/Down regulation | [22] | Holoprosencephaly Single brain ventricle | n/a | n/a | Proboscis Midface hypoplasi |
| IHH | Indian hedgehog | Acrocallosal Syndrome | Inactivating/Down regulation | [23] | Disproportionate Macrocephaly | Short-limbed dwarfism Brachydactyly | n/a | n/a |

## Membrane Bound Receptors

| Gene Symbol | Gene Name | Associated Syndrome (S) | Type of Mutation/ Effect on pathway | Ref | Brain Phenotype | Limb Phenotype | Neoplasms | Dysmorphic |
|---|---|---|---|---|---|---|---|---|
| PTCH1 | Patched 1 | Basal cell nevus syndrome | Inactivating/Up regulation | [24] | Megalencephaly | Brachydactyly Short 4th metacarpal Short thumb terminal phalanx | Medulloblastoma Basal cell carcinoma | Broad facies Frontal and biparietal bossing Mild mandibular prognathism Odontogenic keratocysts of jaws |
| PTCH2 | Patched 2 | Basal cell nevus syndrome | Inactivating/Up regulation | [25] | Megalencephaly | Brachydactyly Short 4th metacarpal Short thumb terminal phalanx | Medulloblastoma Basal cell carcinoma | Frontal bossing Mild mandibular prognathism Odontogenic keratocysts of jaws |
| SMO | Smoothened | Curry-Jones Syndrome | Activating/Up Regulation | [26] | Hemimegalencephaly Megalencephaly Polymicrogyria | Broad thumbs Duplicated thumbs Preaxial polydactyly | Desmoplastic medulloblastoma of cerebellum | Facial asymmetry |

## Cytoplasmic/Nuclear Signaling

| Gene Symbol | Gene Name | Associated Syndrome (S) | Type of Mutation/ Effect on pathway | Ref | Brain Phenotype | Limb Phenotype | Neoplasms | Dysmorphic |
|---|---|---|---|---|---|---|---|---|
| SUFU | SUFU negative regulator of hedgehog signaling | Basal cell nevus syndrome | Inactivating/Up regulation | [27] | Megalencephaly | Brachydactyly Short 4th metacarpal Short thumb terminal | Medulloblastoma Basal cell carcinoma | Broad facies Frontal bossing Prognathism Odontogenic |

| | | | | | | | | phalanx | | keratocysts of jaws |
|---|---|---|---|---|---|---|---|---|---|---|
| **GLI2** | GLI family zinc finger 2 | Culler-Jones syndrome, Holoprosencephaly 9 | Inactivating/Down regulation | [28] | Anterior pituitary hypoplasia Ectopic posterior pituitary Thin pituitary stalk | Postaxial polydactyly | n/a | | | Midface hypoplasia Hypotelorism Cleft lip Cleft palate |
| **GLI3** | GLI family zinc finger 3 | Greig cephalopolysyndactyly syndrome | Inactivating/Down regulation | [29] | Macrocephaly Hydrocephaly Agenesis of corpus callosum | Postaxial polydactyly Broad thumbs Syndactyly Camptodactyly | n/a | | | High forehead Frontal bossing Hypertelorism Downslanting palpebral fissures Broad nasal root |
| **KiF7** | Kinesin family member 7 | Acrocallosal syndrome, Joubert syndrome 12 | Inactivating/Up regulation | [30] | Macrocephaly Hypoplastic or absent corpus callosum | Tapered fingers Fifth finger clinodactyly Brachydactyly polydactyly | n/a | | | Prominent forehead Short philtrum Hypoplastic midface |

Figure 4-3: Summary of Hh associated phenotypes.

As presented in Table 1, we have summarized the key findings of Hh-related syndromes.

The main manifestations are those affecting the development of the brain, limbs, and face.

This reproducible triad marks specific events and processes in development that are

altered by abnormal Hh signaling.



## Brain
Megalencephaly
Holoprosencephaly
Hemimegalencephaly
Absent Corpus Callosum

## Face
Proboscis
Frontal Bossing
Facial Asymetry
Short Piltrum

## Hands
Brachydactyly
Broad Thumbs
Polydactyly
Syndactyly

## Feet
Polydactyly
Syndactyly
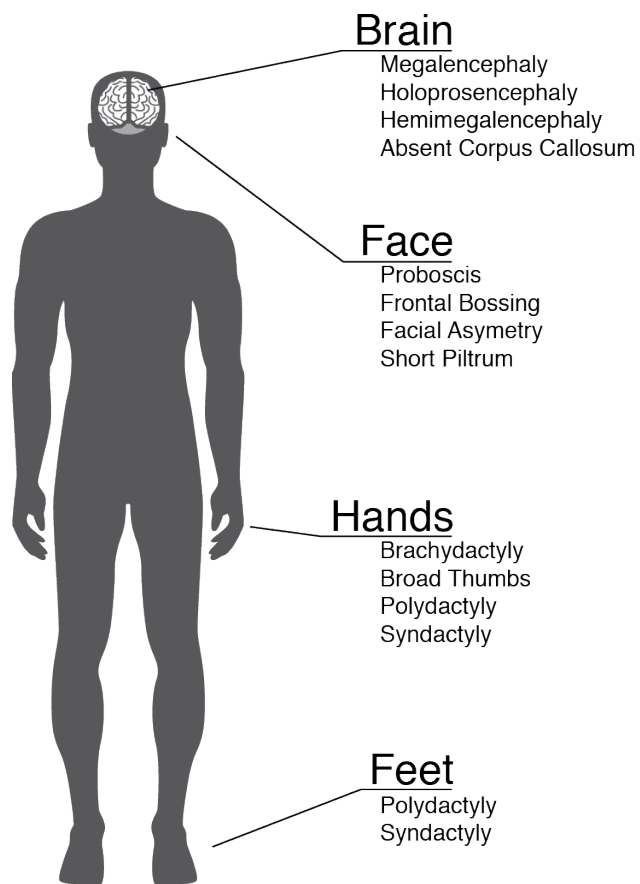
In a cohort of macrocephaly cases we have identified germ-line mutations with activated

Hh signaling. These cases have mutations in PTCH1 and SUFU, both structural copy number

variants (CNVs) diagnosed via chromosomal microarray and single nucleotide variants

(SNVs) diagnosed via clinical exome sequencing (CES). We present phenotypic data for

each of the cases and show that there is striking somatic overgrowth, macrocephaly, and

behavioral phenotypes. This constellation of phenotypes was most similar to mutations in

PTEN and therefore we propose that there might be cross-talk between the activated Hh

pathway and the PI3K/AKT/mTOR signaling cascade. To explore this hypothesis we

generated PTCH1 and SUFU heterozygote cell populations via Crispr/Cas9 and furthermore

treated primary human neural stem cells with SHH ligand and assayed the transcriptional

consequences of Hh activity. Our findings demonstrate that the phenotypic overlap

between Hh and PI3K associated syndromes is due to underlying molecular cross talk.


Materials and Methods

### Crispr/Cas9 Cloning

*PTCH1 and SUFU* w deleted from HEK293T cells utilizing the Crispr/Cas9 plasmid

(pSpCas9(BB)-2A-Puro (PX459) V2.0, #62988[31]) from addgene.   Guide RNAs (gRNAs)

were designed using benching software. gRNAs were selected which showed the highest

"on-target" score[32] and "off-target" score[33]. The 20Bp gRNAs were flanked with CACC-on

the 5'end of their forward oligo and AAAC- on the 5'end of their reverse oligo. These

overhangs facilitate ligation into the parental plasmid once it is digested with BBSI. Briefly

the oligos were annealed and phosphorylated using T4 PNK enzyme (NEB, M0201S),

annealed oligos were then diluted an added to a digestion-ligation reaction containing parental plasmid, tango buffer (Life Tech By5), DTT, ATP, BBSI (Thermo, FD1014) and T7 Ligase (NEB, M03185). After six cycles of $37^0$C for five minutes and $23^0$C for 5 min the reaction was treated with plasmid safe exonulease (Epicentre, E3101K). Finally plasmids were transformed in Stbl3 E.Coli and grown under ampicillin selection. Plasmid mini-preps were performed on three colonies and sanger sequencing confirmed the cloning event using the human U6 primer sequence: 5'-CGATACAAGGCTGTTA-3'.

gRNA Sequences:

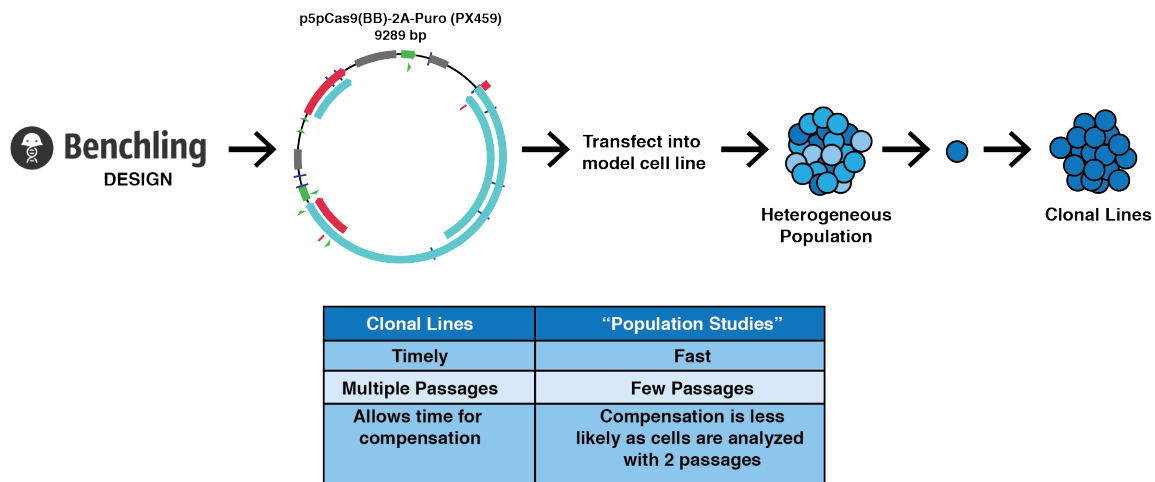| ID | Sequence |
|---|---|
| PTCH1 Upstream 1 F | 5'-**CACC**-GAAGCTTGCTGGGTCTCTACT-3' |
| PTCH1 Upstream 1 R | 5'-**AAAC**-AGTAGAGACCCAGCAAGCTTC-3' |
| PTCH1 Downstream 1 F | 5'-**CACC**-GTTAGGTTAAGGCACACTACT-3' |
| PTCH1 Downstream 1 R | 5'-**AAAC**-AGTAGTGTGCCTTAACCTAAC-3' |
| PTCH1 Downstream 2 F | 5'-**CACC**-GTGTGCCTTAACCTAACGCA-3' |
| PTCH1 Downstream 2 R | 5'-**AAAC-**TGCGTTAGGTTAAGGCACAC-3' |
| SUFU Upstream 1F | 5'-**CACC**-GCCGCCGCCGAGTCTGCCAGA-3' |
| SUFU Upstream 1R | 5'-**AAAC-**TCTGGCAGACTCGGCGGCGGC-3' |
| SUFU Downstream 1F | 5'-**CACC**-GTAGATGGCGTGCAGTCCCG-3' |
| SUFU Downstream 1R | 5'-**AAAC-**CGGGACTGCACGCCATCTAC-3' |
| LAMTOR3 Upstream 1F | 5'-**CACC**-GGACAGGATCTAGAAAACAG-3' |
| LAMTOR3 Upstream 1R | 5'-**AAAC-**CTGTTTTCTAGATCCTGTCC-3' |

| LAMTOR3 Downstream 1F | 5'-**CACC**-GTTGTGACGAAAATTTTCCAG-3' |
| LAMTOR3 Downstream 1R | 5'-**AAAC**-CTGGAAAATTTTCGTCACAAC-3' |

*Cell Culture and Transfection:*

**HEK293T:** Cells were maintained with basal media including DMEM, PSN and 10% fetal bovine serum (FBS). Twenty-four hours before transfection cells were liberated from T25 flask with TrypLE™ Express Enzyme (1X). Cell concentration and viability was determined with the Invitrogen Countess I. After plating $2x10^5$ viable cells onto a 12-well culture dish, volume was brought to 1ml of basal media. On the day of transfection media was aspirated, and 500ul of basal media was added to each well. GeneIn Transfection reagent was combined with 2ug of plasmid, brought to a final volume of 200ul, vortexed and then incubated at room temperature for 15 minutes then added to each well. Cells were incubated for 24 hours, followed by a 12-hour nutrient starvation in DMEM lacking glutamine, glucose and FBS. To model PTCH1, SUFU and LAMTOR3 loss we chose to analyze populations of cells which had been edited, instead of clonally expanding individual cell lines (Figure 4).

Figure 4-4: Experimental design for generation of PTCH1, SUFU, and laMTOR3 deletion populations in HEKS293Ts

Guide RNAs (gRNAs) were designed using Benchling software, which maximizes efficiency and minimizes off target effects. These gRNAs are then cloned into parental Crispr plasmids that also carry puromycin. Following transfection and puromycin selection, we analyzed populations of cells. This is advantageous due to the few passages required which gives the cells less time to compensate, and allows biological differences to be observed.



| Clonal Lines | "Population Studies" |
|---|---|
| Timely | Fast |
| Multiple Passages | Few Passages |
| Allows time for compensation | Compensation is less likely as cells are analyzed with 2 passages |

*Western Blot Analysis*

Cells were lysed on 24 well or 12 well plates with 200µl or 400ul of passive lysis buffer, prepared with phosphatase and protease inhibitors, and incubated by shaking at $4^0C$ for one hour. After lysis tubes were spun at 7500 Rcf for 5 minutes to collect debris. Supernatant was transferred to a new tube then protein concentration determined with the Coommasie Plus Bradford (Life Technologies) reagent following manufacture instructions. Protein samples were diluted to a final concentration of 10µg/20 µl into Western loading buffer with beta-mercaptoethanol and then boiled for 5 minutes. Western blots were run on 12% acrylamide gels followed by transfer onto nitrocellulose membranes utilizing the Transblot Turbo® apparatus from Biorad. The membrane was blocked in 5% bovine serum albumin in Tris buffered saline plus Tween (TBST) for 30 minutes, then incubated in primary antibodies for 72 hours against STAG2 (Cell Signaling #5882, Dilution 1/500) and beta-actin (Cell Signaling #4970, Dilution 1/5000). Blots were then rinsed with Tris buffered saline (TBS) and washed three times with TBST. Blots were then incubated in rabbit secondary antibodies conjugated to horseradish peroxidase at a dilution of 1/3750. Following secondary incubation membranes were rinsed with TBS then washed twice with TBST. Blots were exposed using Western Clarity reagents from BioRad and imaged on the Bio Rad ChemiDoc and viewed in ImageLab Software.

| Antibodies | | | |
|---|---|---|---|
| Antibody | Manufacturer | Cat # | Dilution |
| pmTOR 2448 | Cell Signaling | 5536 | 1:1000 |
| AKT 473 | Cell Signaling | 4060 | 1:2000 |
| B-actin | Cell Signaling | 4970 | 1:4000 |

| | | | |
|---|---|---|---|
| p4EBP1 S65 | Cell Signaling | 9451 | 1:1000 |
| PTEN | Cell-Signaling | 9188 | 1:1000 |
| pTSC2 | Cell-Signaling | 3611 | 1:2000 |
| pGSK3a/b | Cell-Signaling | 9331 | 1:1000 |
| pPTEN | Cell-Signaling | 9551 | 1:1000 |
| pAKT308 | Cell-Signaling | 13038 | 1:1000 |
| pAKT450 | Cell-Signaling | 9267 | 1:1000 |
| P4EBP1 | Cell-Signaling | 2855 | 1:1000 |
| pmTOR2481 | Cell-Signaling | 2974 | 1:500 |
| pS6Kinase | Cell-Signaling | 9234 | 1:1000 |
| pSGK(Ser422) | Santa Cruz | Sc-16745 | 1:200 |
| pRAPTOR (Ser792) | Cell-Signaling | 2083 | 1:1000 |

*Immunofluorescence*

One hundred thousand human neural stem cells were plated on GelTrex (Invitrogen)

coated coverslips. After 24 hours of growth cells were fixed using paraformaldehyde for 20

minutes then blocked with 10% normal goat serum in TBST overnight. The following day

coverslips were washed three times in TBST. Coverslips were incubated in Phalloidin 647

(Thermo, A22287) in 3% BSA in TBST for one hour. Coverslips were then washed three

times in TBST and incubated in secondary antibody (Jackson Laboratories, AffiniPure

Donkey Anti-Rabbit, 711-165-152, Dilution 1/1000 and Invitrogen, Alexa Fluor® 647

Phalloidin, A22287, dilution 1/100) in 3% BSA in TBST for one hour. Coverslips were then

washed three times in TBST and then three times in water. Coverslips were mounted on

glass slides using ProLong® Gold Antifade Mountant with DAPI (Invitrogen, P36931).

Slides were imaged using a Zeiss LSM-800.

*Treatment of primary human neural stem cells with SHH Ligand*

Primary neural progenitor cells pNPCs were taken down to a single cell suspension using Accumax. The cells concentration was determined with the Countess cells and I were plated at a density of $750x10^5$ cells per well in a 6 well plate. Cells were suspended in 3ug/ml SHH ligand for the "treated" wells or standard growth media for the "untreated" wells. Cells were allowed to grow in the presence of SHH for 24 hours before they were harvested for RNA extraction.

*Transcriptional analysis*

The cells were collected following a 24 hour SHH treatment and pelleted by brief centrifugation. 800ul of trizol was added to each cell pellet and the tubes were vortexed and frozen at $-80^0$C. RNA extraction was performed using the Zymo Direct-Zol™ as per manufactured instructions and DNased off the column. RNA was quantified and checked for quality before performing the RT-PCR analysis. For RT-PCR we used 400ng of RNA and creased a cDNA library using the Qiagen RE3 mix. Following generation of cDNA a Sybr Green master mix was created for each sample and aliquots were loaded on the Qiagen Plate, which is manufactured with RT-PCR primers in every well that are validated to quantitate expression of components of the mTOR pathway. The 96 well plates were run on the 7900 HT at a program of $95^0$C for 10 minutes followed by 40 cycles of $95^0$C for 15 second and $60^0$C for 1 minute. The plate setup from Qiagen is as follows:

| | 1 | 2 | 3 | 4 | 5 | 6 | 7 | 8 | 9 | 10 | 11 | 12 |
|---|---|---|---|---|---|---|---|---|---|---|---|---|
| **A** | AKT1 | AKT1S1 | AKT2 | AKT3 | CAB39 | CAB39L | CDC42 | CHUK | DDIT4 | DDIT4L | DEPTOR | EIF4B |
| **B** | EIF4E | EIF4EBP1 | EIF4EBP2 | FKBP1A | FKBP8 | GSK3B | HIF1A | HRAS | HSPA4 | IGF1 | IGFBP3 | IKBKB |
| **C** | ILK | INS | INSR | IRS1 | MAPK1 | MAPK3 | MAPKAP1 | MLST8 | MTOR | MYO1C | PDPK1 | PIK3C3 |
| **D** | PIK3CA | PIK3CB | PIK3CD | PIK3CG | PLD1 | PLD2 | PPP2CA | PPP2R2B | PPP2R4 | PRKAA1 | PRKAA2 | PRKAB1 |
| **E** | PRKAB2 | PRKAG1 | PRKAG2 | PRKAG3 | PRKCA | PRKCB | PRKCE | PRKCG | PTEN | RHEB | RHOA | RICTOR |
| **F** | RPS6 | RPS6KA1 | RPS6KA2 | RPS6KA5 | RPS6KB1 | RPS6KB2 | RPTOR | RRAGA | RRAGB | RRAGC | RRAGD | SGK1 |
| **G** | STK11 | STRADB | TELO2 | TP53 | TSC1 | TSC2 | ULK1 | ULK2 | VEGFA | VEGFB | VEGFC | YWHAQ |
| **H** | ACTB | B2M | GAPDH | HPRT1 | RPLP0 | HGDC | RTC | RTC | RTC | PPC | PPC | PPC |

*Transcription Factor Binding Analysis*

After mTOR transcriptional targets were identified they were screened for common transcription factor binding sites. This was achieved via manually entering the 5kb upstream region for each identified gene into the transcription factor search engine TFSearch. The results from this analysis were manually curated and entered to a spread sheet to identify common shared transcription factors.

# Results

## Clinical Presentation of Cases

Case 1 (PTCH1, SB, CES): Limited clinical information is available on this case, at it was referred to UCLA from an outside physician and subsequently lost to follow up. Briefly the patient presented with somatic overgrowth height 95th percentile and weight >97th percentile, as well as macrocephaly OFC > 97th percentile. Additionally the patient had the diagnosis of autism.

Case 2(PTCH1, RB, CNV) was born at 37 weeks gestation to a 35-year-old mother after an uncomplicated pregnancy. He required a two-week hospital stay due to respiratory distress syndrome. He had difficulty breathing and was admitted for congestion, trouble breathing, and hypoxia. Birth weight was 3500 g (50th percentile) and length 54.5 cm (95th-97th percentile). He also had bilateral inguinal hernias with repair at 6 weeks of age. At 3-years-old he displayed overgrowth with weight (22.8 kg), height (104 cm), and head circumference (58 cm) all above the 97th percentile. Additionally, dysmorphic features and developmental delay were observed. He had a flat face with down slanting palpebral fissures, a short nose with anterior nares, frontal bossing, and a wide forehead. His ears were low set, and he had very small ear canals. He had clinodactyly of the 5th digits bilaterally and very doughy hands. He had a sacral dimple on the back, with hypermobility of the ankles. History of narrow ear canals and chronic serous otitis media requiring tympanostomy tube placement was reported. The parents also reported gastroesophageal reflux disease, constipation, and torticollis, which resolved. The patient has had significant developmental delay. He said very few words at 18 months. He walked after the age of 2 years. He was currently receiving speech therapy twice per week and physical therapy once per week. Brain MRI showed dilated ventricles, with no other abnormalities.

Case 3 (KSS, SUFU WES) was born as a 34-week monamniotic twin via C-Section to a previously 26 year old G2P3 mother and a 36 year old father. She did well postpartum, and met normal developmental milestones in infancy, but afterwards language and learning delays were observed. She had growth curves which were below her healthy twin sister with a noticed increasing head circumference. She also had congenital right microtia. By

age 2 years old headaches without neurologic deficits and clumsiness were reported which prompted imaging studies and found a large cerebellar mass with resultant obstructive hydrocephalus. The diagnosis of a desmoplastic medulloblastoma led to surgical resection via craniotomy, with ventriculo peritoneal shunt placement, high dose chemotherapy, and an autologous hematopoietic stem cell transplant, with complications. At 3 years and 8 months old her height was 94 cm (placing at the 15.71 percentile) weight was 16.8 kg (placing at the 79.54 percentile), and head circumference of 53 cm. Her BMI is 10.01 kg/m2 (placing at the 97.96 percentile). Dysmorphic features included Right sided microtia, hypertelorism, mild downslanting palpebral fissures, and fifth finger clinodactyly.

Case 4 (TB, SUFU CNV) was born full-term to a 39-year-old mother by cesarean due to breech position. The perinatal period was uncomplicated. At time of evaluation he was 18 months old with overgrowth as demonstrated by weight (13.1 kg) was in the 75-90th percentile, height (87.5cm) in the 75-90th percentile, and head circumference (52.5 cm) above the 98th percentile. Additionally, dysmorphic facial features included frontal bossing, bilateral posterior and superior plagiocephaly, depressed nasal bridge. He had clinodactyly of the 4th and 5th finger and 5th toe bilaterally. He had several Mongolian spots on the back and upper buttocks. At the time of evaluation his mother noted that he did not look at her when she called his name until about 12 months. His milestones were delayed, especially in speech. Still little speech use (10 words) though he does respond to his name. He was reported to be "clumsy" and experiences falls. Brain MRI showed multiple areas of ectopic gray matter in the ventricular lining, but they do not appear to be subependymal nodules suggestive of Tuberous sclerosis.

*Identification of Mutations*

Case 1: Clinical Exome sequencing identified a heterozygous c.4014_403del21, p.Trp1339_Arg1345del frameshift variant in the PTCH1 gene. The heterozygous deletion variant was of unknown inheritance as no paternal sample was obtained.

Case 2: Comparative genomic hybridization testing identified a 3.9 Mb heterozygous copy number loss of chromosomal material at region 9q22.31q22.33.

Case 3: Clinical Exome sequencing identified A heterozygous c.111delC frameshift variant in the SUFU gene. The heterozygous c.111delC frameshift variant was confirmed in this patient using Sanger sequencing as an alternate methodology. It was also confirmed to be absent (wildtype) in the mother (R13-36453).

Case 4: Array CGH was performed and showed a 325 Kb deletion at chromosome 10q24.32.

*Deletion of Ptch and SUFU in HEK293Ts*

Following transfection of PTCH1 and SUFU gRNA plasmids and 48-hour puromycin selection we confirmed PTCH1/SUFU deletions via PCR analysis utilizing a primer set, which flanks the cut sites. We observed the presence of an edited band. This band is of the expected size, which confirms that the crispr/cas9 system is cutting efficiently and correctly (Figure 5a,c).  By lessening the Puromycin selection to 24 hours we were additionally able to generate heterozygous Ptch/SUFU populations (Figure 5a). This was

confirmed via RT-PCR analysis of RNA extracted from these cells and additionally western

blot analysis which shows no PTCH1 protein in the homozygotes, intermediated PTCH1

levels in the heterozygotes, and normal PTCH1 levels in the wildtype controls (Figure 5a).


### _Effects of PTCH1 and SUFU Deletion_

We then assayed whether PTCH1 or SUFU deletion alters activation of the

PI3K/AKT/mTOR pathway.  Cells with PTCH1 deletions show strongly increased mTORC1

target p4EBP1, an activated translation initiation factor that increases cell proliferation, we

also observed increases in pmTOR2448 a marker of mTORC1 activity. There were no

changes in pAKT473 or pAKT308 leading us to conclude that this mTORC1 activation was

AKT independent (Figure 5b). Cells with SUFU deletions show stronger increases in

mTORC1 activation marked by pmTOR 2448 and p4EBP1 levels. Additionally there are

increases in pAKT473 and pAKT308 levels which shows that there is activation of mTORC1

and AKT (Figure 5d).


### _PTCH1 deletion causes cellular hyperplasia_

We imaged the PTCH1 cells and show that they form large multinucleated, circular,

irregular clsuters in cell culture.  These abnormal cells are not only larger, but more

prevalent in homozygous PTCH1 deletions than in heterozygous PTCH1 cells (Figure 5e)

Figure 4-5:  Modeling PTCH1 and SUFU Loss in HEK293T with Crispr/Cas9

(a) PCR and RT-PCR showing deletion of critical exon 2 in PTCH1 which can form

heterozygous and homozygous populations  (b) western blot analysis of PTCH1$^{(+/-)}$ cells

which demonstrates increased mTORC1 targets including p4EBP1 (Ser65) and

pmTOR2448; however, there were no increases in AKT473 and AKT308. (c) PCR showing

deletion of critical Exon 1 in SUFU which can form heterozygous and homozygous

populations  (d) western blot analysis of SUFU$^{(+/-)}$ cells which demonstrate increased

mTORC1 targets including p4EBP1 (Ser65) and pmTOR2448 and  increases in AKT473 and

AKT308. (e) Morphological changes observed in PTCH1$^{(+/-)}$ and PTCH1$^{(-/-)}$ cells which

demonstrate increased cell size, and multi nucleated cells (shown by yellow arrows)

Ph=Phallodin.
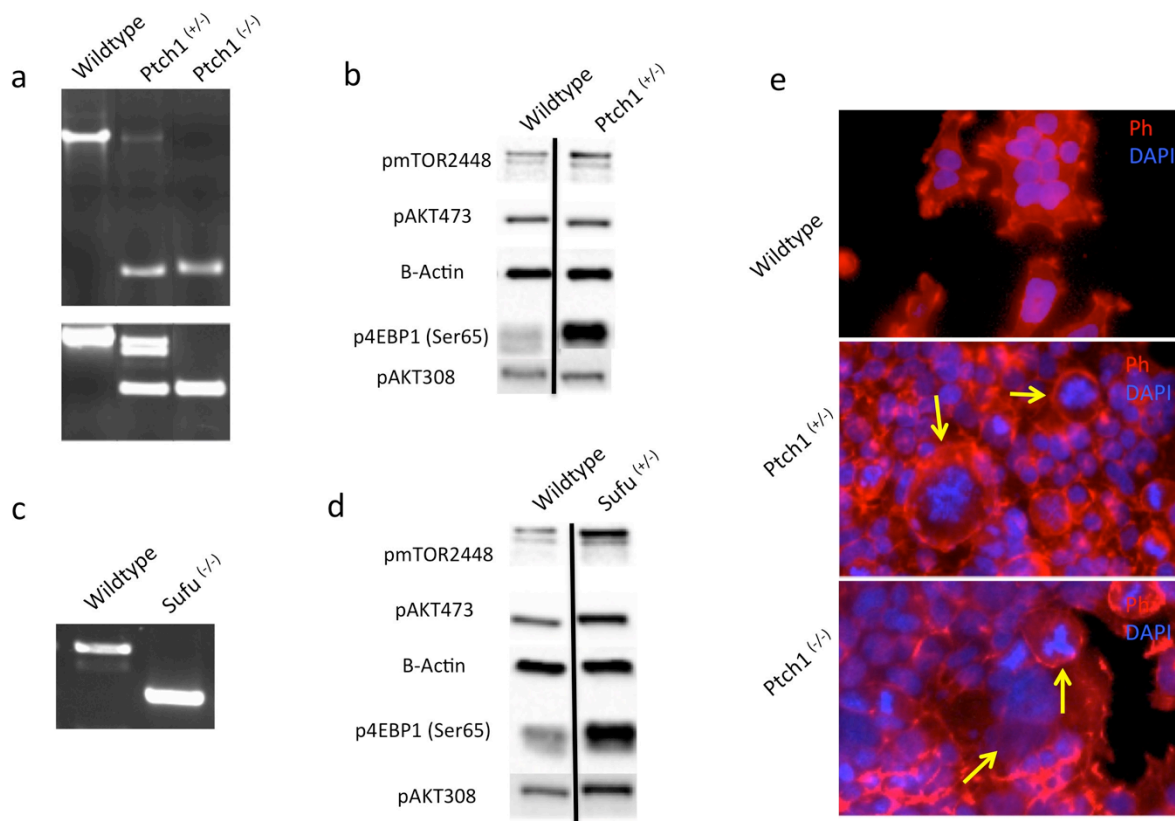
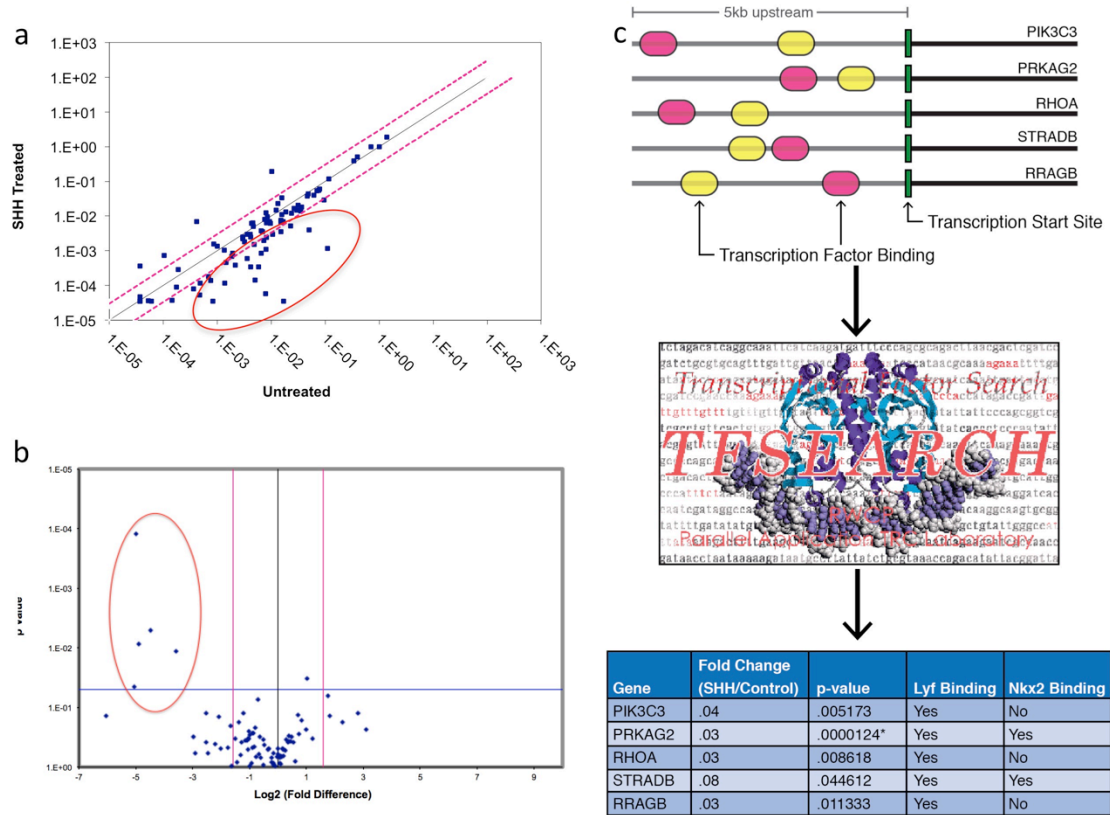*Treating primary human neural stem cells with SHH Ligand*

We treated primary human neural stem cells with SHH Ligand and looked for SHH-mediated expression changes, which may explain the changes in PI3K/AKT/mTOR signaling.  We identified a group of genes with significantly decreased expression following treatment (Figure 7a,b). The strongest candidates due to significance and magnitude are *PIK3C3, PRKAG2, RHOA, STRADB*, and *RRAGB*. Interestingly all these genes with the exception of PIK3C3 are negative regulators of mTOR.


*Transcription factor binding analysis*

We then performed transcription factor binding analysis on the 5Kb upstream region for each of the 5 genes, which were identified. We found an over-representation of binding sites for two transcription factors Lyf1-1 and Nxk2.2. Lyf1-1 binding sites were found in all five candidate genes while the Nkx2.2 binding sites were found in three out of five candidate genes PRKAG2, RHOA and RRAGB.  The presence of these common binding sites suggests that these genes are controlled in a coordinated fashion (Figure 7c).

Figure 4-6: Expression changes in primary neural progenitors following SHH treatment

(a) Scatter plot showing differentially regulated gene expression in SHH treated vs. untreated primary neural progenitor cells. (b) Volcano plot identifying the most significant and greatly affected expression of mTOR related genes in response to SHH treatment. (c) Transcription factor binding analysis that demonstrates that the five strongest candidates identified share a Lyf1 binding site and 2 share a Nxk2.2 binding site. These transcription factors are known to be SHH responsive.



| Gene | Fold Change (SHH/Control) | p-value | Lyf Binding | Nkx2 Binding |
|------|---------------------------|---------|-------------|--------------|
| PIK3C3 | .04 | .005173 | Yes | No |
| PRKAG2 | .03 | .0000124* | Yes | Yes |
| RHOA | .03 | .008618 | Yes | No |
| STRADB | .08 | .044612 | Yes | Yes |
| RRAGB | .03 | .011333 | Yes | No |

## Discussion

*Mutations/Deletions in PTCH1 and SUFU are associated with Overgrowth,*

*Macrocephaly, Developmental delays and dysmorphia.*

We have presented a series of four cases, which help to establish somatic overgrowth,

macrocephaly, developmental delays and dysmorphia as part of the phenotypic

consequences of PTCH1 and SUFU mutations/deletion.  Interestingly, this phenotype is

distinct from that of the basal cell carcinoma syndrome (BCNS, MIM#: 109400) mainly due

to the fact that the reported cases, with the exception of case 3, do not have neoplastic

disease (Table 2) which may be a delayed phenotype as most of our cases are pediactric

and may develop these growths later in life. Most recently, the brain morphology of BCNS

cases was studied and reported to display overgrowth of the cerebrum, thinning of the

corpus callosum and ventricular enlargement[34]. These studied suggested that the brain

phenotypes were similar to those observed in the PI3K/AKT-related overgrowth

syndromes and proposed that they pathways are interacting however they offered no

experimental evidence to support this claim.  Additionally, gain of function mutations in

Smoothened, and activation of Hh, cause the Curry-Jones syndromes which presents with

Hemimegalencepahly[26]. In aggregate, these syndromes are very similar to those in the

PI3K/AKT pathway and we have provided the molecular basis for this cross talk. Lastly the

dysmorphic facial features of our cohort also show similarities to those observed in

PI3K/AKT overgrowth. With down slanting palpebral fissures, ear phenotypes, and 5th

finger clinodactyly being present in at least 2 cases (50%, Table 3).

Table 4-2: Cases with Mutations in the PTCH1 and SUFU with macrocephaly

Summary of each of the four cases presented with their growth parameters, genetic

changes, and presence or absence of specific phenotypes. WES: Whole exome sequencing,

CMA: Chromosomal Microarray, "+": Present, "-": absent.

| Case | Method | Growth Parameters | Genetic Change | Genes of Interest | Macrocephaly | Dysmorphic | Neoplasm | Developmental Delay |
|---|---|---|---|---|---|---|---|---|
| 1 | WES | Wt >97% Ht 95% OFC >97% | Het del c.4014-4034 | *PTCH1* | + | + | - | + |
| 2 | CMA | Wt >97% Ht 95% OFC >97% | Del 9q22.31-33 (96,109,699-973,826) | *PTCH1* | + | + | - | + |
| 3 | WES | Wt >97% Ht 95% OFC >97% | Het c.111 delC | *SUFU* | + | + | + | + |
| 4 | CMA | Wt 75-90% Ht 90-95% OFC >95% | Del 10q24.32 (104,345,460-104,670,581) | *SUFU* | + | + | - | + |

Table 4-3: Specific clinical findings in cases

We focused on the most common phenotypes in this cohort and report on the occurrence of
down slanting palpebral fissures, ear phenotypes, and 5th finger/toe clinodactyly. "+":
present, "-": absent, "?": unknown.

| Case | Flat Face | Down Slanting Palpebral Fissures | Ear Phenotype | Clinodactyly |
|------|-----------|----------------------------------|---------------|--------------|
| 1 | ? | ? | ? | ? |
| 2 | + | + | + | + |
| 3 | - | + | + | + |
| 4 | - | - | - | + |

We also expand upon our cohort by searching the Decipher database for cases with mutations and copy number variations in PTCH1 and SUFU. We have identified 16 cases with mutations/deletions (2 SNVs and 14 CNVs) in PTCH1 (Table 4) and one case with a deletion of SUFU (Table 5). From the cases with PTCH1 Deletions we searched the available phenotypic data from 14 cases to see if there was phenotypic overlap, which would support our claim that these mutations are associated with a novel core triad phenotype of overgrowth, dysmorphia, and developmental delays.  Ten of the fourteen cases reported overgrowth (71%), eleven of the 14 had developmental delays (79%), and ten of the fourteen cases reported dysmorphic facial features (71%). Five of the fourteen cases (36%) reported neoplasms.  We were able to find one additional SUFU deletion, this case presented with developmental delays and dysmorphia however overgrowth was not a reported phenotype.  We also were able to identify duplications involving PTCH1 (n=5) and SUFU (n=4).  From these duplications we see that many cases display undergrowth: three of the five PTCH1 cases (60%) and two of the four SUFU cases (50%). Additionally developmental delays were observed in 60% of PTCH1 cases and 25% of SUFU cases and lastly dysmorphia was observed in 60% of PTCH1 cases and 100% of SUFU cases. To strengthen this reciprocal relationship there are additional reports of familial microcephaly which stratifies with PTCH1 duplications[35].  Collectively these phenotypes help to establish the role of PTCH1 and SUFU in the overgrowth, developmental delay, dysmorphic phenotype and additionally show biological reciprocal relationship to PTCH1 and SUFU duplications, which in many cases are associated with undergrowth, potentially via the same mechanism in reverse.  To directly test this hypothesis we sought to confirm the involvement of the PI3K/AKT/mTOR pathway in these cases.

| Single Nucleotide Variations | | Overgrowth | Developmental Delay | Dysmorphic | Neoplasm |
|---|---|---|---|---|---|
| 276843 | 9:98231437-98231437 T>C | + | + | + | NR |
| 258983 | 9:98241382-98241382 A>C | + | + | + | NR |

| Deletions | | Overgrowth | Developmental Delay | Dysmorphic | Neoplasm |
|---|---|---|---|---|---|
| 321763 | 9:94358815-99785745 deletion | + | + | + | + |
| 268610 | 9:91877380-99121811 deletion | + | + | + | + |
| 248719 | 9:94599654-98659874 deletion | + | + | + | + |
| 268609 | 9:95461101-104307286 deletion | + | + | + | NR |
| 282572 | 9:95441416-104307086 deletion | + | + | + | NR |
| 290013 | 9:98267081-98272376 deletion | + | + | NR | NR |
| 761 | 9:97336045-102370397 deletion | + | + | NR | NR |
| 249750 | 9:96208745-104600969 deletion | + | NR | + | NR |
| 1002 | 9:97336045-102019119 deletion | NR | + | + | + |
| 251468 | 9:96742321-104692852 deletion | NR | + | + | NR |
| 322740 | 9:98181648-98333827 deletion | NR | NR | NR | + |
| 270439 | 9:98218538-110294149 deletion | NR | NR | NR | NR |

| Duplications | | Undergrowth | Developmental Delay | Dysmorphic | Neoplasm |
|---|---|---|---|---|---|
| 256837 | 9:71950016-99525487 duplication | + | + | + | NR |

| | | | | | |
|---|---|---|---|---|---|
| 295745 | 9:220253-141102518 duplication | + | + | + | NR |
| 288238 | 9:204090-141087916 duplication | + | NR | + | NR |
| 285789 | 9:220253-141102518 duplication | NR | + | NR | NR |
| 286236 | 9:220253-141102518 duplication | NR | NR | NR | NR |

Table 4-4: PTCH1 Cases from Decipher

We collected all cases from the decipher database which had genetic mutations in the PTCH1 gene. We were able to find numerous PTCH1 deletions that were associated with overgrowth, developmental delays, dysmorphia, and some with neoplasms. Most interestingly from this collection, we also identified cases with duplications some that present with undergrowth, developmental delay and dysmorphia. "+ ": present, "NR": not reported.

Table 4-5: SUFU Cases from Decipher

We collected a case from the decipher database which had a genetic mutation in the SUFU gene. We were able to find numerous SUFU deletions, which was associated with developmental delays and dysmorphia. Most interestingly from this collection, we also identified cases with duplications some that present with undergrowth, developmental delay and dysmorphia. "+": present, "NR": not reported

| Decipher ID | Genomic Change | Phenotypes | | | |
|---|---|---|---|---|---|
| **Deletions** | | Overgrowth | Developmental Delay | Dysmorphic | Neoplasm |
| 264272 | 10:103852285-104696098 deletion | NR | + | + | NR |
| | | | | | |
| **Duplications** | | Undergrowth | Developmental Delay | Dysmorphic | Neoplasm |
| 2578 | 10:94214092-111401818 duplication | + | + | + | NR |
| 249450 | 10:101711724-104823513 duplication | + | NR | + | NR |
| 249514 | 10:101711724-104823513 duplication | NR | NR | + | NR |
| 328230 | 10:104021180-105357898 duplication | NR | NR | + | NR |

.

*Deletion of PTCH1 and SUFU cause activation of PI3K/AKT/mTOR signaling*

We have shown that deletion of PTCH1 and SUFU using Crispr/Cas9 cause activation of PI3K/AKT/mTOR signaling. However, each gene has specific effects on downstream signaling. Heterozygous PTCH1 loss results in moderate activation of MTOR, demonstrated by pmTOR2448 levels and subsequently increased phosphorylation of a major mTORC1 target p4EBP1 (Thr37/46). This signaling is AKT independent as we observed no activation of AKT at the mTORC1-associated residue 308, or the mTORC2 associated residues 450 or 473. This led us to suspect that the cross talk of the two pathways may be downstream of AKT (Figure). In contrast, loss of SUFU is distinct and demonstrates stronger activation of pmTOR, similar increases in its target p4EBP1 (Thr37/46), but also shows increases in pAKT levels at both residues 308 and 473 but not 450. We propose that the increased pmTOR levels are due to a combinatorial effect of not only the same mechanism demonstrated by PTCH1 mutated cells, but also suggests that cytoplasmic SUFU is cross talking with a negative regulator of AKT, or perhaps even negatively regulating AKT itself. While activation of the PI3K/AKT/mTOR pathway can crosstalk with the SHH pathway in esophagealesophageal adenocarcinoma[36] and pancreatic tumors[37] we are the first to demonstrate the constitutive, ligand independent SHH activation can directly modulate PI3K/AKT/mTOR signaling in both AKT independent and dependent mechanisms. We believe it is this activation of mTOR and subsequent increased phosphorylation of its targets (state specifics) which causes the phenotypic overlap between SHH- and PI3K-related overgrowth disorders.

*Activation of PI3K/AKT/mTOR signaling resulting from PTCH1 Loss is mediated*

*through transcriptional regulation of Negative regulators of mTOR*

We hypothesized that activation of PI3K/AKT/mTOR signaling upon loss of Hh pathway negative regulators was due to Gli-mediated expression changes resulting from activation of SHH signaling. We confirmed this via transcriptional analysis of primary human neural cells treated with SHH Ligand. We were able to identify negative regulators of mTOR, which show decreased expression including RHOA[38], PRKAG2[39], and STRADB. Most interestingly the 5Kb upstream region to these negative regulators were all shown to contain transcription factor binding sites for Lyf1-1 and all except STRADB were shown to have a binding site for Nkx2.2.  The Nkx2.2 homeobox gene was shown to not only be SHH responsive but is additionally integral to determining neuronal identity[40]. We believe that this supports a model by which Gli-mediated alterations in Nkx2.2 decrease the expression and therefore translation of negative regulators of mTOR and lead to it's AKT-independent activation as seen in the PTCH1 mutants (Figure 9).

Figure 4-7: Loss of PTCH1 causes Transcriptional, AKT independent activation of mTOR

Loss of PTCH1 lessens the inhibition of Smoothened, which allows it to activate SUFU and remove the negative inhibition of SUFU on Gli translocation. When Gli translocates to the nucleus it activates the expression of Lyf and Nkx2.2, which inhibits the expression of PRKAG2, RHOA, and STRADB; these are all negative regulators of mTOR. The loss of negative inhibition leads to activation of mTOR, which we have demonstrated via increased phosphorylation of p4EBP1 and mTOR itself



.
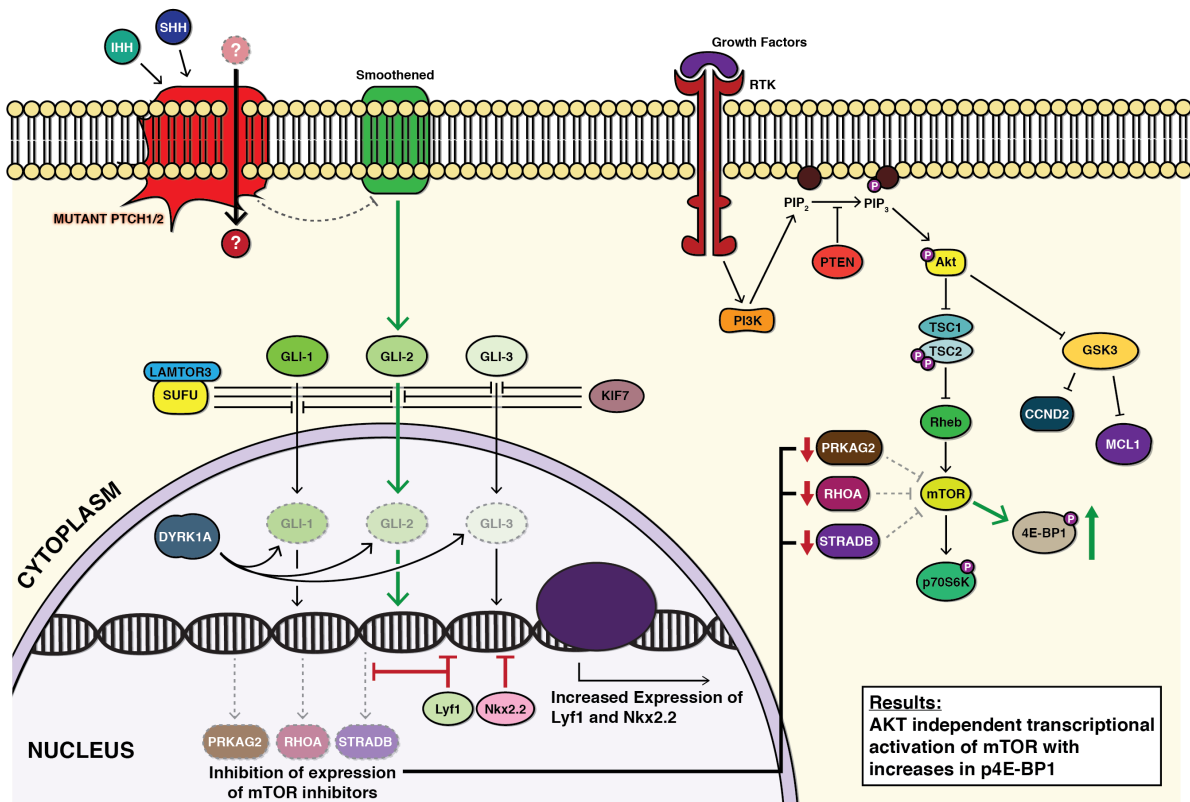
*Activation of PI3K/AKT/mTOR signaling resulting from SUFU Loss is mediated*

*through transcriptional and protein-protein interactions with regulators of mTOR*

When we observed the increases in AKT phosphorylation associated with SUFU deletion

we queried if SUFU is playing an additional role, which mediates cross talk between the

two pathways. We used GeneMania to visualize proteins that have a direct proven physical

interaction with PTCH1 and SUFU. From this analysis we pulled out a potential candidate,

which explains the difference between the PTCH1 and SUFU deletion models outside of the

shared GLI-mediated transcription changes, Late Endosomal/Lysosomal Adaptor, MAPK

And MTOR Activator (LAMTOR3, Figure 10 and 11). As it's name suggests LAMTOR3 is a

direct activator of mTOR, and we propose that SUFU exerts an inhibitory effect on this

protein via direct protein-protein interactions. To briefly test the hypothesis that

LAMTOR3 is modulating mTOR signaling in this cellular background we engineered cells

with LAMTOR3 heterozygous deletions and show that they have decreased pmTOR,

pAKT308 and p4EBP1 which we believe is the direct mechanism via which SUFU has added

pathway activation when compared to PTCH1 deletions which do not demonstrate this

additive effect (Figure 10).

Figure 4-8: LAMTOR3 physically interact with SUFU and activates mTOR

To explain the differences in mTOR activation, we searched for proteins that physically

interact with (a) PTCH1 and (b) SUFU. We identified an activator of mTOR, LAMTOR3. To

see if LAMTOR3 directly interacts with mTOR we (c) engineered LAMTOR knockout cell

lines and show that (d) loss of LAMTOR3 decreases the activity of mTORC1 and

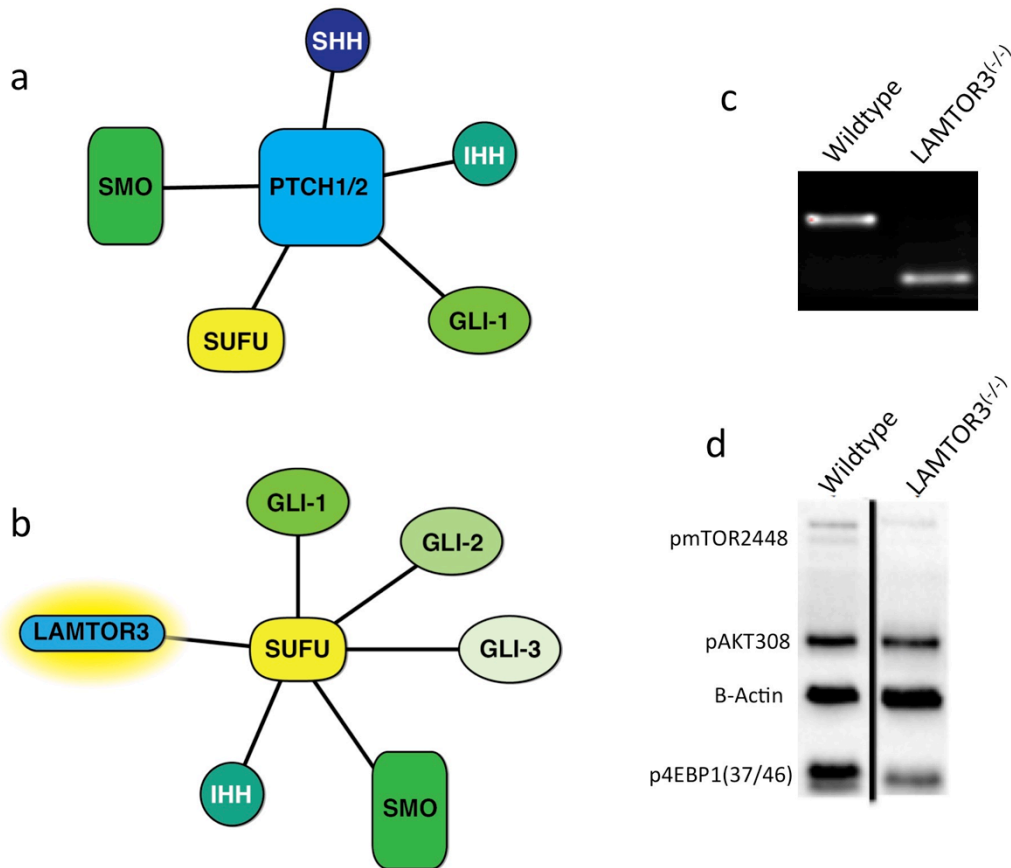additionally pAKT308, which supports the model by which increased LAMTOR3 would

have the opposite effect.

Figure 4-9: Loss of SUFU causes transcription as well as LAMTOR3 mediated AKT activation of mTOR

Loss of SUFU lessens the inhibition on Gli translocation. When Gli translocates to the nucleus, it activates the expression of Lyf and Nkx2.2, which inhibits the expression of PRKAG2, RHOA, and STRADB; these are all negative regulators of mTOR. The loss of negative inhibition leads to activation of mTOR, which we have demonstrated via increased phosphorylation of p4EBP1 and mTOR itself. Additionally loss of SUFU liberates LAMTOR3 from inhibition and allows it to activate AKT, which we have demonstrated via increased phosphorylation of pAKT473 and pAKT308.
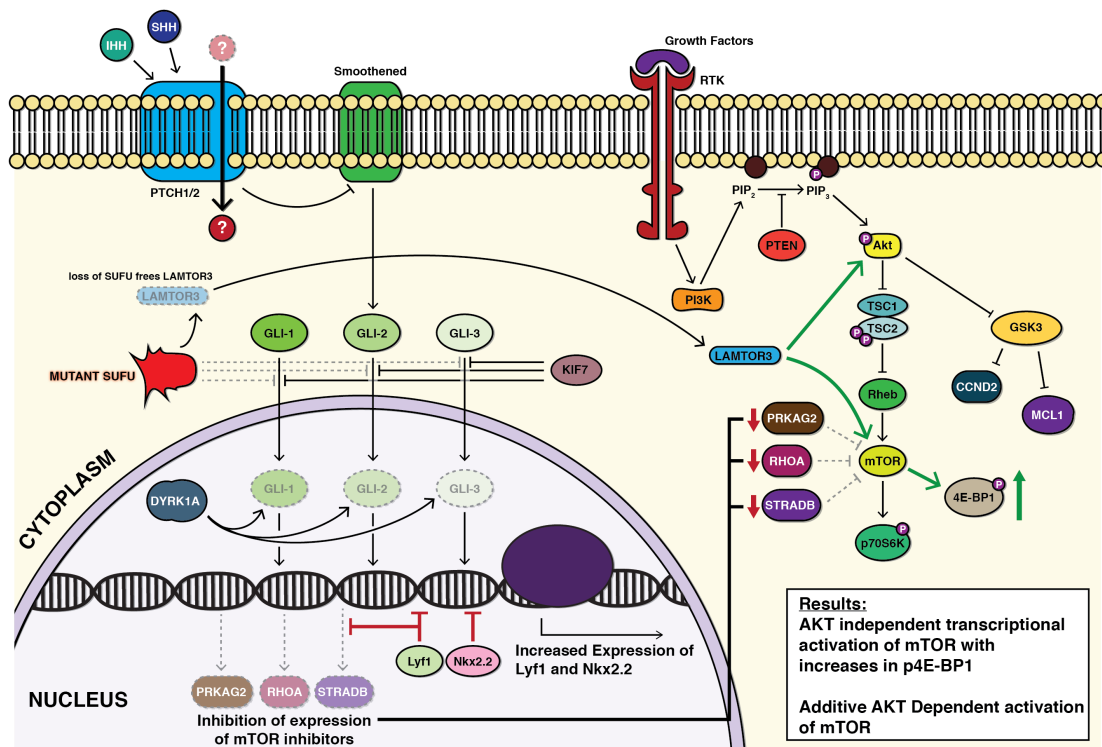
*Patients with mutations in SHH components may benefit from combination therapies of PI3K/mTOR inhibitors.*

Our data shows that individuals with mutations that cause constitutive activation of the SHH pathway have phenotypic similarities to those with over-active PI3K/AKT/mTOR signaling. We therefore propose that these patients may be candidates for combination therapies that are composed of not only SHH but also PI3K/AKT/mTOR inhibitors. These therapies have already been empirically shown to combat certain tumors types including rhabdomyosarcoma[41] and pancreaticpancreatic cancer[42]. Interestingly, in PTEN mutant glioblastoma cells lines, Hh inhibition has shown additive effects[43].   We provide the potential link between these two pathways which explains the benefit on the combined PI3K/SHH inhibition approach and furthermore make a case for the precision therapeutic approach to these cases as patients harboring mutations in SUFU may require higher dose of mTOR inhibition and additionally may require an AKT-inhibitor while patients with PTCH1 mutations will potentially not benefit from these treatments.

## Conclusions

We expand the phenotypic spectrum of patients carrying mutations in PTCH1 and SUFU to include overgrowth, macrocepahly, developmental delays and dysmorphia. We demonstrate that the strong phenotypic overlap between these conditions and those associated with PI3K/AKT/mTOR related overgrowth syndromes is due to cross talk between the two pathways, which is mediated by Gli-associated transcriptional changes. Surprisingly mutations in SUFU not only overlap with the transcriptional changes associated with active Hh signaling but also demonstrate additional PI3K activation, which

may be due to a loss of suspected inhibition of LAMTOR3. We propose that these cases as well as those affected by the more classical basal cell carcinoma nevoid syndrome would benefit from dual inhibition of PI3K/AKT/mTOR and SHH signaling for these reasons.

*References*

1. Ingham, P.W., and Placzek, M. (2006). Orchestrating ontogenesis: variations on a theme by sonic hedgehog. Nat Rev Genet 7, 841-850.

2. Hartl, T.A., and Scott, M.P. (2014). Wing tips: The wing disc as a platform for studying Hedgehog signaling. Methods 68, 199-206.

3. Dessaud, E., McMahon, A.P., and Briscoe, J. (2008). Pattern formation in the vertebrate neural tube: a sonic hedgehog morphogen-regulated transcriptional network. Development 135, 2489-2503.

4. McMahon, A.P., Ingham, P.W., and Tabin, C.J. (2003). Developmental roles and clinical significance of hedgehog signaling. Curr Top Dev Biol 53, 1-114.

5. Lee, R.T., Zhao, Z., and Ingham, P.W. (2016). Hedgehog signalling. Development 143, 367-372.

6. Liu, J., Wang, X., Li, J., Wang, H., Wei, G., and Yan, J. (2014). Reconstruction of the gene regulatory network involved in the sonic hedgehog pathway with a potential role in early development of the mouse brain. PLoS Comput Biol 10, e1003884.

7. Matise, M.P., and Joyner, A.L. (1999). Gli genes in development and cancer. Oncogene 18, 7852-7859.

8. Mao, J., Maye, P., Kogerman, P., Tejedor, F.J., Toftgard, R., Xie, W., Wu, G., and Wu, D. (2002). Regulation of Gli1 transcriptional activity in the nucleus by Dyrk1. J Biol Chem 277, 35156-35161.

9. Borggrefe, T., Lauth, M., Zwijsen, A., Huylebroeck, D., Oswald, F., and Giaimo, B.D. (2016). The Notch intracellular domain integrates signals from Wnt, Hedgehog, TGFbeta/BMP and hypoxia pathways. Biochim Biophys Acta 1863, 303-313.

10. Ma, X., Drannik, A., Jiang, F., Peterson, R., and Turnbull, J. (2017). Crosstalk between Notch and Sonic hedgehog signaling in a mouse model of amyotrophic lateral sclerosis. Neuroreport 28, 141-148.

11. Najafi, M., Abbaszadegan, M.R., Rad, A., Dastpak, M., Boroumand-Noughabi, S., and Forghanifard, M.M. (2016). Crosstalk between SHH and stemness state signaling pathways in esophageal squamous cell carcinoma. J Cell Commun Signal.

12. D'Amico, D., and Canettieri, G. (2016). Translating Hedgehog in Cancer: Controlling Protein Synthesis. Trends Mol Med 22, 851-862.

13. Araujo, S.J. (2015). The Hedgehog Signalling Pathway in Cell Migration and Guidance: What We Have Learned from Drosophila melanogaster. Cancers (Basel) 7, 2012-2022.

14. Dahmane, N., Lee, J., Robins, P., Heller, P., and Ruiz i Altaba, A. (1997). Activation of the transcription factor Gli1 and the Sonic hedgehog signalling pathway in skin tumours. Nature 389, 876-881.

15. Taylor, M.D., Liu, L., Raffel, C., Hui, C.C., Mainprize, T.G., Zhang, X., Agatep, R., Chiappa, S., Gao, L., Lowrance, A., et al. (2002). Mutations in SUFU predispose to medulloblastoma. Nat Genet 31, 306-310.

16. Koike, Y., Ohta, Y., Saitoh, W., Yamashita, T., Kanomata, N., Moriya, T., and Kurebayashi, J. (2017). Anti-cell growth and anti-cancer stem cell activities of the non-canonical hedgehog inhibitor GANT61 in triple-negative breast cancer cells. Breast Cancer.

17. Zou, Q., Yang, Z., Li, D., Liu, Z., and Yuan, Y. (2017). Association of chloride intracellular channel 4 and Indian hedgehog proteins with survival of patients with pancreatic ductal adenocarcinoma. Int J Exp Pathol.

18. Yang, Z., Peng, Y.C., Gopalan, A., Gao, D., Chen, Y., and Joyner, A.L. (2017). Stromal hedgehog signaling maintains smooth muscle and hampers micro-invasive prostate cancer. Dis Model Mech 10, 39-52.

19. Rimkus, T.K., Carpenter, R.L., Qasem, S., Chan, M., and Lo, H.W. (2016). Targeting the Sonic Hedgehog Signaling Pathway: Review of Smoothened and GLI Inhibitors. Cancers (Basel) 8.

20. Gupta, S., Takebe, N., and Lorusso, P. (2010). Targeting the Hedgehog pathway in cancer. Ther Adv Med Oncol 2, 237-250.

21. Sonamoto, R., Kii, I., Koike, Y., Sumida, Y., Kato-Sumida, T., Okuno, Y., Hosoya, T., and Hagiwara, M. (2015). Identification of a DYRK1A Inhibitor that Induces Degradation of the Target Kinase using Co-chaperone CDC37 fused with Luciferase nanoKAZ. Sci Rep 5, 12728.

22. Wong, K., Moldrich, R., Hunter, M., Edwards, M., Finlay, D., O'Donnell, S., MacDougall, T., Bain, N., and Kamien, B. (2015). A familial 7q36.3 duplication associated with agenesis of the corpus callosum. Am J Med Genet A 167A, 2201-2208.

23. Yuksel-Apak, M., Bogershausen, N., Pawlik, B., Li, Y., Apak, S., Uyguner, O., Milz, E., Nurnberg, G., Karaman, B., Gulgoren, A., et al. (2012). A large duplication involving the IHH locus mimics acrocallosal syndrome. Eur J Hum Genet 20, 639-644.

24. Guion-Almeida, M.L., Zechi-Ceide, R.M., and Richieri-Costa, A. (2007). Cerebro-oculo-nasal syndrome: 13 new Brazilian cases. Am J Med Genet A 143A, 3252-3266.

25. Fujii, K., Ohashi, H., Suzuki, M., Hatsuse, H., Shiohama, T., Uchikawa, H., and Miyashita, T. (2013). Frameshift mutation in the PTCH2 gene can cause nevoid basal cell carcinoma syndrome. Fam Cancer 12, 611-614.

26. Twigg, S.R., Hufnagel, R.B., Miller, K.A., Zhou, Y., McGowan, S.J., Taylor, J., Craft, J., Taylor, J.C., Santoro, S.L., Huang, T., et al. (2016). A Recurrent Mosaic Mutation in SMO, Encoding the Hedgehog Signal Transducer Smoothened, Is the Major Cause of Curry-Jones Syndrome. Am J Hum Genet 98, 1256-1265.

27. Evans, D.G., and Farndon, P.A. (1993). Nevoid Basal Cell Carcinoma Syndrome. In GeneReviews(R), R.A. Pagon, M.P. Adam, H.H. Ardinger, S.E. Wallace, A. Amemiya, L.J.H. Bean, T.D. Bird, N. Ledbetter, H.C. Mefford, R.J.H. Smith, et al., eds. (Seattle (WA).

28. Ribeiro, L.A., Guerini Rde, C., and Richieri-Costa, A. (2005). Holoprosencephaly with microphthalmia, hypoplastic ears, vertebral segmentation defects, and congenital heart defects. Am J Med Genet A 136A, 350-351.

29. Sobetzko, D., Eich, G., Kalff-Suske, M., Grzeschik, K.H., and Superti-Furga, A. (2000). Boy with syndactylies, macrocephaly, and severe skeletal dysplasia: not a new syndrome, but two dominant mutations (GLI3 E543X and COL2A1 G973R) in the same individual. Am J Med Genet 90, 239-242.

30. Ali, B.R., Silhavy, J.L., Akawi, N.A., Gleeson, J.G., and Al-Gazali, L. (2012). A mutation in KIF7 is responsible for the autosomal recessive syndrome of macrocephaly, multiple epiphyseal dysplasia and distinctive facial appearance. Orphanet J Rare Dis 7, 27.

31. Ran, F.A., Hsu, P.D., Wright, J., Agarwala, V., Scott, D.A., and Zhang, F. (2013). Genome engineering using the CRISPR-Cas9 system. Nat Protoc 8, 2281-2308.

32. Doench, J.G., Fusi, N., Sullender, M., Hegde, M., Vaimberg, E.W., Donovan, K.F., Smith, I., Tothova, Z., Wilen, C., Orchard, R., et al. (2016). Optimized sgRNA design to

maximize activity and minimize off-target effects of CRISPR-Cas9. Nat Biotechnol 34, 184-191.

33. Hsu, P.D., Scott, D.A., Weinstein, J.A., Ran, F.A., Konermann, S., Agarwala, V., Li, Y., Fine, E.J., Wu, X., Shalem, O., et al. (2013). DNA targeting specificity of RNA-guided Cas9 nucleases. Nat Biotechnol 31, 827-832.

34. Shiohama, T., Fujii, K., Miyashita, T., Mizuochi, H., Uchikawa, H., and Shimojo, N. (2017). Brain morphology in children with nevoid basal cell carcinoma syndrome. Am J Med Genet A 173, 946-952.

35. Derwinska, K., Smyk, M., Cooper, M.L., Bader, P., Cheung, S.W., and Stankiewicz, P. (2009). PTCH1 duplication in a family with microcephaly and mild developmental delay. Eur J Hum Genet 17, 267-271.

36. Wang, Y., Ding, Q., Yen, C.J., Xia, W., Izzo, J.G., Lang, J.Y., Li, C.W., Hsu, J.L., Miller, S.A., Wang, X., et al. (2012). The crosstalk of mTOR/S6K1 and Hedgehog pathways. Cancer Cell 21, 374-387.

37. Sharma, N., Nanta, R., Sharma, J., Gunewardena, S., Singh, K.P., Shankar, S., and Srivastava, R.K. (2015). PI3K/AKT/mTOR and sonic hedgehog pathways cooperate together to inhibit human pancreatic cancer stem cell characteristics and tumor growth. Oncotarget 6, 32039-32060.

38. Gordon, B.S., Kazi, A.A., Coleman, C.S., Dennis, M.D., Chau, V., Jefferson, L.S., and Kimball, S.R. (2014). RhoA modulates signaling through the mechanistic target of rapamycin complex 1 (mTORC1) in mammalian cells. Cell Signal 26, 461-467.

39. Reiter, A.K., Bolster, D.R., Crozier, S.J., Kimball, S.R., and Jefferson, L.S. (2005). Repression of protein synthesis and mTOR signaling in rat liver mediated by the

AMPK activator aminoimidazole carboxamide ribonucleoside. Am J Physiol

    Endocrinol Metab 288, E980-988.

40. Briscoe, J., Sussel, L., Serup, P., Hartigan-O'Connor, D., Jessell, T.M., Rubenstein, J.L., and

    Ericson, J. (1999). Homeobox gene Nkx2.2 and specification of neuronal identity by

    graded Sonic hedgehog signalling. Nature 398, 622-627.

41. Graab, U., Hahn, H., and Fulda, S. (2015). Identification of a novel synthetic lethality of

    combined inhibition of hedgehog and PI3K signaling in rhabdomyosarcoma.

    Oncotarget 6, 8722-8735.

42. Miyazaki, Y., Matsubara, S., Ding, Q., Tsukasa, K., Yoshimitsu, M., Kosai, K., and Takao, S.

    (2016). Efficient elimination of pancreatic cancer stem cells by hedgehog/GLI

    inhibitor GANT61 in combination with mTOR inhibition. Mol Cancer 15, 49.

43. Filbin, M.G., Dabral, S.K., Pazyra-Murphy, M.F., Ramkissoon, S., Kung, A.L., Pak, E., Chung,

    J., Theisen, M.A., Sun, Y., Franchetti, Y., et al. (2013). Coordinate activation of Shh and

    PI3K signaling in PTEN-deficient glioblastoma: new therapeutic opportunities. Nat

    Med 19, 1518-1523.

**Chapter Five**

"Hotspot" mutations in DICER1 cause Glow

Syndrome-associated macrocephaly via

modulation of specific microRNA populations and

resulting activation of PI3K/ATK/mTOR signaling

# Abstract

The *DICER1* gene is located on chromosome 14 and codes for the large multi-domain DICER1 protein. DICER1 resides mostly in the cytoplasm where its best-characterized role is in the processing of precursor micro RNAs (pri-miRNAs) into mature micro RNAs (miRNAs). These RNA species are then associated with the RNA-induced silencing complex (RISC) and cause translational interruption and silencing of target genes.  miRNA regulation has been shown to be a key mechanism for the modulation, balance and responses of numerous biological pathways, developmental processes and disease pathogeneses.  The understanding of DICER1 function has largely been based on somatic mutations that lead to overrepresentation in specific solid tumors and of the association of germ line, sometimes mosaic, mutations which correspond to an increased lifetime risk of developing specific cancers which have been named the DICER1-syndrome.  Additionally, we have previously described mosaic mutations in the RNAse IIIb domain of DICER1 that display global developmental delays, lung cysts, somatic overgrowth, macrocephaly and Wilms tumor. This constellation of phenotypes was classified as GLOW syndrome, an acronym for the core clinical presentations.  Due to the phenotypic overlap of syndromic overgrowth cases with mutations in the PI3K/AKT/mTOR pathway we hypothesized that specific mutations in DICER1 can lead to alterations in miRNA regulation of this pathway and cause the phenotype of somatic overgrowth and macrocephaly.  To test this hypothesis we engineered HEK293T cells with loss of exon 25 of DICER1, a genetic modification that was shown to be synonymous with the "hot spot" RNAse IIIb mutations that cause GLOW syndrome. In HEK293T edited cells we observe activation of the PI3K/AKT/mTOR pathway as demonstrated by increased pS6Kinase and pTSC2 levels. Additionally these cells

demonstrate a striking cellular phenotype and the ability to form spheres when serum is removed from their growth medium. The cells in these spheres are Oct4 and Sox2 positive and exhibit the property of reversion to Oct4 and Sox2 adherent cells with the addition of serum. We queried miRNA expression data and identified a population of miRNAs that increase as a result of these mutations. We have identified the targets of these miRNAs as members of the PI3K/AKT/mTOR pathway and their increase may be the molecular basis for the activation of this important signaling pathway. This work identifies the delicate and essential role for miRNA control of the PI3K/AKT/mTOR pathway. We conclude that the overgrowth and behavioral phenotypes observed in the GLOW syndrome are the result of PI3K/AKT/mTOR activation. Furthermore, we propose that these patients, as well those with the DICER1 syndrome-associated tumors, may be candidates for treatment with mTOR and AKT inhibitors to specifically target these pathologically overactive pathway.

# Introduction

*General DICER1*

The *DICER1* gene is located on chromosome 14 and contains 27 exons, which when

faithfully spliced code, for the DICER1 protein. This protein is 1,922 amino acids in length

and 220kDa in weight. DICER1 contains multiple functional domains which include but are

not limited to the two helicase domains, a double-stranded RNA (dsRNA) binding domain,

the RNAse IIIa and the RNAse IIIb domains[1; 2].   DICER1 is essential for the generation of

mature microRNAs. These small 15-20bp single stranded RNA molecules ultimately

combine with the RNA induced silencing complex (RISC) where in a sequence-specific

manner they target and regulate the translation of complimentary-sequence-specific

mRNAs. miRNAs have far reaching implications and associations with numerous biological

and developmental processes[3; 4].  Specifically, DICER1 resides in the cytoplasm where it

processes premature microRNAs (pri-miRNAs). During this process two populations of

microRNAs are produced, the 3p and 5p miRNAs.


   *3p/5p microRNAs*

pri-mRNAs are transcribed by RNA polymerase II (RNA Pol II) and form dsRNA-hairpin

looped structures which are actively exported from the nucleus. Once in the cytoplasm they

dock to the DICER1 protein, which recognizes their dsRNA hairpin motif.  Once bound,

DICER1 magnesium-dependent exonuclease domains make two distinct cuts liberating the

hairpin and producing two populations of miRNAs. These populations of miRNAs are

named based upon which end of the pri-miRNA they originated. The "5p" miRNA

population arises from the 5 prime ends of the hairpin and the "3p" miRNA population

from the 3 prime ends (Figure 1). These two mature miRNAs are complementary to one another, however most commonly have unrelated targets, as the mRNAs they silence are single stranded and complementation is not a concern. These miRNAs regulate numerous cell processes including proliferation, which was first recognized via the increased prevalence of specific tumors associated with the DICER1-syndrome.

Figure 5-1: Normal function of DICER1

DICER1 resides in the cytoplasm where it receives pri-miRNAs that are actively

transported from the nucleus. Upon recognition of their dsRNA hairpin motif, DICER1

makes two single stranded nicks that liberates two distinct populations of miRNAs: the 3p

and 5p microRNAs. These then associate with Agornot and inhibit the translation of

specific miRNAs.
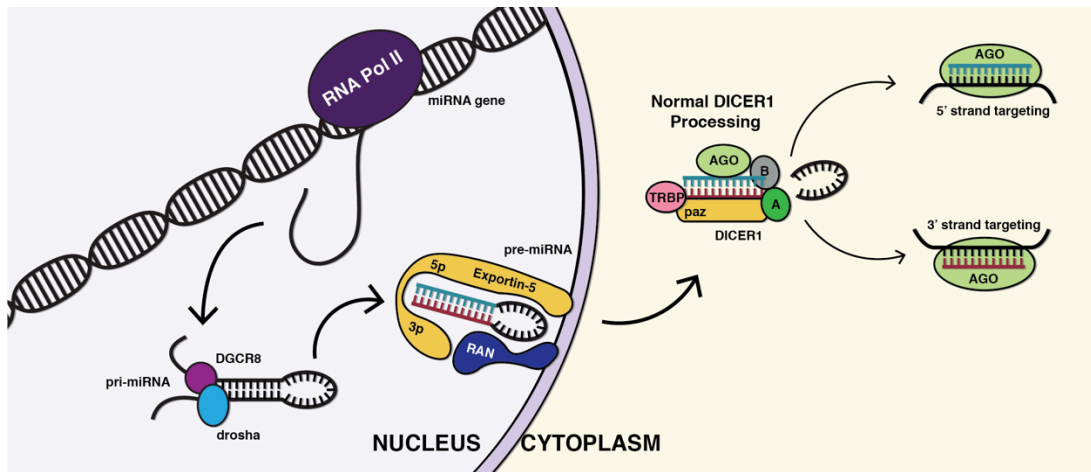
*DICER 1 Syndrome*

The DICER1 syndrome is a cancer predisposition syndrome which was first described due to its association with pleuropulmonaryblastoma tumors (PPB)[5; 6]. These rare pulmonary, pediatric tumors occur during development and are often present at birth. The tumors begin as histologically benign pulmonary cysts, which are prone to malignant transformation and in certain cases sarcoma formation[6]. In addition to PPB there are numerous neoplastic phenotypes which are associated with this syndrome including Sertoli-Leydig cell tumor, cystic nephroma, Wilms tumor, seminoma, embryonal rhabdomyosarcoma, and ovarian sex cord–stromal tumors[7-9] (Figure 2). Most interestingly, macrocephaly has been recently added to the phenotypic spectrum of the DICER1 syndrome; this observation that was first reported in association with the GLOW syndrome[1; 10].

Figure 5-2: Pediatric and Adult manifestation of the DICER1 syndrome

DICER1 syndrome is a cancer predisposition syndrome, which has an overrepresentation of numerous tumors including pinoblastomas, pleuropulmonary blastomas (PPB), pituitary blastomas (PitB), cystic nephroma, ovarian sex cord-stromal tumors (OSCST), Sertoli-Leydig cell tumors (SLCT), nasal chondromesenchymal hamartoma (NCMH), cervix embryonal rhabdomyosarcoma (cERMs), and ciliary body medulloepithelioma (CBME).
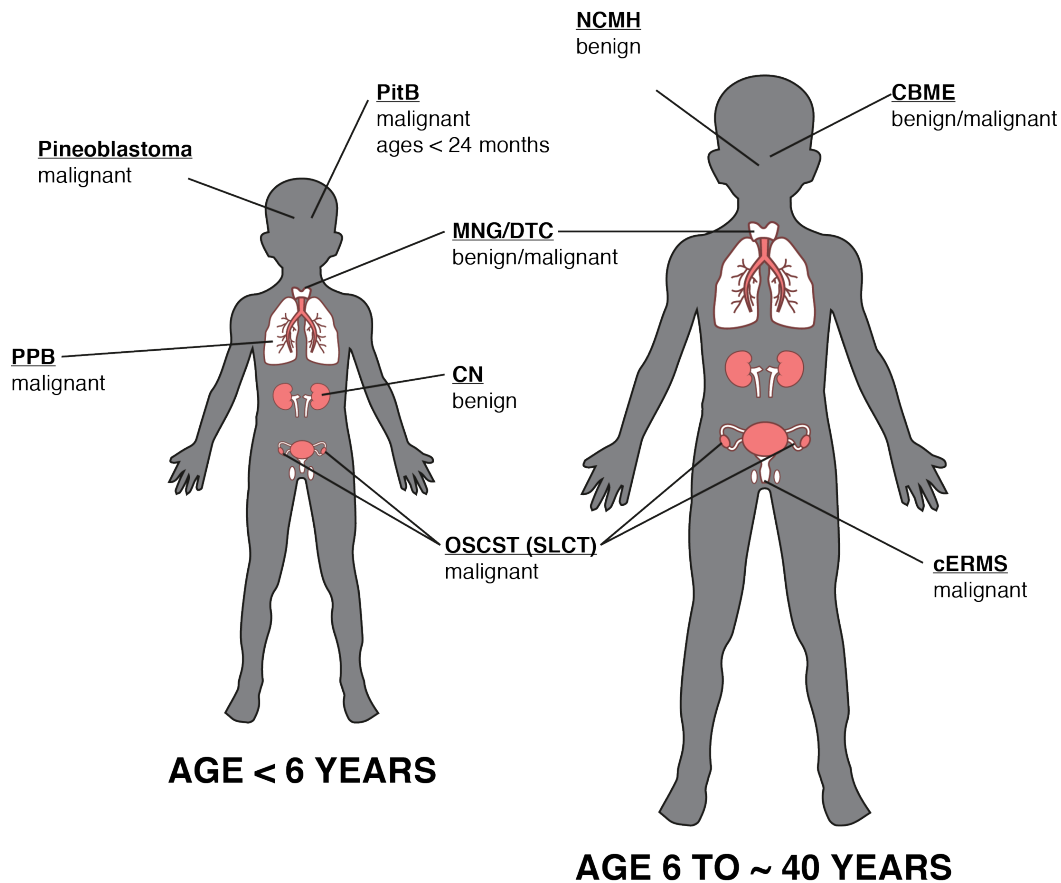
*GLOW Syndrome*

GLOW Syndrome is an overgrowth syndrome which is named as an acronym for its core clinical manifestations including Global developmental delays, Lung Cysts, Overgrowth and Wilms tumor[6]. These patients also demonstrate macrocepahly and dysmorphic facial features including hypertelorism, flattened nasal bridges, and frontal bossing. Additionally, it has been shown that autism is part of the clinical spectrum[1]. The mutations that cause GLOW syndrome are distinct from those that cause the classic DICER-1 syndrome[1]. While the DICER1 syndrome is classically caused by frame shift, nonsense, or other mutations that ablate DICER1 function in a true heterozygous state, GLOW-syndrome mutations are at specific residues within the RNase IIIb domain that only affect the function of this domain. The RNase IIIb domain is one of two RNase domains that cleave the pri-mRNAs. Specifically, the IIIb domain makes the cut that is necessary for the generation of 5p microRNAs. The result of these mutations is a loss of all 5p miRNAs and an increase in specific 3p miRNAs[11]. Analysis of the miRNA expression data showed that the increased 3p microRNAs target central growth signaling pathways including TGF $\beta$ and PI3K/AKT/mTOR[1; 10; 11]. We have hypothesized that it is this specific deregulation of the PI3K/AKT/mTOR signaling pathway that results in the syndromic phenotypes associated with RNase IIIb mutations. To test this hypothesis we have generated HEK293T cells with a specific deletion of exon 25, a genetic mutation which has been shown to be functionally synonymous with the "hot spot" mutations which cause the GLOW syndrome[1; 11; 12]. We then queried if these cells have enhanced activation of PI3K/AKT/mTOR signaling and furthermore if they display abnormal cellular phenotypes.

# Methods

*Crispr/Cas9 Cloning*

*DICER1 Exon25 was* deleted from HEK293T cells utilizing the Crispr/Cas9 plasmid

(pSpCas9(BB)-2A-Puro (PX459) V2.0, #62988[13]) from addgene.   Guide RNAs (gRNAs)

were designed using benching software. gRNAs were selected which showed the highest

"on-target" score[14] and "off-target" score[15]. The 20Bp gRNAs were flanked with CACC-on

the 5'end of their forward oligo and AAAC- on the 5'end of their reverse oligo. These

overhangs facilitate ligation into the parental plasmid once it is digested with BBSI. Briefly

the oligos were annealed and phosphorylated using T4 PNK enzyme (NEB, M0201S),

annealed oligos were then diluted an added to a digestion-ligation reaction containing

parental plasmid, tango buffer (Life Tech By5), DTT, ATP, BBSI (Thermo, FD1014) and T7

Ligase (NEB, M03185). After six cycles of $37^0$C for five minutes and $23^0$C for 5 min the

reaction was treated with plasmid safe exonulease (Epicentre, E3101K). Finally plasmids

were transformed in Stbl3 E.Coli and grown under ampicillin selection. Plasmid mini-preps

were performed on three colonies and sanger sequencing confirmed the cloning event

using the human U6 primer sequence: 5'-CGATACAAGGCTGTTA-3'.

gRNA Sequences:

| ID | Sequence |
|---|---|
| PTEN Upstream 2 F | 5'-**CACC**-GGTGGGTTATGGTCTTCAAA-3' |
| PTEN Upstream 2 R | 5'-**AAAC**-TTTGAAGACCATAACCCACC-3' |
| PTEN Downstream 1 F | 5'-**CACC**-GAGAGGCCCTAGATTTCTATG-3' |

| | |
|---|---|
| PTEN Downstream 1 R | 5'-**AAAC**-CATAGAAATCTAGGGCCTCTC-3' |
| PTEN Downstream 2 F | 5'-**CACC**-GATTCACTGTAAAGCTGGAAA-3' |
| PTEN Downstream 2 R | 5'-**AAAC-**TTTCCAGCTTTACAGTGAATC-3' |
| DICER1-Del25 Upstream 1 F | 5'-**CACC**-GTGTTACTTCTTTAGTAAGGG-3' |
| DICER1-Del25 Upstream 1 R | 5'-**AAAC-**CCCTTACTAAAGAAGTAACAC-3' |
| DICER1-Del25 Downstream 1 F | 5'-**CACC**-GTGGGTTTTTTTCTTTCTAAA-3' |
| DICER1-Del25 Downstream 1 R | 5'-**AAAC-**TTTAGAAAGAAAAAAACCAC-3' |

gRNAs were designed flanking exon 25 (Figure 3).

Figure 5-3:  Crispr Targeting Exon 25

We designed gRNAs that would target specific sequences in the introns flanking exon 25. This deletion has been shown to be functionally equivalent to RNase IIIb hot spot mutations that cause GLOW syndrome[12].

*Cell Culture and Transfection:*

**HEK293T:** Cells were maintained with basal media including DMEM, PSN and 10% fetal bovine serum (FBS). Twenty-four hours before transfection cells were liberated from T25 flask with TrypLE™ Express Enzyme (1X). Cell concentration and viability was determined with the Invitrogen Countess I. After plating $2x10^5$ viable cells onto a 12-well culture dish, volume was brought to 1ml of basal media. On the day of transfection media was aspirated, and 500ul of basal media was added to each well. GeneIn Transfection reagent was combined with 2ug of plasmid, brought to a final volume of 200ul, vortexed and then incubated at room temperature for 15 minutes then added to each well. Cells were incubated for 24 hours, followed by a 12-hour nutrient starvation in DMEM lacking glutamine, glucose and FBS.

*Western Blot Analysis*

Cells were lysed on 24 well or 12 well plates with 200µl or 400ul of passive lysis buffer, prepared with phosphatase and protease inhibitors, and incubated by shaking at $4^0$C for one hour. After lysis tubes were spun at 7500 Rcf for 5 minutes to collect debris. Supernatant was transferred to a new tube then protein concentration determined with the Coommasie (Check spelling) Plus Bradford (Life Technologies) reagent following manufacture instructions. Protein samples were diluted to a final concentration of 10µg/20 µl into Western loading buffer with beta-mercaptoethanol and then boiled for 5 minutes. Western blots were run on 12% acrylamide gels followed by transfer onto nitrocellulose membranes utilizing the Transblot Turbo® apparatus from Biorad. The membrane was blocked in 5% bovine serum albumin in Tris buffered saline plus Tween (TBST) for 30

minutes, then incubated in primary antibodies (listed below) overnight. Blots were then rinsed with Tris buffered saline (TBS) and washed three times with TBST. Blots were then incubated in rabbit secondary antibodies conjugated to horseradish peroxidase at a dilution of 1/3750. Following secondary incubation membranes were rinsed with TBS then washed twice with TBST. Blots were exposed using Western Clarity reagents from BioRad and imaged on the Bio Rad ChemiDoc and viewed in ImageLab Software.

| Antibodies | | | |
|---|---|---|---|
| Antibody | Manufacturer | Cat # | Dilution |
| pmTOR 2448 | Cell Signaling | 5536 | 1:1000 |
| AKT 473 | Cell Signaling | 4060 | 1:2000 |
| B-actin | Cell Signaling | 4970 | 1:4000 |
| p4EBP1 S65 | Cell Signaling | 9451 | 1:1000 |
| PTEN | Cell-Signaling | 9188 | 1:1000 |
| pTSC2 | Cell-Signaling | 3611 | 1:2000 |
| pGSK3a/b | Cell-Signaling | 9331 | 1:1000 |
| pPTEN | Cell-Signaling | 9551 | 1:1000 |
| pAKT308 | Cell-Signaling | 13038 | 1:1000 |
| pAKT450 | Cell-Signaling | 9267 | 1:1000 |
| P4EBP1 | Cell-Signaling | 2855 | 1:1000 |
| pmTOR2481 | Cell-Signaling | 2974 | 1:500 |
| pS6Kinase | Cell-Signaling | 9234 | 1:1000 |
| pSGK(Ser422) | Santa Cruz | Sc-16745 | 1:200 |
| pRAPTOR (Ser792) | Cell-Signaling | 2083 | 1:1000 |

*Statistical Analysis*

Western blots were run in biological sextets, which gave us the power to perform Mann-Whitney U tests for non-parametric data. The p-values for these tests were Bonferroni corrected for multiple tests in the event of numerous comparisons.

*Immunofluorescence*

One hundred thousand human neural stem cells were plated on GelTrex (Invitrogen) coated coverslips. After 24 hours of growth cells were fixed using paraformaldehyde for 20 minutes then blocked with 10% normal goat serum in TBST overnight. The following day coverslips were washed three times in TBST. Coverslips were incubated in primary antibody against STAG2 (Cell Signaling #5882 Dilution 1/250) in 3% BSA in TBST for one hour. Coverslips were then washed three times in TBST and incubated in secondary antibody (Jackson Laboratories, AffiniPure Donkey Anti-Rabbit,  711-165-152, Dilution 1/1000 and Invitrogen, Alexa Fluor® 647 Phalloidin, A22287, dilution 1/100) in 3% BSA in TBST for one hour. Coverslips were then washed three times in TBST and then three times in water. Coverslips were mounted on glass slides using ProLong® Gold Antifade Mountant with DAPI (Invitrogen, P36931). Slides were imaged using a Zeiss LSM-800.

# Results

*Generation of DICER1 Exon 25 deleted HEK293Ts*

We aimed to model the hot spot mutations observed in the GLOW syndrome by deletion of

exon 25 of DICER1. Exon skipping is a documented phenomena which is associated with

functionally identical DICER1 mutations including c.5429A>G and c.5438A>G which cause

Wilms' tumor[12]. This was achieved with Crispr/Cas9 guide RNAs (gRNAs) that target

intronic regions flanking Exon 25 (DICER1$^{delExon25\ (+/-)}$). We confirmed the deletion utilizing

RT-PCR primers with homology to exon 24 and exon 26. We then confirmed the presence

of the smaller RNA band via RT-PCR, which is not present in wildtype cells, transfected

with only Cas9 plasmids. The identified band is of the correct size, which confirms that the

gRNAs are targeting efficiently and correctly (Figure 4a). As has been previously shown

this smaller mRNA lacking exon 25 can be translated *in vivo* into a functional DICER1

protein, which lacks RNase IIIb function[12].


*DICER1$^{delExon25\ (+/-)}$ Cells have activation mTOR signaling*

Once the cellular model of loss of RNase IIIB function was created we hypothesized that

these cells would demonstrate increased or altered PI3K/AKT/mTOR signaling. We

confirmed this hypothesis via western blot analysis of these cells. As a positive control we

utilized PTEN$^{(-/-)}$ cells which have confirmed increased PI3K/AKT/mTOR signaling (Figure

4b-d) . First we confirmed that the cells express less full length DICER1 when compared to

WT and PTEN$^{(-/-)}$ cells. We next confirmed our hypothesis and demonstrate that

DICER1$^{delExon25\ (+/-)}$ cells have increased mTORC1 signaling evidenced by increased

phosphorylation of its two main substrates p4EBP1(Ser65) and pS6Kinase(Thr389). This

activation is significantly greater than WT cells however less than that present in PTEN$^{(-/-)}$ cells. These cells show decreased activation of mTORC2 targets pAKT(Ser473), and pAKT(Thr450). In contrast, the PTEN$^{(-/-)}$ cells demonstrate increased phosphorylation of these same targets, suggesting a potential mTORC1/mTORC2 negative feedback loop which is disrupted in PTEN$^{(-/-)}$ cells, however intact in the DICER1$^{\text{delExon25 }(+/-)}$ model. Additionally, DICER1$^{\text{delExon25 }(+/-)}$ cells do not have changes in autophagy as evidenced by the lack of changes LC3A, in contrast to what is observed in PTEN$^{(-/-)}$ cells. Most interestingly, these cells show a possible decrease in hedgehog signaling as the demonstrated by the decreased *Gli1* expression.

Figure 5-4: Deletion of Exon 25 in DICER1 results in activation of mTORC1

(a) RT-PCR confirming deletion of exon 25 from DICER1 mRNA, the band in the

Crispr/Cas9 cells is the correct size for transcripts lacking exon 25 (b) Western blot

analysis comparing DICER1$^{Delex25(+/-)}$ to PTEN$^{(-/-)}$ cells. (c) Quantification of the western

blots which show significant increases in p4EBP1, pS6Kinase and decreases in pAKT450,

pAKT473 and DICER1. Black vertical bars show standard deviations.
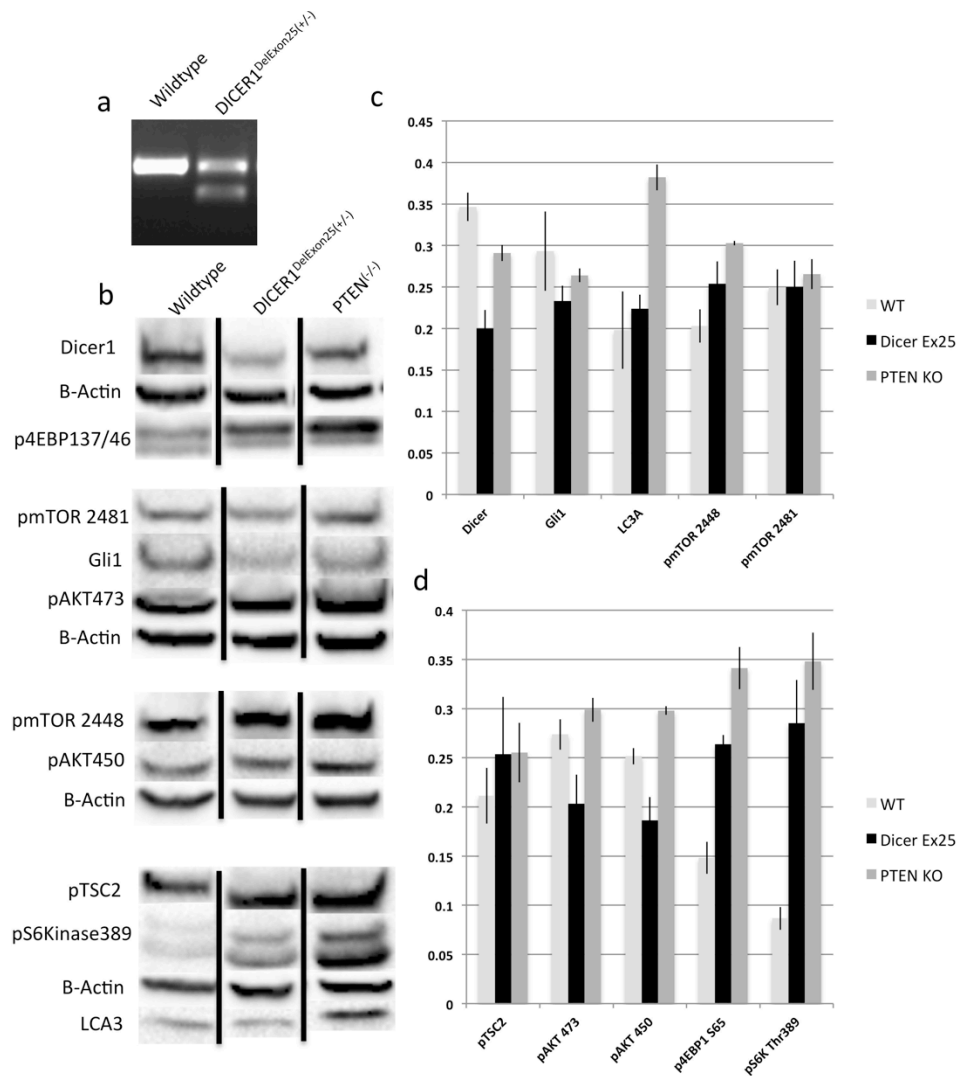
*DICER1$^{delExon25\ (+/-)}$ cells demonstrate the ability to form spheres when serum starved*

We attempted to correct the increased mTOR activation in DICER1$^{delExon25\ (+/-)}$ cells by removing fetal bovine serum (FBS) from their growth media; FBS includes growth factors and insulin that stimulate this pathway. Surprisingly, these cells do not only maintain the ability to grow and divide in the absence of previously documented essential growth factors and hormones, but also begin to form spheres after 72 hours; this is the time point when wildtype cells enter apoptosis due to the lack of nutrients in the environment (Figure 5a). Theses spheres can be maintained in serum free media and proliferate well in stem cell media, which includes F12, B27, EGF, and bFGF. Upon reintroduction of serum, the spheres become adherent, send out projections, and "spread." This pattern is most analogous to the behavior of primary human neural spheres that, upon the withdrawal of FGF and EGF, will first send out radial glial projections before differentiated cells types migrate away from the sphere center. This led us to hypothesize that these cells were "progenitors" of some type and we investigated this with staining for defined progenitor markers (Figure 5b).

*DICER1$^{delExon25\ (+/-)}$ spheres display early progenitor markers including Oct4 and SOX2*

To assess the identity of the cells within the sphere we undertook immunofluorescence staining for the well characterized Oct4 and SOX2 markers of pluripotency. The cells were positive for Oct4, which displays a nuclear staining pattern. Additionally, these cells demonstrate increased DICER1 staining. Upon reintroduction of Serum for 24 hours these cells revert the Oct4 and increased DICER1 staining (Figure 5c) . Additionally, the spheres are positive for SOX2. While this staining pattern is predominately nuclear, it also demonstrates some cytoplasmic staining which may be due to the fact that the antibody is

trapped in the sphere micro environment or that the cells in the sphere are so close together it obstructs antibody penetration. We also show the presence of phosphorylated 4EBP1 (Ser65) in the starved spheres, which is reflective of the presence of activated mTOR signaling in these cells even in the absence of serum. In fact, the p4EBP1 staining is maintained and is similar to that of WT HEK cells in monolayer grown in the presence of serum (Figure 5d).

Figure 5-5: DICER1$^{Del25(+/-)}$ Cells demonstrate the ability to form Oct4$^+$ and SOX2$^+$ spheres in culture

(a) After 72 hours of growth without serum DICER1$^{Del25(+/-)}$ continue to divide and form spheres which detach (b) upon reintroduction of serum the spheres attach and spread. (c) spheres are Oct4 positive (d) spheres are Sox2 positive.
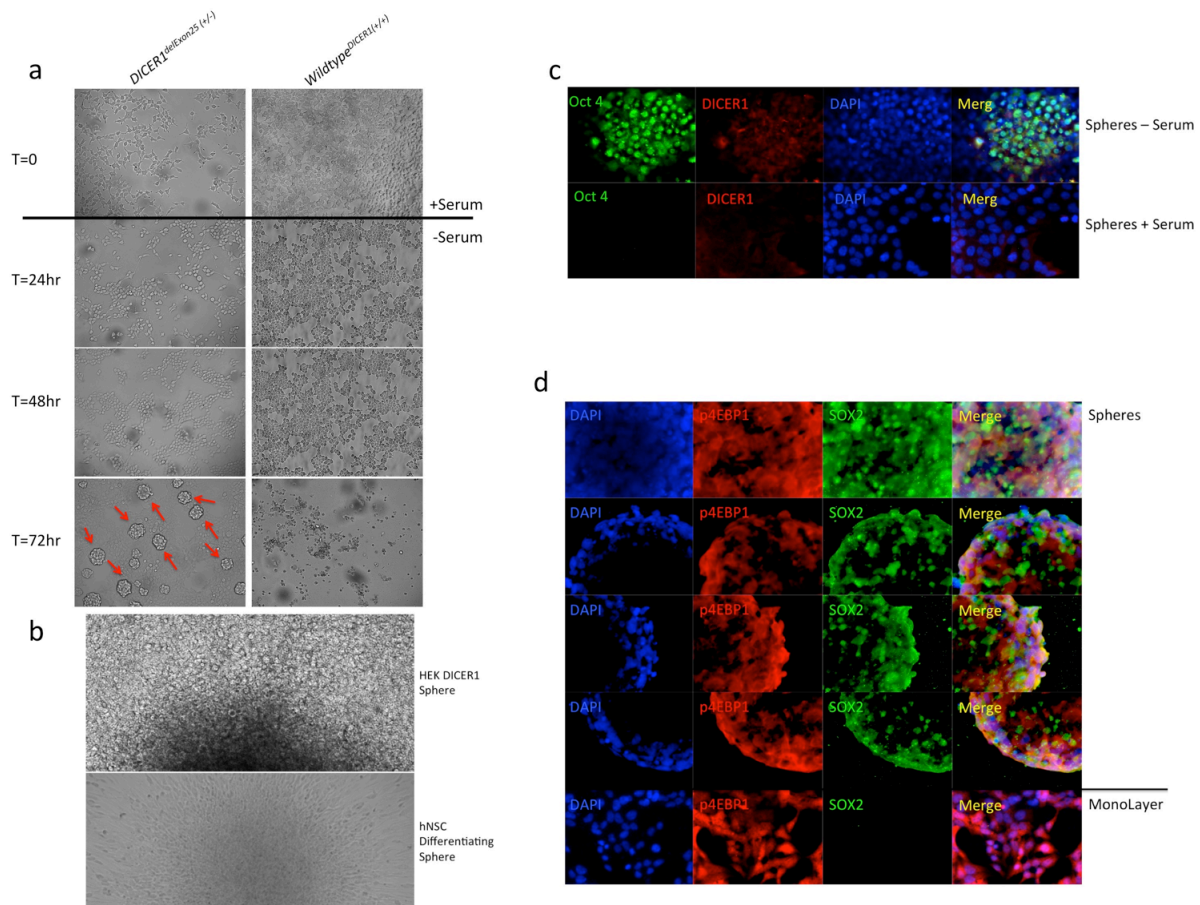
_DICER1_<sup>delExon25 (+/-)</sup> _cells demonstrate extremely abnormal cells phenotypes_

Despite the presence of loss of function biallelic mutations in DICER1 associated with PPB, all cases of Wilms tumor associated with syndromic or somatic distribution of RNAse IIIb domain mutations in DICER1 are always observed in the heterozygous state. This suggests that these mutations are likely associated with the hyperproliferative phenotype of Wilms tumor. We attempted to generate DICER1<sup>delExon25 (-/-)</sup> cells which we hypothesized would demonstrate even more activation of mTOR signaling due to the true lack of all 5p miRNAs. Interestingly, clonal DICER1<sup>delExon25 (-/-)</sup> cells do not proliferate well in culture making the assessment of their signaling impossible. We were able to generate a few of these cells, which demonstrate extremely abnormal cell morphology. Not only are these cells lager than their WT predecessors but also branch extensively (Figure 7). It should be noted that the WT cells that were used for comparison in these figures were cells which underwent all steps of the transfection, genomic editing, and clonal passaging; however, they were not edited during the transfection. Therefore the likelihood that this cell phenotype was due to manipulation outside of the homozygous loss of exon25 is unlikely .

Figure 5-6: Homozygous DICER1<sup>delExon25 (-/-)</sup> *Cells display abnormal phenotypes*

We were able to grow a few DICER1 homozygous deleted cells; they do not grow well in culture, but the few that do survive display severely abnormal cell phenotypes including increased cell size, abnormal branching patterns and non-HEK morphology.
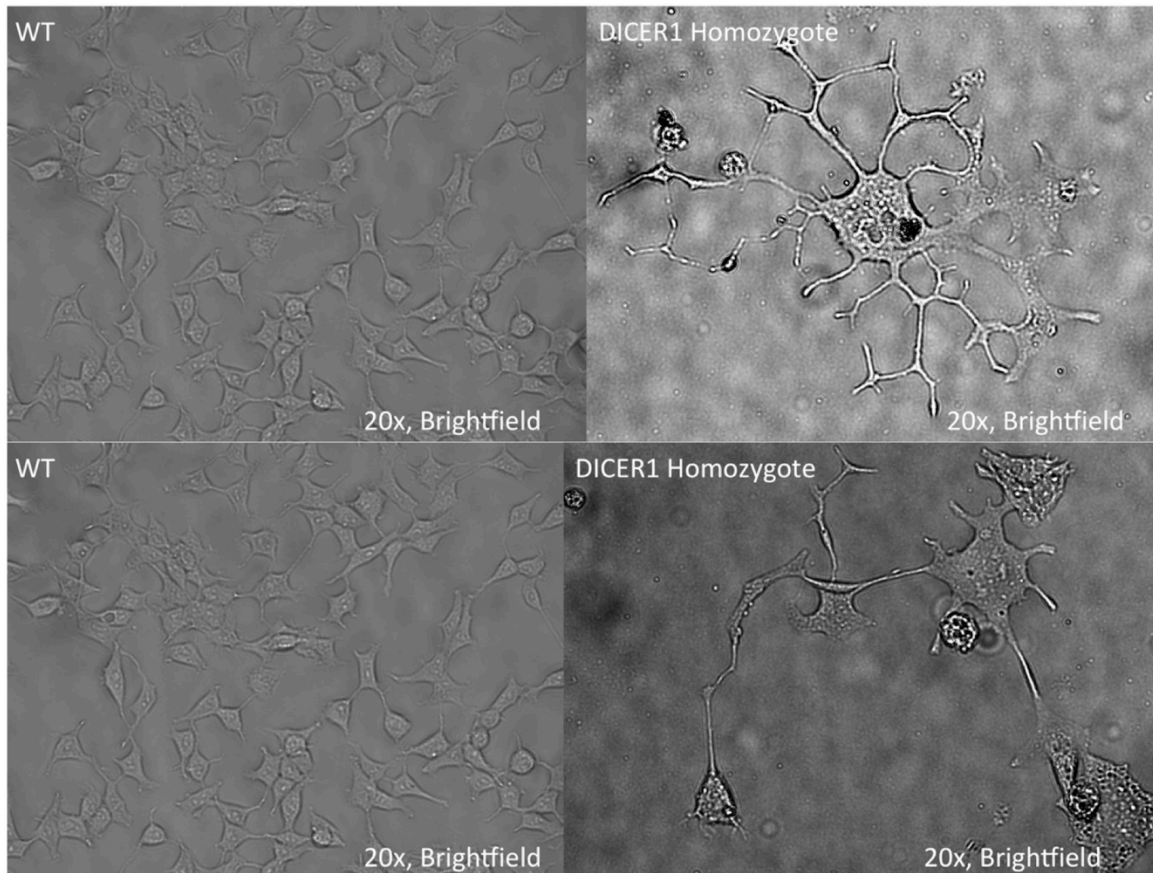
## Discussion

*Deletion of Exon25 of DICER1 activates mTOR signaling*

We have shown that *in vitro* deletion of Exon25 from HEK293T cells activated mTORC1 signaling. Compared to PTEN$^{(-/-)}$ cells this increase is less but still significantly greater than wild type cells. This confirms our hypothesis that the overgrowth phenotypes associated with the GLOW syndrome display phenotypic overlap with PI3K/AKT-related overgrowth syndromes due to a deregulation of this key growth-signaling pathway. Specifically, the presence of macrocephaly with development delay and autism is most similar to PTEN associated autism/macrocephaly syndrome. A signaling event, which seems to be PTEN-specific is the strong activation of mTORC2 which was not seen in the DICER1$^{delExon25\ (+/-)}$ cells. This observation supports the presence of an mTORC1/mTORC2 negative feedback loop, which is disrupted in PTEN$^{(-/-)}$ cells however not in DICER1$^{delExon25\ (+/-)}$. This difference may account for some of the phenotypic differences between PTEN versus GLOW syndrome patients. Namely, the macrocephaly is reproducibly reported to be extreme (OFC > 3SD) in PTEN cases, but more mild in GLOW syndrome cases. Additionally, the stratification of neoplasms to specific tissues within the GLOW syndrome is unique and distinct from those in the PTEN-related neoplastic syndromes, possibly due to this molecular difference. Lastly, we propose that the lung, kidney, and brain are most susceptible to miRNAs imbalance of 3p/5p populations. This results in alterations to the PI3K/AKT signaling and development of these tissues[5; 7; 16]. To further expand upon the mechanism of cross talk between miRNAs and the mTOR-signaling cascade we dissected specific 3p miRNAs, which are increased, and their potential targets.

*Specific miRNA analysis*

The most comprehensive transcriptional understanding of DICER1 "hot spot" mutations was reported by Anglesio et al. from engineered DICER1[(-/-)] ES cells which were then infected with donor lenti-viruses carrying one of four DICER1 "hot spot" mutations (D1709N, D1810Y , E1813Q, and D1709A). This generated a comprehensive expression signature when compared to WT DICER1[(+/+)] ES cells. They convincingly show that the 5p miRNA population is ablated from these cells and additionally that specific 3p miRNAs demonstrate marked increased expression[11] (Figure 8).   We mined this data and screened to identify the 3p miRNAs that show the greatest difference in expression[1; 11].  We have mapped the targets of these miRNAs and show that they target numerous levels and effectors of mTOR signaling. Most upstream they target TSC1 a negative regulator of mTOR signaling that in its absence Rheb is able to activate mTOR. Downstream to this activation event we have furthermore identified target substrates, which seem to focus the activated mTOR signaling into pS6Kinase and ultimately S6, a potent pro-proliferative driver (Figure 9). Our data is confirmatory of this as increases in pS6Kinase(Thr389) were observed.  In addition to the pro-proliferative signal we have observed a cellular phenotype that is affecting cell identity and stemness.

Figure 5-7: DICER1 hotspot mutations and loss of Exon 25 result in loss of 5p miRNAs and increased 3p miRNAs

Mutations in DICER1 that ablate the RNaseIIIb function result in loss of 5p miRNAs and increased 3p miRNAs. Although these mutations are enriched in tumors and present in the glow syndrome, the mechanistic link to overgrowth and proliferation was not known. We have provided evidence that these mutations result in direct activation of mTOR signaling which explains their phenotypic overlap with PI3K-related overgrowth syndromes.
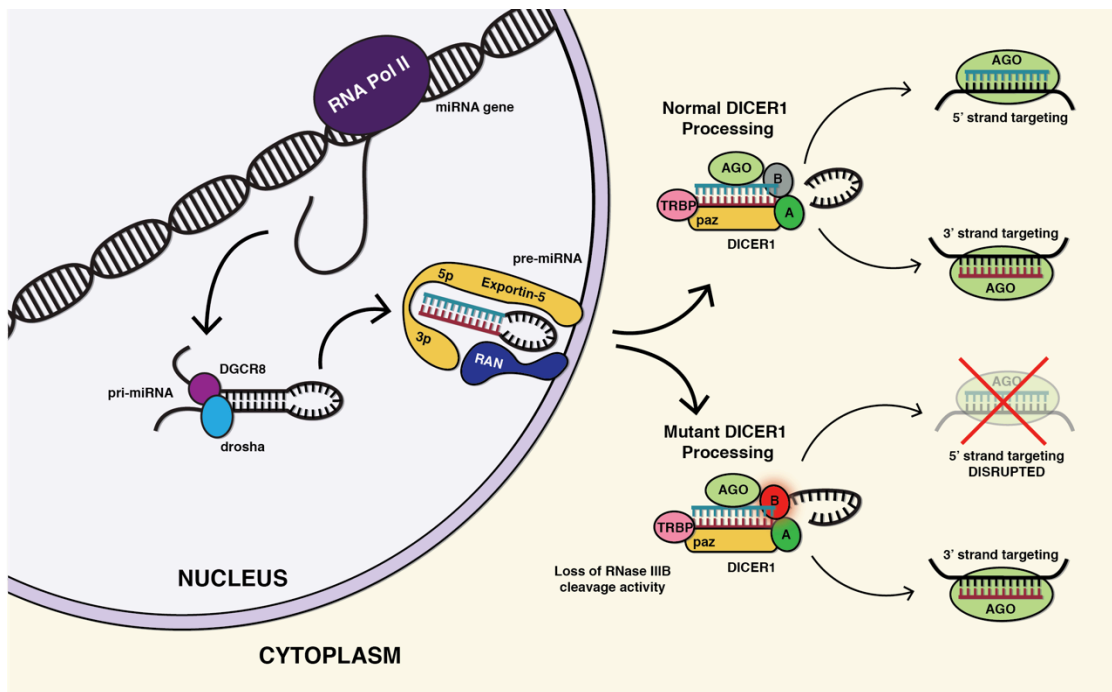
Figure 5-8: Specific increased 3p miRNAs target mTOR signaling

We show that certain miRNAs affected by these pathogenic mutations target negative

regulators of mTOR: namely TSC2. Additionally, downstream targets are effected which

streamlines mTOR signaling into S6kinase activation of cell proliferation/growth. We have

provided evidence for this via the increased pS6Kinase levels on our *DICER1*<sup>*delExon25 (+/-)*</sup> cell

model.
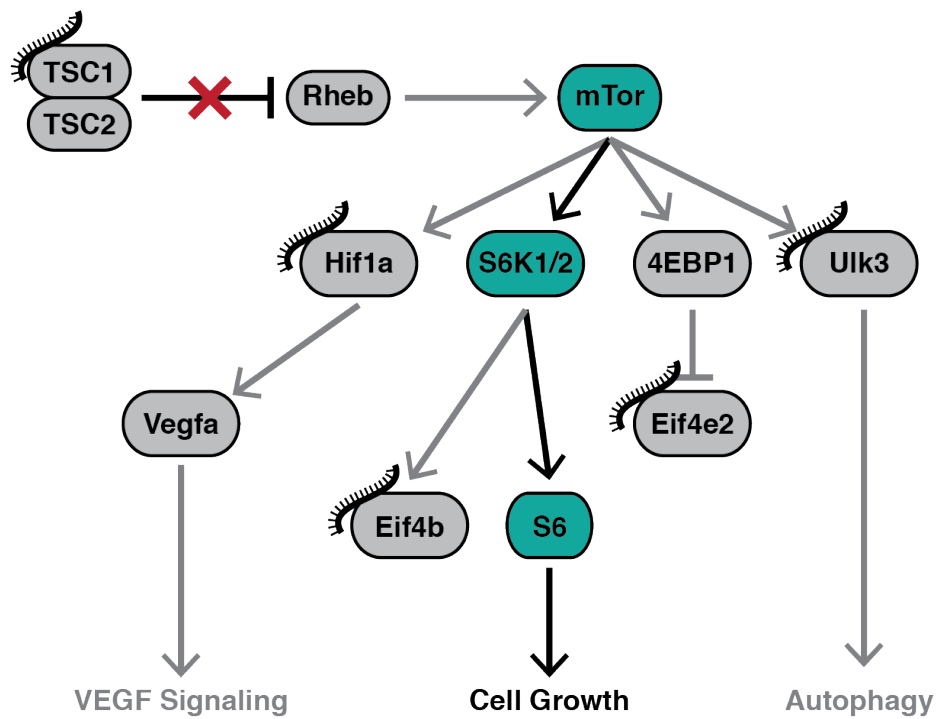
*Deletion of Exon 25 of DICER1 allows cells to form spheres and divide in the absence of*

*serum*

As we have presented, DICER1[delExon25 (+/-)] cells have the ability to grow in the absence of

serum, and additionally form SOX2^{+} and Oct4^{+} spheres. Upon the reintroduction of serum to

these cells they attach to the culture vessel and begin to phenotypically resemble their

kidney predecessors. The role for miRNAs in pluripotency has been proven and classically

described in the epidermis[17]; however, the role of DICER1 mutations and their resulting

tumors is debated[2]. Our data supports that miRNAs are essential in maintaining a

terminally differentiated state and furthermore that loss of specific microRNA populations,

namely the 5p miRNAs, can result in cell identity reversion. In the clinical context this

paradigm is fitting as Wilms tumor blastemal stem cells have been shown to

dedifferentiate, propagate, and add to tumor volume and mass[18]. In fact, Wilms tumor can

also be referred to as nephro<u>blastoma</u>, which are preceded by nephrogenic rests defined by

their embryonal or undifferentiated histology[19]. Similarly the lung cysts, or

pleuropulmonary <u>blastoma</u> tumors (PPB) are reported to arise from primitive, likely stem,

mesenchymal cells[20]. Through this lens the gain in ability to dedifferentiate observed in our

cell model may be reflective of DICER1's essential role in the differentiation process, and

may be furthermore pathogenic in specific tissue types and result in pediatric blastoma–

like tumors. Temporal differentiation is an essential aspect of development and it is not

surprising that disruption of this eloquent coordination results in devastatingly altered

phenotypes.

From our findings we propose that GLOW syndrome, and possibly DICER1 syndrome cases at large, may benefit from the use of PI3K/AKT/mTOR inhibitors such as rapamycin and TORIN-1. Additionally, blastoma-type tumors in these cases, and others, may respond to drugs which promote differentiation. Such chemotherapies have been shown to be effective in acute myeloid leukemia cells[21]. In AML cell treatment facilitates the identification of cancerous cells by natural killer NK cells and ultimate cell lysis and clearance[21]. We propose that a similar response may be seen in pediatric tumors composed of undifferentiated cells, or where cellular dedifferentiation plays an important role including Wilms[18] and pleuropulmonaryblastoma (PPB) tumors[20]. Additionally the mutations associated with the GLOW syndrome present in a mosaic pattern of distribution, most likely due to them not being tolerated when inherited in a more wide spread distribution in keeping with Happle's hypothesis[22]. The tumors in these cases have devastating sequalae as they often metastasize; we proposed that cases identified in the future may benefit from early identification, management and similar interventions.

## Conclusions

We provide functional interaction data between the loss of 5p miRNA populations resulting from DICER1 "hot spot" or loss of exon 25 mutations and activation of the PI3K/AKT/mTOR pathway. This cross talk accounts for the phenotypic overlap observed between these cases and those with PTEN mutations, namely the macrocephaly and behavioral abnormalities including autism. Additionally, we show that DICER1$^{delExon25\,(+/-)}$ cells develop the ability to dedifferentiate and from spheres in the absence of serum. We

propose that the non-PI3K/AKT congruent phenotypes in the GLOW syndrome are due to a disruption of differentiation and the persistence of undifferentiated cells in the newborn. This is exemplified in the tumors types of GLOW syndrome cases: Wilms and pleuropulmonary blastoma (PPB) tumors. We propose the novel of use of pro-differentiation chemotherapies in combination with PI3K/AKT/mTOR inhibition would benefit these cases and may have far reaching implications for the management of the blastoma-like class of pediatric tumors.

## References

1. Klein, S., Lee, H., Ghahremani, S., Kempert, P., Ischander, M., Teitell, M.A., Nelson, S.F., and Martinez-Agosto, J.A. (2014). Expanding the phenotype of mutations in DICER1: mosaic missense mutations in the RNase IIIb domain of DICER1 cause GLOW syndrome. J Med Genet 51, 294-302.

2. Foulkes, W.D., Priest, J.R., and Duchaine, T.F. (2014). DICER1: mutations, microRNAs and mechanisms. Nat Rev Cancer 14, 662-672.

3. Desvignes, T., Batzel, P., Berezikov, E., Eilbeck, K., Eppig, J.T., McAndrews, M.S., Singer, A., and Postlethwait, J.H. (2015). miRNA Nomenclature: A View Incorporating Genetic Origins, Biosynthetic Pathways, and Sequence Variants. Trends Genet 31, 613-626.

4. Yan, S., and Jiao, K. (2016). Functions of miRNAs during Mammalian Heart Development. Int J Mol Sci 17.

5. Schiffman, J.D., Geller, J.I., Mundt, E., Means, A., Means, L., and Means, V. (2013). Update on pediatric cancer predisposition syndromes. Pediatr Blood Cancer 60, 1247-1252.

6. Hill, D.A., Ivanovich, J., Priest, J.R., Gurnett, C.A., Dehner, L.P., Desruisseau, D., Jarzembowski, J.A., Wikenheiser-Brokamp, K.A., Suarez, B.K., Whelan, A.J., et al. (2009). DICER1 mutations in familial pleuropulmonary blastoma. Science 325, 965.

7. Stewart, C.J., Charles, A., and Foulkes, W.D. (2016). Gynecologic Manifestations of the DICER1 Syndrome. Surg Pathol Clin 9, 227-241.

8. Faure, A., Atkinson, J., Bouty, A., O'Brien, M., Levard, G., Hutson, J., and Heloury, Y. (2016). DICER1 pleuropulmonary blastoma familial tumour predisposition syndrome: What the paediatric urologist needs to know. J Pediatr Urol 12, 5-10.

9. Slade, I., Bacchelli, C., Davies, H., Murray, A., Abbaszadeh, F., Hanks, S., Barfoot, R., Burke, A., Chisholm, J., Hewitt, M., et al. (2011). DICER1 syndrome: clarifying the diagnosis, clinical features and management implications of a pleiotropic tumour predisposition syndrome. J Med Genet 48, 273-278.

10. Khan, N.E., Bauer, A.J., Doros, L., Schultz, K.A., Decastro, R.M., Harney, L.A., Kase, R.G., Carr, A.G., Harris, A.K., Williams, G.M., et al. (2017). Macrocephaly associated with the DICER1 syndrome. Genet Med 19, 244-248.

11. Anglesio, M.S., Wang, Y., Yang, W., Senz, J., Wan, A., Heravi-Moussavi, A., Salamanca, C., Maines-Bandiera, S., Huntsman, D.G., and Morin, G.B. (2013). Cancer-associated somatic DICER1 hotspot mutations cause defective miRNA processing and reverse-strand expression bias to predominantly mature 3p strands through loss of 5p strand cleavage. J Pathol 229, 400-409.

12. Wu, M.K., Sabbaghian, N., Xu, B., Addidou-Kalucki, S., Bernard, C., Zou, D., Reeve, A.E., Eccles, M.R., Cole, C., Choong, C.S., et al. (2013). Biallelic DICER1 mutations occur in Wilms tumours. J Pathol 230, 154-164.

13. Ran, F.A., Hsu, P.D., Wright, J., Agarwala, V., Scott, D.A., and Zhang, F. (2013). Genome engineering using the CRISPR-Cas9 system. Nat Protoc 8, 2281-2308.

14. Doench, J.G., Fusi, N., Sullender, M., Hegde, M., Vaimberg, E.W., Donovan, K.F., Smith, I., Tothova, Z., Wilen, C., Orchard, R., et al. (2016). Optimized sgRNA design to maximize activity and minimize off-target effects of CRISPR-Cas9. Nat Biotechnol 34, 184-191.

15. Hsu, P.D., Scott, D.A., Weinstein, J.A., Ran, F.A., Konermann, S., Agarwala, V., Li, Y., Fine, E.J., Wu, X., Shalem, O., et al. (2013). DNA targeting specificity of RNA-guided Cas9 nucleases. Nat Biotechnol 31, 827-832.

16. Doros, L., Schultz, K.A., Stewart, D.R., Bauer, A.J., Williams, G., Rossi, C.T., Carr, A., Yang, J., Dehner, L.P., Messinger, Y., et al. (1993). DICER1-Related Disorders. In GeneReviews(R), R.A. Pagon, M.P. Adam, H.H. Ardinger, S.E. Wallace, A. Amemiya, L.J.H. Bean, T.D. Bird, N. Ledbetter, H.C. Mefford, R.J.H. Smith, et al., eds. (Seattle (WA).

17. Aberdam, D., Candi, E., Knight, R.A., and Melino, G. (2008). miRNAs, 'stemness' and skin. Trends Biochem Sci 33, 583-591.

18. Shukrun, R., Pode-Shakked, N., Pleniceanu, O., Omer, D., Vax, E., Peer, E., Pri-Chen, S., Jacob, J., Hu, Q., Harari-Steinberg, O., et al. (2014). Wilms' tumor blastemal stem cells dedifferentiate to propagate the tumor bulk. Stem Cell Reports 3, 24-33.

19. Beckwith, J.B. (1998). Nephrogenic rests and the pathogenesis of Wilms tumor: developmental and clinical considerations. Am J Med Genet 79, 268-273.

20. Hill, D.A., Jarzembowski, J.A., Priest, J.R., Williams, G., Schoettler, P., and Dehner, L.P. (2008). Type I pleuropulmonary blastoma: pathology and biology study of 51 cases from the international pleuropulmonary blastoma registry. Am J Surg Pathol 32, 282-295.

21. Rohner, A., Langenkamp, U., Siegler, U., Kalberer, C.P., and Wodnar-Filipowicz, A. (2007). Differentiation-promoting drugs up-regulate NKG2D ligand expression and enhance the susceptibility of acute myeloid leukemia cells to natural killer cell-mediated lysis. Leuk Res 31, 1393-1402.

22. Happle, R. (1987). Lethal genes surviving by mosaicism: a possible explanation for sporadic birth defects involving the skin. J Am Acad Dermatol 16, 899-906.

# Chapter Six

*Toxoplasmosis Gondi* causes activation of mTOR signaling in human neural progenitors and may explain the macrocephaly phenotype

## Abstract

In-utero, fetal infections are caused by numerous microbial agents and have potentially devastating effects on the developing embryo. The spectrum of causative agents are known as TORCH infections, an acronym which lists some of the most common microbes (Toxoplasmosis, Other (syphilis, varicella-zoster, parvovirus B19, ZIKA), Rubella, Cytomegalovirus (CMV), and Herpes simplex virus). The presentation of symptoms and the subsequent culturing and testing of maternal and newborn blood, tissues, or secretions can narrow the precise infectious etiology at birth. For example, congenital rubella infection is associated with deafness and cataracts while congenital syphilis presents with hepatomegaly, jaundice, and rash. These clinical manifestations vary based upon stage in development when the infections are contracted as well as specific microbe tropism. Most recently the ZIKA endemic has gained international attention due to its causative association with microcephaly (head circumference <$2^{nd}$ percentile) and developmental delay. The far-reaching accelerated spread of the ZIKA virus has caused an eruption of research into its life cycle, control, epidemiology and pathophysiology. It has been shown that (1) ZIKA can infect human fetal neural progenitor cells (hfNPCs) and (2) ZIKA inhibits the essential growth signaling pathway PI3K/AKT/mTOR. We hypothesized that infections with *Toxoplasmosis Gondi* would have a reciprocal effect on this growth-signaling cascade due to the association of macrocephaly (head circumference > $98^{th}$ percentile) with cases of congenital infections. We have infected both primary human neural progenitor cells (phNPCs) and induced-pluripotent derived neural progenitor cells (ipNPCS) with toxoplasmosis. We show that (1) these cells can be infected with the parasite and (2) that the infected cells demonstrate activation of the PI3K/AKT/mTOR pathway. These findings

establish the molecular underpinnings for a well-recognized congenital syndrome. Taken in combination with the more recent advances in ZIKA pathophysiology our findings support the importance of infection on deregulation of the PI3K/AKT/mTOR pathway and its ultimate effect on determining head size and brain growth in the developing human embryo. We propose that early identification of these cases and emergent treatment with PI3K/AKT/mTOR agonists or antagonist may help to reverse the pathogenic alterations in brain growth.

## Introduction

*In-utero Infections*

Infection during pregnancy with specific infectious agents can lead to vertical transmission and associated congenital abnormalities. These infections are not uncommon and in aggregate are reported to account for 2-3% of all congenital birth defects[1]. Collectively vertical transmission is restricted to a subset of pathogens that are commonly referred to as TORCH an acronym for each of the ones most commonly observed: Toxoplasmosis, Other (syphilis, varicella-zoster, parvovirus B19), Rubella, Cytomegalovirus (CMV), and Herpes simplex virus infections[1].  Each agent is associated with a specific constellation of congenital abnormalities which aide in perinatal diagnosis and dictate management (Table 1).

Table 6-1: Phenotypes associated with congenital TORCH infections

The major causes of congenital TORCH infections are presented with their clinical
manifestations. Any presentation having to do with somatic overgrowth, undergrowth, or
head circumference was bolded as those are the major focus of this report. "IUGR":
interuterine growth retardation

| Pathogen | Toxoplasmosis | Syphilis | Varicella-zoster | Parvovirus B19 | Rubella | Cytomegalovirus (CMV) | Herpes simplex virus |
|---|---|---|---|---|---|---|---|
| **Type** | Parasite | Bacteria | Viral | Viral | Viral | Viral | Viral |
| **Findings** | Chorioretinitis Abnormal cerebrospinal fluid Anemia Seizures Intracranial calcification Jaundice Fever Splenomegaly Lymphadenopathy Hepatomegaly Pneumonitis | Hepatomegaly Jaundice Nasal discharge ("snuffles") Rash Generalized lymphadenopathy Skeletal abnormalities | Ocular defects, such as cataracts, chorioretinitis, Horner syndrome, microphthalmos, and nystagmus, hypoplasia of bone and muscle, aricella pneumonia, hepatitis, and meningoencephalitis | Hydrops and fetal death | Fetal growth restriction Meningoencephalitis Hearing loss Cloudy cornea, cataract infantile glaucoma, retinopathy Interstitial pneumonia Cardiac defects Hepatosplenomegaly, jaundice, diarrhea Radiolucent bone lesions Petechiae and purpura Adenopathy Hemolytic anemia, thrombocytopenia | Petechiae Jaundice at birth Hepatosplenomegaly Small size for gestational age Sensorineural hearing loss Lethargy and/or hypotonia Poor suck Chorioretinitis Seizures Hemolytic anemia Pneumonia | hepatitis with elevated liver transaminases, ascites, and direct hyperbilirubinemia, pneumonia and hemorrhagic pneumonitis, , meningoencephalitis, myocarditis and myocardial dysfunction, disseminated intravascular coagulation (DIC), necrotizing enterocolitis, Skin and mucous membranes lesions |

| Growth Findings | Macrocephaly | Microcephaly IUGR | Microcephaly IUGR | IUGR | Microcephaly IUGR | Macrocephaly | Microcephaly |
|---|---|---|---|---|---|---|---|

Exact presentation at birth is dictated by what stage in development infection occurs and furthermore the pathogen's tropism for specific tissue types[2-10]. Most recently global media and medical attention has been given to the ZIKA virus which fits into the TORCH acronym under the heading of "Other" and is associated with it's own clinical manifestations[11].

### ZIKA Virus

The ZIKA virus epidemic is a global public health crisis[12]. With initial reports originating in Brazil the spread the virus was swift and new cases are currently being documented throughout the western hemisphere and within the Continental United States[12-15]. Maternal infection with ZIKA and subsequent vertical transmission is associated with a reproducible phenotype including microcephaly and developmental delays[16; 17].  Adult infection with ZIKA also displays central nervous system tropism and results in a transient manifestation similar to that of Guillain-Barre syndrome with acute progressive weakness and paralysis[18].  While the adult manifestations are thought to be immune mediated, it has been shown that the perinatal findings of microcephaly and developmental delay are a direct result of down regulation of the AKT/mTOR signaling axis and induction of autophagy[19]. More specifically the viral proteins NS4A and NS4B directly inhibit AKT, which has broad implications for neural cell differentiation and proliferation[19].  We hypothesized that the opposite observation of macrocephaly associated with *T.gondi* infection was due to the activation of the same pathway.

*Toxoplasmosis Gondi*

*T.gondi*, a protozoa (Figure 1), is one of the worlds most common parasites and infects a

number of host species including household cats which is thought to be a common mode of

transmission to pregnant women[20-22]. Infection in the immune competent patient results in

flu-like symptoms or more commonly is asymptomatic. In pregnancy however vertical

infection is associated with a multi-faceted perinatal presentation including premature

birth, anemia, hepatomegaly, motor and developmental delays, intracranial calcifications

and macrocephaly[23]. We hypothesized that the macrocephaly associated with these

infections is due to up regulation of the AKT/mTOR pathway in a reciprocal manner to that

of ZIKA virus.

Figure 6-1: The Protozoan Toxoplasmosis Gondi

The internal structure of the parasite T.gondi is presented. It should be noted that unlike viruses, these microbes contain their own structures and ability to synthesize proteins; this may have potential implications for interpreting results of infection on host cell signaling.
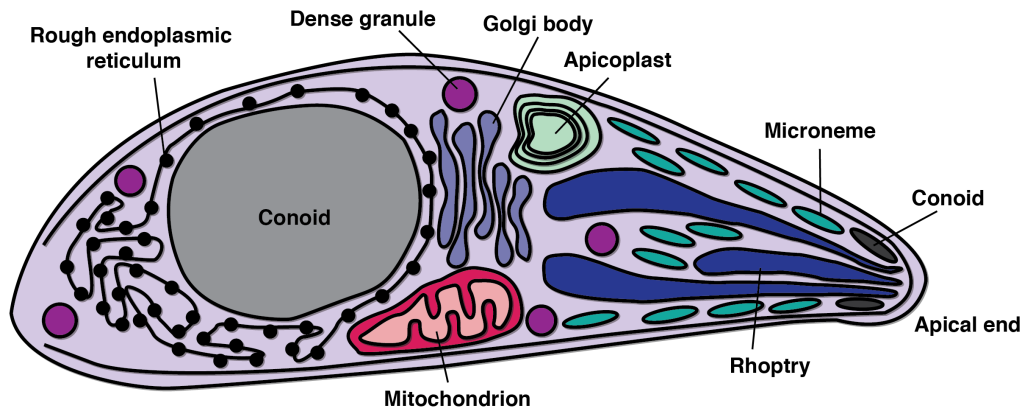


Ultrastructure of a *Toxoplasma gondii* tachyzoite

## Methods

*Growing and infection with Toxoplasmosis Gondi*

T. Gondi was grown in Vero cells with minimum medium (MEM 8.0% FBS and 1.0%

Penicillin strep). Host cells were inoculated with T.Gondi on day zero and then harvested

on day four.  The tachyzoites are harvested using a 27-gauge needle. The supernatant was

then filtered a 5um syringe filter. Following filtration the parasites were centrifuged a five

thousand RPM for ten minutes at 4 degrees Celsius.  The pellet was washed once with PBS

and suspended in one ml of base media. T.Gondi concentration was determined using a

hemocytometer. Cells were infected with a high MOI and allowed to infect for 18 hours

before cell lysis from infection took place.


*Cell Culture*

Cells were maintained in basal media composed of NeuralX  NSC Medium, GlutaGro,

MEM nonessential amino acids, GS22 Neural Supplement, FGF/EGF, and LIF. 24 hours

before infection, cells were liberated from T75 flask with 5ml of TrypLE™ Express Enzyme

(1X) and replated onto a LDEV-free, Geltrex coated 12-well plate. Media was changed and

then either 100 or 200ul of based media +/- *T.gondi* was added.


*Western Blot Analysis*

Cells were lysed on 12 well plates with 400ul of passive lysis buffer, prepared with

phosphatase and protease inhibitors, and incubated by shaking at $4^0$C for one hour. After

lysis tubes were spun at 7500 Rcf for 5 minutes to collect debris. Supernatant was

transferred to a new tube then protein concentration determined with the Coomassie Plus

Bradford (Life Technologies) reagent following manufacture instructions. Protein samples

were diluted to a final concentration of 10μg/20 μl into Western loading buffer with beta-

mercaptoethanol and then boiled for 5 minutes.  Western blots were run on 12%

acrylamide gels followed by transfer onto nitrocellulose membranes utilizing the Transblot

Turbo® apparatus from Biorad. The membrane was blocked in 5% bovine serum albumin

in Tris buffered saline plus Tween (TBST) for 30 minutes, then incubated in primary

antibodies (Listed Below) for 24 hours. Blots were then rinsed with Tris buffered saline

(TBS) and washed three times with TBST. Blots were then incubated in rabbit secondary

antibodies conjugated to horseradish peroxidase at a dilution of 1/3750. Following

secondary incubation membranes were rinsed with TBS then washed twice with TBST.

Blots were exposed using Western Clarity reagents from BioRad and imaged on the Bio Rad

ChemiDoc and viewed in ImageLab Software.

| Antibodies | | | |
|---|---|---|---|
| Antibody | Manufacturer | Cat # | Dilution |
| pmTOR 2448 | Cell Signaling | 5536 | 1:1000 |
| AKT 473 | Cell Signaling | 4060 | 1:2000 |
| B-actin | Cell Signaling | 4970 | 1:4000 |
| p4EBP1 S65 | Cell Signaling | 9451 | 1:1000 |
| PTEN | Cell-Signaling | 9188 | 1:1000 |
| pTSC2 | Cell-Signaling | 3611 | 1:2000 |
| pGSK3a/b | Cell-Signaling | 9331 | 1:1000 |

| | | | |
|---|---|---|---|
| pPTEN | Cell-Signaling | 9551 | 1:1000 |
| pAKT308 | Cell-Signaling | 13038 | 1:1000 |
| pAKT450 | Cell-Signaling | 9267 | 1:1000 |
| P4EBP1 | Cell-Signaling | 2855 | 1:1000 |
| pmTOR2481 | Cell-Signaling | 2974 | 1:500 |
| pS6Kinase | Cell-Signaling | 9234 | 1:1000 |
| pSGK(Ser422) | Santa Cruz | Sc-16745 | 1:200 |
| pRAPTOR (Ser792) | Cell-Signaling | 2083 | 1:1000 |

Western blots were run in biological sextets, which gave us the power to perform Mann-Whitney U tests for non-parametric data. The p-values for these tests were Bonferroni corrected for multiple tests in the event of numerous comparisons.

*Immunofluorescence*

One hundred thousand human neural stem cells were plated on GelTrex (Invitrogen) coated coverslips. After 24 hours of growth cells were fixed using paraformaldehyde for 20 minutes then blocked with 10% normal goat serum in TBST overnight. The following day coverslips were washed three times in TBST. Coverslips were incubated in primary antibody (Listed Below) in 3% BSA in TBST for one hour. Coverslips were then washed three times in TBST and incubated in secondary antibody (Jackson Laboratories, AffiniPure Donkey Anti-Rabbit, 711-165-152, Dilution 1/1000 and Invitrogen, Alexa Fluor® 647 Phalloidin, A22287, dilution 1/100) in 3% BSA in TBST for one hour. Coverslips were then washed three times in TBST and then three times in water. Coverslips were mounted on glass slides using ProLong® Gold Antifade Mountant with DAPI (Invitrogen, P36931). Slides were imaged using a Zeiss LSM-800.

| Staining | | | |
|---|---|---|---|
| **Antibody** | **Manufacturer** | **Cat #** | **Dilution** |
| PTEN | Cell Signaling | 9188 | 1:500 |
| Phalloidin 647 | Thermo | A22287 | 1:250 |
| Rb-Cy3 | Jackson | 711-165-152 | 1:1000 |
| Ms-DL469 | Jackson | | 1:4000 |

# Results

*Primary Human Neural Progenitor Cells (pNSCs) and Induced Pluripotent Derived*

*Human Neural Progenitor Cells (ipNSCs) can be infected with Toxoplasmosis Gondi.*

We first confirmed that both cells types, Primary Human Neural Progenitor Cells (pNSCs) and Induced Pluripotent Derived Human Neural Progenitor Cells (ipNSCs) could be infected with the intracellular parasite *T.gondi*. This was achieved via infection of adherent cells followed by immunofluorescence staining for SAG1, a pathogen specific surface marker. We demonstrate dose-dependent infection, which increases with increased pathogen concentration. Infections show the presence of numerous intracellular SAG1+ pathogen particles. While T.Gondi infection has been shown in murine neural stem cells[24] and established human neuroblasts and microglia cell lines[25] we are the first to demonstrate this tropism for primary human neural progenitors which was additionally confirmed in an induced pluripotent derived neural progenitor cell type.

*Infection with Toxoplasmosis Gondi causes activation of PI3K/AKT Signaling*

We then queried if PI3K/AKT/mTOR signaling was increased in these cells. Western blot analysis was performed 24 hours after infection. These cells show increased AKT signaling as evidenced by the increased levels of pAKT308 and pAKT450. Most interestingly viral infected cells show an additional band, which stains with the primary antibodies for pAKT. They also show increased levels of pmTOR2448, pmTOR2481, and p4EBP1 (Ser65). Lastly these cells show increased levels of the autophagy makers LC3A/B. This increase in pAKT308 was confirmed with immunofluorescence staining at high magnification, which demonstrated that infected cells have higher levels of this substrate in the phosphorylated

form. Additionally, it appears that this antibody recognizes an antigen present in the

parasite.

Figure 6-2: *T. Gondi* infected neural progenitors and activated PI3K/AKT/mTOR signaling

(a) Infection of both human primary and induced pluripotent derived neural progenitors show the ability to be infected with *T. Gondi,* infections increases with increased parasite concentration. (b) Western blot analysis assaying PI3K/AKT activation following infection showing increases in pmTOR2448, pAKT308, LC3A/B, pAKT450 and pmTOR2481, extra band observed in pAKT308 stainin denoted with red arrow. (c) Quantification of western blot analysis (d) confirmation of increased pAKT308 staining via Immunofluorescence.
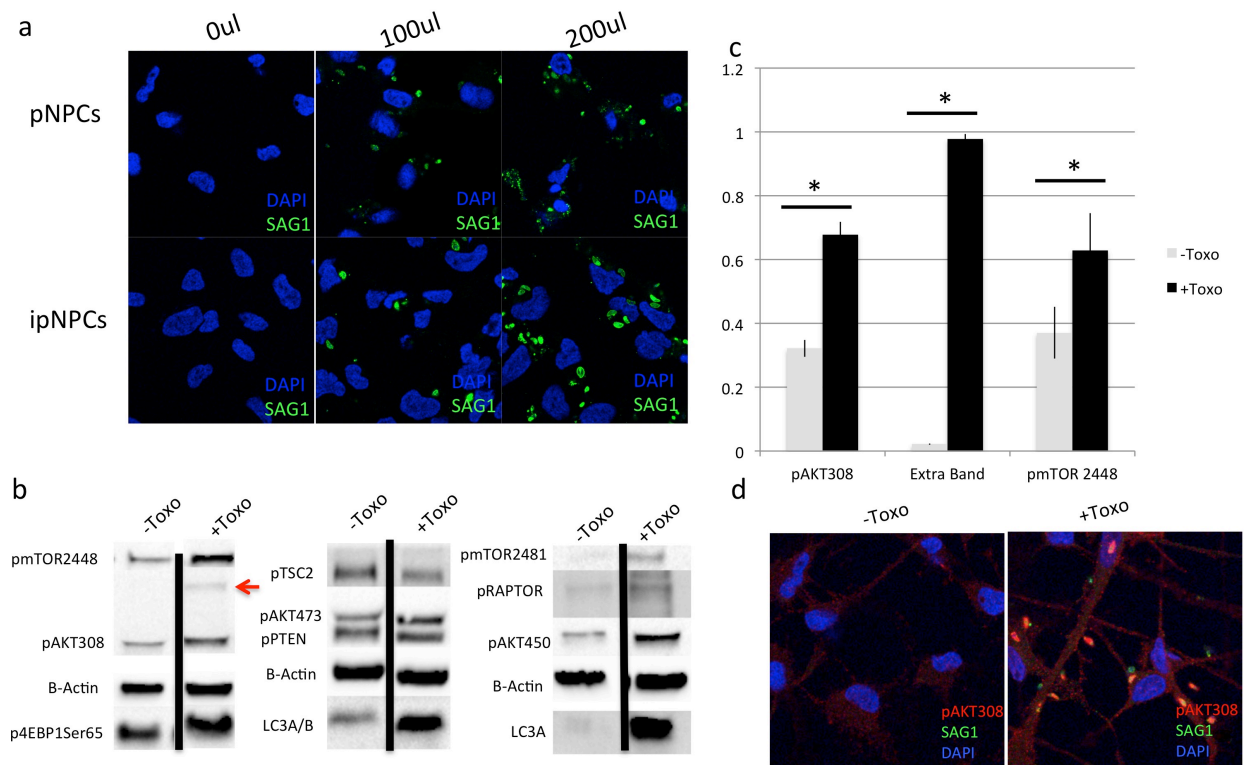
# Discussion

*Neural Progenitors infected with Toxoplasmosis Gondi have activated PI3K/AKT/mTOR signaling*

We have shown that *T. gondi* has the ability to infect neural progenitor cells, which confirms the pathologies and pathogen tropism associated with the central nervous system[23,25]. Furthermore we demonstrate that Toxoplasmosis infection activates the PI3K/AKT/mTOR signaling pathway. The association between toxoplasmosis and mTOR activation has been previously reported in the murine fibroblast cell line 3T3. However, that report shows that the activation of mTOR is AKT independent and activated S6kinase but did not activate p4EBP1[26]. We report a cell type specific and biologically relevant response in human primary and induced pluripotent derived neural progenitor cells, which demonstrate strong activation of AKT, increased levels phosphorylated AKT. We have also shown increases in activated components of the pathway downstream of AKT including pmTOR2448 and p4EBP1Ser65. In combination these events demonstrate coordinated mTORC1 activation in response to Toxoplasmosis infection. Paradoxically we show increases in markers of autophagy including LC3A and LC3B. This was not expected as classical mTOR signaling is thought to inhibit autophagy. We propose that intracellular infection may be triggeran overriding pro-autophagy signal, which accounts for this discrepancy. Specifically autophagy activation could occur concurrent but independent from AKT/mTOR activation[27].

We compare our findings to those most recently reported with ZIKA virus infection, which have demonstrated, in similar cell lines, that infection causes decreased AKT signaling. This deregulation is caused by a direct interaction of the viral proteins NS4A and NS4B with AKT, which is inhibitory and lessens downstream mTOR signaling(ref). ZIKA infection causes decreased neurogenesis and increased autophagy, which may be responsible for the microcephaly phenotypes in congenital cases. Similarly Toxoplasmosis infection activates this same pathway by a mechanism not yet fully understood.  The opposite effects on brain size despite the shared decreases in autophagy leads us to believe that the macrocephaly associated with these *T.gondi* congenital cases may be due to increased progenitor proliferation independent of autophagy. Interestingly, both infections are associated with development delays and intellectual disability supporting the importance of the temporal, faithful maintenance of brain growth during development and the ability of alterations to this trajectory to disrupt normal brain functions (Figure 3).

Figure 6-3: Toxoplasmosis Gondi and Zika Virus exert opposite effects on the neural progenitor cell

As has been previously shown, ZIKA virus can infect neural progenitors and directly inhibits AKT via two viral proteins and causes microcephaly. We have shown that toxoplasmosis gondi infection activates AKT. Therefore, we believe the same mechanism cause congenital T. gondi macrocephaly.
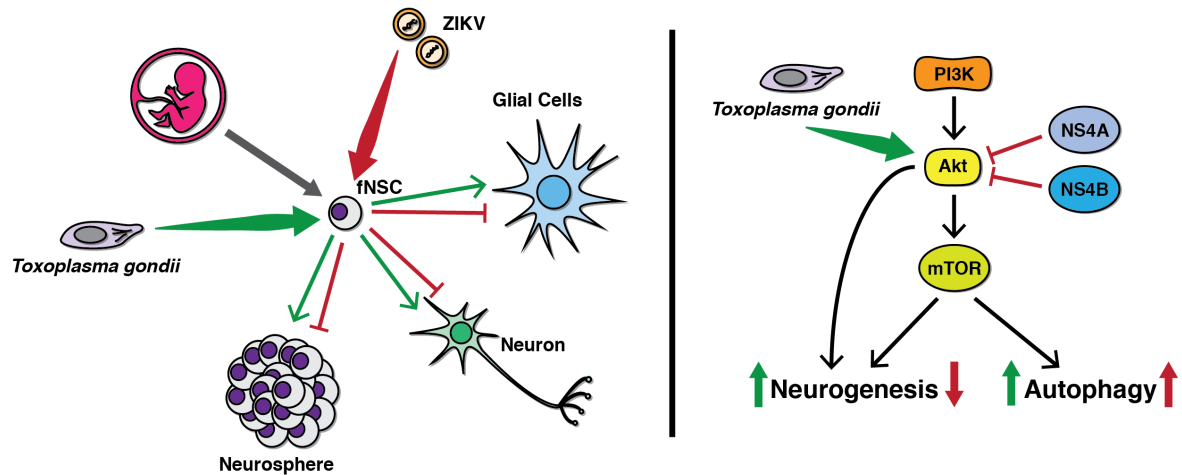
*The precision approach to the patient with congenital Toxoplasmosis or ZIKA infection*

Abnormal head circumference can be the first indication of congenital infections with either ZIKA virus or Toxoplasmosis Gondi. In these cases, emergent testing should be performed to identify the causative pathogen, which may also have important consequences for potential treatments. Multiple biological cues and reactive signaling pathways tightly regulate brain growth. Central to this orchestrated coordination is the PI3K/AKT/mTOR signaling cascade[28]. As we have shown in previous chapters mutations within this pathway and with cross talking intermediates results in abnormal brain growth. In addition to genetic mutation it is becoming evident, through our work and others, that infections can also modulate mTOR signaling. We believe that there is a potential role for PI3K/AKT/mTOR antagonist and agonist in the management of congenital TORCH infections presenting with abnormal head circumference. In utero control of the AKT signaling may represent a focal rheostat, which allows brain growth trajectories to return to normal and possibly result in better outcomes for these cases.

## Conclusions

We demonstrate for the first time *T.gondi* tropism for human neural progenitors. In response to infection this specific cell type shows increased PI3K/AKT/mTOR signaling, which may be responsible for the occurrence of macrocephaly in cases of congenital toxoplasmosis. We propose that this pathophysiology is reciprocal to that seen in congenital ZIKA virus infection which results in decreased AKT signaling and microcephaly. This report in combination with the emerging understanding of ZIKA infection

demonstrates the interplay between intracellular infection and regulation of growth

signaling pathways. We believe that there is a potential role for pharmacological

intervention in these cases as the PI3K/AKT antagonist and agonist are numerous and vary

in mechanism of action and effectiveness. Restoring PI3K/AKT signaling to baseline

regulated levels may be an essential step in treating these cases and improving outcomes.

# References

1. Stegmann, B.J., and Carey, J.C. (2002). TORCH Infections. Toxoplasmosis, Other (syphilis, varicella-zoster, parvovirus B19), Rubella, Cytomegalovirus (CMV), and Herpes infections. Curr Womens Health Rep 2, 253-258.

2. Dreher, A.M., Arora, N., Fowler, K.B., Novak, Z., Britt, W.J., Boppana, S.B., and Ross, S.A. (2014). Spectrum of disease and outcome in children with symptomatic congenital cytomegalovirus infection. J Pediatr 164, 855-859.

3. Prusa, A.R., Kasper, D.C., Pollak, A., Gleiss, A., Waldhoer, T., and Hayde, M. (2015). The Austrian Toxoplasmosis Register, 1992-2008. Clin Infect Dis 60, e4-e10.

4. Berger, F., Goulet, V., Le Strat, Y., and Desenclos, J.C. (2009). Toxoplasmosis among pregnant women in France: risk factors and change of prevalence between 1995 and 2003. Rev Epidemiol Sante Publique 57, 241-248.

5. Workowski, K.A., Bolan, G.A., Centers for Disease, C., and Prevention. (2015). Sexually transmitted diseases treatment guidelines, 2015. MMWR Recomm Rep 64, 1-137.

6. Goderis, J., De Leenheer, E., Smets, K., Van Hoecke, H., Keymeulen, A., and Dhooge, I. (2014). Hearing loss and congenital CMV infection: a systematic review. Pediatrics 134, 972-982.

7. Flagg, E.W., and Weinstock, H. (2011). Incidence of neonatal herpes simplex virus infections in the United States, 2006. Pediatrics 127, e1-8.

8. Roberts, S. (2009). Herpes simplex virus: incidence of neonatal herpes simplex virus, maternal screening, management during pregnancy, and HIV. Curr Opin Obstet Gynecol 21, 124-130.

9. Mahnert, N., Roberts, S.W., Laibl, V.R., Sheffield, J.S., and Wendel, G.D., Jr. (2007). The incidence of neonatal herpes infection. Am J Obstet Gynecol 196, e55-56.

10. Brown, Z.A., Wald, A., Morrow, R.A., Selke, S., Zeh, J., and Corey, L. (2003). Effect of serologic status and cesarean delivery on transmission rates of herpes simplex virus from mother to infant. JAMA 289, 203-209.

11. Coyne, C.B., and Lazear, H.M. (2016). Zika virus - reigniting the TORCH. Nat Rev Microbiol 14, 707-715.

12. Sharma, S., Tandel, K., Dash, P.K., and Parida, M.M. (2017). Zika virus: A public health threat. J Med Virol.

13. Miner, J.J., and Diamond, M.S. (2017). Zika Virus Pathogenesis and Tissue Tropism. Cell Host Microbe 21, 134-142.

14. Diaz, J.H. (2016). Preparing the United States for Zika Virus: Pre-emptive Vector Control and Personal Protection. Wilderness Environ Med 27, 450-457.

15. Reynolds, M.R., Jones, A.M., Petersen, E.E., Lee, E.H., Rice, M.E., Bingham, A., Ellington, S.R., Evert, N., Reagan-Steiner, S., Oduyebo, T., et al. (2017). Vital Signs: Update on Zika Virus-Associated Birth Defects and Evaluation of All U.S. Infants with Congenital Zika Virus Exposure - U.S. Zika Pregnancy Registry, 2016. MMWR Morb Mortal Wkly Rep 66, 366-373.

16. Song, B.H., Yun, S.I., Woolley, M., and Lee, Y.M. (2017). Zika virus: History, epidemiology, transmission, and clinical presentation. J Neuroimmunol.

17. Chibueze, E.C., Tirado, V., Lopes, K.D., Balogun, O.O., Takemoto, Y., Swa, T., Dagvadorj, A., Nagata, C., Morisaki, N., Menendez, C., et al. (2017). Zika virus infection in

pregnancy: a systematic review of disease course and complications. Reprod Health 14, 28.

18. Wijdicks, E.F., and Klein, C.J. (2017). Guillain-Barre Syndrome. Mayo Clin Proc 92, 467-479.

19. Liang, Q., Luo, Z., Zeng, J., Chen, W., Foo, S.S., Lee, S.A., Ge, J., Wang, S., Goldman, S.A., Zlokovic, B.V., et al. (2016). Zika Virus NS4A and NS4B Proteins Deregulate Akt-mTOR Signaling in Human Fetal Neural Stem Cells to Inhibit Neurogenesis and Induce Autophagy. Cell Stem Cell 19, 663-671.

20. Wyrosdick, H.M., and Schaefer, J.J. (2015). Toxoplasma gondii: history and diagnostic test development. Anim Health Res Rev 16, 150-162.

21. Frimpong, C., Makasa, M., Sitali, L., and Michelo, C. (2017). Seroprevalence and determinants of toxoplasmosis in pregnant women attending antenatal clinic at the university teaching hospital, Lusaka, Zambia. BMC Infect Dis 17, 10.

22. Brennan, A., Donahoe, S.L., Beatty, J.A., Belov, K., Lindsay, S., Briscoe, K.A., Slapeta, J., and Barrs, V.R. (2016). Comparison of genotypes of Toxoplasma gondii in domestic cats from Australia with latent infection or clinical toxoplasmosis. Vet Parasitol 228, 13-16.

23. Hampton, M.M. (2015). Congenital Toxoplasmosis: A Review. Neonatal Netw 34, 274-278.

24. Wang, T., Zhou, J., Gan, X., Wang, H., Ding, X., Chen, L., Wang, Y., Du, J., Shen, J., and Yu, L. (2014). Toxoplasma gondii induce apoptosis of neural stem cells via endoplasmic reticulum stress pathway. Parasitology 141, 988-995.

25. Mammari, N., Vignoles, P., Halabi, M.A., Darde, M.L., and Courtioux, B. (2014). In vitro infection of human nervous cells by two strains of Toxoplasma gondii: a kinetic analysis of immune mediators and parasite multiplication. PLoS One 9, e98491.

26. Wang, Y., Weiss, L.M., and Orlofsky, A. (2009). Intracellular parasitism with Toxoplasma gondii stimulates mammalian-target-of-rapamycin-dependent host cell growth despite impaired signalling to S6K1 and 4E-BP1. Cell Microbiol 11, 983-1000.

27. Martin, S., Saha, B., and Riley, J.L. (2012). The battle over mTOR: an emerging theatre in host-pathogen immunity. PLoS Pathog 8, e1002894.

28. Kim, W.Y. (2015). Brain size is controlled by the mammalian target of rapamycin (mTOR) in mice. Commun Integr Biol 8, e994377.

# Chapter Seven

Genetic etiologies of macrocephaly, many roads lead to mTOR some roads lead to Autism.

We have presented data and cases that demonstrate the genetic heterogeneity of macrocephaly. We briefly summarize each chapter of this thesis below:

## Summaries by Chapter

Our data demonstrates that macrocephaly is a distinct clinical finding resulting from numerous genetic etiologies. Biological functional enrichment analysis revealed that these genes are involved in common biological processes including central nervous system development, neurogenesis, generation of neurons, head development, neuron differentiation, and brain development. Interestingly, pathway enrichment analysis demonstrates that these genes cluster within two growth signaling pathways (1) PI3K/AKT/mTOR pathway and (2) the Hedgehog-signaling pathway. The associated phenotypes within macrocephaly-associated syndromes include skeletal, epidermal, and vascular system phenotypes. Closer examination of the neurologic phenotypes revealed that numerous macrocephaly-syndromes are associated with developmental delays, autism, and hypotonia. By demonstrating the overlap of macrocephaly- and autism-associated genes, we have identified a potential novel neural network, which may help to elucidate the causative genetic etiologies of the macrocephaly-autism phenotype. We highlight the overlap between autism and macrocepahly associated genes which confirms the role of pathogenic brain growth in this behavioral phenotype. We focused on understanding the genetic contribution of macrocephaly-associated genes to brain growth by modeling mutations in *PTEN, MTOR, Ptch1, Sufu, DICER1* associated with macrocepahly and developmental delays including autism.

Figure 7-1: Autism-macrocephaly related community

Using GeneNets software we were able to generate this community from the aut-macro gene list. These highly interconnected genes represent a potential novel neural network that is implicated in the development of the autism-macrocephaly phenotype.
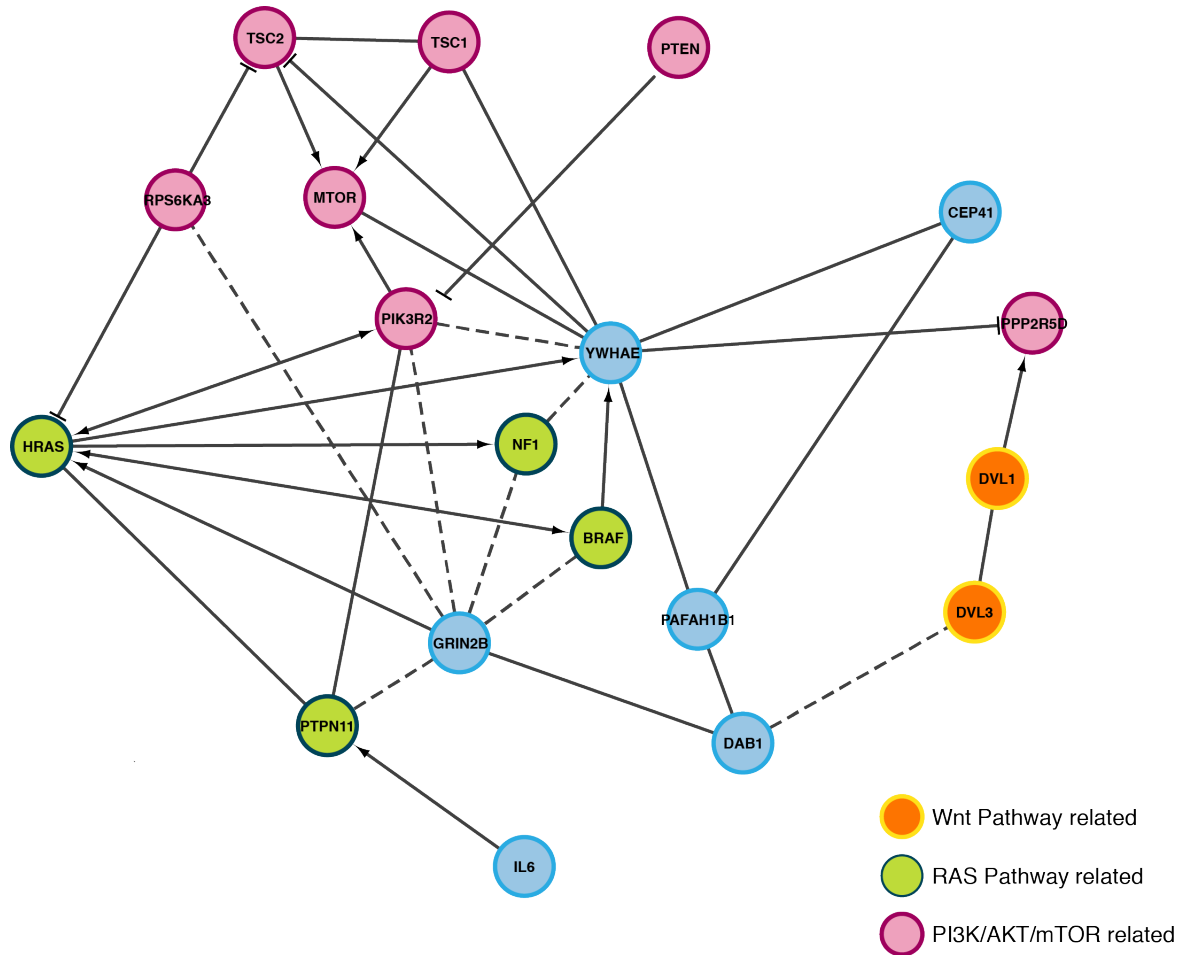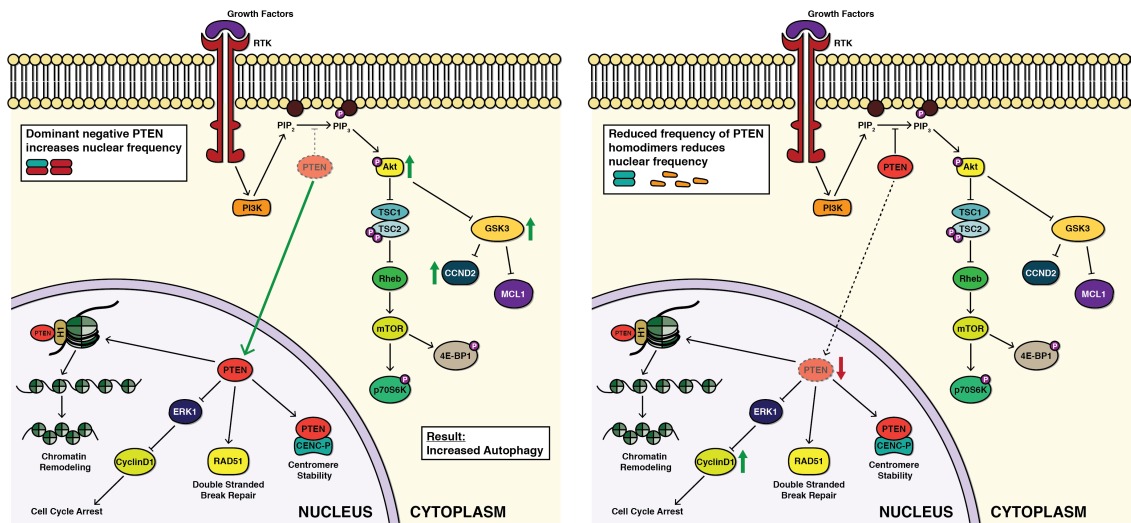
*Chapter 2:*

We use numerous approaches to determine the role that PTEN loss and mutations affect downstream cell signaling. Namely we use a Crispr/Cas9, viral and patient derived induced pluripotent stem cell (iPSC) based approach. Utilizing Crispr/Cas9 we show the importance of the PTEN/mTORC2 axis, which is evidenced by increased phosphorylation of its substrates. From the patient derived iPSCs we demonstrated heterozygous loss of function PTEN variants in neural progenitor cells result in isolated activation of pAKT308 and translocation of PTEN out of the nucleus. Mutations in PTEN predicted to act through a dominant negative mechanism of action are associated with not only increased pAKT308 but also strong pAKT473 activation and decreases in mTORC1 targets such as p4EBP1, increased localization of PTEN into the nucleus, and increased autophagy. These differential effects stress the role of nuclear PTEN in the development of these phenotypes. We propose that these signaling events culminate in functional effects outside of canonical mTOR signaling, mainly deregulation of the cell cycle via alterations to the cyclin proteins. These distinctions help to explain the spectrum of molecular mechanisms that can result in macrocephaly associated autism, and predict varying response to treatment modalities based upon genetic etiology. In addition to PTEN we have modeled mutations in mTOR, which confirm the role of this downstream target of PI3K/AKT signaling in the pathogenesis of macrocephaly.

Figure 7-2: Effect of dominant negative and true loss of function mutations

Out proposed model that explains the difference in dominant negative mutations and true loss of function mutations. The dominant negative mutations are associated with PTEN translocation into the nucleus and increased pAKT308 and 473 while true loss of function mutations are associated with a nuclear sparing staining pattern.

*Chapter 3:*

We have shown that specific macrocephaly-associated phenotypes arise from recurrent gain of function mutations in mTOR and also that these mutations are associated with distinct degrees of mTOR activation. In particular, strong mTOR activating mutations behave similar to gain-of-function mutations in *PIK3CA, AKT3* and *PIK3R2*, while mTOR mutations that only mildly activate its function resemble inactivating mutations in *PTEN*. Supporting this paradigm, inactivating mutations in *PTEN* are repeatedly observed to be germline similar to the E1799K *MTOR* variant, while activating mutations in *PIK3CA, AKT3, AKT1* and *PIK3R2* have a predilection towards mosaic distribution, as observed for the C1483Y and the T1977I mTOR variants. Growth signaling pathways are highly complex and branch extensively; additional pathway intermediates may be playing distinct roles upstream of the activation of AKT, which may cause additional genotype-phenotype variations. Our findings establish gain-of-function mutations in *mTOR* as causative for a range of distinct human macrocephaly-associated phenotypes that result from allele specific effects on pathway activation and mosaic distribution. These findings provide insight into the etiology of human overgrowth and establish mTOR activation as sufficient for deregulation of this process, with implications for therapeutic approaches and prognosis. Mutations in the hedgehog pathway are associated with phenotypes overlapping those in components of the PI3K/AKT signaling cascade, prompting us to hypothesize that these pathways interact.

| C1483Y/F | | | T1977I | | | E1799K | | |
| --- | --- | --- | --- | --- | --- | --- | --- | --- |
| Cases | Phenotype | M/G | Cases | Phenotype | M/G | Cases | Phenotype | M/G |
| **Case 1** | Hemi-Megalencephaly, HMI, Seizures | M | **Case 2** | Hemi-Hypertrophy, Hyperpigmented Skin Lesion, GDD, Macrocephaly | M | **Case 3** | Macrocephaly, Somatic Overgrowth, GDD | G |
| 1[A] | Hemi-Megalencephaly, HMI | M | | | | 2[C] | Macrocephaly, Somatic Overgrowth*, ASD, Iris Coloboma, | G |
| 1[B] | Megalencephaly, Seizures | G? | | | | 3[D] | Macrocephaly, SD, GDD, Seizures, Small Chest | G |

Mosaic Distribution
Global Developmental Delay
Hemi-Megalencephaly
Hypomelanosis of ITO
Seizures

Mosaic Distribution
Global Developmental Delay
Macrocephaly
Hemi-Hyperplasia
Hyperpigmented Skin Lesions

Germline
Global Developmental Delay
Autism Spectrum Disorder
Macrocephaly
Somatic Overgrowth
Seizures

mTOR Activity

Figure 7-3: mTOR activation and associated overgrowth phenotypes

Summary of phenotypic findings associated with mutations in the residues C1483, T1977 and E1799 and corresponding levels of mTOR activation.  M/G: Mosaic/Germline distribution, M: Mosaic Distribution, G: Germline Distribution, G?: single case reported to be germline but not confirmed, HMI: Hypomelanosis of ITO,  GDD: Global developmental delay, SD: speech delay, ASD: Autism Spectrum Disorder, A: Lee et al.[1], B: Smith et al.[2], C: Mroske et al.[3], D: Baynam et al. [4].

*Chapter 4:*

We demonstrate that the strong phenotypic overlap with PI3K/AKT/mTOR related overgrowth syndromes is due to cross talk between the two pathways, which is mediated by Gli-associated transcriptional changes. We have expanded the phenotypic spectrum of PTCH1 and Sufu mutations to include overgrowth, macrocepahly, developmental delays and dysmorphia. Additionally, mutations in SUFU not only overlap with the transcriptional changes associated with active Hh signaling but also demonstrate additional PI3K activation, which may be due to a loss of suspected inhibition of LAMTOR3. We propose that these cases as well as those affected by the more classical basal cell carcinoma nevoid syndrome would benefit from dual inhibition of PI3K/AKT/mTOR and SHH signaling for these reasons.

Figure 7-4: Loss of PTCH1 causes Transcriptional, AKT independent activation of mTOR

Loss of PTCH1 lessens the inhibition of Smoothened, which allows it to activate SUFU and remove the negative inhibition of SUFU on Gli translocation. When Gli translocates to the nucleus it activates the expression of Lyf and Nkx2.2, which inhibits the expression of PRKAG2, RHOA, and STRADB; these are all negative regulators of mTOR. The loss of negative inhibition leads to activation of mTOR, which we have demonstrated via increased phosphorylation of p4EBP1 and mTOR itself.
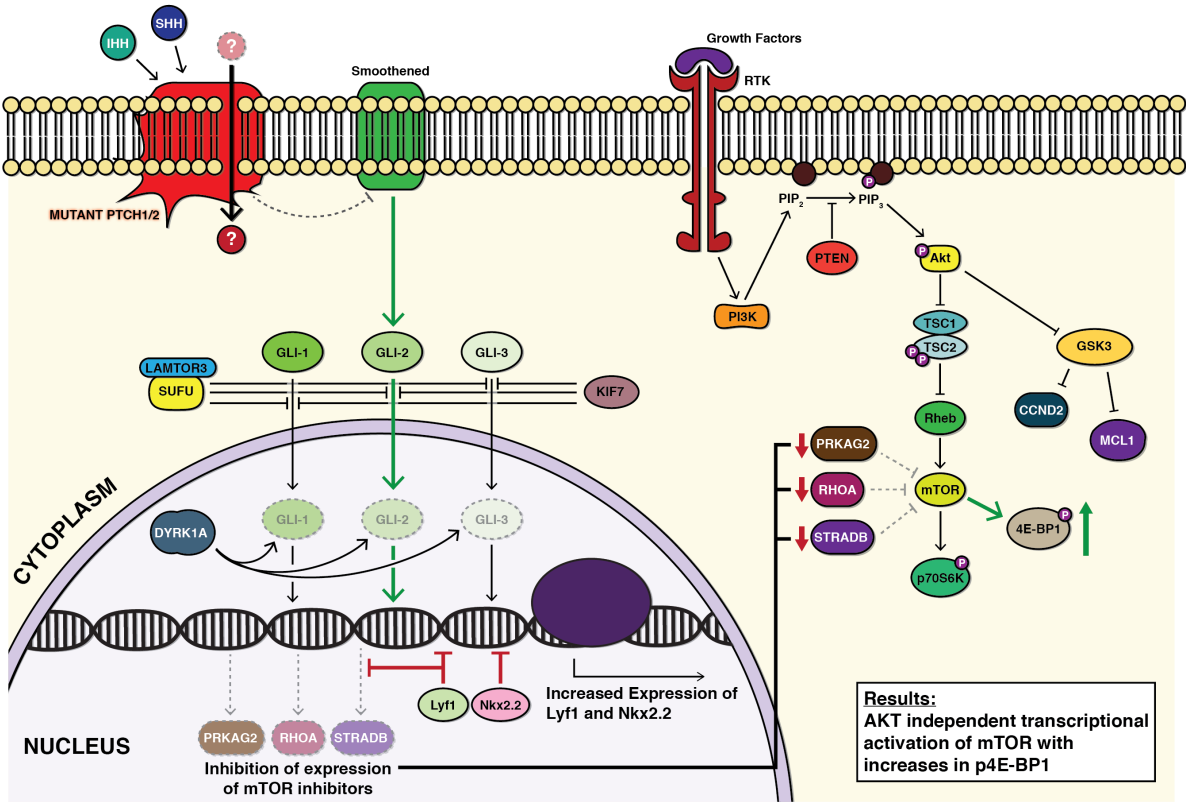
Figure 7-5: Loss of SUFU causes transcription as well as LAMTOR3 mediated AKT activation of mTOR

Loss of SUFU lessens the inhibition on Gli translocation. When Gli translocates to the nucleus, it activates the expression of Lyf and Nkx2.2, which inhibits the expression of PRKAG2, RHOA, and STRADB; these are all negative regulators of mTOR. The loss of negative inhibition leads to activation of mTOR, which we have demonstrated via increased phosphorylation of p4EBP1 and mTOR itself. Additionally, loss of SUFU liberates LAMTOR3 from inhibition and allows it to activate AKT, which we have demonstrated via increased phosphorylation of pAKT473 and pAKT308.
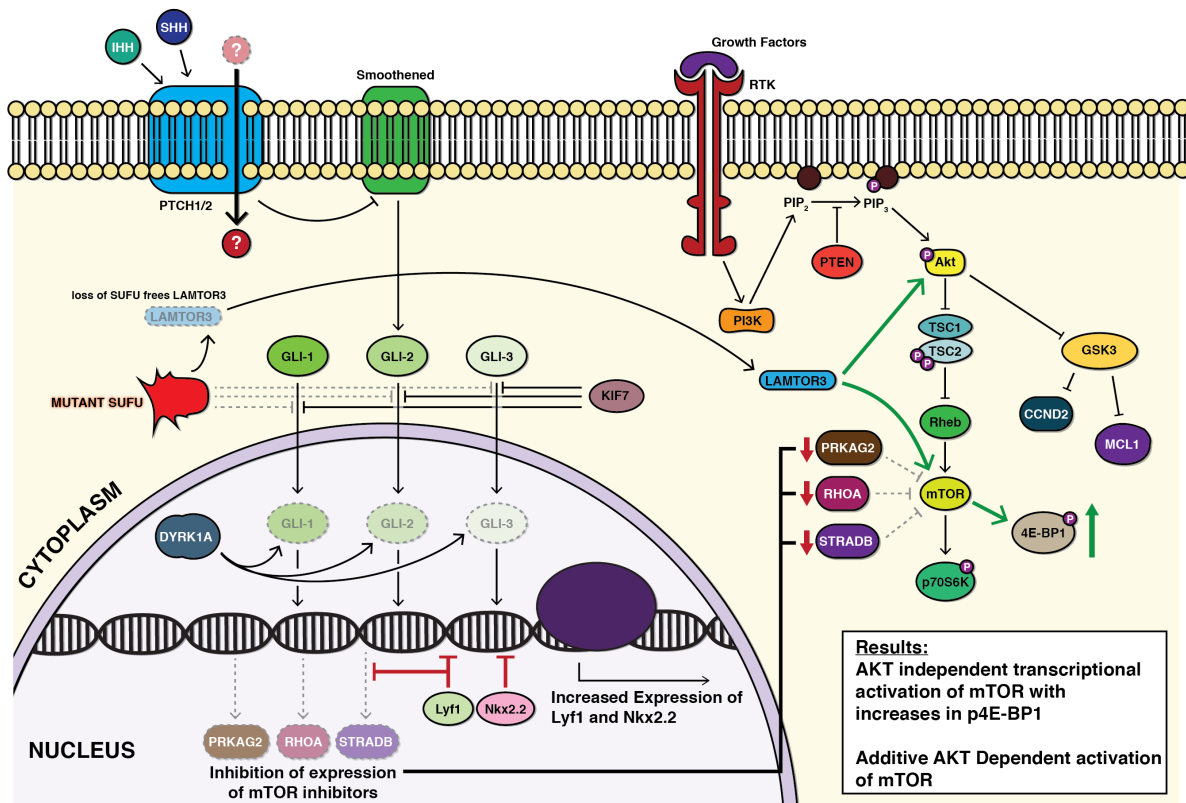
*Chapter 5:*

We have established that macrocephaly and overgrowth associated DICER1 "hot spot" or loss of exon 25 mutations activate the PI3K/AKT/mTOR pathway through loss of 5p miRNAs and increased expression of specific 3p miRNAs. Additionally, we show that DICER1$^{delExon25\ (+/-)}$ cells develop the ability to dedifferentiate and from spheres in the absence of serum. We propose that the non-PI3K/AKT congruent phenotypes in the GLOW syndrome are due to a disruption of differentiation and the persistence of undifferentiated cells in the newborn. This is exemplified in the tumors types of GLOW syndrome cases: Wilms and pleuropulmonary <u>blastoma</u> (PPB) tumors. We propose that the novel use of pro-differentiation chemotherapies in combination with PI3K/AKT/mTOR inhibition would benefit these cases and may have far reaching implications for the management of the blastoma-like class of pediatric tumors.

Figure 7-6: Specific increased 3p miRNAs target mTOR signaling

We show that certain miRNAs affected by these pathogenic mutations target negative regulators of mTOR: namely TSC2. Additionally, downstream targets are effected which streamlines mTOR signaling into S6kinase activation of cell proliferation/growth. We have provided evidence for this via the increased pS6Kinase levels on our *DICER1*^*delExon25 (+/-)* cell model.
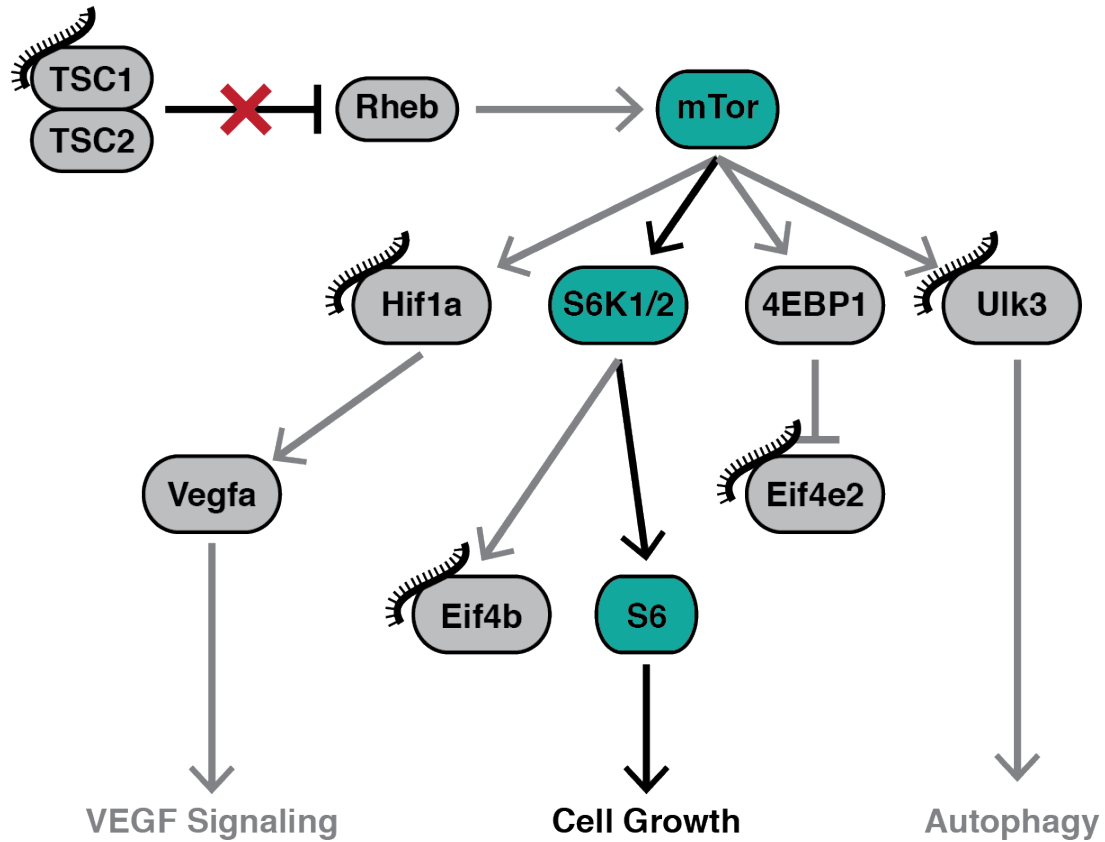
Finally we demonstrate for the first time *Toxoplasmosis gondi* tropism for human neural progenitors. In response to infection this specific cell type shows increased PI3K/AKT/mTOR signaling, which may be responsible for the occurrence of macrocephaly in cases of congenital toxoplasmosis. We propose that this pathophysiology is reciprocal to that seen in congenital ZIKA virus infection which results in decreased AKT signaling and microcephaly. This report in combination with the emerging understanding of ZIKA infection demonstrates the interplay between intracellular infection and regulation of growth signaling pathways. We believe that there is a potential role for pharmacological intervention in these cases as the PI3K/AKT antagonist and agonist are numerous and vary in mechanism of action and effectiveness. Restoring PI3K/AKT signaling to baseline regulated levels may be an essential step in treating these cases and improving outcomes.

Figure 7-7: Toxoplasmosis Gondi and Zika Virus exert opposite effects on the neural progenitor cell

As has been previously shown, ZIKA virus can infect neural progenitors and directly inhibits AKT via two viral proteins and causes microcephaly. We have shown that toxoplasmosis gondi infection activates AKT. Therefore, we believe the same mechanism cause congenital T. gondi macrocephaly.
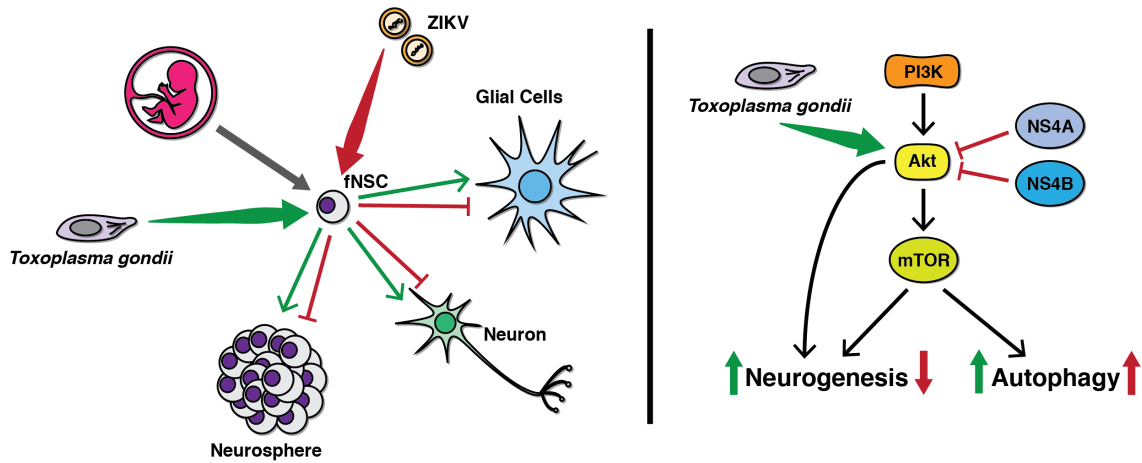
## Summary

We have presented some of the diverse and heterogeneous genetic etiologies of macrocephaly. We hope it has become evident through this work that the PI3K/AKT/mTOR pathway is an essential regulator of neural progenitor proliferation and determines ultimate head size in the developing embryo and child. The convergence of multiple genetic, infectious, and environmental inputs onto this pathway represents a possible pharmacological node where diverse etiologies may benefit from similar therapies. Namely inhibition of aberrant AKT/mTOR activation is the candidate of highest importance in curtailing these phenotypes.

Figure 7-8:
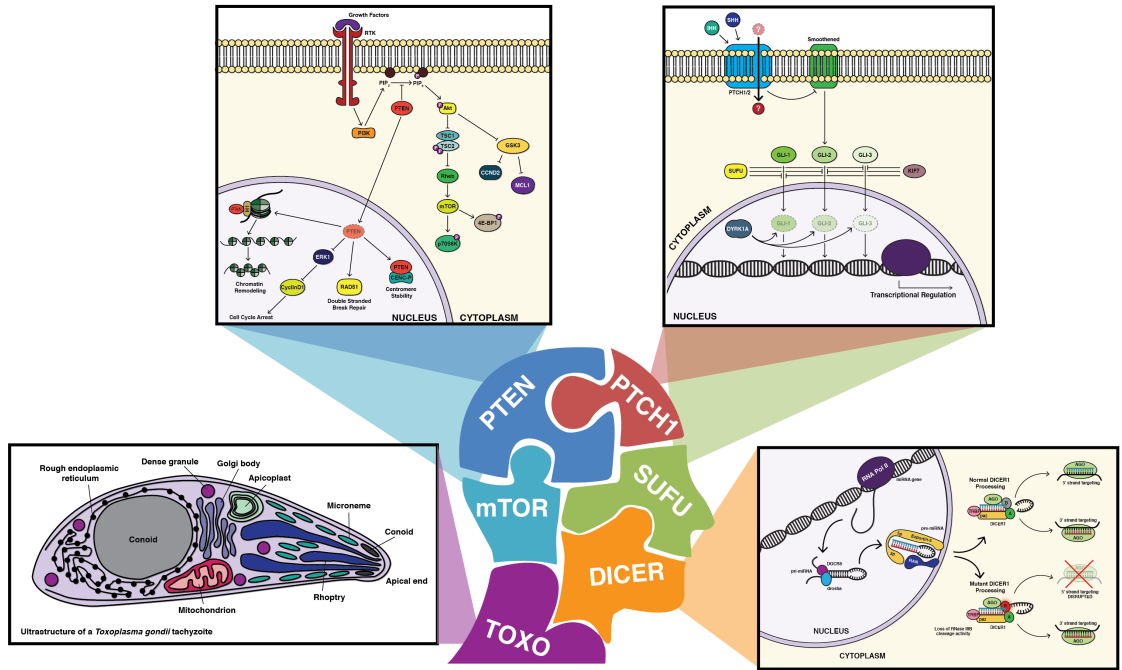
Figure 7-9:
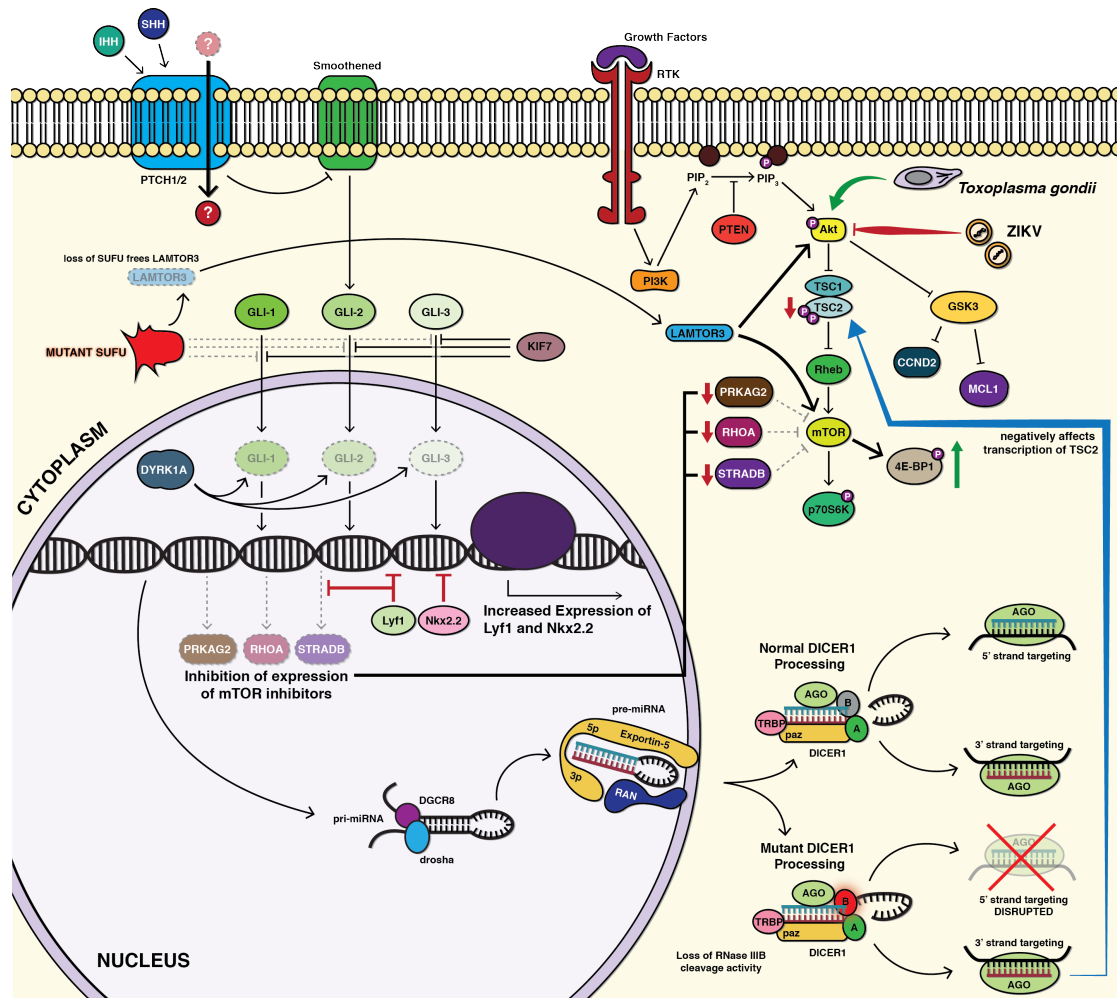
References:

1.  Lee, J.H. *et al.* De novo somatic mutations in components of the PI3K-AKT3-mTOR pathway cause hemimegalencephaly. *Nat Genet* **44**, 941-5 (2012).

2.  Smith, L.D. *et al.* Exome Sequencing Reveals De Novo Germline Mutation of the Mammalian Target of Rapamycin (MTOR) in a Patient with Megalencephaly and Intractable Seizures. *Journal of Genomes and Exomes* **2**, 63-72 (2013).

3.  Mroske, C. *et al.* Germline activating MTOR mutation arising through gonadal mosaicism in two brothers with megalencephaly and neurodevelopmental abnormalities. *BMC Med Genet* **16**, 102 (2015).

4.  Baynam, G. *et al.* A germline MTOR mutation in Aboriginal Australian siblings with intellectual disability, dysmorphism, macrocephaly, and small thoraces. *Am J Med Genet A* **167**, 1659-67 (2015).

# Appendix

# Phenotypic Progression of Skeletal Anomalies in CLOVES Syndrome

**Steven Klein,**[1] **Albert Stroberg,**[2] **Shahnaz Ghahremani,**[3] **and Julian A. Martinez-Agosto**[1]*

[1]Department of Human Genetics, David Geffen School of Medicine at UCLA, Los Angeles, California

[2]Department of Pediatric Orthopedic Surgery, David Geffen School of Medicine at UCLA, Los Angeles, California

[3]Department of Pediatric Radiology, David Geffen School of Medicine at UCLA, Los Angeles, California

Overgrowth syndromes, defined as genetic disorders in which there is disproportionate somatic growth, are challenging to diagnose due to their heterogeneous presentations and possible differing genetic etiologies. CLOVES syndrome is characterized by congenital lipomatous overgrowth, vascular malformations, epidermal nevi, and skeletal abnormalities (Scoliosis). We describe a developmental follow up of the skeletal changes in CLOVES syndrome and a detailed account of its management. We demonstrate the asymmetric growth rate of toes responsible for the macrodactyly observed, and present additional phenotypic findings, including postnatal onset of abdominal symmetry and hepatomegaly. While the etiology of CLOVES is still a mystery, its similarity to Klippel–Trenaunay syndrome suggests a shared defect in a common signaling pathway, and its asymmetric bone overgrowth supports a mosaic genetic defect as its etiology. © 2012 Wiley Periodicals, Inc.

**Key words:** CLOVES Syndrome; Klippel–Trenaunay syndrome; skeletal; overgrowth

## INTRODUCTION

CLOVES syndrome is characterized by four main clinical findings: congenital lipomatous (CL) overgrowth (O), vascular malformations (V), epidermal nevi (E), and skeletal/scoliosis/spinal abnormalities(S) [Sapp et al., 2007; Alomari, 2009a]. Patients presenting with these clinical characteristics are often suspected of having classic disorders of overgrowth including Proteus syndrome ("PS" OMIM 176920), neurofibromatosis type I ("NF-1"OMIM 162200), hemihyperplasia-multiple lipomatosis syndrome ("HHML" OMIM 235000), encephalocraniocutaneous lipomatosis ("ECCL" OMIM 613001), or Klippel–Trenaunay Syndrome (KTS, OMIM 149000) [McCall et al., 1992; Alomari, 2009b]. CLOVES patients present with overgrowth that is distinct from the dysplastic and disorganized nature of that seen in other similar syndromes. The presence of truncal overgrowth and characteristic patterned macrodactyly at birth differentiates CLOVES from other syndromic forms of overgrowth [Sapp et al., 2007]. While the etiology of CLOVES syndrome is still a mystery, the presence of high flow lesions in these patients [Alomari et al., 2011] suggests that it

may be related to KTS. These clinical findings have been associated with the chromosome translocation t(8;14)(q22.3;q13) [Wang et al., 2001; Barker et al., 2006]. The distinction of CLOVES from other overgrowth conditions is an important one as their management and prognosis are different. We describe a developmental follow up of the progressive skeletal changes in CLOVES syndrome through serial X-ray imaging of the skeletal abnormalities, comparing the findings to previously described cases, and present a detailed account of its management.

## CLINICAL REPORT

We report on a female with a history of asymmetric overgrowth, polydactyly, macrodactyly, truncal overgrowth, epidermal nevi, lipoma, and port wine stain. The patient, was born full term via cesarean, secondary to large size, to a 34-year-old G13P13 mother and a healthy, nonconsanguineous father. All 12 siblings are healthy, However, two have been diagnosed with ADHD. The proband is the only family member affected by CLOVES syndrome and there was no history of any birth defects or overgrowth findings in the family. Birth weight was 3,629 g (∼50th centile) and birth length was 53.34 cm (∼90th centile). At birth, it was noted that there was a lipoma on her back and a port wine stain on the vertex of her head. She was born with striking bilateral asymmetric

*Correspondence to:
Julian A. Martinez-Agosto, 695 Charles E. Young Drive South, Gonda Research Center Room 4554B, Los Angeles, CA 90095.
E-mail: julianmartinez@mednet.ucla.edu

macrodactyly (Fig. 3B), postaxial polydactyly (not shown), and cutaneous syndactyly (Fig. 3A) of the right foot.

Examination of radiographs at age of 4 months showed no leg length asymmetry (Fig. 1A), normal spine (Fig. 1C), and normal pelvis (Fig. 1E). The left foot manifested overgrowth of both the soft tissues and underlying bones of the second through fourth digits, with the first and fifth toes being normal (Fig. 1G). The right foot was also overgrown, with macrodactyly of the first through fourth toes including overgrowth of both the soft tissues and underlying bones. There was also a flexion deformity of the right fifth toe, which was curved and projected to the underside of the foot with distorted proximal phalanx (Fig. 2A), as well as enlargement of the fat pads (Fig. 2F).

At 9 months of age, physical exam showed an enlarged right forefoot with asymmetrical increase in soft tissues in both the coronal as well as sagittal dimensions, particularly in the third ray distribution (Fig. 2G). Likewise, the patient had an enlarged fifth ray with abnormal appearance (Fig. 2B). Examination of the left foot showed an enlarged third ray; however, the patient's left forefoot was smaller than the right (Fig. 1H). The growth of her toes was asymmetric, showing the greatest increases in the second (16.1–21.4 mm) and third (28.5–33.7 mm) toes of the left foot and the first (14.8–20.5 mm), third (22.2–27.5 mm), and fourth (22.3–27.3 mm) toes of the right foot. Her first surgery at age 10 months entailed amputation of the second, and fifth toes, and the fifth metatarsal on the right foot, and also the third toe on the left foot.

By 2 years of age, the patient presented with clinical signs of scoliosis and the port wine stain on her head, which measured 2 cm, persisted. Furthermore, several epidermal nevi were noted on her trunk, as well as a hypopigmented lesion and a café-au-lait spot. Her surgical course continued with amputation of the right third and fourth toes with extensive debulking of the plantar fat pads (Figs. 2H and 3C). Signs of asymmetric growth continued to develop on her right side and were more pronounced in the gluteal region.
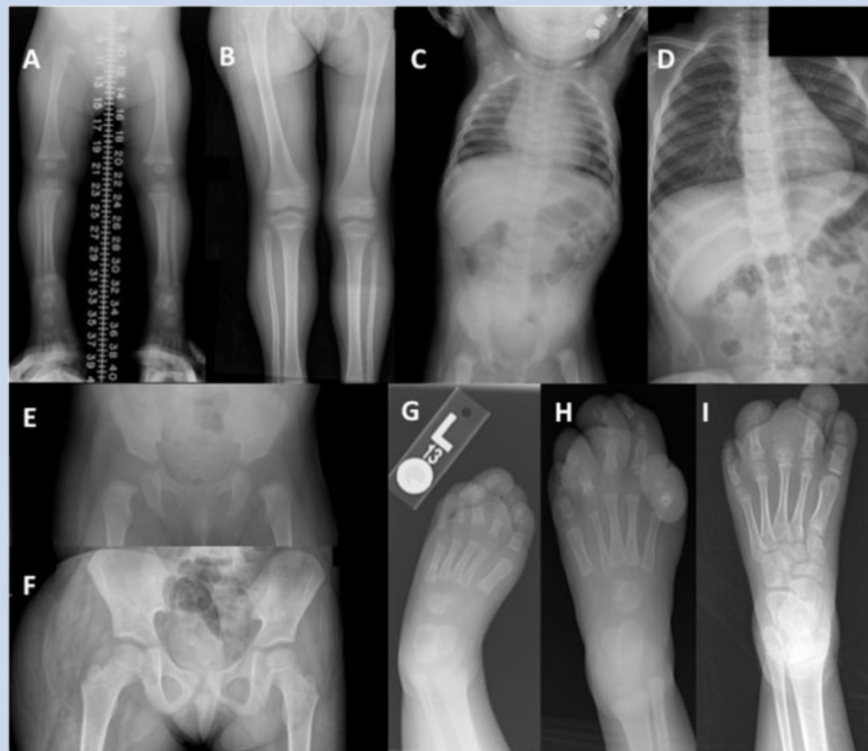


FIG. 1. Skeletal changes from age 4 months to 5 years. A–B: Legs at 4 months (A) showing no leg asymmetry and 45 months old (B) showing right femur length 0.7 cm larger than left. C–D: Spine at 4 months (C) showing normal vertebral alignment. By 45 months (D), levoscoliosis is noted from T5 to T12 of 9° and T12 to L4 of 18°. E–F: Hip at 4 months (E) showing normal bones and bony alignment. At 45 months (F), pelvic obliquity is present. G–I: Left foot at 4 months (G) showing overgrowth of both the soft tissues and underlying bones of the second through fourth digits. By 9 months of age (H, pre-surgery) there was an increase in the soft tissue prominence of the digits with progressive macrodactyly. In addition, the second digit now had a calcified left middle phalanx. At 5 years (I), the distal third toe has been amputated and the growth plate of the third metatarsal was arrested.

FIG. 2. Progressive skeletal changes of the right foot. Right foot dorsal (A–F) and side (F–J) views. The right foot at 4 months (A,F) shows significant overgrowth of the first through fourth toes, including both the soft tissues and underlying bones. There was a flexion deformity of the right fifth toe. The third and fourth metatarsals were relatively enlarged, when compared with the other metatarsals. At 22 months (B,G), interval skeletal maturation with increased development of the tarsal ossification centers and amputation of the second and fifth toes and the fifth metatarsal has occurred. There was increased flattening of the tufts of the second and fourth distal phalanges. By 26 months (C,H), the third and fourth toes were amputated. At age 3 years 9 months (D,I) there was continued interim overgrowth, most prominent by age 5 years (E,J) as seen by the asymmetric overgrowth of the cuboid bone, larger on the right foot than the left.

By 3 years and 9 months of age the feet remained the most affected by asymmetric overgrowth; the macrodactyly was still evident, with deposition of excessive fatty tissue that was compressible and not hard. There was also bony overgrowth on the right foot, with an enlarged cuboid and third metatarsal (Fig. 2D). The right third metatarsal size was significantly larger (74 mm) than the fourth metatarsal (67 mm, Fig. 2D). Interestingly, the left third metatarsal also showed overgrowth (63 mm) compared to the left fourth metatarsal (59.5 mm, Fig. 1I). Examination of spine radiographs at this time also showed lumbar levoscoliosis with a curve of 15° and mild dextroscoliosis of the thoracic spine of 10° (Fig. 1D). The right leg was noted to be longer than the left, mostly due to a 5 mm femoral length difference (right femur measured 28 cm and left femur measured 27.5 cm; right tibia measured 22.9 cm and the left tibia 22.8 cm; Fig. 1B), and associated with a pelvic tilt (Fig. 1F). There was noticeable asymmetry of the gluteal soft tissues (Fig. 1B,F), with muscles infiltrated with fatty tissue and fat infiltrates underneath the achilles tendon.

At age 4 years, she underwent growth plate arrest of the third metatarsal of the left foot and further de-bulking of the plantar fat

pads in the right foot (Fig. 2E,J). A pathology specimen was taken of the fatty tissue during this procedure and showed un-orientated, irregularly shaped, fragmented pieces of red-tan lobulated fatty tissue. By age 5 years her lipoma (Fig. 3E) was again noted, which had increased in size since birth, and her abdomen had asymmetrically increased in size, with greater protuberance on the left side (Fig. 3G).

By age 7 years, the right foot continued to overgrow (Fig. 3B), while the left foot soft tissues were enlarged (Fig. 3D); there was also persistent but unchanged lipoma (Fig. 3F) and abdominal protuberance (Fig. 3H). An abdominal ultrasound showed hepatomegaly. Her height was 135 cm (>98th centile) and her weight was 39.2 kg (>98th centile) and her intellectual development was normal. Finally, examination of the legs showed more evident right leg hemihyperplasia and further illustrated leg length discrepancy (Fig. 3I).

Comparison of rates of growth for metatarsal bones and toes of the left (Fig. 4A) and right (Fig. 4B) feet demonstrated significant asymmetric overgrowth of the right third and fourth, and left third toes that presented with the largest macrodactyly, when compared

303
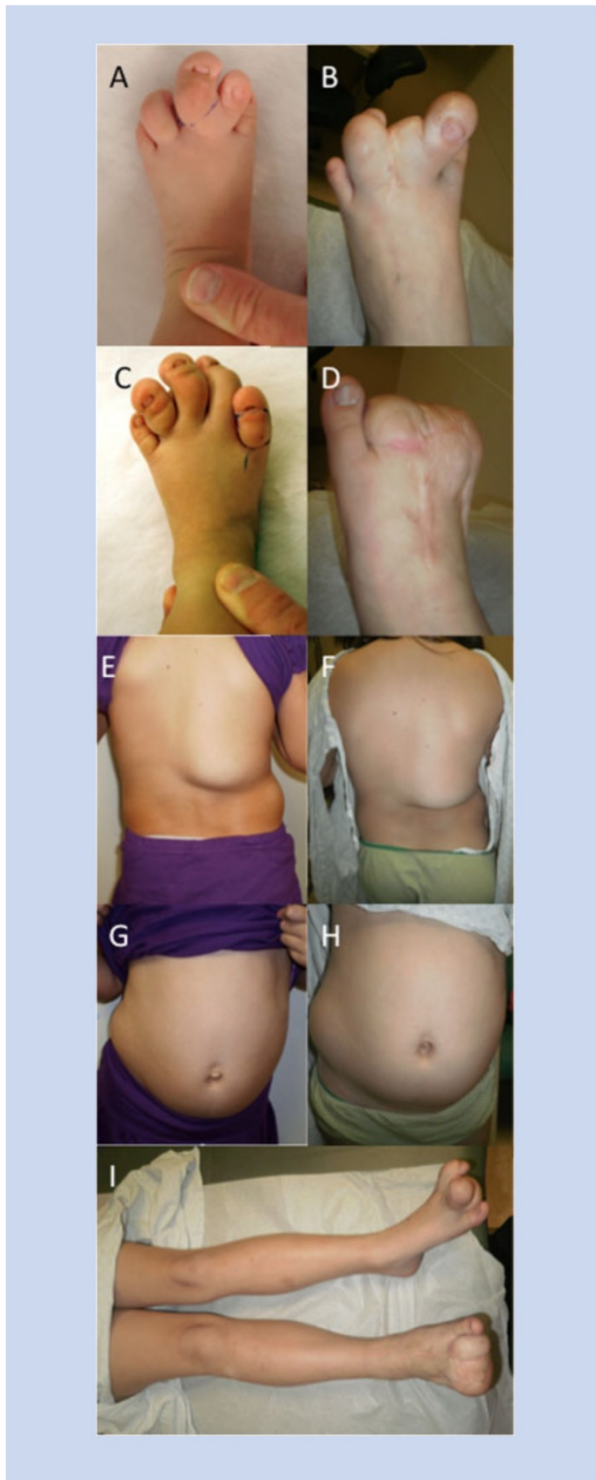
to those without overgrowth (the left first and fifth, Fig. 4). Furthermore: the right third, fourth, fifth, and left third and fourth metatarsals showed a markedly increased growth rate, consistent with the observed overgrowth (Fig. 4).
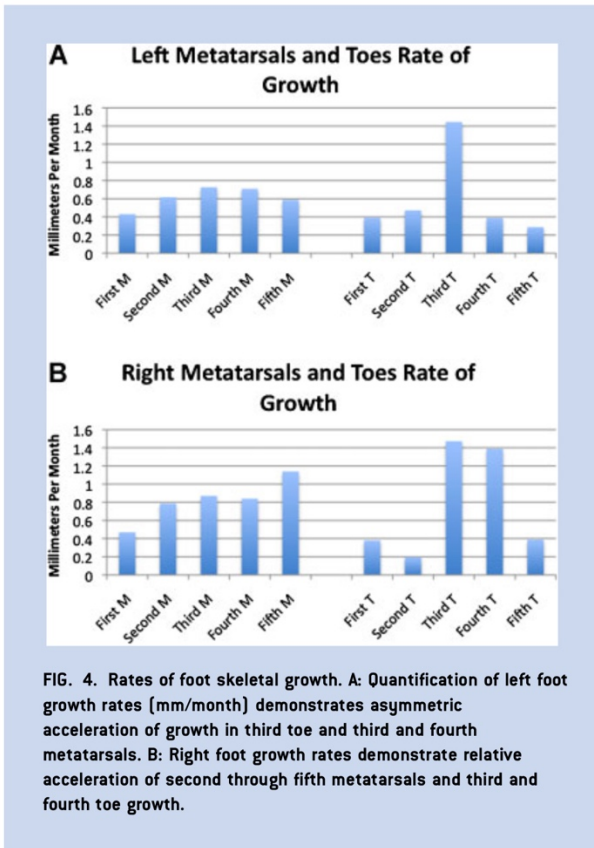
## DISCUSSION

We report on a developmental follow up of the progressive skeletal changes in a case of CLOVES that presented with asymmetric overgrowth, polydactyly, macrodactyly, truncal overgrowth, epidermal nevi, lipoma, and port wine stain. The phenotypic findings were consistent with those previously reported (Table I), most prominently those frequently associated, including asymmetric growth, lipomatous mass, truncal overgrowth, vascular malformations, limb hemihyperplasia, macrodactyly, scoliosis, and epidermal nevi. These physical findings represent the core clinical criteria for the diagnosis of CLOVES syndrome and distinguish these patients from those of other overgrowth conditions. However, the phenotypic similarities, including macrodactyly, asymmetric growth of extremities and the presence of high flow lesions, to those of KTS are suggestive of a common genetic etiology. In particular, we emphasize the presence of hepatomegaly, previously reported in KTS [Haber et al., 1995] but not in CLOVES.

Although it has been reported that some patients with CLOVES syndrome develop CNS findings including hemimegalencephaly and malformation of the corpus callosum that may result in seizures [Gucev et al., 2008], these findings are not common and not present in the patient reported here. Furthermore, there have been some reports of gastrointestinal bleeding associated with CLOVES [Sapp et al., 2007; Fernandez-Pineda et al., 2010; Alomari et al., 2010b, 2011] but this was not observed in the present patient as she has no history of gastrointestinal bleeding or unexplained anemia. Developmentally, the patient showed worsening scoliosis of the spine as well as asymmetric overgrowth of the lower body. The scoliosis was not present at birth; however, scoliosis was first noticed at age 4 years, associated with tilt of the pelvis and asymmetric femoral length, resulting in leg length discrepancy. In addition, the later onset abdominal protrusion in the present patient was likely due to asymmetric growth of soft tissues, as the observed hepatomegaly is unlikely to be the causative etiology.

The surgical treatment of this patient had two main objectives: (1) to debulk excess fatty tissue and (2) to arrest the foot overgrowth. The latter goal was achieved via epiphysiodesis, which

**FIG. 3. External physical findings and their progression. A–B: Left foot macrodactyly at birth showing syndactyly of the second and third toes (A). The second toe continued to overgrow at age 7 years (B). Note amputated toes. C–D: Right foot at birth showing macrodactyly of second through fifth toes (C) all of which were later amputated; however there was still progression of growth of the first toe and an increase in dorsal fat pads by age 7 years (D). E–F: Posterior lipoma at age 2 years (E), showing progressive overgrowth at age 7 years (F). G–H: Abdominal protuberance at age 2 years (G) progressed by age 7 years (H). I: Legs at age 7 years demonstrated asymmetric overgrowth and leg length discrepancy.**

FIG. 4. Rates of foot skeletal growth. A: Quantification of left foot growth rates (mm/month) demonstrates asymmetric acceleration of growth in third toe and third and fourth metatarsals. B: Right foot growth rates demonstrate relative acceleration of second through fifth metatarsals and third and fourth toe growth.

has been proven to be effective in the treatment of worsening overgrowth [Chang et al., 2002]. Our analysis of the progressive phenotypic manifestations in CLOVES syndrome suggests that a number of surveillance studies should be performed to identify complications, including scoliosis, leg length discrepancy, pelvic obliquity, and macrodactyly, as well as abdominal imaging for hepatomegaly. These may prompt surgical intervention as growth proceeds with successful therapeutic outcomes, but with careful attention to the observed poor wound healing in this syndrome [Sapp et al., 2007]. Attempts at resecting the lipomas have had mixed results; it has been reported that some lipomas associated with this syndrome may regrow [Alomari, 2009a]. The vascular abnormalities in these patients can also present complications during surgical procedure and recovery. While being evaluated for surgery, the presence or absence of spinal/paraspinal lesions should also be assessed [Alomari et al., 2011]. These patients need to be followed in the perioperative period for complications including central and thoracic phlebectasia [Alomari et al., 2010a], which can be devastating.

We have described a case of CLOVES syndrome in a girl who was 7 years old at her evaluation. We report additional phenotypic findings, including a developing asymmetrical abdominal protuberance as well as hepatomegaly, and furthermore present the evolution and progression of skeletal phenotypic findings. These

TABLE I. Comparison of the Clinical Findings in Reported CLOVES Cases to Our Patient

| Clinical findings | Feature | Friedberg [1867] [2], n = 1 | Gucev et al. [2008] [7], n = 1 | Fernandez-Pineda et al. [2010] [4], n = 1 | Sapp et al. [2007] [6], n = 7 | Alomari [2009a] [5], n = 18 | Alomari et al. [2011] [1], n = 6 | Our patient | Frequency |
|---|---|---|---|---|---|---|---|---|---|
| General | Asymmetric | + | + | + | 7 | 18 | 1,2 (2) | + | 100% |
| Musculoskeletal | Lipomatous mass | + | + | + | 6 | 18 | 6 | + | 100% |
| | Truncal overgrowth | + | + | + | 7 | 18 | 6 | + | 100% |
| | Limb overgrowth | + | + | + | 4 | 9 | 1,3,4,5,6 (5) | + | 62% |
| | Hand asymmetry | + | − | − | 1 | NK | NK | + | ? |
| | Macrodactyly/syndactyly | + | + | ++ | 5 | 8 | 3,5 (2) | + | 53% |
| | Scoliosis | + | NK | + | 6 | 6 | 3,4,5,6 (4) | + | 53% |
| | Disproportional growth of toes | + | −+ | − | NK | NK | NK | + | ? |
| | Sandal gap | NK | NK | + | NK | 6 | NK | + | ? |
| | Leg length discrepancy | + | −+ | − | 4 | 4 | NK | + | ? |
| Cutaneous | Melanocytic epidermal nevi | + | + | +++ | 7 | 2 | 2,3 (2) | + | 27% |
| Vascular | Low flow malformations | NK | + | ++ | 1 | 18 | NK | + | 82% |
| | Capillary malformation | + | + | | 2 | NK | 2,4,5,6 (4) | + | ? |
| Lymphatics | Extensive fatty-infiltration | NK | NK | NK | | NK | 5 | + | ? |

305

findings may assist in the assessment of prognosis in individuals with CLOVES syndrome in the future. We confirm the accelerated asymmetric skeletal growth rate that occurs postnatally in CLOVES patients, a finding suggestive of a mosaic genetic etiology that awaits molecular confirmation.

## REFERENCES

Alomari AI. 2009a. Characterization of a distinct syndrome that associates complex truncal overgrowth, vascular, and acral anomalies: A descriptive study of 18 cases of CLOVES syndrome. Clin Dysmorphol 18:1–7.

Alomari AI. 2009b. A truly unusual overgrowth syndrome: An alternative diagnosis to Klippel-Trenaunay-Weber syndrome. Intern Med 48: 493–494.

Alomari AI, Burrows PE, Lee EY, Hedequist DJ, Mulliken JB, Fishman SJ. 2010a. CLOVES syndrome with thoracic and central phlebectasia: Increased risk of pulmonary embolism. J Thorac Cardiovasc Surg 140:459–463.

Alomari AI, Thiex R, Mulliken JB. 2010b. Hermann Friedberg's case report: An early description of CLOVES syndrome. Clin Genet 78:342–347.

Alomari AI, Chaudry G, Rodesch G, Burrows PE, Mulliken JB, Smith ER, Fishman SJ, Orbach DB. 2011. Complex spinal-paraspinal fast-flow lesions in CLOVES syndrome: Analysis of clinical and imaging findings in 6 patients. AJNR Am J Neuroradiol 32:1812–1817.

Barker KT, Foulkes WD, Schwartz CE, Labadie C, Monsell F, Houlston RS, Harper J. 2006. Is the E133K allele of VG5Q associated with Klippel-Trenaunay and other overgrowth syndromes? J Med Genet 43:613–614.

Chang CH, Kumar SJ, Riddle EC, Glutting J. 2002. Macrodactyly of the foot. J Bone Joint Surg Am 84-A:1189–1194.

Fernandez-Pineda I, Fajardo M, Chaudry G, Alomari AI. 2010. Perinatal clinical and imaging features of CLOVES syndrome. Pediatr Radiol 40:1436–1439.

Friedberg H. 1867. Riesenwuchs des rechten Beines. Virchow Arch 40: 353–360.

Gucev ZS, Tasic V, Jancevska A, Konstantinova MK, Pop-Jordanova N, Trajkovski Z, Biesecker LG. 2008. Congenital lipomatous overgrowth, vascular malformations, and epidermal nevi (CLOVE) syndrome: CNS malformations and seizures may be a component of this disorder. Am J Med Genet Part A 146A:2688–2690.

Haber M, Reuben A, Burrell M, Oliverio P, Salem RR, West AB. 1995. Multiple focal nodular hyperplasia of the liver associated with hemi-hypertrophy and vascular malformations. Gastroenterology 108: 1256–1262.

McCall S, Ramzy MI, Cure JK, Pai GS. 1992. Encephalocraniocutaneous lipomatosis and the Proteus syndrome: Distinct entities with overlapping manifestations. Am J Med Genet 43:662–668.

Sapp JC, Turner JT, van de Kamp JM, van Dijk FS, Lowry RB, Biesecker LG. 2007. Newly delineated syndrome of congenital lipomatous overgrowth, vascular malformations, and epidermal nevi (CLOVE syndrome) in seven patients. Am J Med Genet Part A 143A:2944–2958.

Wang Q, Timur AA, Szafranski P, Sadgephour A, Jurecic V, Cowell J, Baldini A, Driscoll DJ. 2001. Identification and molecular characterization of de novo translocation t(8;14)(q22.3;q13) associated with a vascular and tissue overgrowth syndrome. Cytogenet Cell Genet 95: 183–188.

# Macrocephaly as a Clinical Indicator of Genetic Subtypes in Autism

Steven Klein, Pantea Sharifi-Hannauer, and Julian A. Martinez-Agosto

An association between autism and macrocephaly has been previously described. A subset of cases with extreme macrocephaly (>3 standard deviation [SD], 99.7th percentile) have been correlated to mutations in the gene phosphatase and tensin homolog (PTEN). However, the phenotypic and genetic characterization of the remaining cases remains unclear. We report the phenotypic classification and genetic testing evaluation of a cohort of 33 patients with autism and macrocephaly. Within our cohort, we confirm the association of PTEN mutations and extreme macrocephaly (>3 SD, 99.7th percentile) and identify mutations in 22% of cases, including three novel PTEN mutations. In addition, we define three phenotypic subgroups: (a) those cases associated with somatic overgrowth, (b) those with disproportionate macrocephaly, and (c) those with relative macrocephaly. We have devised a novel way to segregate patients into these subgroups that will aide in the stratification of autism macrocephaly cases. Within these subgroups, we further expand the genetic etiologies for autism cases with macrocephaly by describing two novel suspected pathogenic copy number variants located at 6q23.2 and 10q24.32. These findings demonstrate the phenotypic heterogeneity of autism cases associated with macrocephaly and their genetic etiologies. The clinical yield from PTEN mutation analysis is 22% and 9% from chromosomal microarray (CMA) testing within this cohort. The identification of three distinct phenotypic subgroups within macrocephaly autism patients may allow for the identification of their respective distinct genetic etiologies that to date have remained elusive. *Autism Res* 2013, 6: 51–56. © 2013 International Society for Autism Research, Wiley Periodicals, Inc.

**Keywords:** autism; macrocephaly; PTEN; overgrowth; hypotonia

## Introduction

Autism was first reported by Kanner [1943], as a developmental disorder in which patients present with severely affected expressive and receptive language skills, stereotypical behaviors, and diminished social interactive skills. The incidence of this condition appears to be as high as 1:100 children. Its etiology is unclear, but a number of studies have demonstrated strong support for a genetic basis for the pathogenesis of autism [Bruining et al., 2010; Iurov, Vorsanova, Saprina, & Iurov Iu, 2010], both from twin and familial studies [Muhle, Trentacoste, & Rapin, 2004; Spence, 2004]. In addition, there are numerous single-gene disorders (Fragile X, OMIM: 300624; Bannayan–Riley–Ruvalcaba, OMIM: 153480; and Rett syndrome, OMIN: 312750) and chromosome abnormalities (e.g., 15q and 1q21.1 duplications) that are associated with autistic behaviors. A few single genes have been identified that cause autism, including CNTNAP2 [Whitehouse, Bishop, Ang, Pennell, & Fisher, 2011] and neuroligins [Etherton, Tabuchi, Sharma, Ko, & Sudhof, 2011]. Cumulatively, these genetic etiologies account for less than 10% of

cases [Brunetti-Pierri et al., 2008], and the exact cause of the remaining 90% remains elusive.

There has been a long-standing association between macrocephaly and autism that was first reported by Kanner [1943, 1968], and this has been confirmed by many studies [Courchesne, 2004; Courchesne, Carper, & Akshoomoff, 2003]. Interestingly, cases of extreme macrocephaly (>3 standard deviations [SD]) have been correlated to mutations in the gene phosphatase and tensin homolog [PTEN; Brunetti-Pierri et al., 2008; Buxbaum et al., 2007; Herman et al., 2007a; McBride et al., 2010]. This has made PTEN testing the standard of care for patients who present with autism and macrocephaly [Herman et al., 2007b]. A number of recent studies have demonstrated the association of copy number variations (CNVs) with autism [Rosenfeld et al., 2010]. The high diagnostic yield of chromosomal microarray analysis (CMA) testing has prompted standard practice guidelines from the American College of Medical Genetics, which recommends this testing modality as part of an autism evaluation [Manning & Hudgins, 2010].

In this study, we report the phenotypic classification, PTEN status, and genetic testing results from a cohort of

33 cases of autism and macrocephaly and describe novel phenotypic subgroups.

## Materials and Methods

This study was approved by the David Geffen School of Medicine Institutional Review Board. A retrospective chart review was carried out for all patients evaluated at the University of California, Los Angeles (UCLA) Medical Genetics clinic from 2008 to 2011 who presented with autism and macrocephaly, defined as a head circumference measurement at least at the 90th percentile (~1.5 SDs) above the mean for age or head circumference above 85th percentile with height below the 50th percentile. Somatic overgrowth was defined as a height and weight above the 95th percentile (~1.8 standard deviations above the mean for age). Disproportionate macrocephaly refers to a height percentile/head circumference percentile ratio of <0.7. Relative macrocephaly refers to a height percentile/head circumference percentile of >0.7. All growth parameter percentiles were calculated using the 2010 Centers for Disease Control and Prevention (CDC) growth charts [Rollins, Collins, & Holden, 2010]. Patients were referred to the clinic by a neurologist or a psychiatrist who evaluated the patients based on the Diagnostic and Statistical Manual of Mental Disorders, Fourth Edition criteria for the diagnosis, including instruments such as the Autism Diagnostic Observation Schedule (ADOS), Pre-Linguistic Autism Diagnostic Observation Schedule (PL-ADOS), Checklist for *Autism* in Toddlers (CHAT), and Screening Tool for *Autism* in Toddlers & Young Children (STAT), Head circumference was obtained by two independent measurements and plotted on standard growth charts by two dysmorphologists. The chromosomal microarray platform was developed by Affymetrix and its performance characteristics determined by UCLA clinical laboratory as required by the CLIA '88 regulations. The assay compared the patient's DNA with 270 HapMap normal controls, using the genome-wide single-nucleotide polymorphism array 6.0. This array platform contains 1.8 million markers for copy number variant detection chosen at ~696 bp spacing throughout the human genome. Oligonucleotide probe information is based on the 36 build of the Human Genome (UCSC, University of California, Santa Cruz, Genome Browser, hg18, March 2006). Nondiagnostic copy number changes are referenced to the Database of Genomic Variants http://projects.tcag.ca/variation/.

## Results

We report on a group of 33 patients evaluated in a medical genetics clinic for autism and macrocephaly, their phenotypic findings, and subgroupings (Table 1)

### *Confirmed PTEN Mutations*

Within our cohort, five patients had confirmed PTEN mutations. Careful phenotypic analysis revealed that (4/5) 80% of those positive for mutations in PTEN presented with "extreme macrocephaly" or head circumference that was greater than or equal to 3 SD (99.7th percentile) above the mean. This extent of macrocephaly was present in a range of ages, from 31 months to 15 years old. One patient (patient 5) whose head circumference was 1–2 SD (92nd percentile) above the mean also carries a novel missense mutation in PTEN, V255A. This mutation is in a well-conserved residue in many species and is reported to be "possibly damaging" by Polyphen software (PP1). Additionally, patients 1 and 3 presented with novel PTEN mutations, P38H and Y68N. The clinical findings for patient 1 were recurrent otitis media, lipomas, and pigmented glans of the penis. This mutation (P38H) is predicted to be "probably damaging" by Polyphen software (PP1), and also the amino acid shows conservation across numerous species. Patient 3 presented with a flattened nasal bridge and plagiocephaly. The mutation (Y68N) is predicted to be "possibly damaging" by Polyphen software (PP1), and the amino acid is well conserved. Additional clinical findings of these patients can be found in Figure 1.

### *Autism With Disproportionate Macrocephaly (ADM)*

Among patients with macrocephaly, we identified a novel phenotype consisting of macrocephaly that was disproportionate to height. There were 10 patients with this phenotype; 9/10 (90%) of these patients had normal PTEN testing. Interestingly, 8/10 (80%) of the patients in this group presented with hypotonia, and 5/10 (50%) of these patients presented with flattened nasal bridges. A complete list of the physical findings of this group can be found in Figure 1. CMA revealed a CNV in one case. Patient 7 had a 767 kb duplication of an interstitial region at the cytogenetic position 6q23.2 and also presented with the clinical findings of bilateral epicanthal folds and a flattened nasal bridge (Table 2).

### *Autism With Relative Macrocephaly*

In our cohort, we identified a group ($n = 12$) with "relative macrocephaly." Of these, 5/12 (42%) presented with bilateral clinodactyly. In comparison with the ADM subgroup, only 2/12 (17%) had hypotonia, and 1/12 (8%) had a flattened nasal bridge. CMA testing revealed a de novo 324 kb deletion of 10q24.32 in patient 26. Additional clinical findings in this patient included flattened nasal bridge and bilateral clinodactyly (Table 2).

**Table 1. Phenotypic Features of Individuals With Autism and Macrocephaly**

| | Individuals with confirmed PTEN Mutations | | | | | ADM (Autism with Disproportionate Macrocephaly) | | | | | | | | | |
|---|---|---|---|---|---|---|---|---|---|---|---|---|---|---|---|
| Number | 1 | 2 | 3 | 4 | 5 | 6 | 7 | 8 | 9 | 10 | 11 | 12 | 13 | 14 | 15 |
| Gender | M | M | M | M | M | M | M | M | M | F | M | M | F | M | M |
| Age | 15 years | 3 years | 4 years | 2 years 6 months | 4 years 4 months | 18 years 11 months | 17 years | 5 years 4 months | 3 years | 3 years 2 months | 6 years 11 months | 17 years 6 months | 7 years | 2 years 8 months | 2 years 9 months |
| Height cm (%ile) | 169 (50) | 102 (>95) | 125.6 (>95) | 99 (>95) | 106.8 (75) | 158 (<5) | 168.3 (15) | 106.5 (20) | 92.5 (25) | 91.8 (25) | 117.5 (25) | 174.5 (48) | 123 (53) | 92 (50) | 95 (60) |
| Weight kg (%ile) | 62.6 (74) | 17.4 (95) | 24.8 (>95) | 13.2 (50) | 18.7 (80) | 91.8 (93) | 73.6 (76) | 17.3 (25) | 14.3 (50) | 14.2 (50) | 35.8 (>95) | 61.9 (30) | 26.5 (80) | 14.5 (73) | 16.6 (95) |
| HC cm (%ile) | 58.5 (>99.7) | 56 (>99.7) | 56 (>99.7) | 55.5 (>99.7) | 53 (92) | 62.5 (>99.7) | 57.3 (85) | 53 (87) | 53 (>97) | 51 (92) | 53.5 (85) | 58 (91) | 54 (>97) | 51 (85) | 53 (>97) |
| HCSD | >3 | >3 | >3 | >3 | 1–3 | >3 | 1–3 | 1–3 | 1–3 | 1–3 | 1–3 | 1–3 | 1–3 | 1–3 | 1–3 |
| HT/HC %ile | .5 | .98 | .98 | .96 | .82 | .05 | .18 | .23 | .25 | .27 | .29 | .53 | .55 | .59 | .62 |
| Hypotonia | – | + | – | – | – | + | + | + | + | + | + | – | + | – | + |
| Flat Nasal Bridge | – | – | – | – | – | + | + | + | – | + | + | + | + | – | + |
| Clinodactyly | – | – | – | – | – | – | – | – | – | + | + | – | + | – | – |
| CMA | ? | ? | ? | ? | – | ? | dup6 q23.2 | – | – | – | – | – | – | – | ? |
| PTEN | P38H | R130X | Y68N | R130L | V255A | – | – | – | – | – | – | – | – | – | ? |

| | ARM (Autism with Relative Macrocephaly) | | | | | | | | | | AMSO (Autism Macrocephaly with Somatic Overgrowth) | | | | | | | |
|---|---|---|---|---|---|---|---|---|---|---|---|---|---|---|---|---|---|---|
| Number | 16 | 17 | 18 | 19 | 20 | 21 | 22 | 23 | 24 | 25 | 26 | 27 | 28 | 29 | 30 | 31 | 32 | 33 |
| Gender | F | F | M | F | M | F | M | M | M | M | M | M | M | F | M | M | M | M |
| Age | 7 years 10 months | 2 years 7 months | 3 years 1 months | 4 years 7 months | 3 years 10 months | 2 years 7 months | 7 years | 3 years 8 months | 4 years 8 months | 6 years | 1 years 6 months | 3 years 2 months | 3 years | 3 years 6 months | 14 years 4 months | 3 years 1 months | 4 years 1 months | 6 years 11 months |
| Height cm (%ile) | 129 (74) | 94 (75) | 98 (73) | 107.5 (74) | 104 (76) | 94.6 (85) | 126.7 (80) | 104.5 (89) | 112 (89) | 120 (80) | 87.5 (95) | 102 (93) | 113 (>95) | 109.8 (>95) | 181.3 (>95) | 104.8 (>95) | 116.7 (>95) | 140.3 (>95) |
| Weight kg (%ile) | 32.3 (91) | 17.6 (>95) | 16.8 (91) | 17.5 (50) | 17.2 (80) | 17.5 (>95) | 24.9 (74) | 18.4 (92) | 21 (90) | 23.3 (80) | 13.1 (80) | 17.1 (90) | 35 (>95) | 20.3 (>95) | 70.3 (92) | 19 (>95) | 22.2 (>95) | 56.7 (>95) |
| HC cm (%ile) | 55.5 (>97) | 53 (>97) | 52 (93) | 52.5 (95) | 53 (96) | 55.5 (>99.7) | 54 (90) | 54 (>97) | 54 (>97) | 53.5 (90) | 52.5 (>99.7) | 52.5 (96) | 55 (>99.7) | 52 (>97) | 57.5 (96) | 53 (>97) | 54.5 (>97) | 56 (>97) |
| HCSD | + | + | + | + | + | >3SD | + | + | + | + | >3SD | + | >3SD | + | + | + | + | + |
| HT/HC %ile | .76 | .77 | .79 | .79 | .79 | .85 | .89 | .91 | .91 | .89 | .95 | .97 | .98 | .98 | .98 | .98 | .98 | .98 |
| Hypotonia | – | – | + | – | – | + | – | – | – | – | – | – | – | + | – | + | – | – |
| Flat Nasal Bridge | + | – | – | + | – | + | – | + | – | – | – | – | + | – | – | – | + | – |
| Clinodactyly | – | – | – | – | + | – | – | + | – | + | + | + | + | – | – | – | – | – |
| CMA | ? | – | ? | – | – | ? | – | – | – | ? | del10 q24.32 | – | ? | – | – | – | – | – |
| PTEN | – | ? | ? | ? | – | ? | – | – | ? | ? | ? | ? | ? | – | ? | – | – | – |

CMA, chromosomal microarray; HC, head circumference; HT, height; %ile, percentile; ?, unknown; +, feature present; −, normal or not present; SD, standard deviation.

| Phenotypic Findings With PTEN Mutations | Phenotypic Findings With ADM | Phenotypic Findings With ARM | Phenotypic Findings With AMSO |
|---|---|---|---|
| Pigmented glans of penis | Malar hypoplasia | Malar hypoplasia | Hemangiomas |
| Recurrent otitis media | Epicanthal Folds | Epicanthal Folds | Palatal pits |
| Lipomas | Two Hair Whorls | Advanced Bone Age | Café-au lait spot |
| Plagiocephaly | Coarse Facial Features | Two Hair Whorls | Supernumerary Nipple |
| High broad forehead | Single Palmar Crease | Everted Lower Eyelids | Hypotonia |
| Nevus | Hemangioma | Strabismus | Brachycephaly |
| Torticollis | Pes Planus | Crowded Dentition | Ligmentous Laxity |
| Flat nasal bridge | Prominent Finger Pads | Stiff Gait | Ear Clefting |
| Brachycephaly | Café au lait spots | Café-au lait spot | Pes Planus |
| Colon Polyps | Advanced bone age | Bilateral 2,3 Toe Syndactyly | Tremor |
| Micrognathia | Cupped Pinna | Pectus Excavatum | Down-slanting Palpebral Fissures |
| Pectus Excavatum | Hemangioma | Macrodactyly | Abnormal pinnae |
| | Abnormal Gait | | Celiac Disease |

**Figure 1.** Phenotypic features of individuals with autism macrocephaly subtypes.

**Table 2. CNVs in Patients with Macrocephaly Autism**

| Study | CNVs | Subgroup | Clinical findings | Parental origin |
|---|---|---|---|---|
| Klein [2012] | Duplication of 6q23.2 (132777055–133543604) | Autism disproportionate macrocephaly | Bilateral epicanthal folds Flattened nasal bridge Strabismus Hyperpigmented lesion | Unknown |
| Klein [2012] | Deletion of 10q24.32 (104345460–104670581) | Autism relative macrocephaly | Flattened nasal bridge Clinodactyly of 4th and 5th finger and 5th toe bilaterally Plagiocephaly | De novo |

*Autism Macrocephaly With Somatic Overgrowth (AMSO)*

An additional subgroup of patients presented with somatic overgrowth (*n* = 6) in addition to macrocephaly. The additional physical findings of this group can be found in Figure 1, including normal bone ages.

## Discussion

Autism is a complex disease, which has highly variable severity and associated physical findings. The evidence for a genetic basis of the disease is compelling, although the large number of genome-wide association studies performed points to many genetic alterations in nonoverlapping associated regions of the genome [Hu, Addington, & Hyman, 2011]. While this is suggestive of a multifactorial etiology, it is also likely that lumping of all autism cases confounds what may be a heterogeneous group of phenotypes and clouds the ability to demonstrate true causality. Approaches at identifying "endophenotypes" offer the ability to parse out possible distinct genetic etiologies and to enhance genotype-phenotype correlations.

We have described a cohort of patients with autism and macrocephaly associated with PTEN mutations, some previously unreported that add to those already described in the literature. All but one of our cases with documented PTEN mutations exhibited "extreme macrocephaly," defined as 3 SD (>99.7 percentile) above the mean. Inter-

estingly, we identified a patient with a PTEN mutation and a head circumference that is between 1–2 SD (92nd percentile) above the mean (patient 5). This extent of macrocephaly is less than what has been reported previously in cases of PTEN-associated macrocephaly autism syndrome [Butler et al., 2005; McBride et al., 2010; Mester, Tilot, Rybicki, Frazier, & Eng, 2011]. In that case, the mutation identified, V255A, is novel and may reflect a hypomorphic allele, which manifests with a lesser degree of macrocephaly. However, further causative studies are needed to confirm that this mutation is in fact pathogenic. We identified two additional novel PTEN mutations, P38H (patient 1) and Y68N (patient 3) that presented with unique clinical findings including brachycephaly, nevi, and plagiocephaly (Fig. 1). The pigmented macules on the glans of the penis along with reported lipomas suggest that patient 1 has Bannayan–Riley–Ruvalcaba syndrome (OMIM 15348) [Hobert & Eng, 2009].

We report a clinical yield of 22% (5/23) for PTEN testing in this cohort, which is larger than the previously reported value of 10% reported by Herman et al. in 2007, perhaps due to our small sample size. We suggest that disproptionate macrocephaly may very well have a genetic etiology different from PTEN, which is evidenced by the lack of PTEN mutations in that cohort. Future genome analysis of this group may uncover a common genetics etiology that would allow for a clinical determinant of the need for PTEN testing.

In our analysis, we found a group (*n* = 6) with not only macrocephaly but also generalized somatic overgrowth. We contend that this represents a distinct subgroup of macrocephaly autism cases. This subgroup will be a cohort amenable for future genomic studies that may contribute to the understanding of autism as well as the etiology of somatic overgrowth. Autistic findings have been described in overgrowth syndromes [Cohen, 2003; Kent, Bowdin, Kirby, Cooper, & Maher, 2008], and this subgroup of macrocephaly autism cases with somatic overgrowth may share genetic defects in a common signaling pathway related to PTEN.

In our remaining patients without somatic overgrowth, we have herein used a novel clinical calculation to separate disproportionate from relative macrocephaly. We contest that the ADM subgroup is a distinct cohort whose genetic etiology for autism and/or macrocephaly may be different from the PTEN-positive and somatic overgrowth subtypes. In particular, hypotonia (90%) and a flattened nasal bridge (50%) are the most common clinical findings that distinguish this group and may, in the future, help to further subdivide these cases into subphenotypes. Recent reports have identified gene mutations that can be associated with autism and disproportionate macrocephaly, including the small GTPase RAB39B [Giannandrea et al., 2010], and GlialCAM [Lopez-Hernandez et al., 2011]; mild mutations in these genes may be associated with this subset of patients who present with autism-macrocephaly in the absence of somatic overgrowth and mutations in PTEN.

We stress the importance of CMA testing in all cases of macrocephaly autism. A significant number of chromosomal CNVs, both duplications and deletions, have been associated with autistic manifestations [Vorstman et al., 2006]. Two separate reports have previously demonstrated that both duplications and deletions can result in autism and macrocephaly [Brunetti-Pierri et al., 2008; Moreno-De-Luca et al., 2010; Naqvi, Cole, & Graham, 2000]. We have observed two CNVs in our cohort: a novel duplication (767kB) at 6q23.2, and an additional de novo variant deletion located at 10q24.32 similar to a previously reported overlapping deletion at 104251636–104668797(genome assembly hg18). This patient presented with severe mental retardation, autistic behavior, hypotonia, macrocephaly, cerebellar vermis agenesis, and partial sight [Jaillard et al., 2010]. The duplicated genomic region at 6q23.2 (132 777 055–133 543 604) was reported as a "copy number change of unknown significance;" however, it contains over 10 genes; some of which have roles in neurological development. A search of copy number variants did not identify any report of this duplication in the general population, indicating that it is clinically relevant.

We report a 22% yield for PTEN testing, a 9% yield with CMA, and 0% with fragile X in cases with macrocephaly.

These yields are significantly higher than previously reported that may be due to the small sample size of this study [Herman et al., 2007b; Shen et al., 2010], suggesting that the use of head circumference as a clinical indicator will increase overall yield in identifying a genetic etiology.

We contend that there is a subgroup of patients with autism and macrocephaly who do not have PTEN mutations and that represent a distinct subgroup of phenotypes amenable for gene association studies. Furthermore, there is a cohort of these patients who present with somatic overgrowth (AMSO), which may represent a distinct genetic etiology. Clinical features, such as macrocephaly, that are associated with autism, allow for subgroups to be established and facilitate genetic association studies, significantly enhancing testing yield.

In conclusion, we report on a group of patients with autism and macrocephaly. We recommend that two distinct subgroups be recognized: (1) ADM, and (2) AMSO, both distinct from autism with relative macrocephaly and can be segregated based on clinical measurements. These will be amenable for genetic characterization in future studies.

### References

Bruining, H., de Sonneville, L., Swaab, H., de Jonge, M., Kas, M., et al. (2010). Dissecting the clinical heterogeneity of autism spectrum disorders through defined genotypes. PLoS ONE, 5, e10887.

Brunetti-Pierri, N., Berg, J.S., Scaglia, F., Belmont, J., Bacino, C.A., et al. (2008). Recurrent reciprocal 1q21.1 deletions and duplications associated with microcephaly or macrocephaly and developmental and behavioral abnormalities. Nature Genetics, 40, 1466–1471.

Butler, M.G., Dasouki, M.J., Zhou, X.P., Talebizadeh, Z., Brown, M., et al. (2005). Subset of individuals with autism spectrum disorders and extreme macrocephaly associated with germline PTEN tumour suppressor gene mutations. Journal of Medical Genetics, 42, 318–321.

Buxbaum, J.D., Cai, G., Chaste, P., Nygren, G., Goldsmith, J., et al. (2007). Mutation screening of the PTEN gene in patients with autism spectrum disorders and macrocephaly. American Journal of Medical Genetics. Part B, Neuropsychiatric Genetics, 144B, 484–491.

Cohen, M.M., Jr. (2003). Mental deficiency, alterations in performance, and CNS abnormalities in overgrowth syndromes. American Journal of Medical Genetics. Part C, Seminars in Medical Genetics, 117C, 49–56.

Courchesne, E. (2004). Brain development in autism: Early overgrowth followed by premature arrest of growth. Mental Retardation and Developmental Disabilities Research Reviews, 10, 106–111.

Courchesne, E., Carper, R., & Akshoomoff, N. (2003). Evidence of brain overgrowth in the first year of life in autism. JAMA, 290, 337–344.

Etherton, M.R., Tabuchi, K., Sharma, M., Ko, J., & Sudhof, T.C. (2011). An autism-associated point mutation in the neuroligin cytoplasmic tail selectively impairs AMPA receptor-mediated synaptic transmission in hippocampus. EMBO Journal, 30, 2908–2919.

Giannandrea, M., Bianchi, V., Mignogna, M.L., Sirri, A., Carrabino, S., et al. (2010). Mutations in the small GTPase gene RAB39B are responsible for X-linked mental retardation associated with autism, epilepsy, and macrocephaly. American Journal of Human Genetics, 86, 185–195.

Herman, G.E., Butter, E., Enrile, B., Pastore, M., Prior, T.W., & Sommer, A. (2007a). Increasing knowledge of PTEN germline mutations: Two additional patients with autism and macrocephaly. American Journal of Medical Genetics Part A, 143, 589–593.

Herman, G.E., Henninger, N., Ratliff-Schaub, K., Pastore, M., Fitzgerald, S., & McBride, K.L. (2007b). Genetic testing in autism: How much is enough? Genetics in Medicine, 9, 268–274.

Hobert, J.A., & Eng, C. (2009). PTEN hamartoma tumor syndrome: An overview. Genetics in Medicine, 11, 687–694.

Hu, V.W., Addington, A., & Hyman, A. (2011). Novel autism subtype-dependent genetic variants are revealed by quantitative trait and subphenotype association analyses of published GWAS data. PLoS ONE, 6, e19067.

Iurov, I., Vorsanova, S.G., Saprina, E.A., & Iurov Iu, B. (2010). Identification of candidate genes of autism on the basis of molecular cytogenetic and in silico studies of the genome organization of chromosomal regions involved in unbalanced rearrangements. Genetika, 46, 1348–1351.

Jaillard, S., Drunat, S., Bendavid, C., Aboura, A., Etcheverry, A., et al. (2010). Identification of gene copy number variations in patients with mental retardation using array-CGH: Novel syndromes in a large French series. European Journal of Medical Genetics, 53, 66–75.

Kanner, L. (1943). Autistic disturbances of affective contact. Nervous Child, 2, 217–250.

Kanner, L. (1968). Autistic disturbances of affective contact. Acta Paedopsychiatrica, 35, 100–136.

Kent, L., Bowdin, S., Kirby, G.A., Cooper, W.N., & Maher, E.R. (2008). Beckwith Weidemann syndrome: A behavioral phenotype-genotype study. American Journal of Medical Genetics. Part B, Neuropsychiatric Genetics, 147B, 1295–1297.

Lopez-Hernandez, T., Ridder, M.C., Montolio, M., Capdevila-Nortes, X., Polder, E., et al. (2011). Mutant GlialCAM causes megalencephalic leukoencephalopathy with subcortical cysts, benign familial macrocephaly, and macrocephaly with retardation and autism. American Journal of Human Genetics, 88, 422–432.

Manning, M., & Hudgins, L. (2010). Array-based technology and recommendations for utilization in medical genetics practice for detection of chromosomal abnormalities. Genetics in Medicine, 12, 742–745.

McBride, K.L., Varga, E.A., Pastore, M.T., Prior, T.W., Manickam, K., et al. (2010). Confirmation study of PTEN mutations among individuals with autism or developmental delays/mental retardation and macrocephaly. Autism Research, 3, 137–141.

Mester, J.L., Tilot, A.K., Rybicki, L.A., Frazier, T.W., 2nd, & Eng, C. (2011). Analysis of prevalence and degree of macrocephaly in patients with germline PTEN mutations and of brain weight in Pten knock-in murine model. European Journal of Human Genetics, 19, 763–768.

Moreno-De-Luca, D., Mulle, J.G., Kaminsky, E.B., Sanders, S.J., Myers, S.M., et al. (2010). Deletion 17q12 is a recurrent copy number variant that confers high risk of autism and schizophrenia. American Journal of Human Genetics, 87, 618–630.

Muhle, R., Trentacoste, S.V., & Rapin, I. (2004). The genetics of autism. Pediatrics, 113, e472–e486.

Naqvi, S., Cole, T., & Graham, J.M., Jr. (2000). Cole-Hughes macrocephaly syndrome and associated autistic manifestations. American Journal of Medical Genetics, 94, 149–152.

Rollins, J.D., Collins, J.S., & Holden, K.R. (2010). United States head circumference growth reference charts: Birth to 21 years. Journal of Pediatrics, 156, 907–913, 913 e1-2.

Rosenfeld, J.A., Ballif, B.C., Torchia, B.S., Sahoo, T., Ravnan, J.B., et al. (2010). Copy number variations associated with autism spectrum disorders contribute to a spectrum of neurodevelopmental disorders. Genetics in Medicine, 12, 694–702.

Shen, Y., Dies, K.A., Holm, I.A., Bridgemohan, C., Sobeih, M.M., et al. (2010). Clinical genetic testing for patients with autism spectrum disorders. Pediatrics, 125, e727–e735.

Spence, S.J. (2004). The genetics of autism. Seminars in Pediatric Neurology, 11, 196–204.

Vorstman, J.A., Staal, W.G., van Daalen, E., van Engeland, H., Hochstenbach, P.F., & Franke, L. (2006). Identification of novel autism candidate regions through analysis of reported cytogenetic abnormalities associated with autism. Molecular Psychiatry, 11, 1, 18–28.

Whitehouse, A.J., Bishop, D.V., Ang, Q.W., Pennell, C.E., & Fisher, S.E. (2011). CNTNAP2 variants affect early language development in the general population. Genes, Brain, and Behavior, 10, 451–456.

ORIGINAL ARTICLE

# Expanding the phenotype of mutations in DICER1: mosaic missense mutations in the RNase IIIb domain of *DICER1* cause GLOW syndrome

Steven Klein,[1] Hane Lee,[1,2] Shahnaz Ghahremani,[3] Pamela Kempert,[4] Mariam Ischander,[5,6] Michael A Teitell,[2,7] Stanley F Nelson,[1,2] Julian A Martinez-Agosto[1,7,8]

**Correspondence to**
Dr Julian A Martinez-Agosto, 695 Charles E. Young Drive South, Gonda Research Center Room 4554, Los Angeles, CA 90095, USA; julianmartinez@mednet.ucla.edu

**ABSTRACT**
**Background** Constitutional DICER1 mutations have been associated with pleuropulmonary blastoma, cystic nephroma, Sertoli-Leydig tumours and multinodular goitres, while somatic DICER1 mutations have been reported in additional tumour types. Here we report a novel syndrome termed GLOW, an acronym for its core phenotypic findings, which include *G*lobal developmental delay, *L*ung cysts, *O*vergrowth and *W*ilms tumour caused by mutations in the RNase IIIb domain of DICER1.
**Methods and results** We performed whole exome sequencing on peripheral mononuclear blood cells of an affected proband and identified a de novo missense mutation in the RNase IIIb domain of DICER1. We confirmed an additional de novo missense mutation in the same domain of an unrelated case by Sanger sequencing. These missense mutations in the RNase IIIb domain of DICER1 are suspected to affect one of four metal binding sites located within this domain. Pyrosequencing was used to determine the relative abundance of mutant alleles in various tissue types. The relative mutation abundance is highest in Wilms tumour and unaffected kidney samples when compared with blood, confirming that the mutation is mosaic. Finally, we performed bioinformatic analysis of microRNAs expressed in murine cells carrying specific Dicer1 RNase IIIb domain metal binding site-associated mutations. We have identified a subset of 3p microRNAs that are overexpressed whose target genes are over-represented in mTOR, MAPK and TGF-β signalling pathways.
**Conclusions** We propose that mutations affecting the metal binding sites of the DICER1 RNase IIIb domain alter the balance of 3p and 5p microRNAs leading to deregulation of these growth signalling pathways, causing a novel human overgrowth syndrome.

## INTRODUCTION
Overgrowth, marked by large body size and mass, has numerous aetiologies. Evaluation in the perinatal period assists in distinguishing normal growth variants from endocrine abnormalities and underlying genetic syndromes. Dysmorphic features, developmental delay and asymmetric growth patterns are signs that suggest a genetic aetiology.[1] There are numerous phenotypically recognisable overgrowth syndromes, classified by their distinct pattern of features. Prominent among these characteristics are macrocephaly and symmetric overgrowth. Examples of these syndromes include Cowden syndrome (CWS1 (MIM 158350)), Bannayan–Riley–Ruvalcaba syndrome (MIM 153480) and macrocephaly/autism syndrome (MIM 605309), all caused by inactivating mutations in Phosphatase and tensin homolog (PTEN),[2 3] as well as SOTOS (MIM 117550) and Weaver syndromes (MIM 277590), which are caused by haploinsufficiency of NSD1[4] and EZH2,[5] respectively. Additional phenotypic findings include epidermal changes, cancer predisposition, and distinct facial features, which help to distinguish these syndromes from one another.

Many overgrowth syndromes present with asymmetric overgrowth of bilateral structures, which has been shown to result from mosaic distribution of genetic mutations.[3 6] The most striking examples of such conditions are Proteus syndrome (MIM 176920), caused by activating mutations in AKT1,[7] and congenital lipomatous overgrowth, vascular malformations and epidermal nevi (MIM 612918) syndrome, caused by activating mutations in PI3KCA.[8] Additionally, megalencephaly-capillary-malformation-polymicrogyria syndrome (MIM 602501), is caused by mosaic activating mutations in PIK3CA, PIK3R2 and AKT3.[9] The mosaic distribution of these mutations has led to the hypothesis that constitutive, gain of function zygotic mutations in these genes are lethal.[6] These sporadic genetic conditions eluded molecular analysis until the advent of massively parallel sequencing technologies which allowed identification of de novo mutations. Given the phenotypic overlap among overgrowth syndromes, it is not surprising that many of their molecular aetiologies cluster in pathways that regulate growth. One such pathway is the PIK3–AKT–mTOR signalling pathway,[10] in which both activating mutations in drivers of the pathway (AKT1, PI3K) and inactivating mutations in negative regulators (PTEN) have been reported as pathogenic.[3 4]

Syndromes of deregulated growth are often associated with cancer predisposition and specific syndromes are associated with particular tumour types including hepatoblastoma, pheochromocytoma and Wilms tumour.[11] Wilms tumour is the most common paediatric renal tumour diagnosed after 1 year of age.[12] Most cases are sporadic and without a clear aetiology. However, in some cases it can be associated with specific genetic syndromes, including Beckwith–Wiedeman syndrome (BWS (MIM 130650)).[13 14]

We describe a unique association of congenital nephromegaly, bilateral Wilms tumour, somatic overgrowth, developmental delay, macrocephaly and bilateral cystic lung lesions in the absence of other known genetic aetiologies that defines a novel genetic syndrome.

## MATERIALS AND METHODS
### DNA extraction
DNA was extracted for each case from peripheral blood mononuclear cells using a QIAGEN QIAamp Blood Mini kit. DNA was also extracted from tumour, bone marrow and unaffected kidney samples using a QIAamp DSP DNA FFPE Tissue Kit.

### Whole exome sequencing
Exome sequencing was performed on DNA extracted from peripheral mononuclear blood cells from Case 1 and his unaffected parents, as well as DNA isolated from tumour samples from Case 2 and was consented under an approved IRB protocol. The sequencing library for each sample was prepared using 3 µg of genomic DNA by following the Agilent SureSelect Target Enrichment System for construction of an Illumina paired-end sequencing library (protocol V.1.0.1). The Agilent SureSelect Human All Exon 50Mb Kit was used for the exome capture. Sequencing was performed as 76 bp paired-end reads generated from three lanes of an Illumina GAIIx instrument, generating a total of ~82 million paired-end reads per sample. Base-calling was performed using the real time analysis software provided by Illumina. The sequence reads were aligned to the human reference genome, human_g1k_v37.fasta, downloaded from the Genome Analysis Toolkit (GATK) resource bundle using Novoalign from the Novocraft Short Read Alignment Package. SAMtools was used to sort the aligned Binary Alignment/Map (BAM) files and potential PCR duplicates were marked using Picard. GATK was used to perform local realignment and base quality recalibration for all three samples. The mean coverage across the protein-coding region of RefSeq genes was 76–80X with approximately 88% of the targeted bases covered by ≥10 reads for each exome. Both single nucleotide variants and insertions and deletions less than 10 bases (INDELs) within the protein coding regions of the RefSeq genes were called using the GATK 'Unified Genotyper' tool. Variants resulting in amino acid changes with minor allele frequencies <1% in the population were selected. Further, to identify de novo variants, novel variants that were heterozygous in the proband and homozygous for the reference base in both parents were selected. The exome capture kit provides 100% coverage of all exons within the DICER1 locus, which allowed reliable detection of additional mutations in the tumour sample of Case 2. We determined copy number using the ratio of read number for every exon of DICER1.

### PCR and Sanger sequencing
We confirmed the mutation in Case 1 identified by WES by performing PCR on DNA isolated from mononuclear blood cells. Primers flanking the mutation were designed using Primer3 software and run with Invitrogen Platinum Taq. To determine if there were additional 'second hit' mutations in DNA isolated from tumour samples, primers published by Hill et al[15] were used with the exception of the primers listed below, which were changed due to the presence of polymorphic SNPs within their annealing sites. All PCR products were purified using an Invitrogen Purelink PCR Purification Kit and sequenced using an Applied Biosystems 3730 Capillary DNA Analyser.

PCR primer sequences:
*Exon 25 F 5'-AAGCTTACGGTTCCACTTCG-3'*
*Exon 25 R 5'-GTGTTGTTGACCAGGGCAGA 3'*
*Exon4F 5'-GGTTCTCTGAAGCGAGTGACAAAA A-3'*
*Exon 4R 5'-GCATCCGGCCTTTATTTGGTTTT-3'*
*Exon 5F 5'-CTTTTCCCATGCTTTCCTGATTTCC-3'*
*Exon 5R 5'-AAGGCTATAACAAGAGAGACATCGCCA-3'*
*Exon 8F 5'-GCTGGGTTACATTTAAGGAGCCATT-3'*
*Exon 8R 5'-AAATCCCAGTTAAACCCCAC-3'*
PCR conditions: 95°C for 3 min followed by 40 cycles of 95°C for 30 s, 55°C for 45 s, and 72°C for 1 min 30 s and finally 72°C for 5 min.

### Pyrosequencing
Pyrosequencing was performed on DNA isolated from blood (Case 1) or bone marrow as a surrogate (Case 2), tumour samples and unaffected kidney samples, isolated from paraffin blocks, from both cases. Pyrosequencing reactions were performed on all samples in triplicate according to the standard vacuum prep protocol for the PSQ 96 MA instrument from QIAGEN. This method has been validated for the quantification of allele distribution within a heterogeneous population of alleles.[16 17]

Pyro primer sequences:
*DICER1 Pyro F 5' GCACAAGCTTACGGTTCCACTTC 3'*
*DICER1 Pyro R 5' CGCGGGTCTTCATAAAGGTG 3'*
*DICER1 Pyro S 5' CTTAGAATTCCTGGG 3'*

### MicroRNA bioinformatics analysis
A list of microRNAs which are differentially expressed in murine cells lines with carrying mutated human DICER1 RNaseIIIb domain 'hot spots' was obtained from the supplemental materials of Anglesio et al.[18] We selected only 3p microRNAs which show an increase of expression which is greater than 50-fold when compared with mouse embryonic stem cell Dicer −/− controls (see online supplementary table S1). These microRNAs were entered into the DIANA miRPath V.4.0 (updated from V.2.0)[19] analysis software (available at http://diana.cslab.ece.ntua.gr/pathways/). We used the cut-off of −ln(p value union) of 20 to identify the pathways which are most significantly shared by these miRNAs.

## RESULTS
### Subjects
#### Case 1
The first affected individual presented as a 9-month-old boy with macrosomia and large kidneys. The patient was born via caesarean section at 38 weeks to a 30-year-old G1P1 mother; paternal age was 31 years at birth. Maternal medical problems during the pregnancy included bleeding and spotting. The mother did not take any medications during the pregnancy and there were no known teratogenic exposures. It was noted that the fetus started kicking late in the pregnancy. Prenatal ultrasound at 24 weeks showed enlarged kidneys. Family history was significant for the mother having double ureters on left side, and frequent urinary tract infections. Birth weight was 10 pounds, 13 ounces (>98th centile). Respiratory distress prompted chest imaging which revealed bilateral lung cysts (figure 1A). Renal ultrasound showed multiple small cysts.

His development milestones were delayed: at 9 months of age, he could not yet roll over and had weak muscle tone. Physical examination at 9 months of age showed a height of 76.5 cm (90th centile), weight of 9.6 kg (75th centile) and head circumference of 52 cm (>98th centile). Additionally, hands were observed with a
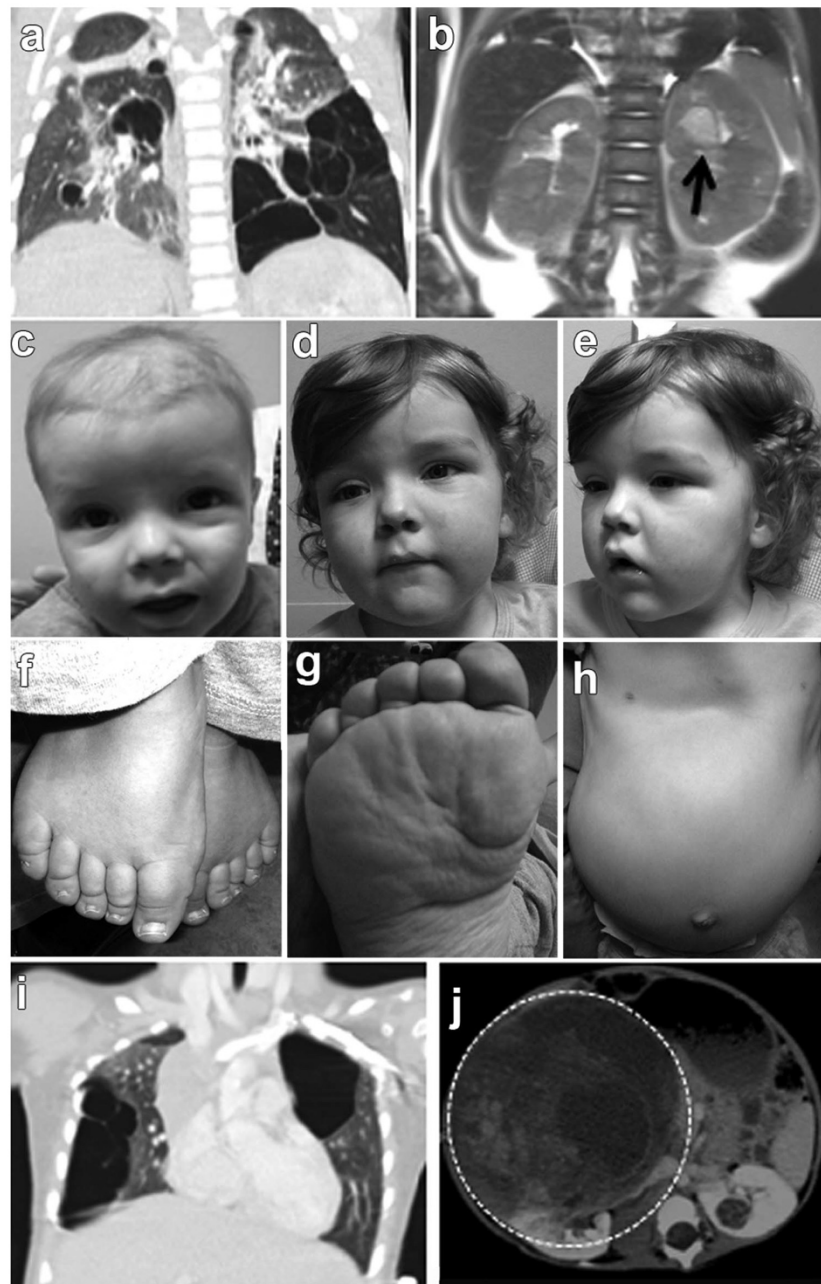
**Figure 1** Phenotypic features of GLOW syndrome. (A) Coronal view of bilateral lung cysts of Case 1. (B) Case 1 at 9 months of age. MRI shows Wilms tumour in the left kidney (arrow). (C–E) Facial features of Case 1 at 9 months (C) and 28 months of age (D–E) including frontal bossing, a very large anterior fontanelle, hypertelorism, anteverted nares, a flat nasal bridge and slight micrognathia. (F–H) Additional findings in Case 1 at 28 months of age included (F) fat pads on dorsum of foot and toes, (G) rugated soles of feet with skin folds and (H) protuberant abdomen. (I) Coronal views of bilateral lung cysts of Case 2 at the age of 21 months. (J) Case 2 at 13 months of age with Wilms tumour (outline) in the right kidney, with associated 'claw sign'.

doughy texture. Hand length was 10.2 cm (>90th centile) and palm length was 6.5 cm (>97th centile). Palmar creases were normal and fingers were tapered. The feet were large and measured 12 cm (75th centile). An abdominal ultrasound confirmed nephromegaly with the left kidney measuring 7.79 cm and the

right kidney measuring 7.71 cm. A soft tissue mass within the superior pole of the left kidney was identified that measured 1.95×1.87×1.54 cm (figure 1B). Nephrectomy was performed and histological examination demonstrated the presence of blastemal predominant Wilms tumour confirmed by WT1 staining. The

kidney histology was abnormal: numerous immature and abnormally developed glomeruli were present with overall underdevelopment of the renal cortex, in addition to dysplastic medullary ray nodules, abnormal medullae and perilobar nephrogenic rests. The reporting pathologist commented that the histology of the kidney was remarkably similar to that of BWS. However, methylation analysis of 11p15 and genetic testing for mutations in CDKN1C were normal. Karyotype of the tumour was normal and showed 46,XY. Additional genetic work up for macrocephaly-associated genes included mutation analysis for folliculin (FLCN), Nuclear receptor binding SET domain protein 1 (NSD1), and PTEN which were all negative. Finally, chromosomal microarray analysis did not identify any copy number variations; however, small to moderate CNVs cannot be ruled out based on the threshold of this clinical test.

At 18 months of age, he had an MRI of the brain that showed enlarged lateral and third ventricles. At 28 months of age, weight was 15.5 kg (92nd centile), height 95 cm (90th centile) and head circumference 55 cm (>98th centile). There were dysmorphic facial and cranial features including frontal bossing, a large anterior fontanelle, slight hypertelorism, anteverted nares, a flat nasal bridge and slight micrognathia (figure 1C–E), as well as umbilical and left inguinal hernias. At the age of 28 months he presented with dimples on the sides of his ankles. There were fat pads on the dorsum of foot and toes (figure 1F), pronounced plantar creases on both sides (figure 1G) and a large protuberant abdomen (figure 1H). Other dysmorphic physical findings included pectus excavatum, kyphosis and a sacral dimple. At the age of 5, he was diagnosed with Wilms tumour of the contralateral kidney as well as autism.

### Case 2
The second affected unrelated individual presented at the age of 14 months with global developmental delay and macrocephaly. Pregnancy was complicated by preeclampsia. Prenatal ultrasounds and laboratory evaluations were normal. Birth weight was 6 pounds, 7 ounces (15th centile). Macrocephaly was noted at birth, but head CT was negative. Family history was significant for a paternal grandmother who had breast cancer at the age of 50 years and skin cancer.

Early in development, global delay was suspected due to delayed rolling at 7 months. He met the following milestones: tracking between 2 and 3 months, reaching between 3 and 4 months, lifting the head between 4 and 5 months, and sitting at 9 months. Global developmental delay was confirmed by 14 months as he was not crawling and not babbling. At 14 months, his growth measurements were weight 13.5 kg (>98th centile), height 81 cm (75th–80th centile) and head circumference 53 cm (>98th centile) demonstrating somatic overgrowth. He had an MRI of the brain that showed mild volume loss, but no signs of hydrocephalus or other brain malformations.

At 18 months of age, he presented with a large firm mass most prominent in the right upper quadrant. CT scan revealed a large mass, arising from the right kidney as well as a multiloculated cystic mass within the upper pole of the left kidney measuring 2.15×2.13×1.84 cm (figure 1J). Left kidney size at this time was 8.1 cm. Right nephrectomy was performed and histological analysis confirmed Wilms tumour. Karyotype for the tumour showed 46,XY. CT of the chest at 21 months demonstrated numerous thin walled cysts throughout the lungs bilaterally (figure 1I). MRI of the brain at the age of 2 showed enlargement of the cerebral spinal fluid (CSF) space in the anterior middle cranial fossa and in the Sylvian fissures bilaterally. At 30 months of age, there was tumour recurrence to the paraspinal area, spleen, contralateral kidney and lungs, which again confirmed to be Wilms' tumour by

biopsy of the paraspinal mass. In addition to macrocephaly, his facial features included a depressed nasal bridge, a left ear pit, frontal bossing and hypertelorism with normal hand and foot creases. He had a karyotype performed on blood, which was normal. A summary of the clinical findings is provided in table 1.

### Sequence analysis
#### Case 1
Whole exome sequencing analysis on DNA isolated from peripheral mononuclear blood cells identified a heterozygous de novo variant in DICER1 (HGA 19g.95560451 A>T, c. 5138 A>T, p.Asp1713Val). The parents shared many rare variants with the proband, confirming biological parentage. Additionally, Sanger sequencing confirmed that this mutation was de novo as it was absent from parental DNA extracted from blood mononuclear cells samples. This variant is not present in dbSNP137, Exome Variant Server Data Release ESP6500SI-V2 or within the UCLA Clinical Genomics Center exome dataset (table 2).

This mutation is 'probably damaging' with a score of 1.0 by Polyphen 2.0 software. The mutation was confirmed by PCR and Sanger sequencing. Somatic mosaicism was suspected due to the skewed coverage distribution for the reference allele (48 reads) compared with the alternate allele (10 reads) in the exome sequencing data and the abundance of the peaks observed on Sanger sequencing (figure 2A).

#### Case 2
DICER1 mutation analysis was performed by Sanger sequencing of the second proband and identified a D1709Y missense mutation (HGA 19, g.95560438 G>T, c. 5125 G>T, p.Asp1709Tyr) located 13 bp from the mutation in Case 1 (figure 2B). This mutation is also probably damaging with a score of 1.0 by Polyphen V.2.0 software.

### Mosaic distribution of the mutations
We performed pyrosequencing on DNA extracted from all available tissue samples to determine the relative abundance of the mutations identified in blood, tumour and unaffected kidney samples. This analysis demonstrated mosaic distribution in each tissue, ranging from 21%–37% in Case 1 (figure 2C) to 28%–47% for Case 2 (figure 2D). In both cases, there is relative enrichment of the mutation in both tumour and unaffected kidney when compared with blood.

The 1709 and 1713 aspartic acid residues reside in the RNase IIIb domain of DICER1 and are conserved across numerous species.[20] Somatic mutations in Arg1709 have been previously reported in a number of cancers (figure 3).[21] More specifically, Arg1709 has been identified as part of a metal binding site essential for 5′ microRNA cleavage from mature pre-microRNAs and a hot spot for somatic mutations in cancer.[21] Similarly, Arg1713 mutated in Case 1 is located adjacent to this metal binding site, and a case of a somatic mutation in Wilms tumour has been reported (figure 3).[22]

### LOH and 'second hit' studies
#### Case 1
There was no evidence of DICER1 copy number loss in the WES data, which was performed on DNA isolated from mononuclear blood cells with all ratios of reads >1. Two additional DICER1 mutations were identified via Sanger sequencing from DNA isolated from tumour, g.95590605C>T, c.1304C>T, p.P453L, located in the Helicase C-Terminal domain (Polyphen 2 Score 0.972: probably damaging) and g.95556912 T>C,

316

**Table 1** Description of patients in the study

|  | Case 1 | Case 2 |
|---|---|---|
| Wilms tumour (initial) | + | + |
| Wilms tumour (contralateral) | + | + |
| Lung cysts | + | + |
| Macrocephaly | + | + |
| Somatic overgrowth | + | + |
| Developmental delay | + | + |
| Dysmorphic features | + | + |
| Autism | + | - |
| Hypertelorism | + | + |
| Flat nasal bridge | + | + |
| Frontal bossing | + | + |
| *DICER1* | c. 5138 A>T | c. 5125 G>T |

c.5529T>C, p.R1898G, located in the double stranded RNA binding domain (Polyphen 2 score 0.969: probably damaging). These mutations are absent from DNA isolated from blood, unaffected kidney as well as parental DNA samples demonstrating that they are tumour-specific de novo somatic mutations. Furthermore, these mutations are unequally distributed within the tumour (see online supplementary figure S1).

Case 2
No evidence of DICER1 copy number loss was identified in the WES data, which was performed on DNA isolated from tumour with all ratios of reads >1. No additional DICER1 mutations were identified by WES.

**Bioinformatics analysis**
We mined microRNA expression data from Dicer1 null mouse embryonic stem cells transfected with a single copy of human *DICER1* affecting the same residue as was seen in Case 2.[18] While the phenotype of mice carrying these mutations is not known, we were able to identify a specific population of microRNAs, which are increased in cells carrying the metal binding site mutations (see online supplementary table S1). Additional analysis using DIANA lab mirPath 2.0 allowed us to identify common target pathways shared by these upregulated microRNAs. Our analysis revealed that the following pathways are targeted by 9/10 of the microRNAs: (1) TGF-β (-ln (p value)=24); and (2) MAPK signalling (-ln (p value)=21) and the mTOR pathway is targeted by 8/10 of the microRNAs (-ln (p value)=26) (see online supplementary table S1).

**Table 2** Filtering of variants identified by whole exome sequencing

|  | Proband | Father | Mother |
|---|---|---|---|
| Total variants | 19 940 | 19 888 | 19 747 |
| Known variants (dbSNP132) | 19 371 | 19 311 | 19 220 |
| Transitions to Transversion ratio (dbSNP132) | 3.2 | 3.2 | 3.3 |
| Amino acid changing variants | 9926 | 10 019 | 9889 |
| Amino acid changing variants with Minor allele frequency<1% | 600 | 627 | 617 |
| High quality de novo variants | 3 |  |  |
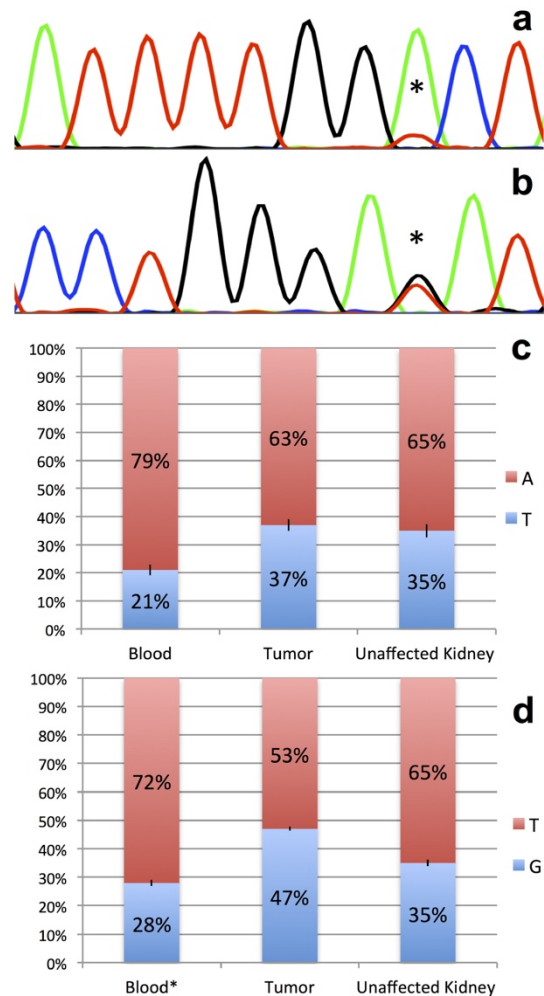


**Figure 2** Postzygotic mosaicism of RNase IIIb mutations in DICER1. (A, B) Sanger sequencing revealed a skewed distribution of allele abundance in Wilms tumour samples for each case. (A) Mutation g.95560451 A>T, c. 5138 A>T, p.1713 D>V identified in Case 1 (marked by asterisk). (B) Mutation g.95560438 G>T, c. 5125 G>T, p.1709 E>K identified in Case 2 (marked by asterisk). (C, D) Pyrosequencing identified mosaic distribution of mutations in different tissues. In both cases, percentage of mutation abundance is represented in blue. (C) Case 1 mutation abundance in blood (21%), tumour (37%) and unaffected kidney (35%). (D) Case 2 mutation abundance in blood (28%), tumour (47%) and unaffected kidney (35%). Standard deviations for Pyrosequencing experiments (C,D) are depicted with black bars.

**DISCUSSION**
DICER1 is a protein that is involved in the microRNA processing pathway.[23] Constitutional DICER1 mutations have been associated with cystic lung disease, cystic nephroma, Sertoli-Leydig tumours and multinodular goitres,[24] while somatic DICER1 mutations have been reported in additional tumour types.[21] [25–29] Despite the wide-ranging effects of microRNAs on gene expression, the recurrent involvement of specific tissue types including the lungs, kidneys, ovaries and thyroid in cases of DICER1 mutations suggests that tissue-
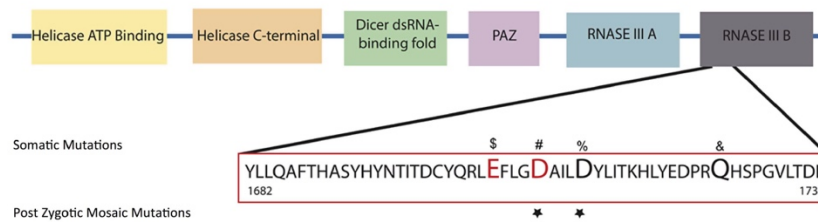
**Figure 3** DICER1 RNase IIIb mutations. Schematic representation of DICER1 protein and its domains. Mutations in the RNAase IIIb domain associated with Sertoli-Leydig cell tumours ($, #), non-epithelial ovarian tumour (#), yolk sac tumour (#), juvenile granulosa-cell tumour (#), Wilms tumour (%) and embryonal rhabdomyosarcomas (&) are presented. Residues identified to be cancer 'hot spots' and known to reduce 5p cleavage and increase 3p microRNAs according to Anglesio et al[18] are depicted in red. Affected residues in GLOW syndrome are marked with a star.

specific microRNAs may play a more prominent role in these organs. The phenotypes associated with DICER1 mutations are varied and reproducible however, to date have not been reported to cause somatic overgrowth, macrocephaly or developmental delay.

The biallelic loss of heterozygosity (LOH) of DICER1 observed in isolated Wilms tumours suggests that DICER1 behaves as a tumour suppressor, requiring a second hit for tumourigenesis to occur.[22] Wu et al have reported three cases of isolated Wilms tumour where there is an inherited frame shift deleterious DICER1 mutation in one allele and an acquired mutation in the RNase IIIa (n=1) or RNase IIIb domain (n=2) in the second allele. Case 1 from our report had two second hit mutations in DICER1 which are heterogeneously distributed

throughout the Wilms tumour (see online supplementary figure S1). This finding in addition to the absence of second hit mutations or LOH in tumour samples from Case 2 suggests that they may not be necessary or sufficient for tumourigenesis in this syndrome. We cannot rule out that we may have missed mutations in intronic or regulatory regions that may affect DICER1 function. It is also important to note that not all Wilms tumours are associated with DICER1 mutations, as Bahubeshi et al[30] have reported a cohort of 50 cases of sporadic Wilms tumours none of which have mutations in DICER1.

Interestingly, of all the mutations reported to date in DICER1, those that alter residues within the RNase IIIb domain are over-represented in sporadic cancers. More specifically, mutations in specific metal binding residues within the RNase

**Table 3** Reported metal binding site and GLOW syndrome mutations in the RNase IIIb domain of DICER-1 and associated phenotypes

| Reference | Coordinates | Protein | Phenotype | S/G/M |
|---|---|---|---|---|
| **This study 1** | **c. 5138A>T** | **p.Asp1713Val (D1713V)** | **GLOW syndrome** | **M** |
| **This study 2** | **c. 5125G>T** | **p.Asp1709Tyr (D1709Y)** | **GLOW syndrome** | **M** |
| Wu *et al* | c.5138A>C | p.Asp1713Ala (D1713A)LOH | Wilms Tumour | S |
| Heravi-Moussavi | c.5113G>A | p.Glu1705Lys (E1705K) | SLCT | S |
| Heravi-Moussavi | c.5125G>A | p.Asp1709Asn (D1709N) | SLCT | S |
| Heravi-Moussavi | c.5126A>G | p.Asp1709Gly (D1709G) | SLCT | S |
| Heravi-Moussavi | c.5127T>A | p.Asp1709Glu (D1709E) | SLCT | S |
| Heravi-Moussavi | c.5428G>C | p.Asp1810His (D1810H) | SLCT | S |
| Heravi-Moussavi | c.5428G>T | p.Asp1810Tyr (D1810Y) | SLCT | S |
| Heravi-Moussavi | c.5428G>A | p.Asp1810Asn (D1810N) | SLCT | S |
| Heravi-Moussavi | c.5437G>C | p.Glu1813Gln (E1813Q) | SLCT | S |
| Heravi-Moussavi | c.5438A>G | p.Glu1813Gly (E1813G) | SLCT | S |
| Heravi-Moussavi | c.5437G>A | p.Glu1813Lys (E1813K) | SLCT | S |
| Heravi-Moussavi | c.5126A>G | p.Asp1709Gly (D1709G) | Juvenile granulosa-cell tumour | S |
| Heravi-Moussavi | c.5125G>A | p.Asp1709Asn (D1709N) | Yolk sac tumour | S |
| Heravi-Moussavi | c.5127T>A | p.Asp1709Glu (D1709E) | Yolk sac tumour | S |
| Heravi-Moussavi | c.5428G>T | p.Asp1810Tyr (D1810Y) | Mature teratoma | S |
| Witkowski | c.5113G>A | p.Glu1705Lys (E1705K) | SCST | S |
| Witkowski | c.5125G>A | p.Asp1709Asn (D1709N) | SLCT | S |
| Witkowski | c.5428G>T | p.Asp1810Tyr (D1810Y) | Mixed* | S |
| Witkowski | c.5429A>T | p.Asp1810Val (D1810V) | SLCT | S |
| Witkowski | c.5437G>A | p.Glu1813Lys (E1813K) | SLCT | S |
| Witkowski | c.5437G>C | p.Glu1813Gln (E1813Q) | SLCT | S |
| Witkowski | c.5437G>C | p.Glu1813Gln (E1813Q) | SLCT | S |
| Witkowski | c.5439G>C | p.Glu1813Asp (E1813D) | SLCT | S |

*, Germ cell tumor with components of immature teratoma and yolk sac tumor.
G, germline mutation; LOH, loss of heterozygosity mutation; M, mosaic mutation; S, somatic mutation; SCST, Sex-cord stromal tumour; SLCT, Sertoli-Leydig cell tumour.
GLOW syndrome mutations described in this report in bold.

IIIb domain are associated with distinct tumour types.[18][29] We suggest that the phenotypic consequence of these metal binding site mutations is overgrowth and cancer predisposition. These specific DICER1 RNase IIIb mutations act differently than those that cause complete DICER1 loss of function suggesting that DICER1 may also behave as an oncogene.[21][29] The higher incidence of metal binding site domain mutations in tumours suggests that they can additionally cause overgrowth, macrocephaly and developmental delay when more widely distributed. Similar to P53, we propose that DICER1 can act both as a tumour suppressor as well as an oncogene depending on the specific mutation present and the functional consequence of those changes on protein function.[31]

The developmental origin of the DICER1 mutation in these cases is likely after zygote formation, which explains their mosaic distribution. It is reasonable to propose that these metal binding site RNase IIIb domain mutations are not tolerated during development and behave differently from haploinsufficient alleles. To support this hypothesis, we have summarised all mutations within the metal binding sites of the RNase IIIb domain of DICER1 and their associated human phenotypes in table 3. As documented in this table, to date there has not been a single case reported of an RNase IIIb metal binding site germline mutation, which in combination with their frequent presence in somatic neoplasms, strengthens the hypothesis that these mutations are not tolerated when inherited.

There are four amino acid residues reported to be metal binding sites (1705, 1709, 1810 and 1813) that are essential for RNase IIIb domain function.[21][29] These metal bindings sites have been labelled as cancer hot spots in DICER1.[21][29] All are reported to have a similar functional consequence when mutated,[18] which is the loss of 5p microRNA synthesis with 3p microRNA synthesis remaining intact. During homeostasis, 5p microRNAs are thought to be the predominant population while 3p microRNAs are normally short-lived and rapidly depleted from cells.[18] Case 2 from our study has a postzygotic mosaic mutation that has been reported to be a hot spot at p. Asp1709Tyr, while the mutation in Case 1 affects an amino acid four residues away, p.Asp1713Val. This mutation has been identified in a sporadic case of Wilms tumour.[22] We propose that when residue 1713 is mutated it has a similar functional consequence to that of the reported hot spots, causing a similar phenotype as residue 1709 when present in a postzygotic mosaic distribution.

Specific 5p microRNAs have been shown to be essential for the regulation of signalling and growth pathways.[32] Furthermore, the balance between specific 3p and 5p microRNAs is essential for the control of growth and prevention of cancer progression.[33] This was shown to be the case for mir28-5p and -3p. Using a transwell assay, overexpression of mir28-5p reduces colorectal cancer (CRC) proliferation and invasion in vitro and, conversely, mir28-3p overexpression increases CRC cell migration and invasion in vitro.[33] We predict that signalling pathways in which the 5p/3p miRNA balance is essential for correct regulation would be especially sensitive to DICER1 RNase IIIb domain mutations.

We performed a bioinformatics analysis in a murine stem cell model of DICER1 mutation (D1709N) to address our prediction that specific pathways may be affected by a 3p/5p microRNA imbalance. We identified 10 candidate dysregulated 3p microRNAs (see online supplementary table S1). Using DIANA miRPath we generated a list of target genes for each microRNA followed by pathway analysis to identify shared targeted signalling pathways. There were three pathways identified:
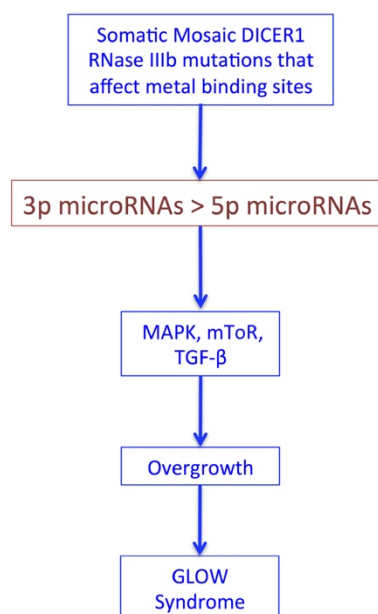


**Figure 4** Model of GLOW syndrome-associated RNase IIIb metal binding site mutations.

mTOR signalling, TGF-β and MAPK signalling, all of which were targeted by 80% (8/10) of the 3p microRNAs identified and two of which were targeted by 90% (9/10) of the 3p microRNAs (TGF-B and MAPK). Many of the targets represent negative regulators of each of these pathways, including PTEN, tuberous sclerosis complex (TSC) (mTOR), SKP1a, Smad7, Snuf1 (TGF-β), NF1, Rasa2, Dusp16, Ppm1a and Evi1 (MAPK). These findings suggest that an imbalance in specific 3p microRNAs may lead to excessive cell and tissue growth and cancer predisposition (figure 4). Furthermore, these pathways may represent potential therapeutic targets.

We support the hypothesis that specific mutations within the metal binding sites of the RNase IIIb domain of DICER1 allow it to behave as an oncogene, distinct from the effects of frame shift or other deleterious DICER1 mutations.[21] The oncogenic microRNA profile manifests as neoplasm formation as well as overgrowth when more widely distributed. We have provided a bioinformatic link between deregulated microRNAs and key growth signalling pathways that provides a potential mechanism by which these mutations may cause tumour formation and overgrowth. While rare cases of nephromegaly[34] and renal hamartomas[35] have been associated with pulmonary cysts, none have been reported to develop Wilms tumour. We therefore suggest that these domain- and site-specific mutations are causal for a unique constellation of associated clinical features representing a novel syndrome. We have termed this syndrome GLOW for its key findings that include *G*lobal development delay, *L*ung cysts *O*vergrowth and *W*ilms tumour. This expands the phenotypic spectrum associated with mutations in the DICER1 gene.

**Author affiliations**
[1]Department of Human Genetics, David Geffen School of Medicine at UCLA, Los Angeles, California, USA
[2]Department of Pathology and Laboratory Medicine, David Geffen School of Medicine at UCLA, Los Angeles, California, USA

[3]Department of Radiology, David Geffen School of Medicine at UCLA, Los Angeles, California, USA
[4]Division of Hematology-Oncology, David Geffen School of Medicine at UCLA, Los Angeles, California, USA
[5]Division of Pulmonary Medicine, David Geffen School of Medicine at UCLA, Los Angeles, California, USA
[6]Department of Pediatrics, Loma Linda University School of Medicine, Loma Linda, California, USA
[7]Jonsson Cancer Center, David Geffen School of Medicine at UCLA, Los Angeles, California, USA
[8]Division of Medical Genetics, Department of Pediatrics, David Geffen School of Medicine at UCLA, Los Angeles, California, USA

## REFERENCES

1 Verge CF, Mowat D. Overgrowth. *Arch Dis Child* 2010;95:458–63.
2 Rodriguez-Escudero I, Oliver MD, Andres-Pons A, Molina M, Cid VJ, Pulido R. A comprehensive functional analysis of PTEN mutations: implications in tumor- and autism-related syndromes. *Hum Mol Genet* 2011;20:4132–42.
3 Pilarski R, Burt R, Kohlman W, Pho L, Shannon KM, Swisher E. Cowden syndrome and the PTEN hamartoma tumor syndrome: systematic review and revised diagnostic criteria. *J Natl Canc Inst* 2013;105:1607–16.
4 Kurotaki N, Imaizumi K, Harada N, Masuno M, Kondoh T, Nagai T, Ohashi H, Naritomi K, Tsukahara M, Makita Y, Sugimoto T, Sonoda T, Hasegawa T, Chinen Y, Tomita Ha HA, Kinoshita A, Mizuguchi T, Yoshiura Ki K, Ohta T, Kishino T, Fukushima Y, Niikawa N, Matsumoto N. Haploinsufficiency of NSD1 causes Sotos syndrome. *Nat Genet* 2002;30:365–6.
5 Weaver DD, Graham CB, Thomas IT, Smith DW. A new overgrowth syndrome with accelerated skeletal maturation, unusual facies, and camptodactyly. *J Pediatr* 1974;84:547–52.
6 Biesecker LG, Spinner NB. A genomic view of mosaicism and human disease. *Nat Rev Genet* 2013;14:307–20.
7 Lindhurst MJ, Sapp JC, Teer JK, Johnston JJ, Finn EM, Peters K, Turner J, Cannons JL, Bick D, Blakemore L, Blumhorst C, Brockmann K, Calder P, Cherman N, Deardorff MA, Everman DB, Golas G, Greenstein RM, Kato BM, Keppler-Noreuil KM, Kuznetsov SA, Miyamoto RT, Newman K, Ng D, O'Brien K, Rothenberg S, Schwartzentruber DJ, Singhal V, Tirabosco R, Upton J, Wientroub S, Zackai EH, Hoag K, Whitewood-Neal T, Robey PG, Schwartzberg PL, Darling TN, Tosi LL, Mullikin JC, Biesecker LG. A mosaic activating mutation in AKT1 associated with the Proteus syndrome. *N Engl J Med* 2011;365:611–19.
8 Kurek KC, Luks VL, Ayturk UM, Alomari AI, Fishman SJ, Spencer SA, Mulliken JB, Bowen ME, Yamamoto GL, Kozakewich HP, Warman ML. Somatic mosaic activating mutations in PIK3CA cause CLOVES syndrome. *Am J Hum Genet* 2012;90:1108–15.
9 Riviere JB, Mirzaa GM, O'Roak BJ, Beddaoui M, Alcantara D, Conway RL, St-Onge J, Schwartzentruber JA, Gripp KW, Nikkel SM, Worthylake T, Sullivan CT, Ward TR, Butler HE, Kramer NA, Albrecht B, Armour CM, Armstrong L, Caluseriu O, Cytrynbaum C, Drolet BA, Innes AM, Lauzon JL, Lin AE, Mancini GM, Meschino WS, Reggin JD, Saggar AK, Lerman-Sagie T, Uyanik G, Weksberg R, Zirn B, Beaulieu CL, Majewski J, Bulman DE, O'Driscoll M, Shendure J, Graham JM Jr, Boycott KM, Dobyns WB. De novo germline and postzygotic mutations in AKT3, PIK3R2 and PIK3CA cause a spectrum of related megalencephaly syndromes. *Nat Genet* 2012;44:934–40.
10 Tatton-Brown K, Weksberg R. Molecular mechanisms of childhood overgrowth. *Am J Med Genet C Semin Med Genet* 2013;163:71–5.
11 Brioude F, Lacoste A, Netchine I, Vazquez MP, Auber F, Audry G, Gauthier-Villars M, Brugieres L, Gicquel C, Le Bouc Y, Rossignol S. Beckwith-Wiedemann syndrome: growth pattern and tumor risk according to molecular mechanism, and guidelines for tumor surveillance. *Horm Res Paediatr* 2013;80:457–65.
12 Huff V. Wilms tumor genetics. *Am J Med Genet* 1998;79:260–7.
13 Niemitz EL, Feinberg AP, Brandenburg SA, Grundy PE, DeBaun MR. Children with idiopathic hemihypertrophy and beckwith-wiedemann syndrome have different constitutional epigenotypes associated with wilms tumor. *Am J Hum Genet* 2005;77:887–91.
14 Scott RH, Stiller CA, Walker L, Rahman N. Syndromes and constitutional chromosomal abnormalities associated with Wilms tumour. *J Med Genet* 2006;43:705–15.
15 Hill DA, Ivanovich J, Priest JR, Gurnett CA, Dehner LP, Desruisseau D, Jarzembowski JA, Wikenheiser-Brokamp KA, Suarez BK, Whelan AJ, Williams G, Bracamontes D, Messinger Y, Goodfellow PJ. DICER1 mutations in familial pleuropulmonary blastoma. *Science* 2009;325:965.
16 Cheesman S, Creasey A, Degnan K, Kooij T, Afonso A, Cravo P, Carter R, Hunt P. Validation of Pyrosequencing for accurate and high throughput estimation of allele frequencies in malaria parasites. *Mol Biochem Parasitol* 2007;152:213–19.
17 Wasson J, Skolnick G, Love-Gregory L, Permutt MA. Assessing allele frequencies of single nucleotide polymorphisms in DNA pools by pyrosequencing technology. *BioTechniques* 2002;32:1144–6, 48, 50 passim.
18 Anglesio M, Wang Y, Yang W, Senz J, Wan A, Heravi-Moussavi A, Salamanca C, Maines-Bandiera S, Huntsman D, Morin G. Cancer-associated somatic DICER1 hotspot mutations cause defective miRNA processing and reverse-strand expression bias to predominantly mature 3p strands through loss of 5p strand cleavage. *J Pathol* 2013;229:400–9.
19 Vlachos IS, Kostoulas N, Vergoulis T, Georgakilas G, Reczko M, Maragkakis M, Paraskevopoulou MD, Prionidis K, Dalamagas T, Hatzigeorgiou AG. DIANA miRPath v.2.0: investigating the combinatorial effect of microRNAs in pathways. *Nucleic Acids Res* 2012;40(Web Server issue):W498–504.
20 Nicholson RH, Nicholson AW. Molecular characterization of a mouse cDNA encoding Dicer, a ribonuclease III ortholog involved in RNA interference. *Mamm Genome* 2002;13:67–73.
21 Heravi-Moussavi A, Anglesio MS, Cheng SW, Senz J, Yang W, Prentice L, Fejes AP, Chow C, Tone A, Kalloger SE, Hamel N, Roth A, Ha G, Wan AN, Maines-Bandiera S, Salamanca C, Pasini B, Clarke BA, Lee AF, Lee CH, Zhao C, Young RH, Aparicio SA, Sorensen PH, Woo MM, Boyd N, Jones SJ, Hirst M, Marra MA, Gilks B, Shah SP, Foulkes WD, Morin GB, Huntsman DG. Recurrent somatic DICER1 mutations in nonepithelial ovarian cancers. *N Engl J Med* 2012;366:234–42.
22 Wu M, Sabbaghian N, Xu B, Addidou-Kalucki S, Bernard C, Zou D, Reeve A, Eccles M, Cole C, Choong C, Charles A, Tan T, Iglesias D, Goodyer P, Foulkes W. Biallelic DICER1 mutations occur in Wilms tumours. *J Pathol* 2013;230:154–64.
23 Carthew RW. Gene regulation by microRNAs. *Curr Opin Genet Dev* 2006;16:203–8.
24 Slade I, Bacchelli C, Davies H, Murray A, Abbaszadeh F, Hanks S, Barfoot R, Burke A, Chisholm J, Hewitt M, Jenkinson H, King D, Morland B, Pizer B, Prescott K, Saggar A, Side L, Traunecker H, Vaidya S, Ward P, Futreal PA, Vujanic G, Nicholson AG, Sebire N, Turnbull C, Priest JR, Pritchard-Jones K, Houlston R, Stiller C, Stratton MR, Douglas J, Rahman N. DICER1 syndrome: clarifying the diagnosis, clinical features and management implications of a pleiotropic tumour predisposition syndrome. *J Med Genet* 2011;48:273–8.
25 Rio Frio T, Bahubeshi A, Kanellopoulou C, Hamel N, Niedziela M, Sabbaghian N, Pouchet C, Gilbert L, O'Brien PK, Serfas K, Broderick P, Houlston RS, Lesueur F, Bonora E, Muljo S, Schimke RN, Bouron-Dal Soglio D, Arseneau J, Schultz KA, Priest JR, Nguyen VH, Harach HR, Livingston DM, Foulkes WD, Tischkowitz M. DICER1 mutations in familial multinodular goiter with and without ovarian Sertoli-Leydig cell tumors. *JAMA* 2011;305:68–77.
26 Schultz KA, Pacheco MC, Yang J, Williams GM, Messinger Y, Hill DA, Dehner LP, Priest JR. Ovarian sex cord-stromal tumors, pleuropulmonary blastoma and DICER1 mutations: a report from the International Pleuropulmonary Blastoma Registry. *Gynecol Oncol* 2011;122:246–50.
27 Foulkes WD, Bahubeshi A, Hamel N, Pasini B, Asioli S, Baynam G, Choong CS, Charles A, Frieder RP, Dishop MK, Graf N, Ekim M, Bouron-Dal Soglio D, Arseneau J, Young RH, Sabbaghian N, Srivastava A, Tischkowitz MD, Priest JR. Extending the phenotypes associated with DICER1 mutations. *Hum Mutat* 2011;32:1381–4.
28 Doros L, Yang J, Dehner L, Rossi CT, Skiver K, Jarzembowski JA, Messinger Y, Schultz KA, Williams G, Andre N, Hill DA. DICER1 mutations in embryonal rhabdomyosarcomas from children with and without familial PPB-tumor predisposition syndrome. *Pediatr Blood Cancer* 2012;59:558–60.
29 Witkowski L, Mattina J, Schonberger S, Murray MJ, Choong CS, Huntsman DG, Reis-Filho JS, McCluggage WG, Nicholson JC, Coleman N, Calaminus G, Schneider DT, Arseneau J, Stewart CJ, Foulkes WD. DICER1 hotspot mutations in non-epithelial gonadal tumours. *Br J Cancer* 2013;109:2744–50.

30  Bahubeshi A, Bal N, Rio Frio T, Hamel N, Pouchet C, Yilmaz A, Bouron-Dal Soglio D, Williams GM, Tischkowitz M, Priest JR, Foulkes WD. Germline DICER1 mutations and familial cystic nephroma. *J Med Genet* 2010; 47:863–6.

31  Sigal A, Rotter V. Oncogenic mutations of the p53 tumor suppressor: the demons of the guardian of the genome. *Cancer Res* 2000;60:6788–93.

32  Maurisa F, Riley MSB, Wahi K, Nuovo GJ, Cole SE. mir-125a-5p-mediated regulation of Lfng is essential for the avian segmentation clock. *Dev Cell* 2013;24:554–61.

33  Almeida MI, Nicoloso MS, Zeng L, Ivan C, Spizzo R, Gafa R, Xiao L, Zhang X, Vannini I, Fanini F, Fabbri M, Lanza G, Reis RM, Zweidler-McKay PA, Calin GA. Strand-specific miR-28-5p and miR-28-3p have distinct effects in colorectal cancer cells. *Gastroenterology* 2012;142:886–96 e9.

34  Weinberg AG, Zumwalt RE. Bilateral nephromegaly and multiple pulmonary cysts. *Am J Clin Pathol* 1977;67:284–8.

35  Graham JM Jr, Boyle W, Troxell J, Cullity GJ, Sprague PL, Beckwith JB. Cystic hamartomata of lung and kidney: a spectrum of developmental abnormalities. *Am J Med Genet* 1987;27:45–59.

# Truncating Mutations in *APP* Cause a Distinct Neurological Phenotype

Steven Klein, BS,[1]
Alexander Goldman, MD,[1]
Hane Lee, PhD,[2]
Shahnaz Ghahremani, MD,[3] Viraj Bhakta,[1]
UCLA Clinical Genomics Center,
Stanley F. Nelson, MD,[1,2,4] and
Julian A. Martinez-Agosto, MD, PhD[1,2,5]

Dominant missense mutations in the amyloid $\beta$ (A$\beta$) precursor protein (*APP*) gene have been implicated in early onset Alzheimer disease. These mutations alter protein structure to favor the pathologic production of A$\beta$. We report that homozygous nonsense mutations in *APP* are associated with decreased somatic growth, microcephaly, hypotonia, developmental delay, thinning of the corpus callosum, and seizures. We compare the phenotype of this case to those reported in mouse models and demonstrate multiple similarities, strengthening the role of amyloid precursor protein in normal brain function and development.

ANN NEUROL 2016;00:000–000

Alzheimer disease (AD) is a neurodegenerative disease, which manifests as progressive memory deterioration and other cognitive decline. Genetic factors that predispose to classic AD as well as early onset AD have previously been described. One genetic predisposition for early onset AD is due to mutations in the gene encoding for amyloid precursor protein (APP), resulting in alterations to the amyloid $\beta$ peptide (A$\beta$).[1,2] A$\beta$ is a 39–43-residue product of proteolysis of APP, which is an integral membrane protein with a long extracellular amino-terminal domain, a single transmembrane domain, and a short cytoplasmic tail.[3] The *APP* gene, on chromosome 21q, is a 400kb gene that is spliced to produce isoforms ranging from 365 to 770 amino acid residues. Studies in mouse models have ascertained that in the constitutive secretory pathway, APP is cleaved within the A$\beta$ region, to form secreted neuroprotective products including but not limited to sAPP$\alpha$.[4] Through alternative pathways, the protein may be internalized to an endosome where intact A$\beta$ is produced, or A$\beta$ may be secreted from cells and found in the cerebrospinal fluid of both AD and healthy individuals.[5] Most mutations in this gene are located just outside of the A$\beta$ region of the protein and are associated with autosomal-dominant early onset AD.[6] Interestingly, to date there have been no reports of human homozygous nonsense or frameshift mutations in the *APP* gene.

## Materials and Methods

This study was approved by the University of California, Los Angeles (UCLA) Institutional Review Board, and informed consent was obtained.

### Single Nucleotide Polymorphism Chromosomal Microarray

The chromosomal microarray platform was developed by Affymetrix and its performance characteristics determined by UCLA clinical laboratory as required by the Clinical Laboratory Improvement Amendments of 1988 regulations. The assay compared the patient's DNA with 270 HapMap normal controls, using the genome-wide single nucleotide polymorphism (SNP) array 6.0. This array platform contains 1.8 million markers for copy number variant detection chosen at ~696bp spacing throughout the human genome. Oligonucleotide probe information is based on Build 36 of the Human Genome (University of California, Santa Cruz, Genome Browser, hg18, March 2006). Nondiagnostic copy number changes are referenced to the Database of Genomic Variants (http://projects.tcag.ca/variation/).

### Clinical Exome Sequencing

Clinical exome sequencing was performed on the patient and his parents at UCLA following the validated protocol as described by Lee et al.[7] Briefly, exome capture was performed using an Agilent Technologies (Santa Clara, CA) SureSelect Human All Exon 50Mb XT kit and sequencing was performed on an Illumina (San Diego, CA) HiSeq2500 as 100bp paired-end runs. Mean coverage across the RefSeq protein-coding exons and flanking intronic sequence ($\pm$2bp)

was 93✕ with >92% of these base positions being sequenced at >9✕. Sequence reads were aligned to the human reference genome (hg19/NCBI Build 37) using Novoalign V2.07.15b (Novocraft, http://www.novocraft.com/). Polymerase chain reaction duplicates were marked using Picard-tools-1.42 (http://broadinstitute.github.io/picard/). Indel (insertions and deletions) realignment, quality score recalibration, variant calling, recalibration, and variant evaluation were performed using the Genome Analysis Toolkit (GATK) v1.1-33.[8] All variants were annotated using Variant Annotator eXtras (VAX)[9] and deposited into a MySQL 5.2 database for filtering. Amino acid–altering de novo, hemizygous, homozygous, compound heterozygous, and inherited heterozygous variants with minor allele frequency <1% (based on data from the 1000 Genomes Project, National Heart, Lung, and Blood Institute Grand Opportunity Exome Sequencing Project, National Institute of Environmental Health Sciences Environmental Genome Project, and HapMap, without the distinction of ethnic background) that were relevant to the patient's phenotype were considered for further analysis. The pathogenicity of a variant was determined according to current American College of Medical Genetics and Genomics sequence interpretation guidelines.

### Western Blot Analysis

Venous blood was drawn from the proband, both parents, and a confirmed unaffected control and immediately spun at $100 \times g$ for 20 minutes to form platelet-rich plasma (PRP). One milliliter of the PRP was transferred to a 1.5ml Eppendorf tube and spun at $100 \times g$ for 20 minutes to pellet the white blood cells. The supernatant was transferred to a 1.5ml Eppendorf tube spun at maximum speed for 10 minutes to pellet platelets. The supernatant was aspirated from the platelet pellet, and the pellet was suspended in 500 μl of passive lysis buffer, prepared with phosphatase and protease inhibitors, and incubated by shaking at 4°C for 1 hour. Afterward, lysis tubes were spun at 7,500 relative centrifugal force for 5 minutes to collect debris. Supernatant was transferred to a new tube, then protein concentration was determined with the Coomassie Plus Bradford (Life Technologies, Carlsbad, CA) reagent following manufacturer instructions. Protein samples were diluted to a final concentration of 5 μg/20 μl into Western loading buffer with beta-mercaptoethanol and then boiled for 5 minutes. Western blots were run on 12% acrylamide gels followed by transfer onto nitrocellulose membranes utilizing the Transblot Turbo apparatus from Bio-Rad (Hercules, CA). The membrane was blocked in 5% bovine serum albumin in Tris-buffered (TBS) saline plus Tween (TBST) for 30 minutes, then incubated in primary antibodies overnight: anti–amyloid precursor protein (Sigma, St Louis, MO; #A8717, dilution = 1/1,000) and α-tubulin (Cell Signaling Technology, Danvers, MA; #2125, dilution = 1/1,000). The next day, blots were rinsed with TBS and washed 3 times with TBST. Blots were then incubated in rabbit secondary antibodies conjugated to horseradish peroxidase at a dilution of 1/3,750. Following secondary incubation, membranes were rinsed with TBS then washed twice with TBST. Blots were exposed using Western Clarity reagents from
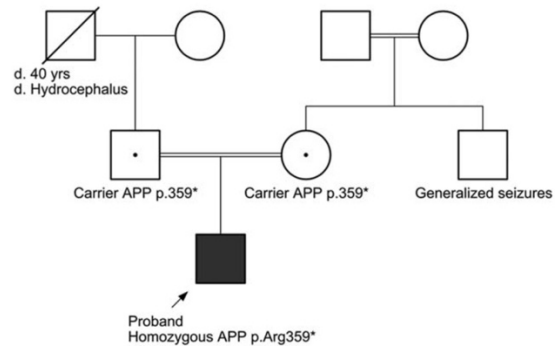


FIGURE 1: Pedigree for affected individual with homozygous truncating *APP* mutations. Three-generation family history was obtained. The pedigree demonstrates that carriers of the heterozygous truncating mutations in *APP* are unaffected. The proband is homozygous for the mutation and affected. Filled square indicates proband. Black dots denote carrier status of each parent. Double lines indicate consanguineous parentage.

Bio-Rad, imaged on the Bio-Rad ChemiDoc, and viewed in Bio-Rad Image Lab Software.

### Results

A 20-month-old male presented with microcephaly, hypotonia, and seizures. He was born prematurely at 33 weeks gestational age via spontaneous vaginal delivery to a G2P0 mother with a history of a previous miscarriage. Family history was significant for consanguinity on the maternal grandmother's side of the family, seizures in a maternal uncle, and the demise of his paternal grandfather from hydrocephalus at age 40 years (pedigree of family history, Fig 1). At birth, length was 45.7cm (75th percentile) and weight was 2,381g (90th percentile). The perinatal period was complicated by poor feeding and seizures (first diagnosed at 1 month of age), which required hospitalization in the neonatal intensive care unit until 2 months of age. Phenobarbital was initiated, which effectively controlled his seizures.

At 3 months of age, delay in developmental milestones was noted. Topiramate was added to the seizure regimen and was effective. Brain magnetic resonance imaging at that time was significant for dolichocephaly, moderate diffuse cerebral atrophy, marked thinning of the corpus callosum, diffuse loss of white matter volume particularly within the bilateral parietal and occipital lobes, and a paucity of myelinated tracts within bilateral frontal lobes with no evidence of infarct, hemorrhage, or mass effect (Fig 2A, B).

Seizure frequency ranged from 2 to 20 per day, and the seizure semiology appeared to be complex partial with left or right head turning and eyes deviating up and to the left followed by tonic axial stiffening with left arm
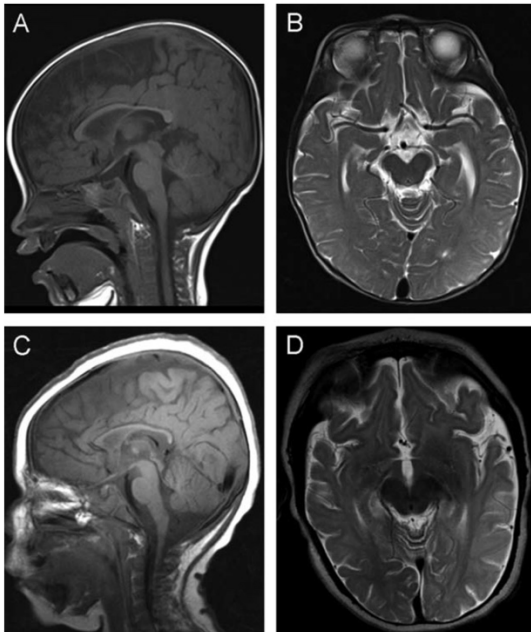
FIGURE 2: Brain findings in *APP* knockout. (A) One-year-old male normal sagittal T1 magnetic resonance imaging (MRI) demonstrating normal myelination and corpus callosum thickness and (B) axial T2 MRI demonstrating lack of focal atrophy and normal T2 signal in subcortical white matter of the left temporal and occipital regions. (C) Proband sagittal T1 MRI demonstrating diffuse hypomyelination with thin corpus callosum and (D) axial T2 MRI demonstrating focal atrophy and hyperintense T2 signal in subcortical white matter of the left temporal and occipital regions.

tonicity, clinically lasting no longer than 90 seconds. A 5-week-long video electroencephalographic recording while the patient was in status epilepticus demonstrated seizure clusters as frequently as 10 per hour with duration up to 25 minutes, with multifocal regions of epileptogenicity. In the postictal state, there was consolable crying, but no signs of fatigue or somnolence.

Additional medical history was significant for global developmental delay, microcephaly, and apneic episodes. Physical examination revealed height of 71cm (<5th percentile), weight of 9.5kg (15 percentile), and head circumference of 41.5cm (<5th percentile) at 13 months, as well as dolichocephaly, mild facial dysmorphia, hypotonia, slightly abnormal ear morphology, and micrognathia. Eye movements were normal. SNP chromosomal microarray analysis was performed to look for microdeletions and duplications associated with seizures and microcephaly, as well as regions of homozygosity that might suggest identity by descent and a recessive genetic etiology. Subsequently, clinical exome sequencing (CES) trio analysis was performed to identify mutations associated with the clinical findings.

### SNP Chromosomal Microarray

No copy number gains or losses of genomic regions of known clinical significance were observed. A total of 138.36Mb of contiguous stretches of homozygosity (each stretch > 5Mb) were identified on chromosomes 3, 4, 5, 9, 13, 16, 20, and 21, suggesting identity by descent. No

**TABLE 1. Variants Identified and Reported by Clinical Exome Sequencing**

| Gene | cDNA Change | Protein Change | Variant Classification | Zygosity | Allele Counts in ExAC Database | Disease Association |
|------|-------------|----------------|------------------------|----------|--------------------------------|---------------------|
| *SETX* | NM_015046.5: c.4738C>T | p.Arg1580Cys | VUS | Homozygous | 1 heterozygous, 0 homozygous | Autosomal-dominant juvenile amyotrophic lateral sclerosis 4 (MIM: 602433); autosomal recessive ataxia–ocular apraxia 2 (MIM: 606002). |
| *CLN8* | NM_018941.3: c.685C>G | p.Pro229Ala | VUS | Heterozygous, maternally inherited | 1,397 heterozygous, 93 homozygous | Autosomal-recessive neuronal ceroid lipofuscinosis 8 (MIM: 600143) |
| *APP* | NM_000484.3: c.1075C>T | p.Arg359* | VUS | Homozygous | 7 heterozygous, 0 homozygous | Autosomal-dominant familial Alzheimer disease1 (MIM: 104300) |

ExAC = Exome Aggregation Consortium; MIM = Mendelian Inheritance in Man; VUS = variant of uncertain significance.

Month 2016

known uniparental disomy-associated human disorders or imprinted genes were located within these regions.

### CES

Of a total 21,790 variants identified by CES, 3 variants were reported: 2 homozygous single nucleotide variants in 2 genes, including a nonsense variant in *APP* gene and a missense variant in *SETX* gene, and 1 heterozygous variant in *CLN8* gene that is associated with autosomal recessive neuronal ceroid lipofuscinosis type 8 (NCL; Table 1). We confirmed the pathogenicity of the *APP* genetic variants by analyzing protein extracts from platelets collected from the trio and a confirmed unaffected control. APP translation is decreased in both heterozygous parents and minimal in the proband when compared to control (Fig 3).

### Discussion

In this study we report for the first time a loss of APP and its phenotypic consequences, including developmental delay, reduced growth, seizures, thin corpus callosum, and hypotonia. Additional variants were identified by CES including a homozygous recessive mutation in *SETX*, a gene associated with juvenile amyotrophic lateral sclerosis type 4 (ALS)[10] and ataxia with ocular apraxia type 2 (AOA2),[11] and a heterozygous variant of uncertain significance in *NCL*.[12] Comparisons of the clinical course of this case to the natural history of these other gene-associated syndromes revealed no clinical signs typically associated with juvenile ALS. However, definitive electromyographic testing was not performed and is needed to rule out ALS anterior horn involvement. Furthermore, ALS and AOA2 usually have onset in adolescence and not the global, multisystem involvement observed in this case. Lastly, NCL lysosomal enzyme testing was normal in this case, demonstrating that enzyme function was intact, and furthermore there are 93 individuals in the Exome Aggregation Consortium (ExAC) database[13] who are homozygous for the same variant the patient was identified with, making the variant likely benign.
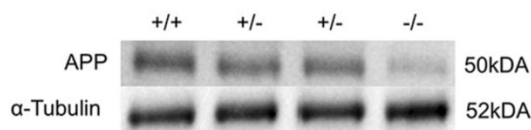


FIGURE 3: Amyloid precursor protein (APP) levels in carriers and affected proband. Western blots compare APP levels of unaffected control (+/+), parental carriers (+/−), and proband (−/−). The carriers are shown to have less APP than the control, and the proband has minimal APP consistent with the genotypes (APP band shown has a molecular weight [MW] of approximately 50kDa, α-tubulin band shown has a MW of approximately 52kDa).

**TABLE 2. Phenotypic Overlap between Human and Murine *APP* Knockouts**

| Phenotype | Mouse | Human |
|---|---|---|
| Decreased growth | + | + |
| Decreased brain weight | + | + |
| Dysgenesis of the corpus callosum | + | + |
| Hypomyelination | na | + |
| Seizures | + | + |
| Defects in locomotor activity/hypotonia | + | + |
| Impaired spatial learning associated with defects in long-term potentiation | + | na |
| Developmental delay | na | + |
| Decreased grip strength | + | na |
| Increased copper levels | + | na |
| Defects in lipid metabolism | + | na |
| Dolichocephaly | − | + |
| Mild facial dysmorphia | − | + |
| Abnormal ear morphology | − | + |
| Micrognathia | − | + |

+ = present; − = absent; na = not assessed.

We next evaluated the role that loss of APP function might play in causing the clinical phenotype by examining the consequence of APP knockout in the murine model. APP1 knockout mice have been generated alone and in combination with other *APP* gene orthologs.[14–20] The APP1 knockout mouse model has revealed a reproducible generalized phenotype including decreased growth,[5] decreased brain weight,[18] dysgenesis of the corpus callosum,[18] seizures,[19] defects in locomotor activity,[20] and impaired spatial learning associated with defects in long-term potentiation.[20] This case shares striking phenotypic overlap with the murine model, including decreased growth, decreased brain weight, thinning of the corpus callosum, hypotonia, and developmental delay (summarized in Table 2).

Loss of APP offers insight into the role of the non-pathogenic products of APP, including but not limited to sAPPα These findings suggest an essential role for intact APP processing in growth, brain development, and behavior in both humans and mice. However, further studies are required to understand the exact contribution

of APP to these processes. The data also demonstrate that APP haploinsufficiency is not associated with a phenotype, as both unaffected parents are heterozygous for the nonsense allele and otherwise healthy. Additionally, searching the ExAC database revealed an absence of homozygote nonsense mutations in the healthy population. Interestingly, from this same analysis we were able to identify 7 additional cases heterozygous for the same mutation as this case (hg19 chr21:g.[27369690C>T], c.1075C>T). These cases are all of Latino descent, as is the case of this family, indicating that this may be a founder mutation. This study expands the human phenotypic data associated with genetic changes in APP and further strengthens the utility of the mouse model in understanding the role of APP. The identification of additional cases in combination with future functional studies will solidify the understanding of the exact role of APP in brain development.

## Acknowledgment

## Author Contributions

S.K. and A.G. wrote the manuscript. H.L., S.F.N., and UCLA Clinical Genomics Center performed the whole exome sequencing and analysis. S.G. reviewed the brain imaging. S.K. and V.B. performed the protein extraction, Western blots, and preparation of the images for publication. J.A.M.-A. wrote/edited the manuscript, oversaw all analysis, and performed clinical phenotyping.

## Potential Conflicts of Interest

Nothing to report.

## References

1. Campion D, Dumanchin C, Hannequin D, et al. Early-onset autosomal dominant Alzheimer disease: prevalence, genetic heterogeneity, and mutation spectrum. Am J Hum Genet 1999;65:664–670.

2. Musiek ES, Holtzman DM. Three dimensions of the amyloid hypothesis: time, space and 'wingmen'. Nat Neurosci 2015;18:800–806.

3. Muller U, Cristina N, Li ZW, et al. Behavioral and anatomical deficits in mice homozygous for a modified beta-amyloid precursor protein gene. Cell 1994;79:755–765.

4. Chow VW, Mattson MP, Wong PC, Gleichmann M. An overview of APP processing enzymes and products. Neuromolecular Med 2010;12:1–12.

5. Zheng H, Jiang M, Trumbauer ME, et al. beta-Amyloid precursor protein-deficient mice show reactive gliosis and decreased locomotor activity. Cell 1995;81:525–531.

6. Brickell KL, Steinbart EJ, Rumbaugh M, et al. Early-onset Alzheimer disease in families with late-onset Alzheimer disease: a potential important subtype of familial Alzheimer disease. Arch Neurol 2006;63:1307–1311.

7. Lee H, Deignan JL, Dorrani N, et al. Clinical exome sequencing for genetic identification of rare Mendelian disorders. JAMA 2014;312:1880–1887.

8. DePristo MA, Banks E, Poplin R, et al. A framework for variation discovery and genotyping using next-generation DNA sequencing data. Nat Genet 2011;43:491–498.

9. Yourshaw M, Taylor SP, Rao AR, et al. Rich annotation of DNA sequencing variants by leveraging the Ensembl Variant Effect Predictor with plugins. Brief Bioinform 2015;16:255–264.

10. Arning L, Epplen JT, Rahikkala E, et al. The SETX missense variation spectrum as evaluated in patients with ALS4-like motor neuron diseases. Neurogenetics 2013;14:53–61.

11. Anheim M, Monga B, Fleury M, et al. Ataxia with oculomotor apraxia type 2: clinical, biological and genotype/phenotype correlation study of a cohort of 90 patients. Brain 2009;132(pt 10):2688–2698.

12. Kousi M, Lehesjoki AE, Mole SE. Update of the mutation spectrum and clinical correlations of over 360 mutations in eight genes that underlie the neuronal ceroid lipofuscinoses. Hum Mutat 2012;33:42–63.

13. ExAC Browser (Beta). Available at: http://exac.broadinstitute.org. Accessed September 1, 2015.

14. Li ZW, Stark G, Gotz J, et al. Generation of mice with a 200-kb amyloid precursor protein gene deletion by Cre recombinase-mediated site-specific recombination in embryonic stem cells. Proc Natl Acad Sci U S A 1996;93:6158–6162.

15. Herms J, Anliker B, Heber S, et al. Cortical dysplasia resembling human type 2 lissencephaly in mice lacking all three APP family members. EMBO J 2004;23:4106–4115.

16. Heber S, Herms J, Gajic V, et al. Mice with combined gene knock-outs reveal essential and partially redundant functions of amyloid precursor protein family members. J Neurosci 2000;20:7951–7963.

17. von Koch CS, Zheng H, Chen H, et al. Generation of APLP2 KO mice and early postnatal lethality in APLP2/APP double KO mice. Neurobiol Aging 1997;18:661–669.

18. Magara F, Muller U, Li ZW, et al. Genetic background changes the pattern of forebrain commissure defects in transgenic mice underexpressing the beta-amyloid-precursor protein. Proc Natl Acad Sci U S A 1999;96:4656–4661.

19. Steinbach JP, Muller U, Leist M, et al. Hypersensitivity to seizures in beta-amyloid precursor protein deficient mice. Cell Death Differ 1998;5:858–866.

20. Tremml P, Lipp HP, Muller U, et al. Neurobehavioral development, adult openfield exploration and swimming navigation learning in mice with a modified beta-amyloid precursor protein gene. Behav Brain Res 1998;95:65–76.

**ORIGINAL ARTICLE**

WILEY AMERICAN JOURNAL OF medical genetics A PART

# De novo loss-of-function variants in *STAG2* are associated with developmental delay, microcephaly, and congenital anomalies

Sureni V. Mullegama[1,2] | Steven D. Klein[3] | Milene V. Mulatinho[1] |

Tharanga Niroshini Senaratne[1] | Kathryn Singh[4,5] | UCLA Clinical Genomics Center[2] |

Dzung C. Nguyen[3] | Natalie M. Gallant[4,5] | Samuel P. Strom[1,2] |

Shahnaz Ghahremani[6] | Nagesh P. Rao[1] | Julian A. Martinez-Agosto[2,3,7] (iD)

[1] Department of Pathology and Laboratory Medicine, David Geffen School of Medicine, University of California, Los Angeles, California

[2] UCLA Clinical Genomics Center, David Geffen School of Medicine, University of California, Los Angeles, California

[3] Department of Human Genetics, David Geffen School of Medicine, University of California, Los Angeles, California

[4] Division of Genetic and Genomic Medicine, University of California, Irvine, California

[5] Miller Children's and Women's Hospital Long Beach, Long Beach, California

[6] Department of Radiology, David Geffen School of Medicine at UCLA, Los Angeles, California

[7] Department of Pediatrics, David Geffen School of Medicine, University of California, Los Angeles, California

**Correspondence**
Julian A. Martinez-Agosto MD, PhD, UCLA Clinical Genomics Center, David Geffen School of Medicine, University of California, 695 Charles E. Young Drive South, Gonda Research Center Room 4605, Los Angeles, CA 90095. Email: julianmartinez@mednet.ucla.edu

**Funding information**
March of Dimes, Grant number: 6-FY12-324, JAM-A; UCLA Children's Discovery Institute; UCLA CART, Grant number: NIH/NICHD P50-HD-055784, JAM-A; NIH/NCATS UCLA CTSI, Grant number: UL1TR000124, JAM-A; Autism Speaks, Grant number: 9172; UCLA-Caltech MSTP NIH, Grant number: T32GM008042; Wellcome Trust

The cohesin complex is an evolutionarily conserved multi-subunit protein complex which regulates sister chromatid cohesion during mitosis and meiosis. Additionally, the cohesin complex regulates DNA replication, DNA repair, and transcription. The core of the complex consists of four subunits: SMC1A, SMC3, RAD21, and STAG1/2. Loss-of-function mutations in many of these proteins have been implicated in human developmental disorders collectively termed "cohesinopathies." Through clinical exome sequencing (CES) of an 8-year-old girl with a clinical history of global developmental delay, microcephaly, microtia with hearing loss, language delay, ADHD, and dysmorphic features, we describe a heterozygous de novo variant (c.205C>T; p.(Arg69*)) in the integral cohesin structural protein, *STAG2*. This variant is associated with decreased STAG2 protein expression. The analyses of metaphase spreads did not exhibit premature sister chromatid separation; however, delayed sister chromatid cohesion was observed. To further support the pathogenicity of *STAG2* variants, we identified two additional female cases from the DECIPHER research database with mutations in *STAG2* and phenotypes similar to our patient. Interestingly, the clinical features of these three cases are remarkably similar to those observed in other well-established cohesinopathies. Herein, we suggest that *STAG2* is a dosage-sensitive gene and that heterozygous loss-of-function variants lead to a cohesinopathy.

**KEYWORDS**

cohesinopathy, cohesin-associated genes, cohesin complex, gene dosage, *STAG2*, X-linked

## 1 | INTRODUCTION

The cohesin complex is a large, evolutionary conserved functional unit involved in DNA replication, gene expression, heterochromatin formation, DNA repair, and sister chromatid cohesion (Di Benedetto et al.,

2013). The cohesin complex consists of four core proteins, SMC1A, SMC3, RAD21, and STAG1/2 (Mannini, Cucco, et al., 2015) (Figure 1A). In addition, there are several proteins that regulate the cohesin complex's interaction with chromosomes (*NIPBL, ESCO2, HDAC8, DDX11, SGOL1, WAPL, PDS5A, PLK1, AURKB,* and *ATRX*) (Figure 1A) (Mannini, Fabien, et al., 2015). Loss-of-function mutations in these genes have been previously associated with multisystem developmental disorders termed

---

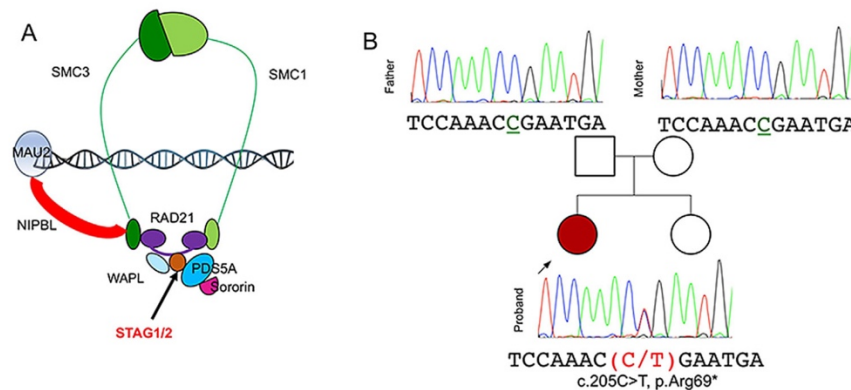Sureni V. Mullegama and Steven Klein are co-first authors.

**FIGURE 1** Characterization of *STAG2* variants. (A) Structure of the cohesin ring and its regulatory proteins. (B) Case 1 family pedigree with sequence analysis by Sanger sequencing showed a heterozygous variant, c.205C>T; p.(Arg69*) in Exon 5 of *STAG2* in the affected proband (red). [Color figure can be viewed at wileyonlinelibrary.com]

"cohesinopathies" (Cucco & Musio, 2016; Skibbens et al., 2013), including Cornelia de Lange syndrome (CdLS, MIM # 122470; *SMC1A*, *SMC3*, *NIPBL*, and *HDAC8*), Roberts/SC phocomelia syndrome (RBS MIM # 268300; *ESCO2*), α-thalassemia/mental retardation syndrome (ATRX, MIM # 301040; *ATRX*), Warsaw breakage syndrome (WBS, MIM # 613398; *DDX11*), Chronic Atrial and Intestinal Dysrhythmia (CAID, MIM # 616201; *SGOL1*), and Cornelia de Lange Syndrome 4 (CdLS4, MIM# 614701; *RAD21* mutations) (Ball, Chen, & Yokomori, 2014; Barbero, 2013; Gerkes, van der Kevie-Kersemaekers, Yakin, Smeets, & van Ravenswaaij-Arts, 2010; McNairn & Gerton, 2008; Musio & Krantz, 2010; Skibbens et al., 2013). Overwhelmingly, these syndromes are characterized by decreased growth, limb malformations, developmental delay, dysmorphic features, and behavioral phenotypes (specifically Attention Deficit Hyperactivity Disorder [ADHD]).

One of the cohesin subunits in which loss-of-function mutations have yet to be associated with any cohesinopathies is the stromal antigen two genes (MIM # 300826; *STAG2*). Recently, 33 chromosome Xq25 duplications involving *STAG2* and *STAG2*-only duplications have been identified in males with intellectual disability, behavioral problems, seizures, malar flatness, and prognathism (Bonnet et al., 2009; Kumar et al., 2015; Leroy et al., 2016; Philippe et al., 2013; Yingjun et al., 2015). The genetic and molecular data in these studies provide compelling evidence that *STAG2* may be a dosage sensitive gene (Kumar et al., 2015). However, no *STAG2* loss-of-function or missense mutations have been identified in individuals with multisystem anomalies and neurodevelopmental delays.

Here, we describe de novo loss-of-function heterozygous *STAG2* variants associated with developmental delay, deafness, craniofacial abnormalities, and congenital heart defects.

## 2 | METHODS

### 2.1 | Patient ascertainment

All samples and information were collected after informed consent was obtained and in accordance with local Institutional Review Board (IRB)

approved protocols from the University of California, Los Angeles. The clinical assessment included a medical record review of, developmental, biochemical, neurological, and genetic evaluations. Fresh peripheral blood samples for molecular and cytogenetic studies were collected from the proband as well as her mother and father.

### 2.2 | Clinical exome sequencing (CES)

CES was performed at the UCLA Clinical Genomics Center, on DNA of the affected girl and both parents, as previously described (Lee et al., 2014). Briefly, exome capture was performed using Agilent SureSelect XT Clinical Research Exome, sequencing was performed on HiSeq2500 as 100 bp paired end runs and variant annotation was performed using GoldenHelix SNP & Variation Suite (Lee et al., 2014; Rehm et al., 2013). Rareness of the variant in the population was measured using the minor allele frequency (MAF) score from Exome Aggregation Consortium (ExAC) database. Variants with greater than 1% MAF in this database were considered common and removed from the final candidate list. In total 23,398 DNA variants were identified, including 21,727 single nucleotide substitutions and 1,671 small deletions/insertions (1–10 bp). The data are consistent with a high quality genomic sequence and fall within normal human genomic variation quality parameters.

### 2.3 | Sanger sequencing

Genomic DNA from the proband and her parents were extracted from peripheral blood using standard protocols. Exon 5 and adjacent intron boundaries of *STAG2* (RefSeq NM_001042749.1) were sequenced using Big Dye Terminator V1.1 cycle sequencing kit and ABI3130xl genetic analyzer following manufacturers guidelines. Primers and PCR conditions are available upon request. The sequencing results were processed with the 4Peaks software (http://nucleobytes.com/4peaks/).

### 2.4 | Western blot analysis

Venous blood was drawn from the proband and both parents, and immediately spun at 100 g for 20 min to obtain platelet rich plasma

(PRP). One milliliter of the PRP was transferred to a 1.5 ml Eppendorf tube and spun at 100 g for 20 min to pellet the white blood cells. The supernatant was discarded and the pellet was suspended in 500 μl of passive lysis buffer, prepared with phosphatase and protease inhibitors, and incubated by shaking at 4°C for 1 hr. After lysis tubes were spun at 7500 Rcf for 5 min to collect debris. Supernatant was transferred to a new tube then protein concentration determined with the Coommasie Plus Bradford (Life Technologies) reagent following manufacture instructions. Western blots were run on 12% acrylamide gels followed by transfer onto nitrocellulose membranes utilizing the Transblot Turbo® apparatus from Biorad. The membrane was blocked in 5% bovine serum albumin in Tris buffered saline plus Tween (TBST) for 30 min, then incubated with either of two independent primary antibodies against STAG2 (Cell Signaling #4,239 Dilution 1/500 and Cell Signaling #5,882 Dilution 1/500) and beta-actin (Cell Signaling #4970, Dilution 1/5,000) for 24 hr. Blots were then rinsed with Tris buffered saline (TBS), washed three times with TBST, and incubated in rabbit secondary antibodies conjugated to horseradish peroxidase at a dilution of 1/3,750. Following secondary incubation membranes were rinsed with TBS then washed twice with TBST. Blots were exposed using Western Clarity reagents from BioRad and imaged on the Bio Rad ChemiDoc and viewed in ImageLab Software. Quantification of band intensity was performed using ImageLab with each band normalized to its independent loading control. Statistical analysis was performed on averages derived from six technical replicates using the Mann–Whitney U Test.

## 2.5 | Immunofluorescence

One hundred thousand human neural stem cells were plated on GelTrex (Invitrogen) coated coverslips. After 24 hr of growth cells were fixed using paraformaldehyde for 20 min then blocked with 10% normal goat serum in TBST overnight. The following day coverslips were washed three times in TBST. Coverslips were incubated in primary antibody against STAG2 (Cell Signaling #5,882 Dilution 1/250) in 3% BSA in TBST for 1 hr. Coverslips were then washed three times in TBST and incubated in secondary antibody (Jackson Laboratories, AffiniPure Donkey Anti-Rabbit, 711-165-152, Dilution 1/1,000 and Invitrogen, Alexa Fluor® 647 Phalloidin, A22287, dilution 1/100) in 3% BSA in TBST for 1 hr. Coverslips were then washed three times in TBST and then three times in water. Coverslips were mounted on glass slides using ProLong® Gold Antifade Mountant with DAPI (Invitrogen, P36931). Slides were imaged using a Zeiss LSM-800.

## 2.5 | Cytogenetic studies

Wright–Giemsa stained metaphase cells were prepared from PHA-stimulated cultures of peripheral blood from the proband and parents following routine G-banding protocols to determine the karyotype status of the three individuals. For sister chromatid cohesion assays, 60 metaphase cells from each of the three individuals in which each chromosome could be clearly resolved as two chromatids were scored. Individual chromosomes were examined for cohesion between the sister chromatids (SC), paying close attention to the centromeric

regions. A chromosome was scored as showing complete separation ("open") if the two chromatids were clearly unattached along their entire length including the centromeric region. A chromosome was scored as showing "partial" separation if one or both SCs showed lack of a centromeric constriction and a potential gap between the SCs was visible at the centromere. For each metaphase cell, the numbers of open, partial, and closed chromosome pairs were scored. Cells were analyzed independently by two observers (once in a blinded fashion). The cells were classified as having premature sister chromatid separation (PSCS) if at least three chromosome pairs per metaphase cell showed the open or partial phenotype, while cells were classified as intermediate if one or two chromosome pairs showed the open or partial phenotype. Statistical analyses were conducted using two-tailed Fisher's Exact tests.

# 3 | RESULTS

## 3.1 | Patient report

Case 1 was a female born at 40 weeks gestation via caesarean section to a 21-year-old primagravida mother and a 23-year-old father. Pregnancy was not significant for any major medical problems, tetratogenic exposures, or hospitalizations. The parents were Latino/Hispanic and family history was negative for any significant morbidities or consanguinity (Figure 1B). Birth weight was 3,629 g (50th–75th centile) and length 51 cm (50th–75th centile). She was admitted to the neonatal intensive care unit (NICU) because of apnea and feeding problems. Examination by a medical geneticist in the NICU documented bilateral microtia (grade 1 on the right and grade 3 on the left), left preauricular pit and tag, left facial palsy (with left eye unable to close), bilateral paramedian lower lip pits, and submucous cleft palate with bifid uvula. Newborn hearing screen results were abnormal. Brain MRI on day 2 of life showed dysgenesis of the splenium of the corpus callosum (Figure 2A and B). Additionally, posterior to the splenium was an 18 mm interventricular subarachnoid cyst and a subgaleal hematoma at the cortex. Echocardiogram showed an apical and muscular ventricular septal defect and chest X-ray showed multiple thoracic vertebral anomalies (Figure 2C and D). Abdominal ultrasound in the neonatal period showed mild left pelviectasis. She was discharged after 2 weeks in the NICU and development was followed: she smiled at 2 months, rolled over at 6 months, sat without support at age 8 months, crawled at 1 year, stood, and walked independently at 18 months, and spoke her first words at 18 months. At age 2 years 7 months a developmental evaluation showed delays in expressive language but no deficits in other areas and no signs of autism were appreciated. At age 4, evaluation of the microtia included a CT scan of the temporal bones that showed left external auditory canal atresia with a fused ossicular mass, absent stapes, and severely stenotic oval window. There was a small pneumatized, aerated middle ear cavity and mastoid antrum. The tympanic segment of the facial nerve was asymmetrically small without normal communication with the anterior genu. On the right, there was absence of the stapes and severe stenosis or absence of the oval window with a medially placed
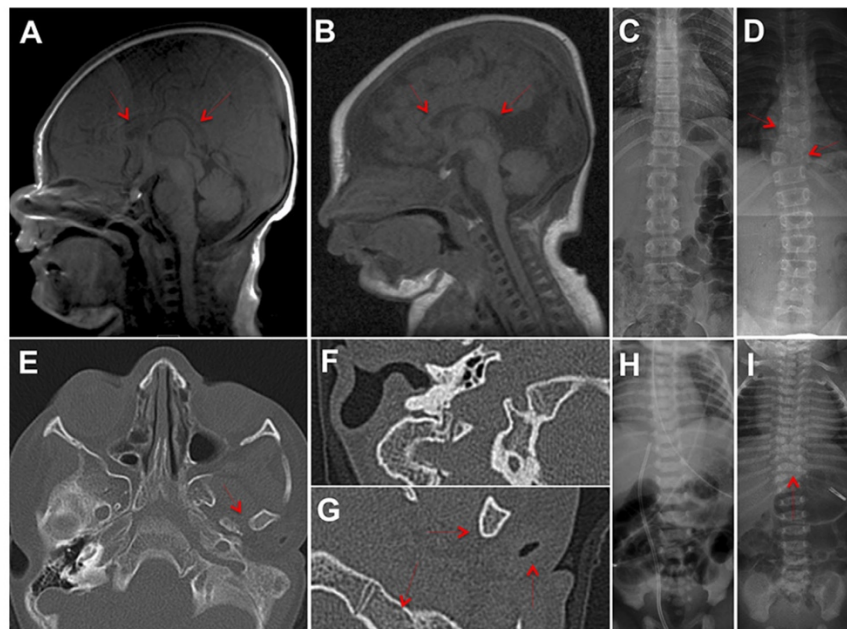
**FIGURE 2** MRI and radiological findings in patients with STAG2 mutations. (A) Healthy three day old female axial T1 weighted MRI view of a normally developed corpus callosum (red arrows). (B) Axial T1 weighted MRI view of patient with STAG2 mutation displaying dysgenesis of the splenium of the corpus callosum (red arrows). (C) Chest X-ray of a healthy 1-day old female demonstrating normal vertebral development. (D) Chest X-ray of a patient with STAG2 mutation demonstrating scoliosis and vertebral abnormalities including hemi-vertebrae and "butterfly" vertebrae (red arrows). (E) Axial view of bilateral auditory canals in a patient with a STAG2 mutation, showing absence of the left auditory canal (red arrow). (F) Higher magnification of the right auditory canal image shows patent canal and normal bone structures. (G) Higher magnification of the left auditory canal demonstrating external auditory canal atresia with a fused ossicular mass, absent stapes, and severely stenotic oval window (red arrows). (H) Chest X-ray of a healthy 8-year-old female demonstrating normal vertebral development. (I) Chest X-ray of a patient with STAG2 mutation demonstrating scoliosis and vertebral abnormalities including hemi-vertebrae (red arrow). [Color figure can be viewed at wileyonlinelibrary.com]

tympanic segment of the facial nerve (Figure 2E–G). At 6 years old, her abdominal ultrasound was repeated and showed left pelviectasis resolution. At 8-years-old, her weight was 24.5 kg (29th centile), and length was 121.7 cm (8th centile) and her head circumference was 48 cm (5th centile) which demonstrated decelerating brain growth and borderline microcephaly and undergrowth. Physical exam at that time was notable for a low anterior hairline, sloping forehead, left eye smaller than the right, asymmetric facial movements, and bilateral fifth finger clinodactyly. She had radiological evidence of scoliosis (Figure 2H and I). Her receptive language was intact but she continued to require speech therapy at school due to delays in expressive language. She was diagnosed with Attention Deficit Hyperactivity Disorder. Karyotype showed a normal female (46,XX). Chromosomal microarray on both BAC and SNP platforms were normal.

## 3.2 | Clinical exome sequencing identifies a de novo loss-of-function heterozygous variant in STAG2

CES performed on Case 1 revealed a de novo heterozygous variant in the *STAG2* gene (NM_001042749.1: c.205C>T, p.Arg69*; Supplementary Table S1). Sanger sequencing analysis of this variant in the parental samples did not detect the variant, suggesting that the change arose de novo in this patient (Figure 1B). ExAC has given this gene a predicted LoF pLI score of 1.00 to suggest loss of function variants in healthy individuals are rare. The c.205C>T, p.Arg69* variant results in a stop-gain (nonsense) change which results in a truncated, predicted non-functional protein product (Figure 3A). The three essential domains of STAG2 (stromal antigen two domain, stromalin conservative domain, and glutamine rich domain) are not present due to this mutation (Figure 1A). Upon searching the DECIPHER database (https://decipher.sanger.ac.uk), we identified two de novo heterozygous *STAG2* variants in two female cases that had phenotype information described in Human Phenotype Ontology (HPO) terms (Table 1). Case 2 has a missense variant; c.1811G>A, p.Arg604Gln (Figure 3A and Supplementary Table S1) (Deciphering Developmental Disorders S, 2015). SIFT and PolyPhen-2 predicted the c.1811G>A (p.Arg604Gln) missense variant to be deleterious and probably damaging (Supplementary Table S1). Case 3 has a frameshift variant that results in a truncated protein product; c.1913_1922del, (p.Ala638Valfs*10) (Figure 3A and Supplementary Table S1). The glutamine rich (GR) domain in STAG2, known to be an activation domain of transcription factors (Xiao & Jeang, 1998), is not present due to Case 3's mutation, which consequently could affect the transcriptional functions of STAG2 (Figure 3A). All three variants are absent from public databases including Exome Aggregation Consortium (ExAC) and 1000 Genome Project (Genomes Project et al., 2012). Since
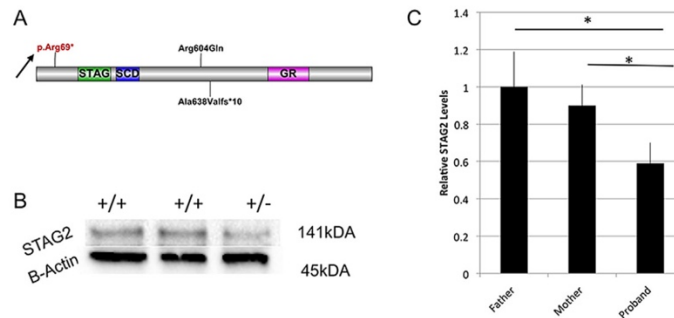
**FIGURE 3** Location and consequence of STAG2 variants. (A) Predicted protein domain structure of STAG2. The 1231 amino acid full-length protein is predicted to contain a STAG domain, a stromalin conservative domain (SCD) and a glutamine-rich region domain (GR). The p.Arg69* mutation is indicated by an arrow. The location of the mutations reported by DECIPHER are depicted (p.Arg604Gln and p.Ala638fs*). (B) Protein expression analysis of STAG2 in patient and her parents reveals decreased levels in proband (±) compared to parents (+/+). (C) Western blot analysis was run using two independent antibodies for STAG2. Quantification of band density with normalization to loading controls demonstrates significant reduction in STAG2 Levels in the proband when compared to either unaffected parental control. *Denotes significant difference ($P < 0.05$, Mann–Whitey U Test ($n = 6$). [Color figure can be viewed at wileyonlinelibrary.com]

STAG2 variants had yet to be associated with any clinical condition, these variants were classified as variants of unknown clinical significance (VOUS) based on the American College of Medical Genetics and Genomics variant assessment (Richards et al., 2015) (Supplementary Table S1).

### 3.3 | Haploinsufficiency of STAG2 is likely pathogenic

The ExAC database demonstrates that STAG2 is extremely intolerant to loss of function variants in healthy populations (43 individuals expected, 0 observed), suggesting that haploinsufficiency is likely pathogenic. Further, the DECIPHER database has given STAG2 a haploinsufficiency score (HI index) of 9.66%, which is a high rank (0–10%), indicating the gene is more likely to exhibit haploinsufficiency (Huang, Lee, Marcotte, & Hurles, 2010).

It is expected that Case 1's STAG2 variant results in a premature termination of translation (Figure 3A). It is likely that nonsense mediated decay could be occurring due this mutation or we could either see the synthesis of a truncated protein lacking the last 1,172 amino acids (Figure 3A). Western blot analysis confirmed that the

mutation is most likely pathogenic as the protein samples prepared from the proband contain less STAG2 than either parent control (Figure 3B–C). Lastly, no alternative splice or truncated variants of smaller size were observed via Western blot analysis (data not shown) indicating that the c.205C>T variant reduces STAG2 protein expression in vivo. However, we cannot rule out the possibility that nonsense mediated decay is occurring.

### 3.4 | Effect of STAG2 haploinsufficiency on sister chromatid cohesion

Since it is well established that STAG2 encodes a subunit of cohesin, a complex that mediates sister chromatid cohesion to ensure accurate chromosome segregation, we next determined if the p.Arg69* variant affects SC cohesion by analyzing metaphase cells for indications of premature sister chromatid separation (PSCS). For each metaphase cell, all sister chromatid pairs were examined to determine if there was no separation ("closed"), clear premature separation at the centromere ("open"), or an intermediate ("partial") phenotype, respectively. Cells were then classified into three categories based on the numbers of

**TABLE 1** Phenotype abnormality comparison between three cases with STAG2 variants

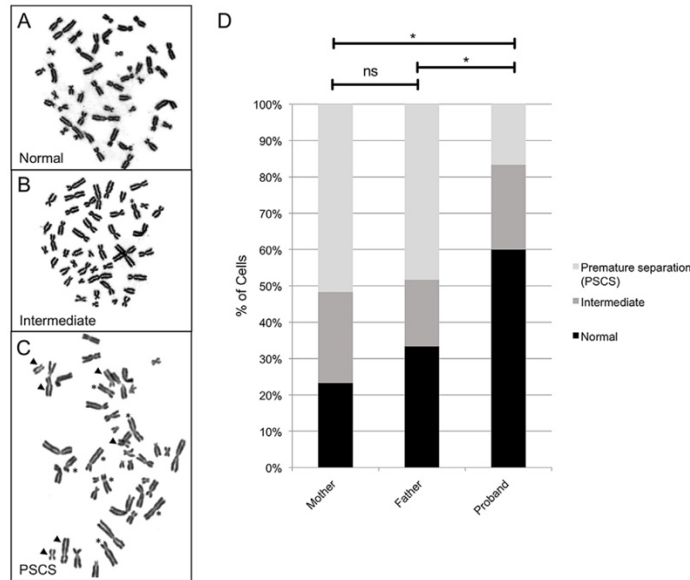| Phenotype abnormalities | HPO term | Case 1 p.Arg69* | Case 2 p.Arg604Gln | Case 3 p.Ala638Valfs*10 |
|---|---|---|---|---|
| Nervous system | HP:0000707 | + | + | + |
| Ear | HP:0000598 | + | + | + |
| Head or neck | HP:0000152 | + | + | + |
| Growth abnormalities | HP:0001507 | + | + | N |
| Limbs | HP:0040064 | + | + | N |
| Skeletal system | HP:0000924 | + | + | N |
| Abdomen | HP:0001438 | N | N | + |
| Respiratory system | HP:0002086 | N | N | + |

+, present; N, not known.

331

**FIGURE 4** Sister Chromatid Cohesion Studies on Affected Proband. (A–C) Metaphases that were described as closed, intermediate, or having premature sister chromatid separation (PSCS) in our assays. Individual chromatid pairs with abnormal phenotypes are highlighted in (B and C), with an arrowhead indicating "open" chromatid pairs, an asterisk indicating pairs with "partial" separation, and all other chromatid pairs being "closed." In (B) there is one partially separated chromatid pair, while in (C) there are six open pairs and seven partial pairs. By our classification, metaphases with 1–2 open/partial chromatid pairs were described as intermediate, and those with three or more open/partial chromatid pairs were described as having PSCS. (D) A graph showing quantification of these results. Sixty metaphases were analyzed from the proband and each parent and classified as described above. In the proband having the STAG2 mutation, PSCS was not increased; in contrast, the proportion of nuclei having PSCS showed a significant decrease compared to either parent (significance calculated using a two-tailed Fisher's Exact test for mother vs. proband ($P = 0.000029$), father versus proband ($P = 0.00075$), and mother versus father ($P = 0.44779$)

chromosome pairs showing the different phenotypes (Figure 4; see Methods section for more details). These studies found that the proband did not show increased PSCS when compared to the parents (Figure 4D). However, the number of metaphases in the PSCS category was significantly reduced in the proband compared to controls (patient vs. mother, $P = 0.000029$; patient vs. father, $P = 0.00075$) (Figure 4D). It was then hypothesized that the STAG2 mutation may have resulted in tighter sister chromatid cohesion. Importantly, the karyotypes were all cytogenetically normal, and there were no significant aneuploidies observed in metaphases from the proband or from the parents.

## 4 | DISCUSSION

Here, we describe de novo heterozygous likely pathogenic STAG2 variants associated with a phenotype that is associated with nervous system (HP:0000707), head or neck (HP: 0000152), and ear (HP:0000598) abnormalities (Table 1). More specifically, the phenotypes include microcephaly, microtia with hearing loss, developmental delay, language delay, ADHD, and dysmorphic features, overlapping with established cohesinopathies (Table 2).

Characterization of our STAG2 variant indicates a loss-of-function mechanism due to decreased STAG2 protein expression. Furthermore, our cytogenetic studies did not reveal significant amounts of PSCS but did show that the mutant cells had tighter sister chromatid cohesion.

The contribution of this alteration in chromosome segregation to the phenotype is not yet fully understood and is complicated by the multifunctional nature of STAG2. For example, STAG2 is also a transcription factor and mutations could affect its binding to specific DNA sequences crucial for proper neurodevelopment and craniofacial development. Additionally, STAG2 is the only cohesin subunit that interacts directly with the zinc finger DNA binding protein (CTCF) (Lake, Boetefuer, Won, & Fan, 2016; Ong & Corces, 2014; Van Bortle, Peterson, Takenaka, O'Connor, & Corces, 2015). CTCF is required for cohesion dependent insulation activity and CTCF mutations have been indirectly implicated in intellectual disability (Van Bortle et al., 2015). About 50–80% of CTCF binding sites in the genome are occupied by the cohesin complex (Lake et al., 2016; Ong & Corces, 2014; Van Bortle et al., 2015). Thus, a nonfunctional cohesin complex results in the disruption of CTCF-mediate intrachromosomal interactions (Lake et al., 2016; Ong & Corces, 2014; Van Bortle et al., 2015). We propose that disruption of STAG2's other functions, such as the regulation of gene expression, may contribute more to the phenotype than the effects on sister chromatin segregation similarly noted in other cohesinopathy genes (Deardorff et al., 2012; Remeseiro, Cuadrado, & Losada, 2013; Skibbens et al., 2013).

Additionally, from this work, we have shown that not all mutations in cohesin complex core subunits affect sister chromatid separation equally. The cellular phenotype most recently described with RAD21 mutations was not replicated in our analysis (Deardorff et al., 2012). This
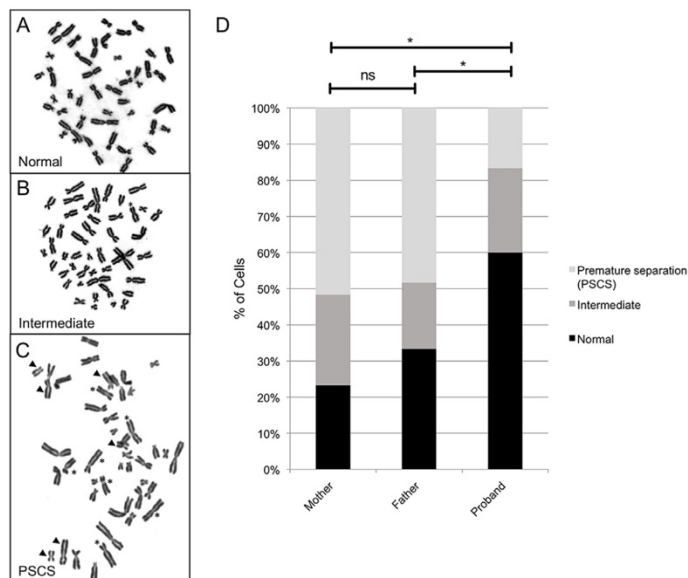
**FIGURE 4** Sister Chromatid Cohesion Studies on Affected Proband. (A–C) Metaphases that were described as closed, intermediate, or having premature sister chromatid separation (PSCS) in our assays. Individual chromatid pairs with abnormal phenotypes are highlighted in (B and C), with an arrowhead indicating "open" chromatid pairs, an asterisk indicating pairs with "partial" separation, and all other chromatid pairs being "closed." In (B) there is one partially separated chromatid pair, while in (C) there are six open pairs and seven partial pairs. By our classification, metaphases with 1–2 open/partial chromatid pairs were described as intermediate, and those with three or more open/partial chromatid pairs were described as having PSCS. (D) A graph showing quantification of these results. Sixty metaphases were analyzed from the proband and each parent and classified as described above. In the proband having the STAG2 mutation, PSCS was not increased; in contrast, the proportion of nuclei having PSCS showed a significant decrease compared to either parent (significance calculated using a two-tailed Fisher's Exact test for mother vs. proband ($P = 0.000029$), father versus proband ($P = 0.00075$), and mother versus father ($P = 0.44779$)

chromosome pairs showing the different phenotypes (Figure 4; see Methods section for more details). These studies found that the proband did not show increased PSCS when compared to the parents (Figure 4D). However, the number of metaphases in the PSCS category was significantly reduced in the proband compared to controls (patient vs. mother, $P = 0.000029$; patient vs. father, $P = 0.00075$) (Figure 4D). It was then hypothesized that the STAG2 mutation may have resulted in tighter sister chromatid cohesion. Importantly, the karyotypes were all cytogenetically normal, and there were no significant aneuploidies observed in metaphases from the proband or from the parents.

## 4 | DISCUSSION

Here, we describe de novo heterozygous likely pathogenic STAG2 variants associated with a phenotype that is associated with nervous system (HP:0007707), head or neck (HP: 0000152), and ear (HP:0000598) abnormalities (Table 1). More specifically, the phenotypes include microcephaly, microtia with hearing loss, developmental delay, language delay, ADHD, and dysmorphic features, overlapping with established cohesinopathies (Table 2).

Characterization of our STAG2 variant indicates a loss-of-function mechanism due to decreased STAG2 protein expression. Furthermore, our cytogenetic studies did not reveal significant amounts of PSCS but did show that the mutant cells had tighter sister chromatid cohesion.

The contribution of this alteration in chromosome segregation to the phenotype is not yet fully understood and is complicated by the multi-functional nature of STAG2. For example, STAG2 is also a transcription factor and mutations could affect its binding to specific DNA sequences crucial for proper neurodevelopment and craniofacial development. Additionally, STAG2 is the only cohesin subunit that interacts directly with the zinc finger DNA binding protein (CTCF) (Lake, Boetefuer, Won, & Fan, 2016; Ong & Corces, 2014; Van Bortle, Peterson, Takenaka, O'Connor, & Corces, 2015). CTCF is required for cohesion dependent insulation activity and CTCF mutations have been indirectly implicated in intellectual disability (Van Bortle et al., 2015). About 50–80% of CTCF binding sites in the genome are occupied by the cohesin complex (Lake et al., 2016; Ong & Corces, 2014; Van Bortle et al., 2015). Thus, a nonfunctional cohesin complex results in the disruption of CTCF-mediate intrachromosomal interactions (Lake et al., 2016; Ong & Corces, 2014; Van Bortle et al., 2015). We propose that disruption of STAG2's other functions, such as the regulation of gene expression, may contribute more to the phenotype than the effects on sister chromatin segregation similarly noted in other cohesinopathy genes (Deardorff et al., 2012; Remeseiro, Cuadrado, & Losada, 2013; Skibbens et al., 2013).

Additionally, from this work, we have shown that not all mutations in cohesin complex core subunits affect sister chromatid separation equally. The cellular phenotype most recently described with RAD21 mutations was not replicated in our analysis (Deardorff et al., 2012). This

further suggests that the cohesin complex as a whole may affect global transcription and its alterations converge on transcriptional deregulation of key developmental genes. The lack of consensus on sister chromatid separation cellular phenotypes despite overwhelming clinical overlap leads us to believe that there is an additional mechanism contributing to cohesinopathy-associated phenotypes. Furthermore, comparison of *STAG2* associated phenotypes with those of well-known cohesinopathies, revealed an overall phenotypic gestalt which is remarkably similar, suggesting common molecular etiologies (Table 2).

Recently, 33 chromosome Xq25 duplications involving *STAG2* have been identified in males with intellectual disability, behavioral problems, seizures, malar flatness, and prognathism (Bonnet et al., 2009; Kumar et al., 2015; Leroy et al., 2016; Philippe et al., 2013; Yingjun et al., 2015). In this study, we illustrate how *STAG2* LOF variants can lead to a unique phenotype as well. Comparing the phenotype of loss-of-function variants in *STAG2* to *STAG2* duplications, we see that while there is a slight overlap of phenotypic features in these *STAG2* patients, the phenotype of loss-of-function variants in *STAG2* result in a more severe phenotype than *STAG2* duplications and is more similar to other cohesinopathies (Table 1 and S2). Based on this study, we suggest that *STAG2* should be added to the expanding list of dosage-sensitive genes that are responsible for neurodevelopmental disorders (Vissers & Stankiewicz, 2012).

Finally, the number of X-linked genes in which de novo mutations cause disorders specifically in females are limited (Grozeva et al., 2015; Kumar et al., 2015; Tzschach et al., 2015). The utilization of next generation sequencing methods has increased the identification of novel X-linked gene mutations in females with developmental delay with multiple congenital malformations (Retterer et al., 2016; Yang et al., 2013). *STAG2* is a gene located on chromosome Xq25. From studies that have determined X-chromosome inactivation (XCi) status of over 400 X-linked genes, *STAG2* was found to be a gene that undergoes inactivation (Cotton et al., 2013). In our study, all our cases are females with de novo heterozygous mutations in *STAG2*. It is conceivable that pathogenic loss-of-function *STAG2* variants that affect canonical STAG, SCD, and GR domains are lethal in males with a 46, XY karyotype similar to males with pathogenic loss-of-function *MECP2* variants in canonical MBD and TRD domains are considered to be lethal (Bianciardi et al., 2016) (Rett syndrome; MIM 300005). Furthermore, the variable clinical severity in both females and males could be dependent on the type of variant (missense versus truncation), location (within a functional domain), and skewed XCi (Chae, Hwang, Hwang, Cheong, & Kim, 2004; Weaving et al., 2003). For example, a female that carries a pathogenic *STAG2* variant but has favorably skewed XCi may have mild or no symptoms. Additionally, *STAG2* male cases that are mosaic or have a 47,XXY karyotype could possibly exist and have a milder phenotype.

Overall, our findings solidify that *STAG2* is a dosage sensitive gene and furthermore provide evidence that loss-of-function mutations in *STAG2* result in a cohesinopathy. The shared phenotype includes abnormalities of the nervous system, head, neck, and ear. Additional features identified in the DECIPHER cases were limited to standardized terms from the HPO. This information has the benefit of standardizing

phenotypes and allowing for coded data sharing. However, it also introduces generalizations that lack specific clinical details. Despite this, the shared phenotypic data as presented in Table 1 suggests that these variants are likely pathogenic and furthermore contribute to the disease process. Further studies on the cellular and molecular function of STAG2, and other cohesin complex components, may reveal the exact mechanism of dosage sensitivity and its effects on normal development.

## CONFLICT OF INTEREST

No conflicts of interests.

## REFERENCES

Ball, A. R. Jr., Chen, Y. Y., & Yokomori, K. (2014). Mechanisms of cohesin-mediated gene regulation and lessons learned from cohesinopathies. *Biochimica Et Biophysica Acta, 1839*(3), 191–202.

Barbero, J. L. (2013). Genetic basis of cohesinopathies. *The Application of Clinical Genetics, 6*, 15–23.

Bianciardi L., Fichera M., Failla P., Di Marco C., Grozeva D., Mencarelli M. A., . . . Ariani F. (2016). MECP2 missense mutations outside the canonical MBD and TRD domains in males with intellectual disability. *J Hum Genet, 61*(2), 95–101.

Bonnet, C., Leheup, B., Beri, M., Philippe, C., Gregoire, M. J., & Jonveaux, P. (2009). Aberrant GRIA3 transcripts with multi-exon duplications in a family with X-linked mental retardation. *American Journal of Medical Genetics Part A, 149A*(6), 1280–1289.

Chae, J. H., Hwang, H., Hwang, Y. S., Cheong, H. J., & Kim, K. J. (2004). Influence of MECP2 gene mutation and X-chromosome inactivation on the Rett syndrome phenotype. *Journal of Child Neurology, 19*(7), 503–508.

Cotton, A. M., Ge, B., Light, N., Adoue, V., Pastinen, T., & Brown, C. J. (2013). Analysis of expressed SNPs identifies variable extents of expression from the human inactive X chromosome. *Genome Biology, 14*(11), R122.

Cucco, F., & Musio, A. (2016). Genome stability: What we have learned from cohesinopathies. *American Journal of Medical Genetics Part C, 172C*(2), 171–178.

Deardorff, M. A., Wilde, J. J., Albrecht, M., Dickinson, E., Tennstedt, S., Braunholz, D., . . . Kaiser, F. J. (2012). RAD21 mutations cause a human cohesinopathy. *American Journal of Human Genetics, 90*(6), 1014–1027.

Deciphering Developmental Disorders S (2015). Large-scale discovery of novel genetic causes of developmental disorders. *Nature, 519*(7542), 223–228.

Di Benedetto, D., Di Vita, G., Romano, C., Giudice, M. L., Vitello, G. A., Zingale, M., . . . Fichera, M. (2013). 6p22.3 deletion: Report of a patient with autism, severe intellectual disability and electroencephalographic anomalies. *Molecular Cytogenet, 6*(1), 4.

Genomes Project C., Abecasis G. R., Auton A., Brooks L. D., DePristo M. A., Durbin R. M., . . . McVean G. A. (2012). An integrated map of genetic variation from 1,092 human genomes. *Nature, 491*(7422), 56–65.

Gerkes, E. H., van der Kevie-Kersemaekers, A. M., Yakin, M., Smeets, D. F., & van Ravenswaaij-Arts, C. M. (2010). The importance of chromosome studies in Roberts syndrome/SC phocomelia and other cohesinopathies. *European Journal of Medical Genetics, 53*(1), 40–44.

Grozeva, D., Carss, K., Spasic-Boskovic, O., Tejada, M. I., Gecz, J., Shaw, M., . . . Raymond, F. L. (2015). Targeted next-generation sequencing analysis of 1,000 individuals with intellectual disability. *Human Mutation, 36*(12), 1197–1204.

Huang N., Lee I., Marcotte E. M., & Hurles M. E. (2010). Characterising and predicting haploinsufficiency in the human genome. *PLoS Genet, 6*(10), e1001154.

Kumar, R., Corbett, M. A., Van Bon, B. W., Gardner, A., Woenig, J. A., Jolly, L. A., . . . Gecz, J. (2015). Increased STAG2 dosage defines a novel cohesinopathy with intellectual disability and behavioral problems. *Human Molecular Genetics, 24*(25), 7171–7181.

Lake, R. J., Boetefuer, E. L., Won, K. J., & Fan, H. Y. (2016). The CSB chromatin remodeler and CTCF architectural protein cooperate in response to oxidative stress. *Nucleic Acids Research, 44*(5), 2125–2135.

Lee, H., Deignan, J. L., Dorrani, N., Strom, S. P., Kantarci, S., Quintero-Rivera, F., . . . Nelson, S. F. (2014). Clinical exome sequencing for genetic identification of rare mendelian disorders. *JAMA, 312*(18), 1880–1887.

Leroy, C., Jacquemont, M. L., Doray, B., Lamblin, D., Cormier-Daire, V., Philippe, A., . . . Malan, V. (2016). Xq25 duplication: The crucial role of the STAG2 gene in this novel human cohesinopathy. *Clinical Genetics, 89*(1), 68–73.

Mannini, L., Cucco, F., Quarantotti, V., Amato, C., Tinti, M., Tana, L., . . . Musio, A. (2015). SMC1B is present in mammalian somatic cells and interacts with mitotic cohesin proteins. *Scientific Reports, 5*, 18472.

Mannini, L., Fabien, C. L., Cucco, F., Amato, C., Quarantotti, V., Rizzo, I. M., . . . Musio, A. (2015). Mutant cohesin affects RNA polymerase II regulation in Cornelia de Lange syndrome. *Scientific Reports, 5*, 16803.

McNairn, A. J., & Gerton, J. L. (2008). Cohesinopathies: One ring, many obligations. *Mutation Research, 647*(1-2), 103–111.

Musio, A., & Krantz, I. D. (2010). Cohesin biology and the cohesinopathies: Abstracts from the second biennial conference, Pontignano, Italy, 2009. *American Journal of Medical Genetics Part A, 152A*(7), 1630–1640.

Ong, C. T., & Corces, V. G. (2014). CTCF: An architectural protein bridging genome topology and function. *Nature Reviews Genetics, 15*(4), 234–246.

Philippe, A., Malan, V., Jacquemont, M. L., Boddaert, N., Bonnefont, J. P., Odent, S., . . . Cormier-Daire, V. (2013). Xq25 duplications encompassing GRIA3 and STAG2 genes in two families convey recognizable X-linked intellectual disability with distinctive facial appearance. *American Journal of Medical Genetics Part A, 161A*(6), 1370–1375.

Rehm, H. L., Bale, S. J., Bayrak-Toydemir, P., Berg, J. S., Brown, K. K., Deignan, J. L., . . . Lyon, E. (2013). ACMG clinical laboratory standards for next-generation sequencing. *Genetics in Medicine, 15*(9), 733–747.

Remeseiro, S., Cuadrado, A., & Losada, A. (2013). Cohesin in development and disease. *Development, 140*(18), 3715–3718.

Retterer, K., Juusola, J., Cho, M. T., Vitazka, P., Millan, F., Gibellini, F., . . . Bale, S. (2016). Clinical application of whole-exome sequencing across clinical indications. *Genetics in Medicine, 18*(7), 696–704.

Richards, S., Aziz, N., Bale, S., Bick, D., Das, S., Gastier-Foster, J., . . . Committee ALQA. (2015). Standards and guidelines for the interpretation of sequence variants: A joint consensus recommendation of the American college of medical genetics and genomics and the association for molecular pathology. *Genetics in Medicine, 17*(5), 405–424.

Skibbens, R. V., Colquhoun, J. M., Green, M. J., Molnar, C. A., Sin, D. N., Sullivan, B. J., & Tanzosh, E. E. (2013). Cohesinopathies of a feather flock together. *PLoS Genetics, 9*(12), e1004036.

Tzschach, A., Grasshoff, U., Beck-Woedl, S., Dufke, C., Bauer, C., Kehrer, M., . . . Bauer, P. (2015). Next-generation sequencing in X-linked intellectual disability. *European Journal of Human Genetics, 23*(11), 1513–1518.

Van Bortle, K., Peterson, A. J., Takenaka, N., O'Connor, M. B., & Corces, V. G. (2015). CTCF-dependent co-localization of canonical smad signaling factors at architectural protein binding sites in D. melanogaster. *Cell Cycle, 14*(16), 2677–2687.

Vissers, L. E., & Stankiewicz, P. (2012). Microdeletion and microduplication syndromes. *Methods in Molecular Biology, 838*, 29–75.

Weaving, L. S., Williamson, S. L., Bennetts, B., Davis, M., Ellaway, C. J., Leonard, H., . . . Christodoulou, J. (2003). Effects of MECP2 mutation type, location and X-inactivation in modulating Rett syndrome phenotype. *American Journal of Medical Genetics Part A, 118A*(2), 103–114.

Xiao, H., & Jeang, K. T. (1998). Glutamine-rich domains activate transcription in yeast *Saccharomyces cerevisiae*. *The Journal of Biological Chemistry, 273*(36), 22873–22876.

Yang, Y., Muzny, D. M., Reid, J. G., Bainbridge, M. N., Willis, A., Ward, P. A., . . . Eng, C. M. (2013). Clinical whole-exome sequencing for the diagnosis of mendelian disorders. *New England Journal of Medicine, 369*(16), 1502–1511.

Yingjun, X., Wen, T., Yujian, L., Lingling, X., Huimin, H., Qun, F., & Junhong, C. (2015). Microduplication of chromosome Xq25 encompassing STAG2 gene in a boy with intellectual disability. *European Journal of Medical Genetics, 58*(2), 116–121.

**SUPPORTING INFORMATION**

Additional Supporting Information may be found online in the supporting information tab for this article.